Contribution à la conception d'un système de radio impulsionnelle ultra large bande intelligent

Rizwan Akbar

université de bretagne occidentale

THÈSE / UNIVERSITÉ DE BRETAGNE OCCIDENTALE
sous le sceau de l'Université européenne de Bretagne

pour obtenir le titre de
DOCTEUR DE L'UNIVERSITÉ DE BRETAGNE OCCIDENTALE
Mention : Sciences et Technologies de l'Information et de la Communication – Spécialité Communication Numérique
École Doctorale SICMA

présentée par
Rizwan AKBAR
Préparée à l'Université de Bretagne Occidentale
(CNRS, UMR 6285 Lab-STICC)

Contribution à la conception d'un système de radio impulsionnelle ultra large bande intelligent

Thèse soutenue le 15 Janvier 2013
devant le jury composé de :

Bernard UGUEN
Professeur, Université de Rennes 1 / *Rapporteur*

Laurent CLAVIER
Professeur, Institut MINES Telecom - Telecom Lille 1 / *Rapporteur*

Jean-François DIOURIS
Professeur, Ecole Polytech de l'Université de Nantes / *Examinateur*

Emanuel RADOI
Professeur, Université de Bretagne Occidentale / *Directeur de thèse*

Stéphane AZOU
Professeur, Ecole Nationale d'Ingénieurs de Brest/ *Encadrant*

Acknowledgements

The research work presented in this thesis was carried out in the *Laboratoire des Sciences et Techniques de l'Information, de la Communication et de la Connaissance* (Lab-STICC UMR CNRS 6285), at University of Brest, France.

First and foremost, I would like to express my deepest gratitude to Allah Almighty, who gave me the strength and courage to achieve this milestone.

After Him, I feel myself highly indebted to my supervisor Professor Emanuel Radoi. He first gave me the opportunity to work with him in my Master's internship, at the time when I was going through the roughest patch of my education career and was in desperate need of motivation and self-confidence. His technical insight, sense of humor and genuine concern for me made working with him a memorable experience. The patience and optimism shown by him towards me had been exemplary all throughout. This thesis would not have been possible without his constant motivation, invaluable guidance and ample support. It has truly been a privilege to work with him.

I would also like to thank my co-supervisor Professor Stéphane Azou for his kindness, continuous association, useful critical comments and the availability.

I am also extremely grateful to all the jury members for their precious time to review my thesis and their constructive remarks.

I would also like to sincerely thank all the members of research team, including the permanents and the doctoral students, who warmly welcomed me and provided me the best environment to work on my thesis. A special thanks to Mélanie, who has been very kind to me throughout and always provided help to me in every possible manner she could have, despite of my inexplicably reserved attitude.

I am also grateful to my family, who has always been there to support me. In particular, I would like to mention my elder brother Adnan, with whom I always had absorbing exchange of arguments on different topics which many times used to help me to relax during the exhausting research periods.

And finally, I want to dedicate this thesis to my late father, who passed away during this time period. Whatever I am today is just because of him. He always used to be very proud and cherish the achievements of his children and I am sure he would have been the most happy person if he had been alive today. You were missed on my Ph.D. defense and will always be.

Résumé étendu en Français

Introduction

Nous assistons depuis quelques années à l'essor considérable des communications sans fil à courte portée, qui est dû au déploiement sans cesse croissant et à très large échelle des réseaux locaux sans fil (WLAN) et personnels (PAN). Cependant, la technologie sans fil traditionnelle ne peut pas répondre aux contraintes des services émergeants, qui exigent souvent du haut débit de données pour être opérationnels. Ce besoin a fortement motivé le développement de la technologie ultra-large bande (UWB), qui est caractérisée par l'émission d'impulsions de très courte durée (de l'ordre de la nanoseconde), avec un très faible niveau de puissance. Les caractéristiques particulières des signaux UWB autorisent à la fois des hauts débits de données, l'immunité aux trajets multiples et une capacité de pénétration élevée.

L'évolution fortement croissante des communications sans fil a également eu comme conséquence l'encombrement du spectre RF, qui est devenu une ressource rare. En outre, le modèle traditionnel d'attribution statique des bandes de fréquence conduit à une faible efficacité d'utilisation des ressources spectrales. Les organismes de régulation en ont pris conscience et souhaitent promouvoir une plus grande flexibilité dans le partage du spectre. L'outil qui semble le mieux adapté pour atteindre cet objectif est la radio cognitive (CR), un concept qui est apparu il y a une dizaine d'années et qui n'a cessé de s'imposer depuis comme une solution d'avenir dans le domaine des communications sans fil.

Un système de radio cognitive est capable de découvrir, d'analyser et finalement d'acquérir la connaissance de son environnement, en s'y adaptant dynamiquement et intelligemment par des mécanismes d'apprentissage [MI99b]. Les premiers travaux consacrés à la radio cognitive étaient liés au concept d'accès dynamique au spectre, c'est-à-dire la sélection dynamique des canaux de fréquences afin de permettre le partage et la réutilisation du spectre. Il s'agit dans ce cas d'un accès opportuniste au spectre pendant les périodes où les utilisateurs primaires (PU) ne sont pas actifs. Cette approche, adoptée par la communauté de la radio cognitive, contraste avec l'utilisation superposée du spectre alloué aux utilisateurs primaires, qui est à la base du développement des systèmes UWB.

Alors que les technologies CR et UWB répondent de façon différente au problème de partage du spectre, nous proposons de combiner leurs avantages dans le cadre d'un nouveau concept, appelé radio cognitive ultra-large bande (UWB CR). Ainsi, puisque les systèmes UWB couvrent une très large bande passante, leur fonctionnement se superpose à celui de plusieurs systèmes de communication et des services ayant différentes caractéristiques techniques et opérationnelles, tels que les réseaux WLAN, WiMax, les systèmes mobiles de $3^{\text{ième}}$ et $4^{\text{ième}}$ génération, etc. [Mis07]. Le faible niveau de puissance utilisé par les systèmes UWB devrait permettre d'éviter les interférences, mais des problèmes peuvent toujours exister, car :

- bien que le système UWB soit conçu pour fonctionner en dessous d'un masque de densité spectrale de puissance défini par les autorités de régulation, certaines imperfections des composantes utilisées ou certaines configurations des paramètres de modulation peuvent tout de même dans certains cas conduire à des interférences gênantes pour les utilisateurs primaires

prioritaires dans des bandes de fréquence étroites ;

– les systèmes UWB eux-mêmes peuvent être perturbés par d'autres systèmes à bande étroite utilisant des niveaux de puissance largement supérieurs ; dans ce cas il peut être plus judicieux de découper cette partie du spectre du signal UWB, car la bande étant étroite cela ne se traduira pas par une réduction significative de ses performances ;

Par rapport à un système UWB standard, un système UWB CR sera donc muni d'un module de détection spectrale, qui permettra de détecter les utilisateurs primaires et de modifier son fonctionnement afin d'éviter toute interférence réciproque. La différence par rapport à un système CR standard est que le système UWB pourra continuer à utiliser tout le temps quasiment la même bande de fréquence, seules des bandes de fréquence étroites correspondant aux différents utilisateurs primaires pouvant être évitées par une conception adaptative de la forme d'onde.

Par ailleurs, les systèmes UWB CR conduisent à un gain de performances par rapport aux systèmes UWB standard. En effet, la capacité cognitive de ces systèmes peut être mise à profit pour transmettre plus de puissance dans les bandes où les utilisateurs primaires peuvent être identifiés et évités. Ainsi, la signalisation et la transmission de données associées peuvent être façonnées de telle sorte qu'une partie du spectre soit utilisée en mode opportuniste (overlay) et une autre partie en mode superposé (underlay), ce qui conduira à une augmentation du débit de données et de la portée du système UWB.

Objectis de la thèse

L'objectif principal de cette thèse est d'étudier quelques-uns des éléments clés dans la réalisation d'un système radio UWB impulsionnel à saut temporel (TH-IR-UWB) intelligent (ou cognitif). En effet, à côté de ses nombreuses caractéristiques uniques et intéressantes, l'approche IR-UWB présente aussi un certain nombre de défis, tels que le taux d'échantillonnage élevé, la réalisation des antennes ultra-large bande, la présence des interférences à bande étroite, la synchronisation, l'estimation de canal et la portée limitée.

Les principaux aspects qui ont fait l'objet de notre travail de recherche, dans le cadre de cette de doctorat, sont résumés ci-dessous :

Interférences à bande étroite (NBI) en UWB

La puissance d'émission très faible et la très large bande passante devraient en principe permettre aux systèmes UWB de coexister avec d'autres systèmes à bande étroite sans interférer avec eux. Toutefois, le fonctionnement du récepteur UWB peut être perturbé par les signaux à bande étroite. Bien que leur effet soit limité seulement à une petite fraction du spectre du signal UWB, leur puissance largement supérieure à ceux des signaux UWB peut considérablement affecter les performances du système UWB. Par conséquent, les récepteurs UWB devraient intégrer des techniques de suppression des NBI pour améliorer leurs performances en termes de taux d'erreur et de portée.

Conception adaptive de la forme d'onde du signal UWB

La forme d'onde du signal UWB est contrainte par les masques définis par les différents organismes de régulation à travers le monde pour la puissance isotrope rayonnée équivalente (EIRP). L'impulsion UWB doit donc être conçue afin d'assurer une efficacité spectrale maximale, tout en restant compatible avec les spécifications du masque spectral considéré. Autrement dit, il s'agit de remplir au maximum le gabarit spectral imposé afin de maximiser la puissance transmise. De plus, les impulsions UWB doivent également être suffisamment adaptatives pour modifier leur spectre afin d'éviter les NBI. Comme le spectre occupé par les systèmes IR-UWB est directement lié à la forme d'onde du signal UWB émis, sa conception adaptative optimisée représente un aspect critique et essentiel dans le contexte de radio cognitive que nous avons défini précédemment.

Synchronisation

L'objectif de la synchronisation est de fournir les mêmes références de temps pour le couple récepteur/émetteur. Dans les systèmes IR-UWB, l'absence de la porteuse, le faible rapport cyclique, et la distorsion du signal par le canal de propagation et les antennes, font de la synchronisation un problème complètement différent et bien plus difficile que dans le cas des systèmes à bande étroite. Par ailleurs, vu que les systèmes IR-UWB utilisent des impulsions extrêmement courtes ayant un très faible niveau de puissance, les imperfections de synchronisation sont très pénalisantes en réception pouvant même rendre impossible la détection des symboles.

Estimation des paramètres du canal UWB

Le choix du récepteur Rake cohérent, en raison de ses performances presque optimales dans le cas des systèmes IR-UWB, rend l'estimation du canal UWB indispensable. En effet, la largeur de bande très importante conduit à une résolution temporelle très fine, et par conséquent à de très nombreux trajets multiples. Puisque la puissance totale est répartie entre ces trajets multiples, le niveau de puissance de chacun sera très réduit, ce qui se traduit par un très faible rapport signal à bruit (SNR) au niveau du récepteur. Ces conditions particulières de fonctionnement des systèmes IR-UWB rendent nécessaire le développement de méthodes d'estimation du canal spécifiques et robustes pour les scénarios pratiques d'utilisation de ces systèmes.

Chapitre 1 : Concepts et défis liés aux communications UWB

Caractérisation générale des systèmes UWB

En 2002, la FCC (Federal Communications Commission) a défini les signaux UWB comme ayant une bande passante fractionnelle à -10 dB supérieure à 20% et/ou une largeur de bande absolue de plus de 500 MHz [FCC02a]. La largeur de bande fractionnaire d'un système de communications est définie par la relation suivante :

$$B_f = 2\frac{f_H - f_L}{f_H + f_L}$$

où f_H et f_L désignent respectivement les limites supérieure et inférieure du spectre mesurées à -10 dB.

En règle générale, la largeur de bande des signaux UWB varie de 500 MHz à plusieurs GHz. Leur spectre s'étend donc sur des bandes de fréquence déjà occupées par d'autres technologies, ce qui a rendu nécessaire une réglementation contraignante sur leur utilisation et notamment des limitations très strictes sur les puissances émises. Cependant, les règles adoptées ne sont pas identiques partout à travers le monde, celles-ci étant plus contraignantes en Europe qu'aux Etats-Unis, et surtout qu'en Asie, à l'exception du Japon. Ces règles sont définies par la FCC aux Etats-Unis et par l'organisme de normalisation européen dans le domaine des télécommunications (ETSI) en Europe.

L'élaboration d'une norme européenne pour les systèmes UWB est en cours, des études étant menées en étroite collaboration entre l'ETSI et le groupe SE24 de la conférence européenne des postes et des télécommunications (CEPT), qui est chargée plus particulièrement d'analyser l'impact des systèmes UWB sur les systèmes existants. En février 2007, la commission européenne des communications (CEC) a donné le feu vert pour l'utilisation des systèmes UWB.

Les masques spectraux pour les communications UWB en environnement indoor en Europe et aux Etats-Unis sont représentés à titre d'exemple sur la figure 1.

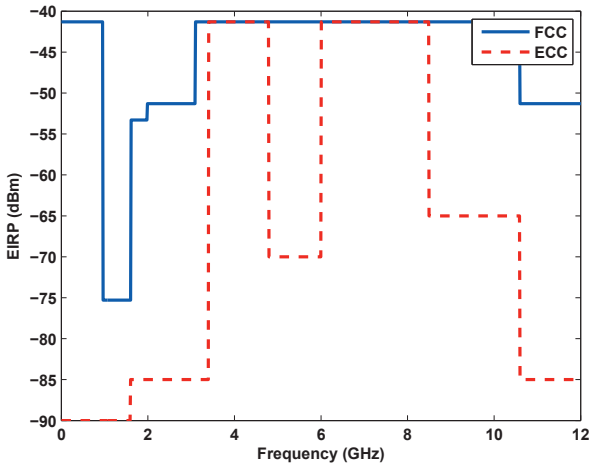

Figure 1: Masques spectraux définis par les autorités de régulation en Europe et aux États-Unis

Les systèmes UWB ont un certain nombre d'avantages qui les rendent attrayants pour les applications de communication grand public. En particulier, les systèmes UWB peuvent être caractérisés par [Gha04b] :

- des capacités de transmissions hauts débits ;
- une très bonne résolution temporelle permettant de réaliser simultanément une localisation précise et la transmission de données ;
- immunité aux trajets multiples et aux interférences ;
- complexité potentiellement faible et coût d'implémentation réduit.

Le travail de recherche présenté dans cette thèse concerne plus précisément les systèmes TH-IR-UWB. Les modulations considérées sont la modulation de phase binaire (BPSK) et la modulation de la forme des impulsions UWB (PSM). Le signal émis se propage à travers le canal UWB en environnement indoor proposé par le groupe de travail IEEE 802.15.3a et est démodulé à l'aide d'un récepteur Rake cohérent. L'architecture générale du système TH-IR-UWB considéré est représentée sur la figure 2, ses différents éléments étant brièvement décrits ci-dessous.

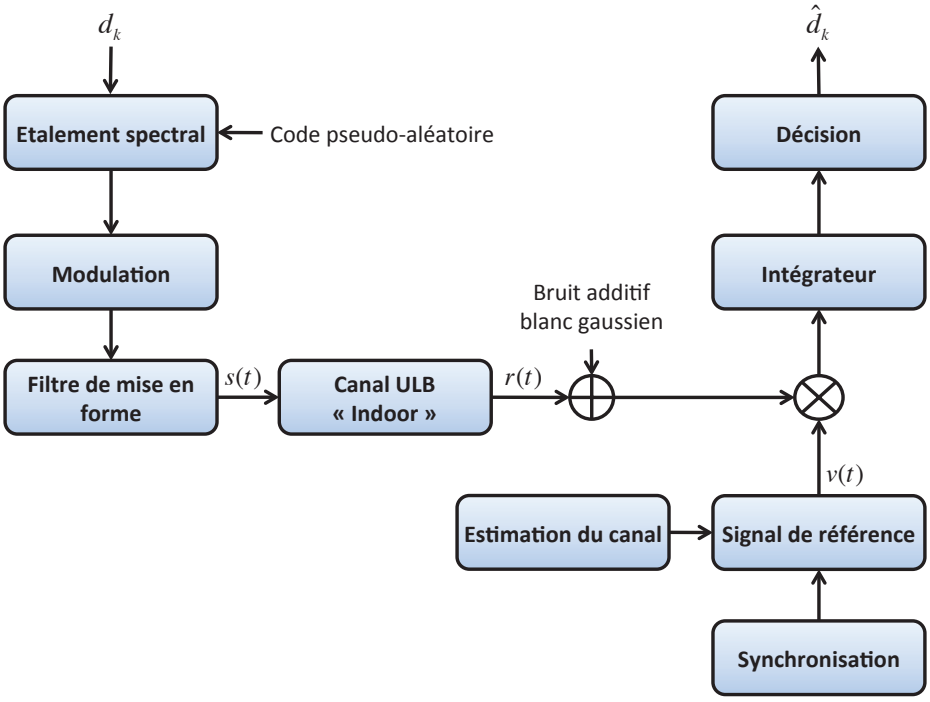

Figure 2: Architecture générale d'un système TH-IR-UWB

Radio Impulsionnelle UWB (IR-UWB)

Développé à partir d'études sur le radar, le concept de radio impulsionnelle UWB est basé sur l'émission d'impulsions de très courte durée (environ 100 ps à 1 ns). En règle générale, ce type d'impulsions présentent un spectre très large (de l'ordre de 1 à quelques GHz). Il s'agit par conséquent, d'une transmission mono-bande.

Différentes formes d'impulsions ont été adoptées pour les applications UWB, dont les plus simples sont représentées par l'impulsion gaussienne et ses dérivées, notamment à l'ordre 1 et 2. Les versions dérivées de l'impulsion gaussienne lui sont préférées à cause de sa composante continue non nulle. Ce type de transmission n'exige pas de porteuse, car le signal se propage bien dans le canal radio. Il s'agit donc d'une transmission en bande de base.

Modulation de phase binaire (BPSK)

Ce type de modulation offre une bonne robustesse aux variations du canal et simplifie la synchronisation. Le signal transmis par le $k^{\text{ième}}$ utilisateur peut être exprimé par :

$$s^k_{bpsk}(t) = (2d_k - 1)\psi(t)$$

où $\psi(t)$ est l'impulsion UWB élémentaire.

L'une des raisons de l'utilisation de la modulation BPSK, notamment par rapport à la modulation d'impulsions en position (PPM), est le gain en performances de 3 dB en termes de SNR.

Modulation de la forme des impulsions UWB (PSM)

Dans le cas de cette modulation, l'information est codée par des impulsions de formes différentes. Il est donc nécessaire de pouvoir disposer d'un ensemble adapté d'impulsions pour les modulations d'ordre supérieur, telles que les fonctions polynomiales de Hermite (MHP) [Wei04a], les ondelettes [Con99], ou les fonctions prolates sphéroïdales [Zhu03]. Le signal PSM peut être représenté par :

$$s^k_{psm}(t) = (1 - d_k)\psi_0(t) + (d_k)\psi_1(t) = \psi_{d_k}(t)$$

Lorsque les signaux utilisés sont orthogonaux ils rendent également possible l'accès multiple, qui peut être obtenu en attribuant un groupe d'impulsions orthogonales à chaque utilisateur. Les transmissions sont alors mutuellement orthogonales et n'engendrent pas d'interférence entre utilisateurs. Des résultats intéressants en termes de taux d'erreur binaire (BER), sont présentés dans [Wei04a], pour deux utilisateurs transmettant des signaux modulés PSM basés sur les MHP, chacun constituant une interférence pour l'autre. Une amélioration significative des performances est obtenue par rapport à une modulation PPM traditionnelle.

Accès multiple basé sur les sauts temporels (TH-UWB)

Les besoins d'accès multiple, ainsi que la contrainte de très faible puissance des systèmes IR-UWB ont conduit à un schéma de transmission UWB amélioré, où chaque symbole transmis est codé par plusieurs impulsions décalées dans le temps selon un code de saut temporel. Plus précisément, la position de chaque impulsion est déterminée par une séquence pseudo-aléatoire (PN). L'énergie par symbole peut être ainsi augmentée de manière à obtenir la portée de la transmission exigée par l'application considérée. Par ailleurs, les différents utilisateurs, qui se distinguent par leur code TH unique, peuvent transmettre en même temps.

La structure du signal utilisant un code TH et une modulation PSM, transmis par le $m^{\text{ième}}$ utilisateur, a la forme suivante [Opp04, DB06] :

$$s^{(m)}(t) = \sum_{i=-\infty}^{\infty} \sum_{j=0}^{N_f-1} \psi_{d_i^{(m)}}(t - iT_s - jT_f - c_j^{(m)}T_c)$$

où $d_i^{(m)}$ est le $i^{\text{ième}}$ bit de données transmis par l'utilisateur m, et N_f est le nombre d'impulsions correspondant à chaque symbole d'information.

Selon ce schéma, la durée symbole T_s est divisée en N_f trames de durée T_f , chacune de ces trames étant à son tour subdivisée en intervalles de durée T_c. Chaque trame contient une impulsion dans la position déterminée par le symbole à coder et la séquence pseudo-aléatoire TH $c_j^{(m)}$ (unique pour chaque utilisateur m).

Modèle du canal UWB IEEE 802.15.3a

Le modèle développé par le groupe de normalisation IEEE 802.15.3a [Mol03] pour les WPAN haut débit s'inspire largement du modèle de Saleh-Valenzuela (SV) [Sal87]. Il en diffère principalement par le fait que c'est un modèle réel et que la décroissance des amplitudes suit une loi de type log-normale au lieu d'une décroissance exponentielle (ainsi les premiers trajets ne sont pas nécessairement les plus forts). De plus, des termes de fading indépendants sont appliqués à chaque trajet et à chaque cluster.

Des paramètres sont fournis pour caractériser les taux d'arrivée des clusters Λ et des rayons λ, ainsi que les coefficients de décroissance exponentielle inter et intra-clusters (Γ et γ). Quatre jeux de paramètres sont fournis pour modéliser quatre types de canaux appelés CM 1 - 4. Le modèle CM1 caractérise un environnement de type LOS (Line of Sight), les modèles CM2 et CM3 des environnements de type NLOS (Non LOS) et le CM4 un environnement en non-visibilité extrême. Ce modèle assez complet a le mérite d'être une référence pour les études de systèmes UWB. Il s'applique dans les environnements indoor à courte portée.

Récepteur Rake

En raison de sa très large bande passante, le signal UWB reçu est composé d'un grand nombre de trajets multiples séparables. Le récepteur Rake exploite la diversité temporelle inhérente des trajets multiples et tente d'accumuler le maximum d'énergie, de manière cohérente. Cependant, en raison du grand nombre de trajets multiples, une accumulation d'énergie importante nécessite un récepteur Rake ayant un nombre de doigts important. Ainsi, selon [Raj03], pour capter 80% de l'énergie du signal reçu, le récepteur Rake nécessite plus de 200 doigts.

En fonction de la configuration considérée (LOS ou NLOS) et de l'environnement (résidentiel, bureaux ou industriel), les différents canaux UWB nécessitent un nombre différent de doigts. Pour le modèle l'IEEE 802.15.3a, le nombre de doigts pour couvrir 85% de l'énergie du signal varie de quelques dizaines à des centaines pour les configurations LOS et NLOS. Par conséquent, seul un sous-ensemble de trajets multiples est utilisé pour accumuler l'énergie à la réception. Les récepteurs Rake sélectif (S-RAKE) et partiel (P-RAKE) utilisent un nombre limité de doigts, mais sont moins efficaces et sont plus sujets aux erreurs. Un compromis est à trouver par conséquent, entre la qualité et la complexité du récepteur.

Le signal reçu est corrélé au niveau de chaque doigt avec un signal de référence, et les résultats sont ensuite combinés en utilisant différents schémas, dont les plus connus correspondent au rapport maximum (MRC - Maximum Ratio Combining) et au gain constant (EGC - Equal Gain Combining). Dans le cas du schéma MRC, les amplitudes des trajets multiples sont estimées et utilisées en tant que vecteur de pondération. Par conséquent, la performance du récepteur Rake MRC dépend de la connaissance parfaite du canal. Dans le cas du schéma EGC, tous les trajets multiples sont combinés avec un gain égal, seule l'estimation des retards et des polarités correspondants étant

nécessaire. Il est plus donc plus simple à mettre en œuvre que le récepteur Rake MRC, mais au prix d'une réduction des performances.

Chapitre 2 : Radio Cognitive UWB : de la détection à l'adaptation spectrale

Ce chapitre explore le concept d'intégration de l'UWB avec la radio cognitive. Il est démontré qu'un bénéfice mutuel peut être obtenu en combinant ces deux technologies intéressantes. A partir de cette idée, nous concentrons tout d'abord nos efforts sur la détection spectrale, qui est un élément clé de la radio cognitive, en proposant une nouvelle approche basée sur la théorie des matrices aléatoires finies. Dans un deuxième temps, nous proposons une méthode basée sur l'adaptation de la forme d'onde UWB et sur les résultats fournis par l'algorithme de détection spectrale, permettant l'utilisation efficace des ressources spectrales disponibles, tout en évitant les interférences avec d'autres systèmes radio.

Principe de la radio cognitive UWB

Le développement de la radio cognitive est motivé par plusieurs facteurs. Il s'agit principalement de l'encombrement du spectre RF couplé à une sous-utilisation des bandes de fréquences sous licence, qui est aussi à l'origine de l'émergence de l'UWB. De nouvelles solutions sont clairement nécessaires pour exploiter efficacement les ressources spectrales, et l'UWB et la CR s'intègrent parfaitement à cette évolution technologique, qui vise l'accès ouvert et dynamique au spectre.

Afin de pouvoir utiliser les "trous" ou les "espaces blancs" du spectre, la FCC a publié un document intitulé "Notice of Proposed Rule Making" [FCC03], qui suggère l'utilisation de la radio cognitive pour mettre en œuvre le partage négocié ou opportuniste du spectre. Selon la FCC : "Un système de radio cognitive est capable de changer ses paramètres à l'émission en fonction de l'interaction avec l'environnement dans lequel il évolue". Exprimé d'une autre manière, un système de radio cognitive est capable de prendre connaissance de son environnement et de s'y adapter intelligemment [MI99b], en suivant un cycle cognitif.

Ce cycle cognitif décrit les activités impliquant l'intelligence du système, telles que la détection, l'apprentissage et l'adaptation. Selon le cycle cognitif générique proposé par Mitola [MI99c], pour qu'un système puisse s'adapter à son environnement radio, il doit être capable de :

- *explorer, découvrir et analyser, pour finalement connaître l'environnement* : dans cette étape les capteurs du système et les algorithmes de traitement du signal associés jouent le rôle principal ;
- *décider de la meilleure configuration de ses paramètres*: pour prendre cette décision le système exploite la connaissance de l'environnement acquise lors de la première étape et tout ce qu'il a appris précédemment grâce à son l'intelligence inhérente ;
- *se reconfigurer* : cette fonction, réalisée généralement par les mécanismes de la radio logicielle, consiste à mettre en œuvre, de manière dynamique et autonome, le résultat de la décision prise à l'étape précédente.

L'approche d'utilisation opportuniste du spectre, qui est caractéristique pour les systèmes de radio cognitive et sous-entend la capacité de détection des utilisateurs primaires, contraste avec l'approche d'utilisation superposée du spectre, simultanément avec les utilisateurs primaires, adoptée par les systèmes UWB. En même temps, les systèmes IR-UWB possèdent intrinsèquement de

nombreuses fonctionnalités intéressantes, telles que le niveau d'interférences négligeable avec les systèmes existants, la flexibilité de la forme des signaux et de la bande passante occupée, l'adaptabilité du débit de données et de la qualité de service, la puissance d'émission et le coût limités, qui sont aussi recherchées dans les systèmes de radio cognitive.

Nous proposons alors de combiner ces deux approches sous la forme de la radio cognitive UWB. L'avantage du point de vue de la radio cognitive est que le système peut continuer à transmettre, même lorsque toutes les bandes sont occupées par des utilisateurs primaires, grâce au très faible niveau de puissance caractéristique pour les signaux UWB. Dans l'autre sens, les systèmes UWB dotés de capacités cognitives pourraient être autorisés à augmenter le niveau de puissance dans les bandes où les utilisateurs primaires peuvent être détectés et évités, avec à la clé une amélioration de leurs performances en termes de portée, débit et taux d'erreur. Néanmoins, avant que le principe d'un système de radio cognitive UWB soit accepté par les autorités de régulation, il faut pouvoir démontrer ses capacités de détection spectrale et de redéfinition rapide de la forme d'onde afin d'éviter les interférences avec les utilisateurs primaires. Nos contributions sur ces deux aspects clés pour le développement des fonctions cognitives des systèmes UWB seront détaillées par la suite.

Détection spectrale

Plusieurs facteurs participent à la difficulté du problème de détection spectrale : le faible SNR des utilisateurs primaires, l'incertitude sur le bruit, la dispersion temporelle des canaux de propagation, la durée et la fréquence de détection, etc. [Yuc09,Zen10]. Du point de vue de la détection du signal, les techniques de détection spectrale peuvent être classées en deux grandes catégories, cohérentes et non-cohérentes. Le premier type de méthodes détectent les utilisateurs primaires de manière cohérente, en comparant le signal reçu ou ses caractéristiques avec les éléments similaires issus d'une connaissance a priori de ces utilisateurs. Pour le deuxième type de méthodes, aucune connaissance a priori n'est nécessaire pour effectuer la détection spectrale.

Techniques traditionnelles de détection spectrale

Plusieurs algorithmes ont été proposés dans la littérature pour la détection spectrale des utilisateurs primaires. Ils sont basés sur la détection d'énergie, la détection de caractéristiques cyclostationnaires, le filtrage adapté, la forme d'onde, etc. Le détecteur d'énergie est la méthode la plus simple mais ses performances sont limitées si le bruit est non-stationnaire et sa variance est inconnue. Les méthodes cohérentes telles que celles basées sur la forme d'onde et le filtrage adapté sont plus robustes que la détection d'énergie ou de caractéristiques, mais demandent des informations préalables sur le signal de l'utilisateur primaire ou des modèles connus et des symboles pilotes. Les méthodes basées sur les caractéristiques de cyclostationnarité sont plus robustes que le détecteur d'énergie lorsque le bruit devient non-stationnaire, ce qui est le cas en présence d'interférences introduites par le canal. Cependant, ces méthodes sont sensibles aux évanouissements du canal et aux dérives de la fréquence d'échantillonnage [Tka07].

Détection spectrale basée sur la théorie des matrices aléatoires

Des résultats récents de la théorie des matrices aléatoires (RMT) rendent possible le développement d'algorithmes de détection spectrales aveugles, performants et robustes, en utilisant les valeurs

propres de la matrice de covariance du signal reçu [Zen07, Car08, Zen09a, Pen09b], et en particulier le nombre de conditionnement standard (SCN) de cette matrice. Le principal avantage des méthodes RMT utilisant le critère du SCN par rapport aux méthodes traditionnelles est qu'elles ne nécessitent aucune information préalable sur le signal primaire ou sur la puissance du bruit. Le caractère aveugle de cette approche est particulièrement intéressant pour la détection spectrale dans des bandes de fréquences encombrées, où le bruit de fond agrégé tend vers un bruit additif blanc gaussien, ayant une puissance dépendante du nombre d'utilisateurs actifs. Malheureusement, cet avantage potentiel est compromis par le fait que la plupart de ces méthodes sont asymptotiques et donc peu adaptées au cas où le nombre d'échantillons est fini et faible. Notre contribution sur ce point est constituée par une approche de détection spectrale aveugle, performante et robuste, utilisant des statistiques de test calculées à partir de la matrice de covariance du signal reçu et des seuils de détection déterminés en utilisant la RMT.

Approche proposée pour la détection spectrale en radio cognitive UWB

Modèle du signal reçu

Dans le cas d'un seul utilisateur primaire dans du bruit additif, blanc et gaussien, le $i^{\text{ième}}$ échantillon du signal reçu est donné par :

$$h(i) = \sqrt{\beta}s(i) + n(i)$$

où β est le SNR, $s(i)$ représente le signal de l'utilisateur primaire intégrant l'effet du canal, et les échantillons du bruit $n(i) \sim \mathcal{N}_{\mathbb{C}}(0,1)$ sont des variables aléatoires indépendantes et identiquement distribuées (i.i.d.) selon la loi normale standard complexe circulairement symétrique.

Le problème de détection de l'utilisateur primaire est formulé comme un test d'hypothèses, où la décision peut être :

- absence des utilisateurs primaires (hypothèse $\mathcal{H}_0$) ;
- présence d'un utilisateur primaire, dont le signal est à enveloppe constante, c'est-à-dire $s(i) = s$, avec s une constante complexe inconnue de module unitaire $|s| = 1$ (hypothèse $\mathcal{H}_1^c$) ;
- présence d'un utilisateur primaire, avec $s(i)$ i.i.d. selon $\mathcal{N}_{\mathbb{C}}(0,1)$, qui correspond au cas où le signal n'est pas à enveloppe constante et/ou est sujet aux évanouissements rapides non-corrélés de Rayleigh (hypothèse $\mathcal{H}_1^r$).

Conformément au modèle présenté ci-dessus, si un nombre $M = K \times N$ d'échantillons est disponible, le récepteur peut construire une des matrices aléatoires suivantes :

$$\mathbf{H} = \begin{cases} \mathbf{H}_n & \text{si } \mathcal{H}_0 \text{ est vraie} \\ \sqrt{\beta}.\mathbf{H}_s + \mathbf{H}_n & \text{si } \mathcal{H}_1 \text{ est vraie} \end{cases}$$

Notre objectif est de développer des algorithmes pour résoudre ce problème de test d'hypothèses, en utilisant les résultats récents de la RMT concernant l'analyse propre et le SCN des matrices de Wishart $\mathbf{W} \triangleq \mathbf{H}\mathbf{H}^{\dagger}$, où † indique l'opérateur hermitien (transposition & conjugaison).

Tests basés sur la distribution du SCN

Pour la grande majorité des techniques de détection spectrale basées sur la RMT et proposées dans la littérature [Yuc09], le seuil de détection est déterminé à partir d'une probabilité de fausse alarme (P_{fa}) ou d'une probabilité de fausse détection (P_{md}) donnée. Ainsi, lorsque le SCN est utilisé comme statistique de test, pour un niveau donné de la P_{fa}, le seuil de détection est calculé par :

$$\gamma_{SCN} \triangleq F_{SCN}^{-1}\left(1 - P_{fa}\right)$$

où F_{SCN} est la fonction de répartition (cdf) du SCN sous l'hypothèse $\mathcal{H}_0$.

Par conséquent, les performances de l'algorithme de détection spectrale basé sur le SCN dépendent de la qualité d'estimation de sa fonction de répartition.

Tandis que des modèles asymptotiques pour la fonction F_{SCN} sont fournis par la RMT depuis longtemps, des modèles précis de cette distribution dans le cas d'un nombre d'échantillons réduit ont été plus difficile à développer. Ainsi, une expression analytique de la distribution du SCN des matrices de Wishart non-corrélées duales et finies (correspondant à l'hypothèse $\mathcal{H}_0$) n'a été que récemment proposée dans [Mat10]. La précision du modèle a été validée à l'aide du test d'ajustement de chi2, le taux d'acceptation étant de l'ordre de 99%. Les expressions exactes et relativement simples de la densité de probabilité et de la fonction de répartition peuvent être facilement utilisées pour déterminer le seuil γ_{SCN} et mettre en place l'algorithme de détection spectrale.

Cependant, sous l'hypothèse $\mathcal{H}_1^c$ la distribution du SCN est difficile à évaluer, en raison du caractère non-centré des matrices de Wishart dans ce cas, qui ne permet pas d'obtenir des expressions simples pour les distributions des valeurs propres extrêmes. En échange, il est possible d'obtenir des distributions exactes et asymptotiques des valeurs propres extrêmes pour les matrices de Wishart centrées corrélées [Tan83, Zan08, Bai08]. L'idée est alors de transformer les matrices de Wishart non-centrées, caractéristiques pour l'hypothèse $\mathcal{H}_1^c$, en matrices de Wishart centrées corrélées, plus faciles à exploiter.

Cette idée est à la base de l'algorithme de détection spectrale proposée dans [Zha12]. Néanmoins, nous avons constaté que lorsque le nombre d'échantillons est faible, le test d'ajustement de chi2 indique une faible adéquation entre la distribution proposée et les valeurs du SCN calculées à partir de données simulées. Nous proposons comme solution la distribution des valeurs extrêmes généralisée (GEV) et montrons qu'elle est bien plus adaptée aux données obtenues sous l'hypothèse $\mathcal{H}_1^c$, avec un taux d'acceptation proche de 1 pour des valeurs de SNR élevées. Par conséquent, un test de validation pour cette hypothèse peut être effectué en utilisant le modèle de la distribution GEV pour F_{SCN}, afin d'obtenir un niveau donné de la probabilité de fausse détection P_{md}. Le seuil de détection est calculé dans ce cas par :

$$\gamma_{SCN} \triangleq F_{SCN}^{-1}(P_{md})$$

Il est à noter que le test basé sur [Mat10] peut être considéré comme complètement aveugle, car il n'a besoin d'aucune connaissance a priori sur le signal ou la puissance de bruit, alors que le test basé sur le modèle GEV pour la distribution du SCN sous l'hypothèse $\mathcal{H}_1^c$ est semi-aveugle, car il demande une estimation du SNR pour déterminer le seuil. Les résultats des simulations montrent que ces deux tests présentent des performances presque similaires en termes de P_{fa} et

P_{md}. Comme le premier test est complètement aveugle, nous allons l'utiliser comme méthode de choix pour détecter les utilisateurs primaires sous l'hypothèse $\mathcal{H}_1^c$.

Dans le cas de la troisième hypothèse, les distributions du SCN correspondant à $\mathcal{H}_0$ et $\mathcal{H}_1^r$ se superposent et ne peuvent pas être par conséquent séparées. En effet, dans ce cas les échantillons du signal de l'utilisateur primaire $s(i)$ et les échantillons du bruit $n(i)$ sont i.i.d., ce qui signifie que les statistiques de test basées sur le SCN ne peuvent pas être utilisées pour les algorithmes de détection spectrale sous l'hypothèse $\mathcal{H}_1^r$. Nous avons donc cherché une solution pour ce dernier cas de figure basée directement sur les valeurs propres à la place du SCN.

Tests basés sur la distribution des valeurs propres

L'expression de la distribution de l'ensemble des valeurs propres de la matrice $\mathbf{W}$ sous l'hypothèse $\mathcal{H}_0$ est donnée par le modèle de Bronk-Shin-Lee (BSL) [Bro65,Shi03]. Le même modèle à un facteur d'échelle près s'applique aussi dans le cas de l'hypothèse $\mathcal{H}_1^r$ [Alf04]. Néanmoins, bien que le test d'ajustement du chi2 valide l'adéquation de la distribution BSL aux données simulées pour de forts SNR, les résultats sont beaucoup moins concluants en termes de taux d'acceptation pour de faibles SNR. En plus, le schéma de détection spectrale est plus complexe dans ce cas.

Afin de maintenir la faible complexité du schéma de détection spectrale, tout en assurant une bonne adéquation aux données simulées, nous proposons d'utiliser comme statistique de test la somme des valeurs propres (EVS) ou la trace de la matrice $\mathbf{W}$, qui est similaire à l'énergie du signal [Zen09a]. Par conséquent, le test basé sur l'EVS est équivalent à la détection d'énergie, qui est optimale pour des signaux i.i.d. [Kay88b]. Nous proposons d'approcher la distribution de l'EVS par la loi gamma afin de mettre en place un algorithme de détection spectrale robuste dans le cas de l'hypothèse $\mathcal{H}_1^r$. En effet, contrairement à la distribution BSL, la loi gamma permet d'obtenir un taux d'acceptation proche de 1 pour l'EVS tant pour les faibles que pour les forts SNR. En échange, tout comme le test basé sur la distribution BSL, le test proposé est semi-aveugle, car il exige l'estimation de la puissance du bruit.

Évaluation des performances et approche à deux étapes pour la détection spectrale

Les performances des algorithmes présentés ci-dessus sont évaluées par simulations numériques pour les trois hypothèses. Le nombre d'échantillons considérés est égal à 20 ($K = 2$, $N = 10$) et les résultats obtenus sont moyennés sur 10^4 réalisations. Des échantillons du signal reçu à enveloppe constante ou i.i.d. selon $\mathcal{N}_{\mathbb{C}}(0, 1)$ sont générés aléatoirement afin de valider les tests basés respectivement sur le SCN et sur l'EVS. Les courbes correspondantes sont tracées sur les figures 3a et 3b respectivement.

Il est à noter que le premier test permet d'obtenir une valeur de la P_{md} de moins de 10% pour une $P_{fa} = 0.05$ et SNR $\geq 3\,$dB, alors que le deuxième test conduit à des résultats encore meilleurs.

Les capacités complémentaires des deux tests nous ont amenés à proposer une approche à deux étapes pour la détection spectrale. Ainsi, le test basé sur le SCN est appliqué en premier aux données reçues. Comme les résultats ci-dessus l'ont montré, il sera capable de détecter de manière complètement aveugle la présence des signaux à enveloppe constante ou fortement corrélées (hypothèse $\mathcal{H}_1^c$). Si aucun utilisateur primaire n'est détecté, le processus continue par une deuxième

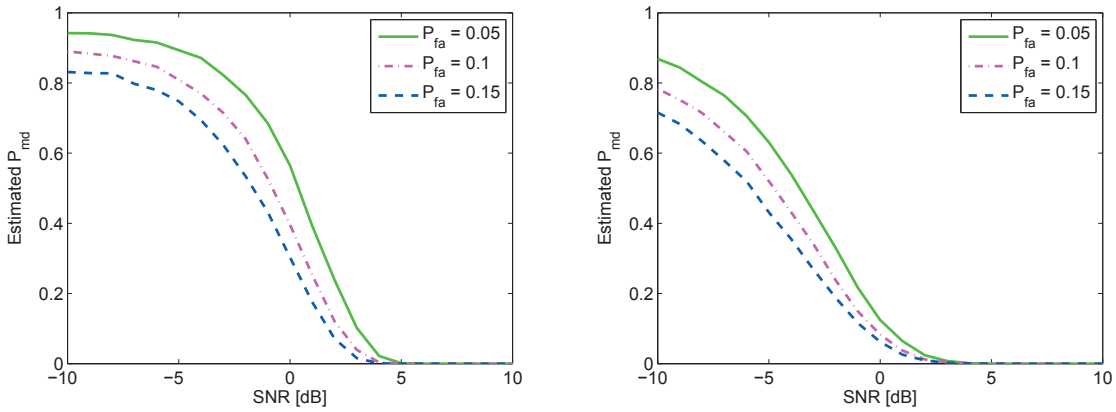

Figure 3: Performance des algorithmes de détection spectrale en fonction du SNR à niveau fixé de la P_{fa} pour (a) le test basé sur le SCN sous l'hypothèse $\mathcal{H}_1^c$ (b) le test basé sur l'EVS sous l'hypothèse $\mathcal{H}_1^r$

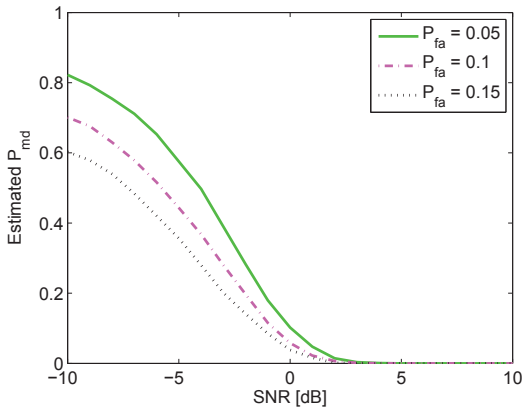

Figure 4: Performances du schéma de détection spectrale à deux étapes pour des signaux à enveloppe constante, aléatoires corrélés et aléatoires non-corrélés

étape de détection, utilisant le test basé sur l'EVS, afin de lever l'ambiguïté entre les hypothèses $\mathcal{H}_0$ et $\mathcal{H}_1^r$.

Afin d'évaluer les performances de ce schéma à deux étapes, des échantillons de signaux reçus, correspondant aux trois hypothèses, sont générés de façon aléatoire à chaque itération. Les courbes obtenues pour trois niveaux de la P_{fa} sont représentées sur la figure 4. Il est à noter que la détection en deux étapes améliore encore les performances en termes de Pmd par rapport aux deux autres tests pris individuellement.

Conception adaptative de la forme d'onde des signaux UWB

La conception de la forme d'onde des signaux UWB est un élément clé pour le concept de radio cognitive UWB proposé. En effet, cette fonction permet de contrôler finement l'occupation spectrale du système IR-UWB et rend possible l'utilisation opportuniste du spectre.

Les signaux UWB doivent être compatibles avec les masques spectraux pour l'EIRP définis par les différents organismes de régulation. En même temps, le domaine défini par le masque FCC

considéré doit être occupé de manière efficace, ce qui revient à émettre le maximum d'énergie tout en restant compatible avec les spécifications de celui-ci. Le troisième objectif est à la fois d'augmenter le débit transmis et de réduire au minimum les interférences inter-symbole en utilisant plusieurs impulsions UWB mutuellement orthogonales. Enfin, dans le contexte de la radio cognitive UWB, les signaux générés doivent également être suffisamment adaptables pour que leur puissance d'émission soit en dessous du masque spectral autorisé dans les bandes occupées (mode underlay) et comparable à celle des utilisateurs primaires dans les bandes qu'ils libèrent temporairement (mode overlay).

La conception des impulsions UWB a fait l'objet de nombreuses recherches depuis plusieurs années et plusieurs solutions ont été proposées dans la littérature, telles que les impulsions Gaussiennes, les impulsions de Hermite modifiées, les fonctions prolates sphéroïdales, les impulsions inspirées par la conception de filtres numériques ou basées sur les vecteurs propres, etc. [Par03, Zhu03, Oue05]. Cependant, chacune de ces formes d'ondes présente certaines limitations. Par exemple, les impulsions Gaussiennes n'utilisent pas les ressources spectrales de manière efficace, les impulsions de Hermite modifiées et les impulsions prolates sphéroïdales exigent des décalages en fréquence et des filtres passe-bande pour s'adapter aux masques spectraux, alors que les impulsions basées sur les vecteurs propres ont comme inconvénients la complexité d'implémentation et une fréquence d'échantillonnage élevée.

Conception optimisée d'impulsions UWB

Dans cette thèse, nous proposons une approche pour la conception adaptative d'impulsions UWB orthogonales à efficacité spectrale maximale [Akb10a]. Cette approche utilise comme éléments de base les fonctions B-splines [Sch46], qui sont des fonctions de support temporel limité et polynomiales par morceaux. Lorsque l'ordre des polynômes vaut 1, ces fonctions se réduisent à des impulsions rectangulaires, et lorsque l'ordre tend vers l'infini, elles convergent vers des fonctions de bande limitée [Kam88]. Du point de vue de l'implémentation, il existe un circuit analogique [Kam95] et un filtre numérique rapide [Ich98] pour la génération des B-splines.

L'idée de base de cette approche est que les impulsions UWB, comme tout signal d'ailleurs, peuvent être représentées par des combinaisons linéaires de fonctions B-splines [Mat05] :

$$\psi_l(t) = \sum_{k=0}^{N_s-1} c_{l,k}\varphi_m(t-kT), \quad l = 1, 2, \ldots, L$$

où $\varphi_m(t)$ est une fonction B-spline d'ordre m et durée T, $N_s = L+m-1$ est le nombre de fonctions B-splines, L est le nombre d'impulsions UWB générés et $c_{l,k}$ sont les coefficients de pondération réels obtenus par une procédure d'optimisation.

Le problème de génération d'impulsions UWB est un problème d'optimisation non-linéaire (maximisation de l'efficacité spectrale), sous des contraintes linéaire (moyenne nulle) et non-linéaires (orthogonalité, masque spectral). Afin de résoudre ce problème, nous avons utilisé l'algorithme génétique (GA), qui est bien connu pour être plus efficace que les méthodes traditionnelles numériques lorsque la fonction objectif est discontinue, non-différentiable et caractérisée par des gradients non-définis en de nombreux points [Mic95].

Nous illustrons la conception de la forme d'onde UWB par l'exemple présenté ci-dessous, où nous

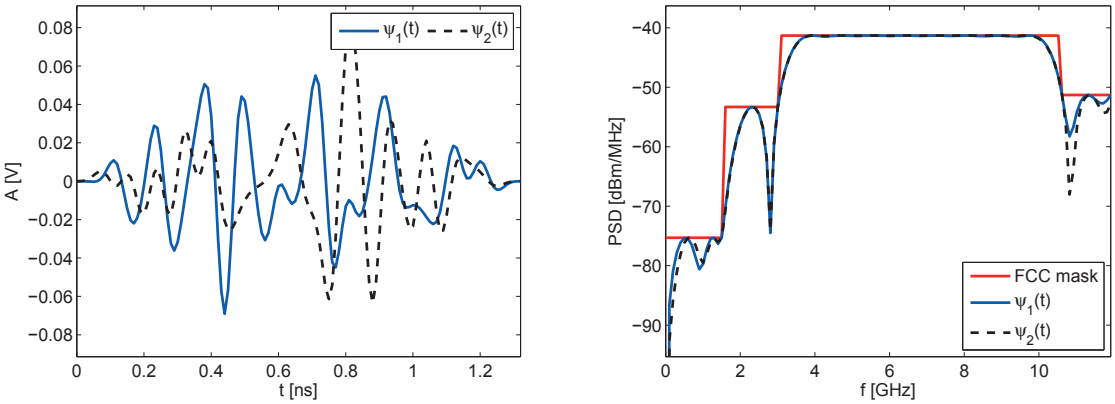

(a) (b)

Figure 5: Deux impulsions UWB générées avec $N_s = 30$ fonctions B-splines (a) et leurs densités spectrales de puissance (b)

avons utilisé des fonctions B-splines d'ordre $m = 3$, une fréquence d'échantillonnage $f_s = 100\,\text{GHz}$, et $N_{fft} = 500$ points pour le calcul de la densité de puissance du signal généré. Les impulsions UWB obtenues, représentées sur la figure 5, ont une durée égale à 1.28 ns, sont conformes au masque spectral considéré, et sont caractérisées par une bonne efficacité spectrale (environ 91.5%).

Chapitre 3: Synchronisation dans les systèmes IR-UWB

Ce chapitre est consacré au problème de la synchronisation dans les systèmes IR-UWB, qui est une étape clé dans leur fonctionnement, avec une influence déterminante sur les performances obtenues. Plusieurs facteurs rendent cette tâche beaucoup plus difficile que dans le cas des systèmes de communications traditionnels. En effet, la résolution temporelle très fine des systèmes IR-UWB conduit à un espace de recherche de solutions pour la synchronisation de taille très importante, tandis que leur niveau de puissance extrêmement faible exige le traitement de longues séquences de données afin de développer un critère de synchronisation fiable. De plus, le signal émis est déformé par les antennes et les canaux à trajets multiples denses, inconnus et sélectifs en fréquence [Cas02, Cra02], ce qui augmente encore la complexité du défi représenté par la synchronisation. En raison de la très courte durée des impulsions UWB, plusieurs trajets multiples peuvent constituer des solutions satisfaisantes, ce qui entraîne de multiples phases d'acquisition. Ces aspects découlant des caractéristiques uniques de la transmission IR-UWB démontrent l'importance du problème de synchronisation dans les systèmes IR-UWB et implicitement le besoin d'algorithmes simples, rapides et efficaces.

Etat de l'art

Les schémas de synchronisation dans les systèmes IR-UWB peuvent être divisés en deux grandes classes selon l'approche adoptée, qui peut être basée sur l'estimation ou sur la détection.

La première approche [Akb12a, Akb12b] utilise une estimation de l'instant d'arrivée, qui est généralement obtenue en maximisant une statistique sur un ensemble de valeurs candidates. Les méthodes de cette classe, basées sur le maximum de vraisemblance (ML) [Lot02], les moindres carrés (LS) [Car06], la décomposition en sous-espaces orthogonaux [Mar03a, Mar03b, Kus03] ou la cyclostationnarité [Yan03, Tia02], ne font donc pas appel à un comparateur à seuil. Cependant, la plupart de ces algorithmes souffrent d'une complexité de mise en œuvre élevée ou sont contraints par une connaissance a priori sur les paramètres de transmission. Afin de réduire la complexité de mise en œuvre, plusieurs schémas de synchronisation utilisant l'échantillonnage au taux symbole ou trame ont également été développés. Certains de ces schémas sont basés sur la corrélation de segments du signal reçu de durée égale à la durée symbole [Yan05, Far05], d'autres s'appuient sur la transmission périodique de symboles de moyenne non nulle [Luo04, Luo06a, Luo06b, Luo07] ou utilisent les propriétés de corrélation de certains codes binaires [Yin08] .

Les méthodes de synchronisation basées sur une approche de type détection évaluent habituellement des décalages temporels candidats par rapport à un certain critère, puis les comparent à un seuil afin de prendre une décision. Ces décalages temporels candidats peuvent être évalués de manière sérielle, parallèle ou hybride. Plusieurs algorithmes de synchronisation qui évitent le processus de recherche de valeurs candidates ont été développées dans [Hom02, Gez03, Aed04, Wan07]. Par ailleurs, une classe de stratégies optimales de recherche de ces valeurs est présentée dans [Suw05, Suw07], qui fournit également des limites fondamentales pour le temps de synchronisation moyen (MST) et démontre que la recherche sérielle conventionnelle conduit à un MST maximum. Un algorithme intéressant, qui exploite l'orthogonalité des impulsions UWB est aussi proposé dans [Ren09].

Chacune des deux approches (estimation et détection) a ses avantages et inconvénients. Ainsi, l'approche de type estimation offre une meilleure précision, car le critère de maximisation est évalué pour chaque décalage temporel candidat, le prix à payer étant un temps de synchronisation plus

long. Par ailleurs, l'approche de type détection a l'avantage de pouvoir appliquer des techniques efficaces de recherche, telles que "bit reversal" ou "look-and-jump-by-K-bins", mais la solution obtenue n'est pas optimale, car celle-ci ne dépend pas seulement du critère de synchronisation, mais aussi de la technique de recherche et du seuil utilisés. Par conséquent, le choix de l'algorithme de synchronisation sera forcément le résultat d'un compromis entre la complexité de la mise en œuvre et le niveau de précision nécessaire.

Dans cette thèse, nous proposons plusieurs algorithmes de synchronisation non-supervisés (NDA) et à faible complexité pour les systèmes IR-UWB. Nous avons préféré les algorithmes NDA, car la transmission de données n'est pas interrompue dans ce cas pendant la phase de synchronisation. Un autre avantage de ces algorithmes est leur capacité de fonctionner dans des scénarios "cold start-up", où le récepteur ne connaît pas l'instant de début de la transmission. Les contributions de notre travail de recherche sur la synchronisation dans les systèmes IR-UWB portent essentiellement sur des algorithmes qui, en disposant d'un minimum de connaissance a priori, sont capables de fournir:

- une synchronisation grossière rapide, avec une résolution pouvant aller jusqu'à T_f, pour les systèmes IR-UWB utilisant une modulation BPSK ;
- une synchronisation flexible permettant d'atteindre un niveau de résolution souhaité, pour les systèmes IR-UWB utilisant une modulation PSM.

Paramètre de synchronisation

Le signal reçu après passage dans le canal de propagation UWB, de réponse impulsionnelle $h(t) = \sum_{l=0}^{L-1} \lambda_l \delta(t-\tau_l)$, est donné par :

$$r(t) = \sum_i d(i) \sum_{j=0}^{N_f-1} g(t - iT_s - jT_f - c_j T_c - \tau_0) + n(t)$$

où $n(t)$ est un bruit additif blanc gaussien, de densité spectrale de puissance bilatérale $N_0/2$, et $g(t) = \sum_{l=0}^{L-1} \lambda_l \psi(t-\tau_{l,0})$ représente la réponse du canal à une seule impulsion UWB $\psi(t+\tau_0)$, avec $\tau_{l,0} = \tau_l - \tau_0$ le retard relatif du l^{ime} trajet multiple.

En supposant que le récepteur devient actif à un moment $t_0 \geq \tau_0$ et en considérant $\tau_0 = 0$, qui sert comme référence dans ce scénario, le signal observé peut être écrit sous la forme :

$$\begin{aligned} x(t) &= r(t+t_0) \\ &= \sum_i d(i) \sum_{j=0}^{N_f-1} g(t - iT_s - jT_f - c_j T_c + t_0) + n(t+t_0) \\ &= \sum_i d(i) \sum_{j=0}^{N_f-1} g(t - (i-N)T_s - jT_f - c_j T_c - t_\phi) + n(t + NT_s - t_\phi) \end{aligned}$$

où $t_0 = NT_s - t_\phi$, avec $N = \lceil t_0/T_s \rceil$.

Vu que le récepteur cherche le début du premier symbole d'information après t_0, c'est-à-dire l'instant $t = t_0 + t_\phi$, il en résulte que le paramètre de synchronisation qui doit être estimé est $t_\phi \in [0, T_s)$.

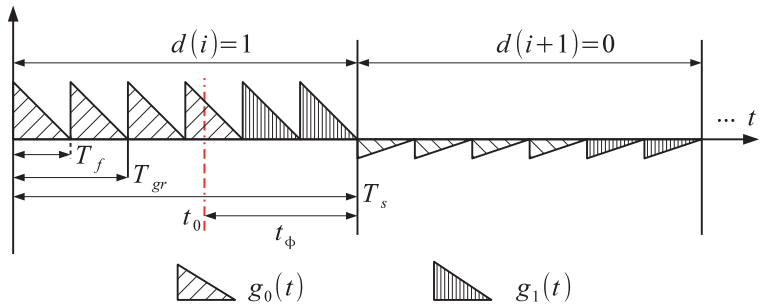

Figure 6: Signal reçu avec le paramètre de synchronisation t_ϕ.

Synchronisation rapide pour les systèmes IR-UWB utilisant une modulation BPSK

La méthode que nous proposons dans ce contexte est non-supervisée et ne fait appel à aucune recherche séquentielle. Ainsi, l'algorithme décrit dans [Akb12c] utilise une série d'impulsions UWB mutuellement orthogonales et une modulation d'amplitude binaire (BPAM) asymétrique de moyenne non nulle. A partir de cette structure particulière du signal UWB, la méthode proposée exploite les énergies estimées sur les intervalles de début et de fin du signal reçu, afin de réaliser la synchronisation au niveau trame.

Algorithme de synchronisation basé sur l'orthogonalité des signaux transmis (OSS)

Le schéma proposé utilise un couple d'impulsions orthogonales, transmises de manière judicieuse, afin d'obtenir la synchronisation. Le signal reçu dans ce cas est représenté sur la figure 6.

Il est clair d'après la figure 6, que chaque symbole est divisé en trois groupes, chacun d'une durée T_{gr}. Les deux premiers groupes transmettent la même impulsion $g_0(t)$, tandis que le troisième groupe utilise l'impulsion orthogonale $g_1(t)$. Les symboles porteurs d'information $d(i)$ prennent les valeurs $\{\theta, -1\}$ de manière équiprobable, avec une moyenne non nulle, où $\theta > 1$. Notre algorithme concerne la synchronisation au niveau trame, c'est-à-dire $|t_\phi - \hat{t}_\phi| \leq T_f$. Le paramètre de synchronisation t_ϕ est décomposé en erreur de niveau groupe et sous-groupe, c'est-à-dire $t_\phi = mT_{gr} + \epsilon$, où $m = \lfloor t_\phi / T_{gr} \rfloor$, $m \in \{0, 1, 2\}$ et $\epsilon \in [0, T_{gr})$. L'algorithme identifie d'abord l'erreur de niveau groupe et affine ensuite la synchronisation en estimant l'erreur de niveau sous-groupe.

Le point de départ est constitué par l'estimation des énergies des intervalles de début et de fin des groupes appartenant à la durée symbole observée, par des opérations d'accumulation-intégration sur les différents groupes. Ces opérations, notées X_1, X_2, X_3, sont effectuées sur les groupes successifs (X_1), sur le deuxième et le troisième groupe (X_2) et sur le premier et le troisième groupe respectivement (X_3). Selon le décalage m au niveau groupe, ces trois corrélations permettent d'obtenir soit l'énergie des intervalles de début ou de fin des groupes, soit la variance du bruit. En utilisant ces estimations énergétiques et des règles logiques il est possible de déterminer les valeurs de $\hat{m}$ and $\hat{\epsilon}$. Le paramètre de synchronisation peut être alors évalué par :

$$\hat{t}_\phi = \hat{m} T_{gr} + \hat{\epsilon}$$

L'algorithme proposé fournit l'estimation exacte de t_ϕ lorsque $\lceil \epsilon / T_f \rceil$ est un entier. Cependant,

si ce n'est pas le cas, l'algorithme permettra tout de même de réaliser la synchronisation avec une erreur inférieure à la durée de la trame.

Synchronisation flexible pour les systèmes IR-UWB utilisant une modulation PSM

Dans le cas de ces systèmes, nous proposons deux algorithmes à complexité réduite et amélioration significative des performances, qui sont capables de converger quel que soit le niveau de précision souhaité pour la synchronisation.

Pour un système IR-UWB utilisant une modulation PSM et des codes TH, le signal reçu s'exprime sous la forme :

$$r(t) = \sum_{i} \sum_{j=0}^{N_f-1} g_{d(i)}(t - iT_s - jT_f - c_j T_c - \tau_0) + n(t)$$

De manière similaire, le paramètre de synchronisation t_ϕ est défini comme suit :

$$\begin{aligned} x(t) &= r(t + t_0) \\ &= \sum_{i} \sum_{j=0}^{N_f-1} g_{d(i)}(t - (i-N)T_s - jT_f - c_j T_c - t_\phi) + n(t + NT_s - t_\phi) \end{aligned}$$

Il est à noter que dans ce cas $g(t)$ est fonction des symboles porteurs d'information $d(i)$, puisque la PSM utilise l'orthogonalité des signaux pour moduler (et démoduler) les données. Ce principe est différent de celui de la méthode OSS décrite ci-dessus, où les impulsions orthogonales permettant de réaliser la synchronisation ne changent pas d'un symbole à l'autre.

Algorithme de synchronisation basé sur la détection d'énergie (EDS)

Cet algorithme, que nous avons proposé dans [Akb11], utilise de simples opérations de superposition-addition, suivies d'une détection d'énergie pour estimer le paramètre de synchronisation. Il a l'avantage de pouvoir fonctionner aussi pour des modulations PSM d'ordre supérieur, où la signalisation orthogonale est particulièrement plus intéressante que la PAM [Pro00].

La synchronisation est réalisée en modifiant judicieusement le format du signal PSM standard. Ainsi, tel qu'il est indiqué sur la figure 7, deux modifications y ont été apportées. Tout d'abord, la première trame de chaque symbole est réservée à la synchronisation et n'est pas utilisée pour transmettre des données. Deuxièmement, chaque symbole est représenté par une série d'impulsions de polarité alternante, c'est-à-dire que le symbole de données $d(i)$ est transmis en utilisant alternativement les signaux $\psi_{d(i)}(t)$ et $-\psi_{d(i)}(t)$. Cette variation particulière de la polarité des impulsions conduit à une moyenne du signal d'observation nulle, à l'exception de la première trame, qui n'est pas porteuse d'information, résultat qui peut être exploité par le détecteur d'énergie pour estimer le début du symbole, à savoir le paramètre de synchronisation. Ainsi, la fonction objectif qui permet l'estimation de t_ϕ peut être formulée comme suit :

$$\hat{t}_\phi = \arg \max_{\tau \in [0, T_s)} \int_0^{T_I} \bar{x}^2 \left([t + \tau]_{T_s} \right) dt$$

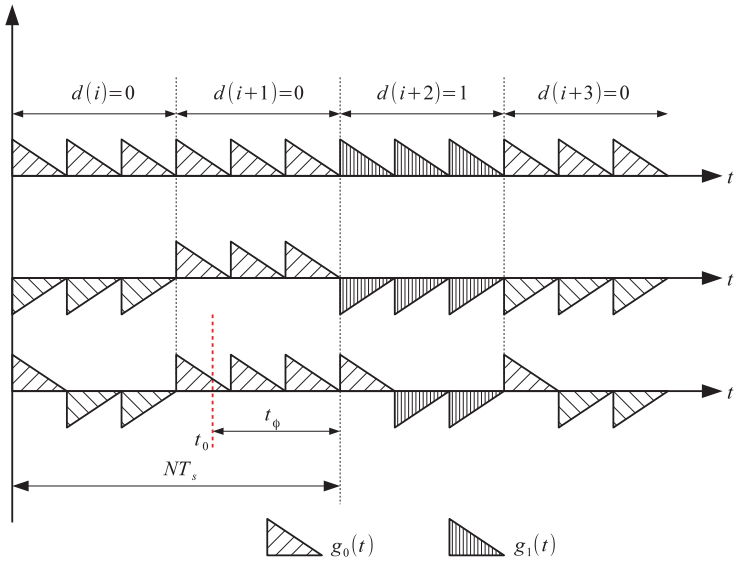

Figure 7: Le signal reçu avec le paramètre de synchronisation t_ϕ et $N_f = 3$ a) format standard du signal PSM, b) signal avec polarité alternante des impulsions, et c) format du signal PSM modifié, dont la première trame n'est pas porteuse d'information

où $\bar{x}(t)$ est la moyenne de signal d'observation et T_I est l'intervalle d'intégration ; l'opérateur $[.]_{T_s}$ permet de réaliser une extension périodique de $\bar{x}(t)$, dont le support est égal à T_s.

La durée d'intégration T_I détermine l'énergie du signal accumulée et influe sur la précision de la synchronisation. Idéalement, T_I devrait être égale à la somme entre le délai introduit par le canal et la durée de l'impulsion UWB, c'est à dire $T_I = T_g$. Cependant, si cette valeur n'est pas connue, elle peut être fixée à $T_I = T_f - N_h T_c$ en présence de codes TH et à $T_I = T_f$ dans les autres cas, à condition que l'énergie accumulée soit suffisante.

Algorithmes de synchronisation basés sur des codes bipolaires

L'idée de base de ces algorithmes est de multiplier les trames de chaque symbole par des codes bipolaires **b**, ayant une fonction d'autocorrélation périodique (PACF) de la forme suivante :

$$R(n) = \sum_{j=0}^{N_f-1} b_j b_{[j+n]_{N_f}} = \begin{cases} N_f & \text{si } n = kN_f \\ \pm 1 & \text{sinon} \end{cases}$$

avec $k = 0, 1, 2, \cdots$.

Parmi les codes bipolaires ayant cette propriété on peut citer les séquences M, les codes de Barker, etc. A la réception, les mêmes codes sont utilisés pour estimer le paramètre de synchronisation. Leur PACF fait que si le décalage temporel τ est égal à l'erreur de synchronisation, les impulsions constituant le code bipolaire sont sommées en phase, ce qui conduit à une accumulation maximale d'énergie. D'autre part, si τ est différent de t_ϕ, les impulsions ne sont plus sommées en phase et l'énergie accumulée est bien moindre.

Cependant, cette approche ne fonctionne que si tous les symboles utilisent la même impulsion UWB élémentaire, ce qui n'est pas le cas pour la PSM, où la forme d'onde des impulsions UWB correspondant aux symboles successifs varie en fonction de $d(i)$ et la PACF n'a plus l'expression

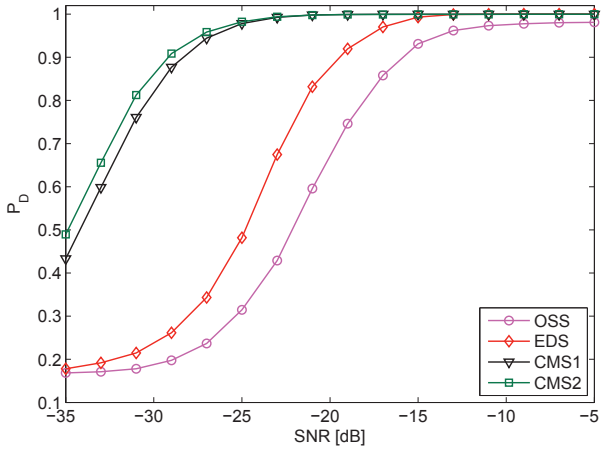

Figure 8: Comparaison des algorithmes proposés en termes de probabilité de détection, pour $K = 64$ symboles, dans le canal CM1

indiquée ci-dessus. Dans cette thèse, nous proposons deux méthodes pour contourner ce problème et rendre ainsi possible l'utilisation des codes bipolaires pour réaliser la synchronisation dans le cas de la PSM. La seule condition est que la forme d'onde de l'impulsion UWB élémentaire reste la même pour toutes les trames multipliées par un même code bipolaire.

La première méthode, appelée **CMS1**, alterne la polarité d'une des impulsions UWB et double l'amplitude de l'autre. Par exemple, considérons que la polarité des impulsions correspondant aux symboles $d(i) = 0$ change alternativement et que l'amplitude des impulsions correspondant aux symboles $d(i) = 1$ est doublée. A la réception, si le signal est moyenné sur un nombre suffisant de durées symbole, les impulsions correspondant aux symboles $d(i) = 0$ s'annulent les unes les autres en raison de leurs polarités alternées. Ainsi, à l'issue de cette étape de traitement, le signal ne contient plus qu'un seul type d'impulsion UWB, ce qui rend possible la synchronisation basée sur les codes bipolaires.

La seconde méthode, appelée **CMS2**, emploie des impulsions UWB ayant des propriétés de corrélation particulières et ne peut être utilisée que pour la PSM binaire. Le signal d'observation est corrélé avec les deux impulsions élémentaires $\psi_0(t)$ and $\psi_1(t)$.

$$y(t) = \int_{-\infty}^{\infty} x(\tau)\psi_0(\tau - t)d\tau + \int_{-\infty}^{\infty} x(\tau)\psi_1(\tau - t)d\tau$$

Considérons la corrélation des impulsions UWB $\Gamma_{a,b}(t) = \int_{-\infty}^{\infty} \psi_a(\tau)\psi_b(\tau - t)d\tau$, $[a, b] = \{0, 1\}$, et soit également $\Psi_a(t) = \Gamma_{0,a}(t) + \Gamma_{1,a}(t)$, $a = \{0, 1\}$. Alors, si $\Psi_0(t) = \Psi_1(t)$, c'est-à-dire que les fonctions d'autocorrélation et d'intercorrélation de $\psi_0(t)$ et $\psi_1(t)$ sont les mêmes, les conditions d'utilisation des codes bipolaires sont de nouveau réunies. Cet algorithme requiert donc une procédure de conception des impulsions élémentaires capable d'assurer ces propriétés de corrélation. Nous avons ainsi utilisé la même procédure d'optimisation basée sur le GA, expliquée dans le chapitre précédent, en incluant les nouvelles contraintes.

Evaluation des performances

Les performances des algorithmes de synchronisation proposés ont été évaluées en termes de probabilité de détection, définie comme $P_D = \Pr\left[|\hat{t}_\phi - t_\phi| \leq T_\delta\right]$. Chaque symbole est constitué de

$N_f = 13$ ($N_f = 12$ pour la méthode OSS, qui requiert un nombre de trames multiples de 3), et chaque trame contient $N_c = 15$ chips. Le canal à trajets multiples utilisé dans nos simulations correspond au modèle CM1 indoor, proposé par le groupe de travail l'IEEE 802.15.3a [Mol03], ayant une valeur effective de la dispersion du retard $\tau_{rms} = 5\,\text{ns}$. Le paramètre de synchronisation t_ϕ est généré de manière aléatoire à partir d'une distribution uniforme sur $[0, T_s)$, à chaque étape de la simulation de Monte Carlo. Le code bipolaire considéré exprimé sous forme décimale vaut $\mathbf{b} = 202$. L'intervalle d'intégration T_I est égal à $T_f - N_h T_c$, donc aucune information concernant l'étalement temporel du canal n'est nécessaire. Enfin, le SNR est défini comme le rapport P_g/σ^2 où P_g est la puissance reçue par impulsion (après la convolution de l'impulsion transmise avec la réponse impulsionnelle du canal).

La figure 8 présente une comparaison des algorithmes proposés en termes de probabilité de détection, en l'absence d'interférences IFI/ISI. Ces résultats confirment le fait que les méthodes basées sur la maximisation d'une fonction critère sur tous les décalages temporels candidats, conduisent à de bien meilleures performances, l'amélioration la plus significative étant réalisée par les algorithmes basés sur l'utilisation des codes bipolaires, grâce à leurs propriétés de corrélation particulières.

Estimation du canal dans les systèmes IR-UWB

Dans ce chapitre, nous abordons le problème de l'estimation du canal UWB, qui est un autre aspect critique pour le fonctionnement des récepteurs Rake cohérents.

Le canal de propagation indoor apparaît différemment aux systèmes UWB par rapport aux systèmes à bande étroite. En effet, les signaux UWB sont caractérisés par une résolution temporelle très fine, ce qui conduit à des canaux sélectifs en fréquence, ayant un nombre très important de trajets multiples. Un récepteur Rake constitué de plusieurs corrélateurs parallèles peut être alors utilisé afin de capter l'énergie du signal distribuée sur ces trajets multiples. Il en résulte que les performances d'un système IR-UWB intégrant un récepteur Rake dépendent fortement de la qualité de l'estimation du canal.

L'expression ci-dessous décrit un modèle typique de la réponse impulsionnelle d'un canal à trajets multiples :

$$h_{\boldsymbol{\alpha},\boldsymbol{\tau}}(t) = \sum_{l=1}^{L} \alpha_l \delta(t - \tau_l)$$

où $\{\alpha_l, \tau_l\}_{l=0}^{L-1}$ sont respectivement les gains et les retards correspondant aux trajets multiples.

Le signal reçu $y(t)$ est constitué par une somme pondérée de répliques atténuées et retardées du signal transmis $s(t)$, à savoir :

$$y(t) = \sum_{l=1}^{L} \alpha_l s(t - \tau_l) + \eta(t)$$

où $\eta(t)$ désigne le bruit supposé additif, blanc et gaussien.

L'objectif est d'estimer les paramètres inconnus du canal $\{\boldsymbol{\alpha}, \boldsymbol{\tau}\}$ à partir du signal reçu $y(t)$.

Etat de l'art

Plusieurs algorithmes sont proposés dans la littérature pour estimer les paramètres du canal, à la fois dans les domaines temporel et fréquentiel. Parmi ceux-ci nous pouvons rappeler l'approche de type moindres carrés (LS) proposée dans [Car03], le critère basé sur le maximum de vraisemblance (ML) présenté dans [Lot02, Win02], l'estimateur NDA quasi-ML développé dans [Che10], ou l'algorithme SAGE (space alternating generalized expectation maximization) introduit dans [Han03].

L'apport de l'approche EM (expectation maximization) pour l'estimation des paramètres du canal de communication d'un système UWB M-PPM a également été étudié dans [Mek08], tandis que l'implémentation de l'estimateur ML sous la forme d'une procédure d'annulation successive des interférences (SIC) est effectuée dans [Han06].

L'étude de la propagation UWB et la modélisation du canal associé, dans les environnements indoor, font apparaître au niveau de sa réponse impulsionnelle une distribution des trajets multiples par groupes (clusters). S'appuyant sur cette structure particulière de la réponse impulsionnelle du canal UWB, une méthode d'estimation de ses paramètres en deux étapes est présentée dans [Car04]. Enfin, vu que le rapport des spectres des signaux reçu et émis se réduit à une somme d'exponentielles complexes, toutes les méthodes d'estimation spectrale haute-résolution proposées dans la littéra-

ture [Roy89,Rao92,Sto97] peuvent être appliquées pour résoudre le problème d'estimation du canal UWB.

Les méthodes d'estimation du canal basées sur le ML, qui évaluent la similarité entre les signaux reçu et estimé, sont relativement simples à mettre en œuvre et fournissent une faible erreur quadratique moyenne, même à faible SNR. Ces méthodes présentent en même temps certains inconvénients dans le cas de l'UWB. Il s'agit principalement de la résolution limitée, ce qui les rend moins adaptées pour les canaux UWB. L'estimation se dégrade aussi de manière significative pour les trajets multiples de faible amplitude noyés dans le bruit.

Les algorithmes haute-résolution basés sur la décomposition en sous-espaces orthogonaux (OS), tels que MUSIC et ESPRIT [Mar87], sont capables théoriquement de fournir une résolution infinie, mais en pratique, montrent certaines limites. Tout d'abord, puisque la matrice d'autocorrélation des données n'est généralement pas connue, son estimation introduit des erreurs. D'autre part, ils requièrent comme paramètre d'entrée le nombre de trajets multiples du canal, qui n'est pas connu non plus. Là encore, son estimation en utilisant différents critères, tels que ceux d'Akaike (AIC) ou Rissanen (MDL) [Wax85], est susceptible d'introduire des erreurs. Ces erreurs d'estimation deviennent très importantes pour les faibles SNR et dégradent considérablement les performances des algorithmes haute-résolution, qui deviennent inutilisables dans ce cas.

Approche conjointe ML/OS pour l'estimation du canal IR-UWB

L'algorithme que nous proposons pour l'estimation du canal IR-UWB [Akb10b] est basé sur une approche conjointe ML/OS. Son idée de base consiste à combiner les deux approches afin de profiter de leurs avantages et de s'affranchir de leurs limites respectives. Cet algorithme consiste en trois étapes :

- estimation grossière du canal en utilisant une implémentation SIC du ML ;
- sélection des trajets multiples valides, parmi ceux estimés à la première étape, en utilisant l'opérateur de projection sur le sous-espace bruit ;
- soustraction des trajets multiples, validés à l'étape précédente, du signal reçu, et estimation des trajets multiples restants par l'algorithme MUSIC.

Plus précisément, l'algorithme utilisé lors de la première étape est SSR (Search, Substract and Readjust) [Fal06]. L'idée est simplement de calculer à chaque itération la corrélation entre le signal reçu et le signal de référence au moyen d'un filtre adapté (MF) et de trouver le plus grand pic, qui est susceptible de représenter le trajet multiple courant. L'amplitude de ce pic est déterminée à l'aide du critère ML, puis soustraite du signal reçu. Le signal obtenu suite à cette soustraction est utilisé à l'itération suivante pour estimer un nouveau trajet multiple, et ainsi de suite jusqu'à ce qu'un nombre N donné d'itérations soit atteint.

En parallèle avec la première étape la matrice d'autocorrélation des données est estimée et son analyse propre effectuée. Les vecteurs propres correspondant aux plus petites valeurs propres sont regroupés pour former la matrice $\mathbf{V}_n$ et l'opérateur de projection sur le sous-espace bruit :

$$\Pi_n^{\perp} = \mathbf{V}_n \mathbf{V}_n^H$$

Cet opérateur de projection est alors utilisé pour valider chacun des trajets multiples extraits lors de la première étape. Dans le cas sans bruit, les vrais et les faux pics sont clairement séparés. Dans le cas bruité, il est plus difficile, mais toujours possible, de classer la plupart d'entre eux, en utilisant un seuil adapté pour les valeurs de projection.

Le signal reconstruit à partir de l'ensemble de trajets multiples validés de cette façon est ensuite soustrait du signal reçu. Enfin, l'algorithme MUSIC appliqué au signal différence permet d'extraire les trajets multiples restants. L'estimation du canal finale est alors constituée par la réunion des trajets multiples valides déterminés avec la méthode SSR et de ceux extraits du signal différence par l'algorithme MUSIC.

Evaluation des performances de la méthode proposée

Les performances des différents algorithmes sont évaluées au moyen de deux paramètres. Le premier est l'erreur quadratique moyenne normalisée, calculée entre le signal reçu et le signal reconstruit à partir du canal estimé, et définie par :

$$S_n\left(\boldsymbol{\tau},\boldsymbol{\alpha}\right) = \frac{\|\mathbf{y} - \hat{\mathbf{y}}_{\boldsymbol{\tau},\boldsymbol{\alpha}}\|^2}{\|\mathbf{y}\|^2} \tag{2}$$

Ce paramètre utilisé seul ne donne pas toujours une bonne indication sur la précision du résultat obtenu, dans la mesure où plusieurs réponses impulsionnelles conduisent à des signaux reçus relativement proches. C'est pourquoi, les performances des algorithmes sont évaluées également par un deuxième paramètre, qui est le coefficient de corrélation entre les profils du canal idéal et estimé :

$$S_{ac}(\boldsymbol{\tau},\boldsymbol{\alpha}) = \frac{\langle \mathbf{h}, \hat{\mathbf{h}}_{\boldsymbol{\tau},\boldsymbol{\alpha}} \rangle}{\|\mathbf{h}\|.\|\hat{\mathbf{h}}_{\boldsymbol{\tau},\boldsymbol{\alpha}}\|} \tag{3}$$

où $\hat{\mathbf{h}}_{\boldsymbol{\tau},\boldsymbol{\alpha}}$ représente la réponse impulsionnelle du canal et $\langle . \rangle$ est le produit scalaire.

La solution recherchée devrait ainsi être performante aussi bien en termes de S_n que de S_{ac}.

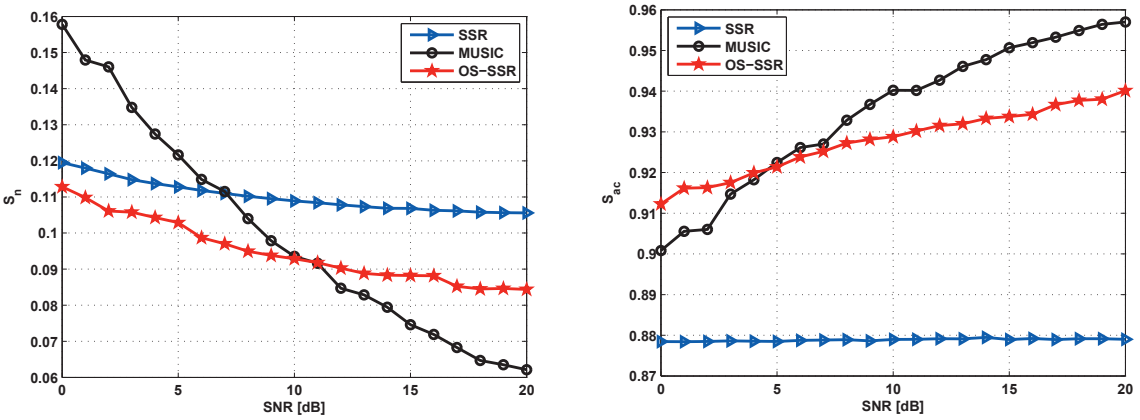

(a) S_n (b) S_{ac}

Figure 9: Performances des algorithmes d'estimation du canal IR-UWB en fonction du SNR, pour $K = 64$ symboles, dans le canal CM1

La figure 9 montre la variation des performances des différents algorithmes en fonction du SNR,

en termes de S_n and S_{ac}, en considérant le modèle du canal IR-UWB CM1, décrit pas le standard l'IEEE 802.15.3a. A chaque itération, le canal est généré de façon aléatoire, puis tronqué au-delà du $20^{\text{ième}}$ trajet multiple. Les résultats obtenus sont moyennés sur 1000 réalisations du canal.

Il est à noter que la méthode proposée (OS-SSR) fournit de meilleurs résultats que l'estimation SSR à la fois en termes de S_n et de S_{ac}. Le comportement de l'algorithme MUSIC est tout à fait différent, car ses performances sont supérieures à celles de la méthode OS-SSR pour des valeurs du SNR élevées, mais se dégradent plus rapidement lorsque le niveau du bruit augmente. Ainsi, la méthode proposée peut être considérée comme une bonne synthèse entre ces deux techniques.

Conlusions

Dans le cadre de cette thèse, nous avons tout d'abord focalisé notre travail de recherche sur le couplage entre la radio cognitive et les systèmes TH IR-UWB. En effet, l'une des préoccupations majeures lors de leur déploiement est constituée par les interférences potentielles **de** et **vers** les systèmes IR-UWB, engendrées par l'existence des réseaux à bande étroite dans différentes sous-bandes du domaine UWB. Par conséquent, le premier élément analysé dans cette thèse est la possibilité d'éviter les NBI en munissant ces systèmes de capacités cognitives. Ainsi, nous proposons une approche à double sens : une décision est tout d'abord prise sur la présence/absence de l'utilisateur primaire en utilisant des algorithmes de détection spectrale rapides et efficaces, et ensuite la forme d'onde de l'impulsion UWB est modifiée lors d'une phase d'adaptation de l'occupation spectrale afin de minimiser les interférences. Le deuxième volet important de la thèse concerne les paramètres critiques pour les performances du récepteur Rake cohérent, à savoir la synchronisation et d'estimation du canal UWB.

Les principales contributions de ce travail de thèse sont résumées ci-dessous :

- Approche de détection spectrale à double seuil et faible nombre d'échantillons, adaptée à la fois aux PU utilisant des signaux à enveloppe constante et aux PU dont les échantillons du signal sont i.i.d. selon $\mathcal{N}_{\mathbb{C}}(0,1)$;
- Procédure de conception adaptive de la forme d'onde IR-UWB, qui maximise l'efficacité spectrale et peut intégrer différentes contraintes linéaires et/ou non-linéaires correspondant aux différents objectifs du traitement ;
- Algorithme rapide de synchronisation NDA pour les systèmes IR-UWB utilisant la modulation BPSK, basé sur l'orthogonalité des impulsions UWB ;
- Algorithmes de synchronisation NDA efficaces pour les systèmes IR-UWB utilisant la PSM (binaire et M-aire), basés sur la détection d'énergie ou les codes bipolaires ;
- Méthode de conception à faible complexité des récepteurs SAT conjointement avec la synchronisation pour les systèmes IR-UWB utilisant la PSM ;
- Approche conjointe ML/OS pour l'estimation du canal IR-UWB permettant de réaliser une bonne synthèse entre robustesse au bruit et qualité de l'estimation.

Contents

List of Figures

List of Tables

Acronyms and Abbreviations

A-PAM asymmetric pulse amplitude modulation
A-Rake All-Rake
ACP autocorrelation property
ADC analog-to-digital converter
AIC Akaike Information Criterion
AWGN additive white gaussian noise

BPAM binary pulse amplitude modulation
BPSK binary phase shift keying
BSL Bronk-Shin-Lee

CAF cyclic autocorrelation function
CDF cumulative distribution function
CEPT European Conference of Postal and Telecommunications Administrations
CIR channel impulse response
CM correlation matching
CMS code matching based synchronization
CMS1 code matching based synchronization - proposition 1
CMS2 code matching based synchronization - proposition 2
CR cognitive radio
CSD cyclic spectrum density
CSI channel state information

DA data-aided
DC direct current
DD differential detector
DS-CDMA Direct Sequence Code Division Multiple Access
DSP digital signal processor
DSSS direct sequence spread spectrum

ECC European Communications Committee
ED energy detector
EDS energy detection based synchronization
EGC equal gain combining
EIRP effective isotropic radiation power
EM expectation-maximization
ETSI European Telecommunications Standards Institute
EVS eigenvalues' sum

FCC Federal Communication Commission
FFT fast fourier transform
FHSS frequency-hoping spread spectrum
FRMT finite random matrix theory

GA genetic algorithm
GEV Generalized extreme value

GLRT generalized likelihood ratio test
GOF goodness-of-fit
GPS Global Positioning System

IFI inter-frame interference
IPI inter-pulse interference
IR-UWB impulse radio UWB
ISI inter-symbol interference
ISM industrial, scientific and medical

LOS line of sight
LPI/LPD low probability of interception/low probability of detection
LS least-square

MAI multi-access interference
MB-OFDM multi-band orthogonal frequency division multiplexing
MC/MB multicarrier/ multiband
MDL Maximum Description Length
MF matched filter
MHP modified Hermite polynomials
MIMO multiple input multiple output
ML maximum-likelihood
MP Marchenko-Pastur
MPC multipath components
MRC maximum ratio combining
MST mean synchronization time
MUI multi-user interference
MUSIC MUltiple Signal Classification

NBI narrowband interference
NDA non-data-aided
NLOS non line of sight
NMSE normalized mean squre error

OFDM orthogonal frequency division multiplexing
OM orthogonal modulation
OOK on-off keying
OS orthogonal subspace
OSS orthogonal signaling based synchronization

P-RAKE Partial RAKE
PACF periodic autocorrelation function
PAM pulse amplitude modulation
PDF probability density function
PDP power delay profile
PPM pulse position modulation
PR pseudorandom
PRF pulse repition frequency
PSD power spectral density

PSM pulse shape modulation
PSWF prolate spheroidal wave functions

QPSK quadrature phase shift keying

RF radio frequency
RLAN remote local area network
rms root mean square
RMT random matrix theory
ROC receiver operating characteristic

S-PAM symmetric PAM
S-RAKE Selective RAKE
SAGE space alternating generalized expectation maximization
SAT synchronized aggregate template
SCN standard condition number
SIC successive interference cancellation
SIMO single input multiple output
SISO single input single output
SNR signal-to-noise ratio
SS spectrum sensing
SSR search, subtract and readjust
SV Saleh-Valenzuela

TDT timing with dirty template
TH time-hopping
TH-IR-UWB time-hopping based impulse radio UWB
ToA time-of-arrival
TR Transmitted Reference
TW Tracy-Widom
TWC Tracy-Widom-Curtiss

UNII unlicensed national information infrastructure
UWB ultra wide band

WBAN wireless body area network
WLAN wireless local area network
WPAN wireless personal area network
WRAN wireless regional area network
WSN wireless sensor network

Notations

$\lceil . \rceil$	Integer ceil operation
$[.]_B$	Modulo operator with base B
$\lfloor . \rfloor$	Integer floor operation
$\mathbb{C}_{K \times N}$	$K \times N$ complex matrix
$\mathbf{1}_{K \times N}$	$K \times N$ All-ones matrix
$\mathbf{A}^*$, $\mathbf{A}^T$, $\mathbf{A}^\dagger$	Complex conjugate, transpose, and conjugate transpose (Hermitian) of matrix $\mathbf{A}$, respectively
$\mathbf{I}_K$	$K \times K$ identity matrix
$\mathcal{N}_{\mathbb{C}}(\mathbf{m}, \mathbf{\Sigma})$	Complex circularly Gaussian distribution with parameters $\mathbf{m}$ and $\mathbf{\Sigma}$
$\mathrm{E}[.]$	Statistical expectation
τ_{max}	Maximum Channel Delay Spread
N_c	Number of chips
N_f	Number of frames
P_A	Probability of acquisition
P_d	Probability of detection
P_{fa}	Probability of false-alarm
P_m	Probability of miss-detection
T_c	Chip duration
T_f	Frame duartion
T_s	Symbol duration
t_0	Receiver Initialization Instant
t_ϕ	Synchronization parameter defined as $t_\phi = T_s - t_0$
$x \sim f(x)$	$f(x)$ is the distribution of x
$x \star y$	Convolution of x and y

General Introduction

The demand for wireless connectivity and crowding of unlicensed spectra has pushed the regulatory agencies to promote more flexibility in spectrum sharing. The regulatory bodies around the world today are providing new opportunities for unlicensed spectrum usage with fewer restrictions on radio parameters. Among the recent innovations in the field of wireless communications, the scientific community is particularly interested in the ultra wide band (UWB), which utilizes frequency bands of 500 MHz to several GHz. UWB technology is evolving fast as with its strict power spectral density (PSD) limitations, there is a possibility to coexist with other technologies by using the spectrum allocated to them in underlay mode. The stringent requirements on UWB power emission help to keep the interference to minimum and thus the spectrum is used with an increased efficiency. UWB, which is the focus of this thesis, is therefore a potential technology for large number of new applications including wireless local area network (WLAN) and wireless personal area network (WPAN) applications.

Given the ultra large bandwidth, UWB signals are immune to multipath fading and have the ability to communicate with high data rates. The limitation is the distance over which communication can be held with sustainable low bit error rates. Furthermore, UWB signaling can potentially be implemented with very low cost and low power consumption components, representing an interesting solution for remote control and sensor network applications. In a pulsed UWB communication system, the information is encoded in very narrow pulses. The ability of pulsed UWB to resolve individual multipath components is exploited in the recent research for short range communication applications.

The main objective of this thesis is to investigate some of the key elements in the realization of an intelligent (or cognitive) time-hopping based impulse radio UWB (TH-IR-UWB) system. The modulation used is either binary phase shift keying (BPSK) or pulse shape modulation (PSM). The transmitted signal propagates through UWB indoor channel proposed by IEEE 802.15.3a Task Group and finally demodulated using a coherent Rake receiver.

Albeit of many unique features of impulse radio UWB (IR-UWB), there are also equally challenging design issues such as high sampling rates, wideband antennas, narrowband interference mitigation, limited range and receiver related issues. The following issues have been addressed in the framework of this thesis research work:

Narrowband interference (NBI) in UWB. The very low transmission power and large bandwidth enable UWB systems to co-exist with other narrowband systems without interfering with them. However, the effect of the narrowband signals on the UWB signal can be significant and may jam the UWB receiver completely. Even though the narrowband signals interfere with only a small fraction of the UWB signal spectrum, due to the large relative power of the narrowband signals with respect to the UWB signal, the performance and capacity of UWB systems can be affected considerably. Therefore, the UWB receivers might need to employ NBI suppression techniques to improve the performance, capacity, and range of communication.

Adaptive UWB waveform design. UWB pulses have to comply with the masks defined by different regulatory bodies around the world for the effective isotropic radiation power (EIRP).

At the same time, the allowed spectral resource is to be efficiently occupied, so that maximum energy can be transmitted while remaining compatible with the specifications of the considered spectral mask. Further, the UWB pulses also need to be enough adaptive so that they can be able to leave occupied portion of the spectrum to avoid NBI. As the spectrum occupied by IR-UWB systems is directly affected by the shape of UWB pulse, its careful design is very critical and essential for an opportunistic spectrum usage.

Synchronization. Synchronization can be roughly described as the process of providing the same time reference for the receiver as is used for the transmitter. In UWB, synchronization is more difficult compared with other narrowband systems. Fast and accurate acquisition with low overhead is desired. The carrierless nature of UWB signals, their very low duty cycle operation, and the pulse distortion caused by the propagation channel and radiating element, all make the timing synchronization a completely different problem for the case of UWB systems. In addition to this, UWB systems employ extremely-short pulses with very low-power. Consequently, timing requirements are stringent because even minor timing misalignment results in lack of energy capture which may render symbol detection impossible.

UWB Channel Parameters Estimation. As we opt for coherent Rake receiver due to its near optimal performance in our considered system, the channel estimation is indispensable. In UWB, the transmission bandwidth is extremely large, which leads to multiple resolvable paths. Since the total power is distributed over many multipath components, the power in each of these individual paths will be very low. The very low-power of UWB signals results in a very low signal-to-noise ratio (SNR) at the receiver. Thus, specific channel estimation techniques are required for UWB signals by taking into consideration the very low SNR of practical UWB working scenarios.

The research work related to this thesis has been carried out within the “Communications” research team, which is a part of the Lab-STICC CNRS UMR 6285, while its main contributions are targeted on the research axis “Intelligence and Furtivity of Communications”, developed at UBO.

UWB systems, and more specifically, UWB signal analysis and processing, is an unifying, though very recent, research topic for our team. Its capabilities in this research field has been increasingly reinforced these last years by the acquisition of an UWB experimental platform as well as by its involvement in Lab-STICC transverse research projects aiming at very precise indoor localization using UWB signal processing.

The main reason for our research team interest in this emerging research field is the great potential of UWB signals in terms of data rate, data security and spectral efficiency, which are very interesting issues for LAN and wireless PAN applications, as already stated above, but also for electronic warfare purposes for example. Indeed, the very low PSD of these signals makes their detection and interception a very challenging task, their inherent low probability of interception/low probability of detection (LPI/LPD) nature being quite effective against COMINT techniques.

On the other hand, the knowledge and experience acquired by working on UWB waveforms and system design could be very helpful for solving the furtivity dual problem, which is represented by the UWB signals interception and parameter estimation, in a non-cooperative context. Their impulsive and non-gaussian nature can be mainly exploited to set up new detection and parameter estimation methods, the final goal being to recover the information confined by the exchanged messages.

While this thesis deals rather with the first aspects listed above, this last problem has been also investigated by our research team through a thesis already defended [Sta11], whose main objective was to propose new methods for UWB signal parameter blind estimation.

Thesis Organization

This document is divided into 4 chapters, which are organized as follows.

Chapter 1

In this chapter, the main concepts of UWB radio are presented. First, the spectrum regulations throughout the world are discussed. Thereafter, an overview of pulsed UWB technology, popular transmission and modulation schemes, its key benefits and applications for wireless transmission are described. UWB channel models are discussed and some of the receiver systems for UWB signals are also illustrated. Finally, the thesis framework is defined starting from some challenging problems in the UWB communication field.

Chapter 2

This chapter explores the concept of integrating UWB with Cognitive Radio. First, the salient features of cognitive radio are reviewed and a close resemblance between the UWB features and cognitive radio requirements is observed. Due to this similarity, UWB technology itself can be considered a potential candidate for realizing cognitive radio technology. On the other hand, by incorporating some cognitive radio features into UWB systems, some of the challenges faced by these systems can also be eliminated. Therefore, a mutual benefit exists by fusing these two interesting technologies together. Owing to this observation, we then focus on the spectrum sensing which is a key element of cognitive radio and propose a rapid method using finite random matrix theory. Next, an adaptive UWB waveform is designed which can help to efficiently utilize the available spectral resources and can also mitigate the interference from other systems.

Chapter 3

This chapter addresses the timing synchronization issue in IR-UWB systems. First, the eventual challenges linked with synchronization in IR-UWB are discussed and a literature review is presented. Motivated by certain limitations of these methods, we then propose several low-complexity synchronization methods, each signifying its merits under particular operating scenarios. Extensive simulation results are provided to validate the robustness of the proposed schemes along with discussion about the practical feasibility.

Chapter 4

In this chapter, we address the channel estimation problem which is another critical issue for the realization of coherent Rake receivers. First, a literature review is presented regarding channel estimation in IR-UWB. It was found that most of the methods available in literature are based on

either maximum-likelihhod or orthogonal subspace approaches. Motivated by certain limitations of these methods, we then propose a joint ML/OS channel estimation method. The simulation results prove the increased efficiency of the proposed algorithm in terms of resolution and accuracy.

In the end, the significance of the results and perspectives are discussed in the thesis conclusion.

Chapter 1

UWB Communications Concepts and Challenges

- Abstract -

In this chapter, the main concepts of UWB radio are presented. First, the spectrum regulations throughout the world are discussed. Thereafter, an overview of pulsed UWB technology, popular transmission and modulation schemes, its key benefits and applications for wireless transmission are described. UWB channel models are discussed and some of the receiver systems for UWB signals are also illustrated. Finally, the thesis framework is defined starting from some challenging problems in the UWB communication field.

Contents

1.1 Introduction

In the recent years, both the wireless and the wired transmissions have experienced an amazing growth due to the rapid advances in semiconductor research and the increasingly demand for high-data rate services. This fact has paved the way for the advent of the so-called next generation communication systems, among which, future short-range wireless systems are experiencing an unprecedented transformation. There are unlimited demands on wireless communication systems to support higher speeds (data rates), higher precision, more reliable connections, more simultaneous users, etc. Meanwhile, the frequency resource is always limited. Depending on the characteristics of the radio channels, the distances, other requirements of the applications, and most importantly, the requirement to avoid interference to other systems, these electro-magnetic waves, also called as wireless signals, need to operate in certain frequency bands. As a result of increasing demands from all the commercial, industrial, scientific and government applications, the whole radio frequency spectrum, ranging from 3 KHz to 300 GHz, is now virtually occupied.

Ultra-Wideband (UWB) technology arrives as an alternative to partly solve the frequency resource scarcity problem mentioned above. Although this underlay approach does not solve the problem completely, it does not require a new licensed frequency allocation, which is always rare and expensive. UWB technology is evolving fast as with its strict PSD limitations, there is a possibility to coexist with other technologies by using the spectrum allocated to them in underlay mode. The interference from UWB signals to the existing wireless systems is minimized by imposing limitations on the UWB radiated emission powers under different frequency range.

Not only does UWB technology avoid the frequency resource scarcity problem, but it also brings many new promising features compared to the existing "narrowband" wireless systems. Naturally, the ultra-wide bandwidth signal suggests a better obstacle penetration, higher data rate, and higher precision ranging (at centimeter level) applications. Impulse Radio (IR) UWB systems, which use ultrashort pulses (sub-nanosecond duration), has the ability to resolve multipath channels. Moreover, IR UWB can operate independently in baseband (without a carrier), which, unlike the traditional narrowband systems, eliminates the need for up/down converters in the transmitter/receiver analog circuits. These features together make UWB an ideal candidate for low-complexity, low-power, short-range wireless communication systems.

1.2 What is UWB?

1.2.1 Definition

Many terms have been adopted for ultra wideband communications such as impulse radio, carrier-free radio, baseband radio, time domain radio, non-sinusoidal radio, orthogonal function radio and

relative bandwidth radio etc. [Bar00]. The first definition for a signal to be qualified as UWB is due to the United States Defense Advanced Research Projects Agency (DARPA) in 1990 which adopted the measure of fractional bandwidth for this purpose. The fractional bandwidth of a signal can be determined as

$$B_f = 2\frac{f_H - f_L}{f_H + f_L} \tag{1.1}$$

where f_H and f_L are respectively the higher and the lower frequency boundaries at a threshold (e.g. 3 dB) below the strongest radiated emission. This first definition of UWB signal stated that a signal can be classified as UWB when the -3 dB fractional bandwidth is greater than 25%. In 2002, the Federal Communication Commission (FCC) defined a UWB signal as any signal having a -10 dB fractional bandwidth larger than 20% [FCC02a]. In addition to this, a signal was also considered to be UWB if the signal bandwidth is equal or greater than 500 MHz. Fig. 1.1 presents a comparative illustration of the UWB spectrum occupation and other existing narrowband systems..

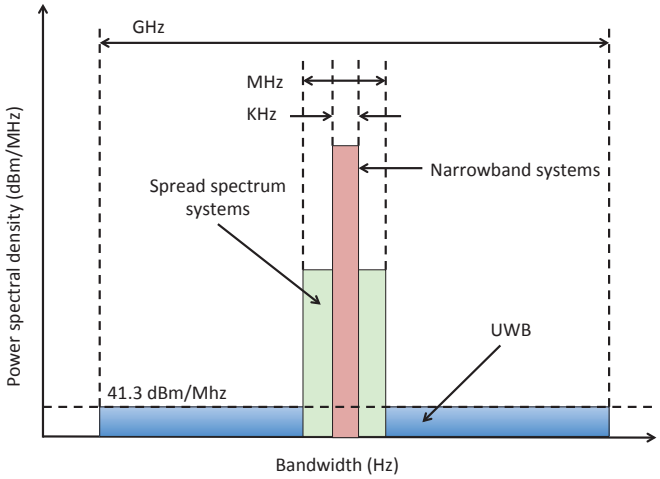

Figure 1.1: Comparison of the spectrum allocation for different wireless radio systems

1.2.2 Historical Overview

Although, often considered as a recent technology in wireless communications, UWB has actually experienced over 40 years of technological developments. In fact, UWB has its origin in the spark-gap transmission design of Marconi and Hertz in the late 1890s. In other words, the first wireless communication system was based on UWB. Owing to technical limitations, narrowband communications were preferred to UWB.

In early 60s, the initial research in UWB was focused on radar applications due to the nature of broadband signals, which provide a strong temporal resolution. A comprehensive survey of early research in this field was presented by Bennett and Ross [Ben78], while Taylor [Tay94] presents the foundations of the technology applied to UWB radar. Regular research advances have been made since the mid-60s, as revealed by the historical study of Barrett [Bar00].

However, the use of UWB signals in the field of radio communication was not envisaged before the end of the 20^{th} century. In 1990, the department of defense of United States of America (USA) government published the results of its evaluation of the UWB technology, which focused exclusively on the radar, since no other application of UWB communication systems were then

proposed [Fow90]. More recently, research has been focused on UWB signals for radio communication [Sch93], developing the main characteristics of this technique: a temporal resolution in the order of nanoseconds due to the frequency bandwidth, low duty cycle allowing multiple access without a transmission carrier, which simplifies the architecture of radio systems [Foe01].

Since 1998, the FCC launched a first study on UWB. In February 2002, a first regulatory report is published, allowing wireless communications in particular in the band of 3.1 GHz - 10.6 GHz with strong constraints on the power spectral density [FCC02a].

1.2.3 Principal Characteristics of UWB

UWB has a number of advantages that makes it attractive for consumer communication applications. In particular, UWB systems [Gha04b]

- provide high data rates
- have very good time domain resolution allowing for ranging and communication at the same time
- have immunity to multipath and interference
- have potentially low complexity and low equipment cost.

The high rates are perhaps the most compelling aspect from a user's point of view and also from a commercial manufacturer's position. With UWB, transmission rates of over 100 Mbps have been demonstrated, and the potential for higher data rates over short distances is there. The high data rate capability of UWB can be best understood by examining the Shannon's famous capacity equation:

$$C = B\log_2\left(1 + \frac{P}{N}\right) \tag{1.2}$$

where C is the channel capacity in bits/second, B is the channel bandwidth in Hz, P is the mean signal power and N is the noise power. This equation tells us that the capacity of a channel grows linearly with the bandwidth B, but only logarithmically with the signal power P. Since the UWB channel has an abundance of bandwidth, it can trade some of the bandwidth against reduced signal power and interference from other sources. Thus, from Shannon's equation we can see that UWB systems have a great potential for high capacity wireless communications.

Thanks to their very large bandwidth, UWB signals have a very high temporal resolution, typically in the order of a nanosecond (ns). Being able to measure the delay of a transmitted signal with a precision of 0.1 to 1 ns, UWB systems provide some information about the position of the transmitter with a precision of 3 to 30 cm. Thus, it is possible to have both precise ranging and high speed data communication in the same wireless terminal providing the possibility for new devices and applications.

The low complexity and low cost of single band UWB systems arises from the ability of UWB systems to directly modulate a pulse onto an antenna. Unlike conventional radio systems, the UWB transmitter produces a very short duration pulse, which is able to propagate without the need for an additional radio frequency (RF) mixing stage. The very wideband nature of the UWB signal means that it spans frequencies commonly used as carrier frequencies. Thus, the signal will propagate well without the need for additional up-conversion and amplification stages.

In single band UWB modulation, the short duration of transmitted pulses provides a fine resolution of reflected pulses at the receiver. In multiband UWB, the spectral flexibility provides robustness against interference by removing the interfering frequency bands.

1.2.4 Disadvantages of UWB

While UWB has all the above advantages, it also has some major weaknesses:

- narrowband interference
- powerful signal processing capabilities
- wideband antennas
- limited range.

Since UWB signal uses a wide RF bandwidth, its interference with existing narrow band turns out to be a critical problem. This interference could be in two directions: one direction is that narrow band signals can interfere to UWB receivers, such as IEEE 802.11a that shares 5 GHz frequency band with UWB signals; the other direction is that UWB signals may interfere into narrow band receivers. For instance, Global Positioning System (GPS) signals are usually of low power density, so it is vulnerable to UWB interference. However, without sacrificing much system performance, the interference of UWB to legacy systems can be mitigated through pulse shaping filter and different modulation schemes.

Also, as the UWB pulses are very short in time domain, high-speed analog-to-digital converters (ADCs) and high-speed digital signal processing are essential for UWB systems to digitize and process UWB signals.

UWB systems require wide-band antennas. Traditional frequency selective antennas could not keep constant amplitude and constant group delay for a wide frequency bandwidth. Instead, wide-band antennas, such as discone antenna, logarithmic antenna, etc., have to be adopted. However, wide-band antennas are bigger and more expensive than narrow-band antennas, designing a small and inexpensive antenna is crucial for UWB technology to be widely deployed.

UWB communication systems are limited in range. In order to make UWB interference to other radio systems insignificant, the transmission power of UWB signals has to be bounded under the emission mask imposed by the regulatory bodies. The low output power leads to smaller coverage area. In general, with high gain antenna, UWB signals may cover up to one kilometer. But with regular antennas, the range of UWB signals is usually from ten to twenty meters.

1.2.5 UWB Applications

In recent years, an increasing request appeared for high speed wireless connectivity between a host (e.g., a PC) and associated peripherals such as wireless modem, camcorder, video player and so on. This increasing need led to the development of many standards for wireless communication systems over short distances. One can quote Bluetooth, the family of WiFi standards (IEEE802.11), Zigbee (IEEE802.15.4) and the recent standard 802.15.3, which are used for WLAN and WPAN. However, most of these technologies use the industrial, scientific and medical (ISM) and unlicensed national information infrastructure (UNII) bands with maximum bandwidths of about 10 MHz.

A UWB link functions as a "cable replacement" with data rate requirement that ranges from 100 Kbps for a wireless mouse to several hundreds of Mbps for rapid file sharing or download of video files. In summary, UWB is seen as having the potential for applications which to date have not been fulfilled by the aforementioned wireless short range technologies. Fig. 1.2 depicts the positioning of the UWB compared to WLAN/WPAN standards in terms of data rate and maximum range. As observed, the potential applications of UWB technology concern two technical areas: very high data rate transmission over short distances (typically 200 Mbps up to 10 m), and low data rate communications with ranges of 100 m with positioning capabilities. It is noticed that in contrast with the WiFi standard, the high data rate mode of UWB belongs to the family of short range WPANs. However, the potential data rate of UWB exceeds the performance of all current WLAN and WPAN standards. In the low data rate mode, the IEEE802.15.4a standard targets UWB systems with centimeter accuracy in ranging as well as with low power and low cost implementation. These features allow a new range of applications, including military applications, medical applications (e.g., monitoring of patients), search-and-rescue applications, logistics (e.g., package tracking), and security applications (e.g., localizing authorized persons in high-security areas).

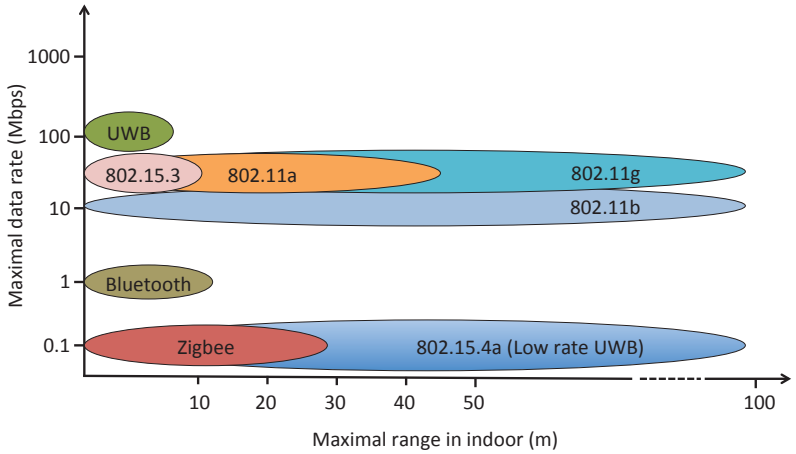

Figure 1.2: Maximal range and data rate of principal WLAN/WPAN standards.

1.3 UWB Regulations

Devices utilizing UWB spectrum are subject to stringent requirements because the UWB spectrum underlays other existing licensed and unlicensed spectrum allocations. In order to optimize spectrum use and to reduce interference to existing systems, regulatory bodies in both Europe and the United States impose very restrictive rulings to UWB devices. Figure 1.3 compares the spectral occupation and emitted power of different radio systems. The essence of these rulings is that the PSD of the modulated UWB signal must satisfy predefined spectral masks specified by spectrum-regulating agencies.

In the United States, the FCC requires that UWB devices for indoor applications occupy more than 500 MHz of bandwidth in the 3.1 - 10.6 GHz band, according to the spectrum mask of Fig. 1.4. As observed, the PSD must not exceed -41.25 dBm/MHz of bandwidth. This limit is low enough not to cause any interference to other services sharing the same bandwidth. Cellular phones, for example, transmit up to 30 dBm per MHz, which is equivalent to 10^7 higher PSD than UWB

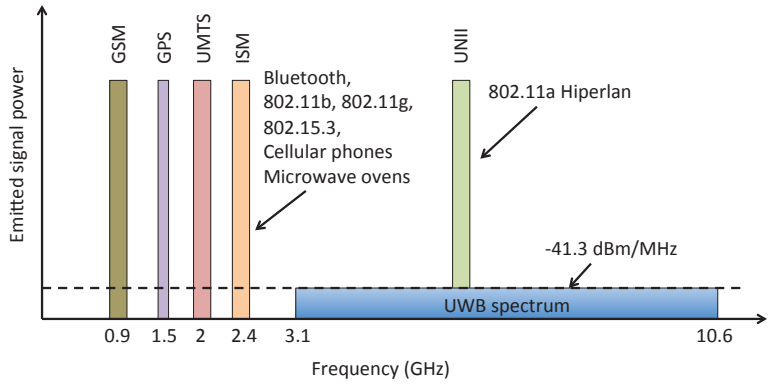

Figure 1.3: Different radio systems present in UHF and SHF bands.

transmitters are permitted.

The European Commission is responsible for adopting technical measures to ensure harmonized conditions with regard to the availability and efficient use of the radio spectrum in the European Union internal market. The studies are carried out in close cooperation with group SE24 of the European Conference of Postal and Telecommunications Administrations (CEPT), which more particularly analyzes the possible impact of UWB on the existing systems. Similarly, the European Telecommunications Standards Institute (ETSI) established the Task Group ERM TG31 to develop a set of standards for short-range devices using UWB technology. It was not until 2006 that CEPT could provide a viable first regulation ensuring coexistence with other systems communications.

In February 2007, the European Communications Committee (ECC) permitted the emission in the UWB. The commission decision contains two separate masks for before and after 31st December 2010 [ECC]. Figure 1.4 shows the emission masks defined by CEPT for UWB communications. The emission limits strongly differentiates from U.S. regulations mainly because of a greater concern about problems of interference and coexistence with other radio technologies. With an adjustment due to the 2009 amendment has lead to the regulations described in Fig. 1.4 to be even more stricter, and advocates over the long term use of the band of 6 to 8.5 GHz.

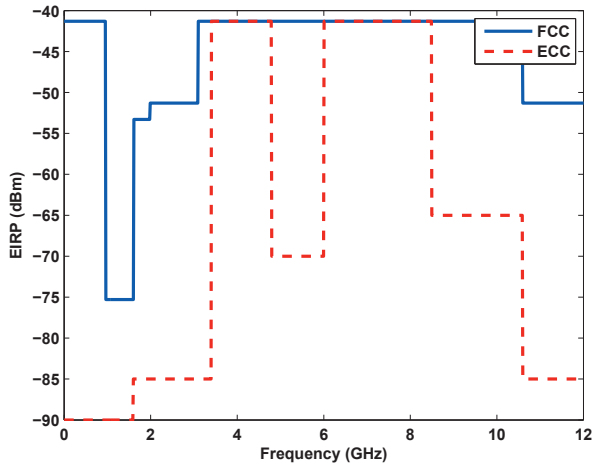

Figure 1.4: UWB Spectral Mask by different regulatory authorities.

1.4 Transmission Techniques for UWB

Several transmission techniques have been studied for UWB and can be divided into:

- Monoband Approach → Impulse radio UWB (IR-UWB)
- Multiband Approach → Multi-band orthogonal frequency division multiplexing (MB-OFDM)

In general, we can contrast these two techniques characterizing the first as a "series" approach in which the symbol stream is transmitted serially, and the second a "parallel" approach where multiple symbols are transmitted at any instant.

1.4.1 Impulse Radio UWB

Single band UWB modulation (also called impulse radio) is based on continuous transmission of very short-time impulse radio which are typically the derivative of Gaussian pulses. Each pulse has an ultra wide spectral occupation in the frequency domain. This type of transmission does not require the use of additional carrier modulation as the pulse will propagate well in the radio channel. The technique is therefore a baseband signal approach. As Impulse radio is carrier-less, so it only has base-band processing and no intermediate frequency (IF) processing is needed. This makes impulse radio devices much cheaper than other communication devices.

1.4.2 Multi-band Orthogonal Frequency Division Multiplexing

A second solution, in the context of high data-rate is the multi-band approach with orthogonal frequency division multiplexing (OFDM) modulation, proposed by IEEE 802.15 Task Group 3a [Bat04]. MB-OFDM technology to divide the whole bandwidth into 14 subbands of approximately 528 MHz. A signal symbol is spread over all the subbands, modulated and transmitted by all the subcarriers simultaneously. One big advantage of this approach is that all the results of OFDM, a pretty mature technology, can be applied immediately. By dividing the whole bandwidth into subbands, the signal can be shaped to fit virtually any spectral mask.

In this technique, the spectrum defined by the FCC is divided into 14 non overlapping sub-bands of 528 MHz each. These sub-bands are then divided into five groups. Fig. 1.5 presents these sub-bands classified into different groups. In each sub-band, OFDM modulation is applied and the signal is distributed among 128 subcarriers which leads to a sub-carrier separation of $\Delta f = 4.125$ MHz. Quadrature phase shift keying (QPSK) modulation is used as a modulation scheme for each sub carrier. This configuration allows a flexible management of radio spectrum. Also, it is quite easier to abide by the regulations on the spectral mask of different countries. Multiple access within the users of a same group of a particular sub-band is made by the use of time-frequency codes. In a group of sub-bands, the communication of a particular user passes regularly from one band to another. This pattern of the change of bands depends on the time-frequency code, which is unique for every user. The advantages of MB-OFDM radio access technology lies mainly in its low complexity. If the frequency bands are limited to the first group of bands, existing RF systems and components can also be used for the implementation of the system. However, the transmitted signals are not pulse-based, therefore, this technology does not benefit from some advantages linked to the ultra wide bandwidth such as the robustness to the channel variations.

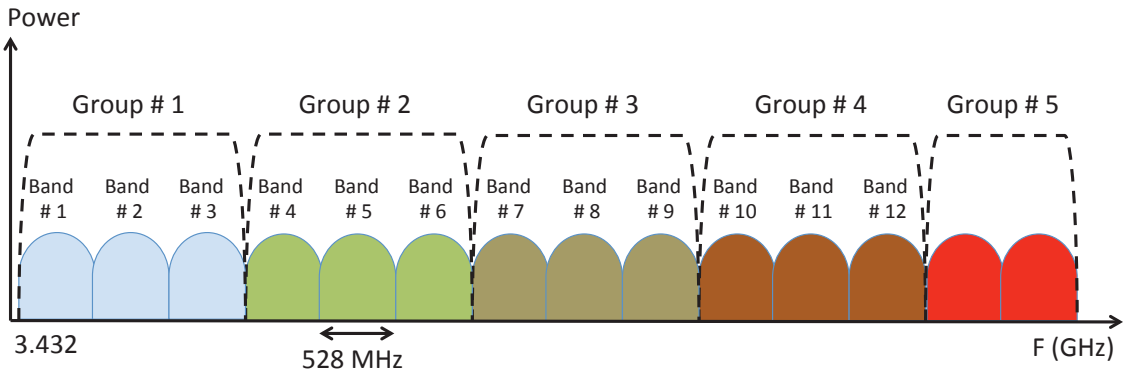

Figure 1.5: Division of the UWB spectrum from 3.1 to 10.6 GHz into band groups containing subbands of 528 MHz in MB-OFDM systems.

1.5 UWB Data Modulation Methods

A number of modulation schemes may be used with UWB systems. The potential modulation schemes include both orthogonal and antipodal schemes. As a helpful categorization of modulation methods, two basic types of modulation methods can be defined for UWB communication. These are shown in Fig. 1.6 as *time-based* techniques and *shape-based* techniques.

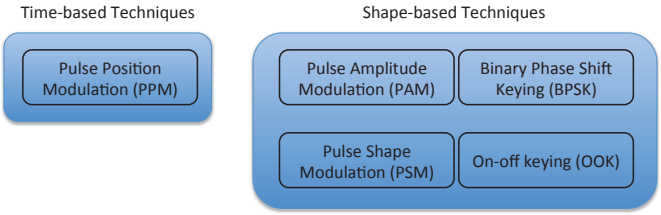

Figure 1.6: Division of different modulation methods for UWB communications.

1.5.1 Pulse Position Modulation (PPM)

By far the most common method of modulation in the initial UWB literature is pulse position modulation (PPM) where each pulse is delayed or sent in advance of a regular time scale. Thus, a binary communication system can be established with a forward or backward shift in time. By specifying specific time delays for each pulse, an M-ary system can also be created. The transmitted signal for a PPM modulated signal can be written as

$$s_{ppm}^{k}(t) = \psi(t - d_k\delta) \tag{1.3}$$

where $d_k \in \{0, 1\}$ represents the k^{th} transmitted bit and δ is the time shift bewteen the modulation states. The value of δ may be chosen according to the autocorrelation characteristics of the pulse. For instance, to implement a standard PPM with orthogonal signals, the optimum value of $\delta(\delta_{\text{opt}})$ which results in zero autocorrelation is such as

$$\rho(\delta_{\text{opt}}) = \int_{-\infty}^{\infty} \psi(\tau)\psi(\delta_{\text{opt}} - \tau)d\tau = 0 \tag{1.4}$$

The advantages of PPM mainly arise from its simplicity and the ease with which the delay may

be controlled. On the other hand, for the UWB system extremely fine time control is necessary to modulate pulses to subnanosecond accuracy.

1.5.2 Pulse Amplitude Modulation (PAM)

pulse amplitude modulation (PAM) is an alternative to PPM. In PAM, the amplitude of the transmitted pulse is varied to encode data symbols for different modulation states. Theoretically, an unlimited number of levels of amplitude can be used but in general, amplitude modulation is not the preferred way for most short range communication. The major reasons include the fact that, an amplitude-modulated signal which has a smaller amplitude is more susceptible to noise interference than its larger amplitude counterpart. Furthermore, more power is required to transmit the higher amplitude pulse.

Binary Phase Shift Keying (BPSK) Due to aforementioned reasons, in practice, PAM is often limited to two states ($\pm$). In these conditions, 2-PAM modulation is a form of bi-phased modulation or BPSK. BPSK provides good robustness to the channel variations and simplifies the synchronization. The transmitted signal for 2-PAM can be written as

$$s^k_{bpsk}(t) = (2d_k - 1)\psi(t) \tag{1.5}$$

where $\psi(t)$ is the ultra-short UWB pulse. One of the reasons for the use of BPSK modulation, especially in comparison with pulse position modulation (which is a mono-phase technique) is the 3-dB gain in power efficiency. This is simply a function of the type of modulation method. That is, BPSK modulation is an antipodal modulation method, whereas pulse position modulation, when separated by one pulse width delay for each pulse position, is an orthogonal modulation method.

On-off keying (OOK) Another variant of the PAM is on-off keying (OOK) where a pulse is transmitted when data symbol is '1' and no pulse is transmitted when data symbol is '0'. The transmitted signal for OOK can be written as

$$s^k_{ook}(t) = d_k\psi(t) \tag{1.6}$$

OOK has a reduced complexity and low implementation cost. The transmitter for OOK consists of a simple RF switch which turns on and off to represent data. This saves power of the transmitter as well. At the receiver end, the signal can be detected by using either coherent or non coherent receivers. The major difficulty of OOK is the presence of multipath, in which echoes of the original or other pulses make it difficult to determine the absence of a pulse. Moreover, on-off keying is a binary modulation method and cannot be extended to an M-ary modulation.

1.5.3 Pulse Shape Modulation (PSM)

PSM is an alternative to PAM and PPM modulations. As depicted in Fig. 1.7d, in PSM the information data is encoded by different pulse shapes. This requires a suitable set of pulses for higher order modulations. The transmitted signal for PSM can be represented as

$$s^k_{psm}(t) = (1 - d_k)\psi_0(t) + (d_k)\psi_1(t) = \psi_{d_k}(t) \tag{1.7}$$

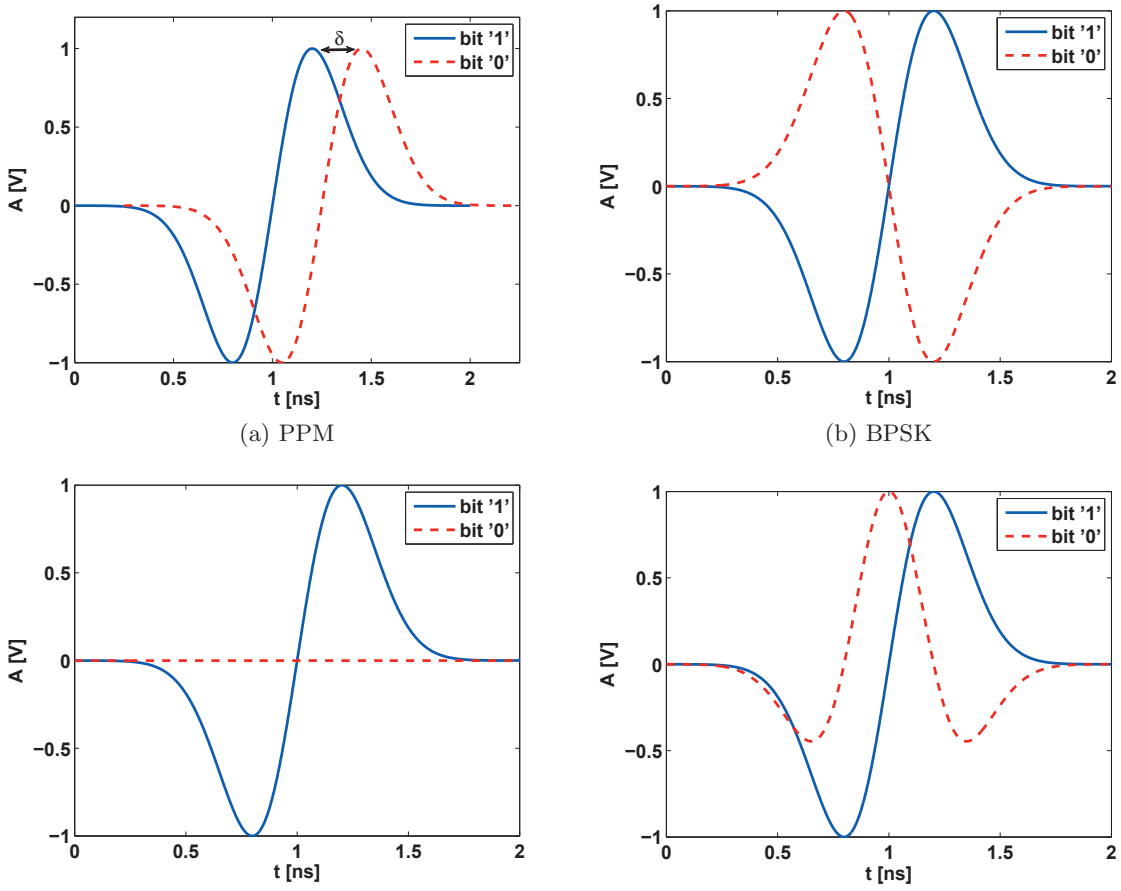

(a) PPM (b) BPSK

(c) OOK (d) PSM

Figure 1.7: IR-UWB modulation schemes

Modified Hermite polynomial functions [Wei04a], wavelets [Con99], and prolate spheroidal wave functions (PSWF) [Zhu03] have been proposed in the literature as pulse sets for PSM systems. The orthogonality of signals used in PSM is a desirable property since it permits an easier detection at the receiver. It is also possible to combine two modulation schemes to create higher-order modulations, called as hybrid modulations. For example, we can create a modulation of 64 states by combining a 32-PPM modulation with a 2-PAM modulation.

1.6 Spectrum randomization and multiple access

Up to now, we assumed that each symbol was transmitted by a single pulse. This continuous pulse transmission can lead to strong lines in the spectrum of the transmitted signal. The regularity of these energy spikes may interfere with other communication systems over short distances. In practical systems, due to the very restrictive UWB power limitations, such a described UWB system shows a high sensitivity to interference from existing systems.

In order to minimize the potential interference from UWB transmissions and provide multiple access capability, a randomizing technique is applied to the transmitted signal. This makes the spectrum of the UWB signal more noise-like. The two main randomizing techniques used for IR-UWB systems are *time-hopping* (TH) and *direct-sequence* (DS). The TH technique randomizes the position of the transmitted UWB impulse in time whereas the DS approach is based on continuous

transmission of pulses composing a single data bit. The DS-UWB scheme is similar to conventional DS spread-spectrum systems where the chip waveform has a UWB spectrum.

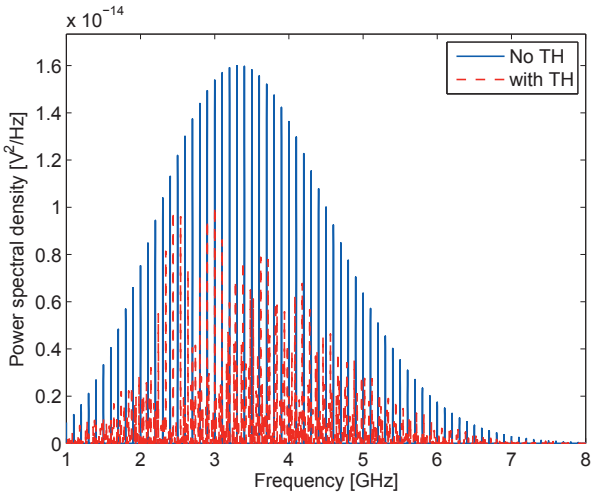

Figure 1.8: Spectrum of UWB pulse train with and without the randomization technique.

The spectrum of a pulse train with and without randomizing technique is depicted in Fig. 1.8. As can be seen, the spectrum contains strong spectral lines at multiples of the pulse repetition frequency. The envelope of the spectrum is that of a single UWB pulse which in this case is of the Gaussian second derivative. Randomizing the position in time of the generated pulses using data modulation and other randomizing techniques will affect the spectrum in such a way that the energy spikes are spread all over the spectrum, which is therefore smoothed. Figure 1.8 also shows the spectrum of a pulse train that includes time hopping based randomization. We can verify that the TH code has the effect of diminishing the number of peaks with highest power contribution since the same power is distributed over a large number of spectral lines.

1.6.1 Data Modulation with Time-Hopping (TH-UWB)

As described above, the multiple access and power limit considerations motivate the use of an improved UWB transmission scheme where each data symbol is encoded by the transmission of multiple impulse radios shifted in time. In the TH scheme, the position of each impulse is determined by a pseudo-random (PR) code. In this way, more energy is allocated to a symbol and the range of the transmission is increased. Besides, different users, distinguished by their unique TH code, can transmit at the same time.

A typical TH format for the m-th user is written as follows [Opp04, DB06].
For PAM modulation

$$s^{(m)}(t) = \sum_{i=-\infty}^{\infty} \left[\sum_{j=0}^{N_f-1} \psi(t - iT_s - jT_f - c_j^{(m)} T_c) \right] d_i^{(m)} \tag{1.8}$$

For PPM modulation

$$s^{(m)}(t) = \sum_{i=-\infty}^{\infty} \sum_{j=0}^{N_f-1} \psi(t - iT_s - jT_f - c_j^{(m)} T_c - d_i^{(m)} \delta) \tag{1.9}$$

and for PSM modulation

$$s^{(m)}(t) = \sum_{i=-\infty}^{\infty} \sum_{j=0}^{N_f-1} \psi_{d_i^{(m)}}(t - iT_s - jT_f - c_j^{(m)} T_c) \tag{1.10}$$

where $d_i^{(m)}$ is the i-th data bit of user m. Here, N_f is the number of impulses transmitted for each information symbol. In this improved scheme, the total symbol transmission time T_s is divided into N_f frames of duration T_f and each frame is itself sub-divided into slots of duration T_c. Each frame contains one impulse in a position determined by the PR TH code sequence $c_j^{(m)}$ (unique for the m-th user) and the symbol to be encoded. The TH spreading can be combined with PAM, PPM, and PSM. However, OOK cannot take advantage of the TH spreading because of the blank transmission in the case of bit "0".

1.6.2 Data Modulation with Direct-sequence (DS-UWB)

In DS-UWB, the pulse waveform takes the role of the chip in a spread spectrum system [Voj03]. Similar in spirit to spread spectrum techniques, DS-UWB employs sequences of UWB pulses (analogous to "chips"). Each user is distinguished by its specific pseudo random sequence which performs pseudo random inversions of the UWB pulse train. A data bit is then used to modulate these UWB pulses. The resulting signal will then be a continuous transmission of UWB pulses whose number depends on the length of the pulse itself and the bit rate defined by the system.

The DS-UWB scheme is suitable for PAM, OOK and PSM modulations. Since PPM is intrinsically a time-hopping technique, it is not used for DS-UWB transmission. The expression characterizing the DS spreading approach in the case of PAM and OOK modulations for user m is given by [DB06]

$$s^{(m)}(t) = \sum_{i=-\infty}^{\infty} \left[\sum_{j=0}^{N_c-1} \psi(t - iT_s - jT_c) c_j^{(m)} \right] d_i^{(m)} \tag{1.11}$$

where $d_i^{(m)}$ is the i-th data bit, $c_j^{(m)}$ is the j-th chip of the PR code, $\psi(t)$ is the pulse waveform of duration T_p, T_c is the chip length (equal to T_p), N_c is the number of pulses per data bit, and m stands for the user index. The PR sequence has values in $\{-1, +1\}$ and the bit length is $T_s = N_c T_c$.

For PSM, the signal model for the m-th user is

$$s^{(m)}(t) = \sum_{i=-\infty}^{\infty} \sum_{j=0}^{N_c-1} \psi_{d_i^{(m)}}(t - iT_s - jT_c) c_j^{(m)} \tag{1.12}$$

where the bit $d_i^{(m)}$ determines the choice of the UWB pulse waveform to be transmitted. Figure 1.9 compares the temporal behavior of binary TH-UWB and DS-UWB transmission techniques.

1.7 UWB Propagation Channels

Accurate knowledge of the wireless propagation channel is of great importance when designing radio systems. A realistic radio channel model that provides insight into the radio wave propagation mechanisms is essential for the design and successful deployment of wireless systems. The type of

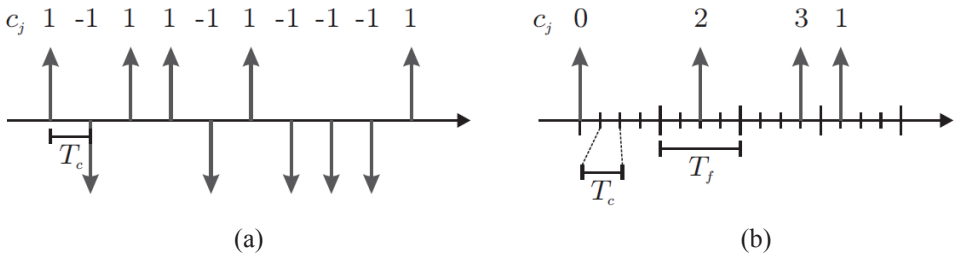

Figure 1.9: Time domain representation of IR-UWB spreading techniques. (a) TH-UWB (b) DS-UWB

channel model that is desired depends critically on the carrier frequency, bandwidth, the type of environment, and the system under consideration. For example, different types of channel models are needed for indoor and outdoor environments, and for narrowband, wideband and UWB systems.

In a wireless system, the transmitted signal interacts with the physical environment in a complex manner. The signal arriving at the RX is in general a summation of both direct LOS and several multipath componentss (MPCs). Multipath occurs due to the three basic multipath propagation mechanisms, namely, reflection, diffraction, and scattering of the transmitted signal. All three of these phenomena cause radio signal distortions and give rise to signal fades, as well as additional signal propagation losses in a wireless communication system. If however, the transmitted signal has a large bandwidth as in UWB, diverse frequency components are attenuated in different ways. The signal thus undergoes a frequency selective fading and therefore, the received power varies with the frequency. Due to this reason, the conventional channel models developed for narrowband transmissions are inadequate for UWB transmission.

The channel impulse response (CIR) of narrow band signals can be modeled as the sum of different MPCs [Par00]. The channel model will only be deterministic if all the echoes of the received signal are resolvable. However, because of the narrow bandwidth, not all of the MPCs are resolvable. Therefore, the CIR can be written as

$$h(t,\tau) = \sum_{i=1}^{N} a_i \delta(t-\tau_i) = \sum_{i=1}^{\acute{N}} \sum_{k} \tilde{a}_{ik} \delta(t-\tau_i) = \sum_{i=1}^{\acute{N}} c_i \delta(t-\tau_i) \tag{1.13}$$

where N is the number of MPCs, while $\acute{N}$ is the number of resolvable MPCs where one resolvable MPC consists of k physical MPCs and c_i is the resultant amplitude of the resolvable multi-path components. In the case of UWB systems, CIR differs from the narrowband propagation channel in many respects

- Due to the fine temporal resolution, the number of physical MPCs which form one resolvable MPC is lower
- Each of the MPCs is subjected to some distortions due to the frequency dependent effects

From [Mol05], the CIR for a UWB channel can be written as

$$h(t,\tau) = \sum_{i=1}^{N} a_i(t) \xi_i(t,\tau) \star \delta(t-\tau_i) \tag{1.14}$$

where $\star$ is the convolution operator and $\xi_i(t,\tau)$ denotes the (time-averaging) distortion of the i-th

echo due to the frequency selectivity of the interactions with the environment.

Depending upon the bandwidth of the UWB signal, the UWB channels can be categorized as *sparse* and *dense*. The *sparse* channel is the one in which the arrival time of certain MPCs is larger than the inverse of the bandwidth of the channel. Therefore, every resolvable MPC might not carry significant amount of energy. On the other hand, in the *dense* channel, the inter arrival time of the MPCs is smaller than the resolvable bandwidth. This significantly impacts the design of Rake receivers [Mol05]. Dense or sparse power delay profile (PDP) depend on the considered bandwidth and the considered environment. Channels with larger bandwidths are more likely to be sparse than the channels with lesser bandwidths. However, large number of reflecting and diffracting objects in the propagation environment will lead to dense channels even for extremely large bandwidths. For instance, dense channels are observed for a large bandwidth of 7.5 GHz in an industrial environment [Kar04a], while residential environments [Cho05] show sparse behavior at that bandwidth. More information on UWB channels can be found in [Mol05].

In order to understand and summarize the characteristics of UWB channels, several statistical models have been developed. We now discuss the two widely adopted models proposed by IEEE to evaluate the performance of the standards IEEE 802.15.3a and IEEE 802.15.4a. These two models are based on the well-known Saleh-Valenzuela (SV) model [Sal87].

1.7.1 IEEE 802.15.3a Channel Model

The IEEE 802.15.3a Working Group, tasked with defining a PAN physical layer standard based on UWB and compatible with the medium access control standard of IEEE 802.15.3-2003, formed a subgroup for the development of a common UWB channel model, as a unique channel characterization is absolutely necessary when selecting parts of the new standard [Mol03]. The model aims to capture the multipath characteristics of typical indoor environments, where IEEE 802.15.3a devices are expected to operate. In addition to the UWB channel measurements performed in the last couple of years, a number of measurement campaigns were carried out by the participants of the task group. A summary of these measurements can be found in [Foe02].

Among the many indoor channel models considered, the final version adopted for the evaluation of the new standard is the one based on a modified SV model [Sal87] that best fits the measurements. As a result of the very fine time resolution UWB waveforms provide, reflections from different objects tend to arrive in clusters. For instance, reflections from a desk result in a cluster of paths, which is followed by another cluster created by the wall a few meters behind the desk, etc. This phenomenon is also observed in the SV model even though it is proposed for indoor channels with comparably smaller bandwidths that are on the order of 100 MHz.

In the original SV model, inter-arrival times between multipath components are exponentially distributed (see Fig. 1.10). Moreover, the multipath components are distinguished based on the cluster and the ray within the cluster. Thus four parameters are required to describe each environment: the cluster arrival rate, the ray arrival rate within the cluster, the cluster decay factor and the ray decay factor, where the decay factors are derived from the PDP. However, due to ultra-wide bandwidths the amplitude statistics of the paths do not follow a Rayleigh distribution as in the original SV model. The measurements in UWB channels indicate that rather the amplitude statistics fit either a lognormal or a Nakagami distribution. Therefore, before adopting for the IEEE 802.15.3a standard channel model, the SV model had to be modified by employing a lognormal

amplitude distribution.

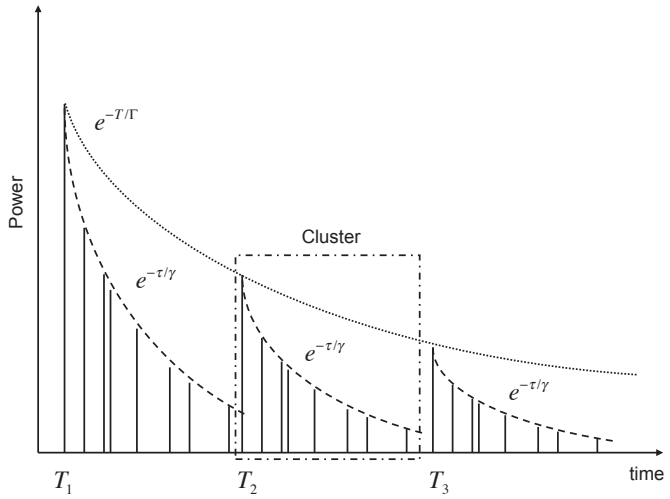

Figure 1.10: Power delay profile of Saleh-Valenzuela model.

A. Power Delay Profile

The multipath model approved by the IEEE 802.15.3a committee has the following discrete time impulse response [Mol03]

$$h_i(t) = X_i \sum_{l=0}^{L-1} \sum_{k=0}^{K-1} \alpha_{k,l}^i \delta(t - T_l^i - \tau_{k,l}^i) \tag{1.15}$$

where $\alpha_{k,l}$ is the gain of the k-th path in the l-th cluster, T_l is the delay of the l-th cluster, $\tau_{k,l}$ is the delay of the k-th path relative to the l-th cluster arrival time, $\delta(.)$ is the Dirac delta function, X_i represents the log-normal shadowing and i refers to the i-th realization.

The cluster arrivals and the ray arrivals within clusters follow a Poisson process and the power of these clusters and rays decays exponentially with increasing delay from the first ray. Thus, they have the probability density function (PDF) representations given by

$$p(T_l|T_{l-1}) = \Lambda \exp[-\Lambda(T_l - T_{l-1})], \quad l > 0 \tag{1.16}$$

$$p(\tau_{k,l}|\tau_{k-1,l}) = \lambda \exp[-\lambda(\tau_{k,l} - \tau_{k-1,l})], \quad k > 0 \tag{1.17}$$

Here, T_l is also the arrival time of the first path of the l-th cluster, i.e., $\tau_{0,l} = 0$, Λ stands for the cluster arrival rate and λ is the arrival rate of a path within each cluster.

The channel coefficients are determined through

$$\alpha_{k,l} = p_{k,l} \varrho_l \varpi_{k,l} \tag{1.18}$$

Signal inversion caused by reflections is indicated by the variable $p_{k,l}$, the random equiprobable + or - signs of the channel coefficients while amplitude statistics are found to best fit the log-normal distribution rather than the Rayleigh that was used in the original SV model. In addition, the large-scale fading is also lognormally distributed. In particular, $20\log_{10}\varrho_l\varpi_{k,l}$ is a normal (Gaussian) random variable with the mean $\mu_{k,l}$ and the variance $\sigma_1^2 + \sigma_2^2$, where σ_1^2 and σ_2^2 are due to the fading on each cluster and ray, respectively. Such a normal random variable is described

shortly with $\mathcal{N}(\mu_{k,l}, \sigma_1^2 + \sigma_2^2)$. If the mean energy of the first arriving path is Ω_0, and Γ and γ are the cluster decay factor and the ray decay factor, respectively, then

$$\mathrm{E}[(\varrho_l \varpi_{k,l})^2] = \Omega_0 \exp(-T_l/\Gamma) \exp(-\tau_{k,l}/\gamma) \tag{1.19}$$

From this, $\mu_{k,l}$ can be given as

$$\mu_{k,l} = \frac{10\ln\Omega_0 - 10T_l/\Gamma - 10 - \tau_{k,l}/\gamma}{\ln(10)} - \frac{\left(\sigma_1^2 + \sigma_2^2\right)\ln(10)}{20} \tag{1.20}$$

And finally, for each channel realization, the total power of the power delay profile is normalized to unity, and subsequently a "bulk shadowing" is superimposed, i.e., the total impulse response is multiplied with a random variable X_i that is lognormally distributed with a standard deviation σ_x. This makes sure that the total PDP shows the correct shadowing distribution, and it is not necessary to compute analytically the interrelationship between the cluster shadowing variance and the bulk shadowing variance.

Note that, a complex tap model was not adopted here. The complex baseband model is a natural fit for narrowband systems to capture channel behavior independently of carrier frequency, but this motivation breaks down for UWB systems where a real valued simulation at RF may be more natural.

B. Temporal Dispersion

The time dispersion of UWB channels can be quantified by their mean excess delay time and rms (root mean square) delay spread [Rapp02]. These two parameters are important for evaluating the performance of digital systems. Delay spreads restrict the transmitted data rates and could limit the capacity of the system when multi-user systems are considered. The mean excess delay τ_m is the first moment of the power delay profile and can be defined as

$$\tau_m = \frac{\sum_k \alpha_k^2 \tau_k}{\sum_k \alpha_k^2} \tag{1.21}$$

The rms delay spread τ_{rms} defined as the square root of the second central moment of the power delay profile, i.e.,

$$\tau_{rms} = \frac{\sum_k \alpha_k^2 \left(\tau_k - \tau_m\right)^2}{\sum_k \alpha_k^2} \tag{1.22}$$

If the coherence bandwidth is the bandwidth over which the frequency correlation function is above 0.5, then the coherence bandwidth is approximately [Rap02]

$$B_c \approx \frac{1}{5\tau_{rms}} \tag{1.23}$$

From the rms delay spread values listed in Table 1.1, the coherence bandwidths of CM1, CM2, CM3, and CM4 channel models will be approximately 40 MHz, 25 MHz, 13.3 MHz, and 8 MHz respectively.

If the pulse repition frequency (PRF) is less than the channel coherence bandwidth, the inter-frame interference (IFI) and inter-symbol interference (ISI) won't be a problem for the UWB

communication system. However, when the PRF is above the channel coherence bandwidth, signals of multi-paths will cause IFI/ISI at receivers. The highest UWB coherence bandwidth, which is about 40 MHz, is far less than the expected UWB symbol rates, which are usually above hundreds of mega hertz. Therefore, IFI/ISI issues will be persistent with UWB communications.

C. Path loss Model

A key parameter for any wireless system is the path loss (PL), i.e., the ratio of the received power (averaged over both the small-scale and the large-scale fading) to the transmit power. PL in free-space propagation is given by $(\lambda/4\pi d)^2$, which predicts predicts that signal power will decrease with the square of increasing frequency. This shows the presence of both distance and frequency dependency in PL. For UWB systems, PL at different frequencies can be noticeably different. This is related to the fact that the free-space attenuation, as well as the effect of basic propagation processes like diffraction and reflection at dielectric walls, changes with frequency. Therefore, the conventional PL model used in narrowband analysis needs to be investigated more closely in order to justify its application to UWB systems.

PL modeling can be simplified by assuming that the frequency dependence and the distance dependence can be treated independently of each other:

$$PL(f,d) = PL(f).PL(d) \tag{1.24}$$

The distance dependency of PL, $PL(d)$, is same as in most narrowband channels. Specifically, the PL in dB is usually described by

$$PL_{\mathrm{dB}}(d) = PL_0 + 10n\log_{10}\left(\frac{d}{d_0}\right) + S \tag{1.25}$$

where the reference distance d_0 is set to 1 m, PL_0 is the PL at the reference distance. The PL exponent n depends on whether or not a line of sight (LOS) connection exists between the transmitter and receiver or not ($n = 2$ for free-space). Added (on a decibel scale) to the PL is the shadowing fading parameter S, which is (again in decibels) a Gaussian-distributed random variable with zero mean and standard deviation σ_S.

The frequency dependence of the PL is usually given as

$$\sqrt{PL(f)} \propto f^{-\kappa} \tag{1.26}$$

where κ is the frequency dependency decaying factor. Many simulations in literature use the simplified free-space PL model $PL_{\mathrm{dB}}(d) = PL_0 + 20\log_{10}(d)$. However, performance measures obtained under this model are utterly unrealistic for NLOS situations. The final report of the 802.15.3a channel modeling subgroup recommends the use of the Ghassemzadeh pathloss model, developed in [Gha04a].

D. Paramterization

The parameters of the standard channel model have been adjusted to fit the measurements made for a number of different scenarios that consider the existence of a LOS path as well as the distance between the transmitter and the receiver. This in turn has given rise to four channel models. The CM1 model, which is based on LOS channel measurements and the CM2 model, which does not

	CM1	CM2	CM3	CM4
Target Channel Characteristics				
Mean excess delay (τ_m) [ns]	5.05	10.38	14.18	
RMS delay spread (τ_{rms}) [ns]	5.28	8.03	14.28	25
NP_{10dB} (number of paths within 10dB of the strongest path)			35	
$NP_{85\%}$ (number of paths that capture 85% of channel energy)	24	36.1	61.54	
Model Parameters				
Cluster arrival rate (Λ) [1/ns]	0.0233	0.4	0.0667	0.0667
Ray arrival rate (λ) [1/ns]	2.5	0.5	2.1	2.1
Cluster decay factor (Γ)	7.1	5.5	14.00	24.00
Ray decay factor (γ)	4.3	6.7	7.9	12
Standard deviation of cluster lognormal fading term (σ_1) [dB]	3.4	3.4	3.4	3.4
Standard deviation of ray lognormal fading term (σ_2) [dB]	3.4	3.4	3.4	3.4
Standard deviation of lognormal fading term for total multipath realizations (σ_x) [dB]	3	3	3	3
Model Characteristics				
Mean excess delay (τ_m) [ns]	5.0	9.9	15.9	30.1
RMS delay spread (τ_{rms}) [ns]	5	8	15	25
NP_{10dB} (number of paths within 10dB of the strongest path)	12.5	15.3	12.9	41.2
$NP_{85\%}$ (number of paths that capture 85% of channel energy)	20.8	33.9	64.7	123.3
Channel energy mean [dB]	-0.4	-0.5	0.0	0.3
Channel energy standard deviation [dB]	2.9	3.1	3.1	2.7

Table 1.1: Characteristics and parameters for the 4 environments of IEEE 802.15.3a channel model

have LOS, have up to 4 m coverage. A longer distance, up to 10 m coverage, is targeted with the CM3 channel in the absence of the LOS path. The CM4 channel model was generated to fit a 25 ns root mean square (rms) delay spread to represent an extreme non line of sight (NLOS) multipath channel [Foe02]. As this model was developed by the IEEE 802.15.3a standardization group for UWB communications systems in order to compare standardization proposals for high-data-rate WPANs, the considered environments were office and residential indoor scenarios with a range of less than 10m.

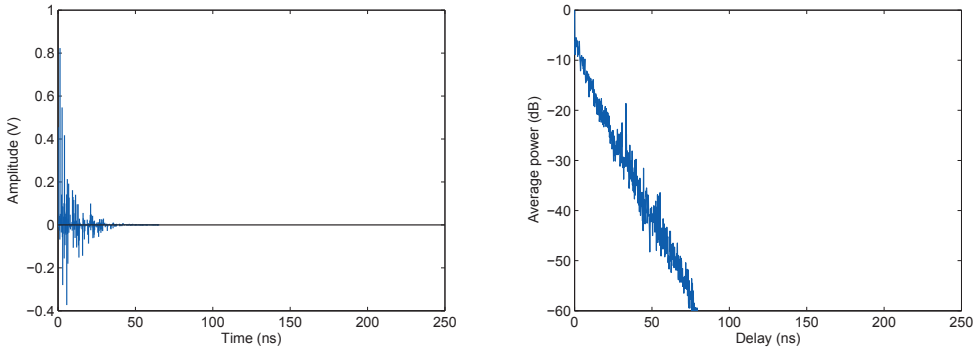

(a) Impulse Response (b) Power Decay Profile

Figure 1.11: IEEE 802.15.3a CM1 channel model

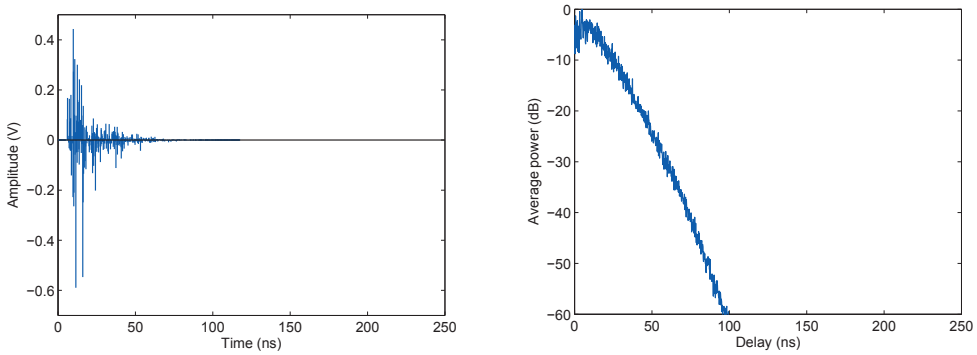

(a) Impulse Response (b) Power Decay Profile

Figure 1.12: IEEE 802.15.3a CM2 channel model

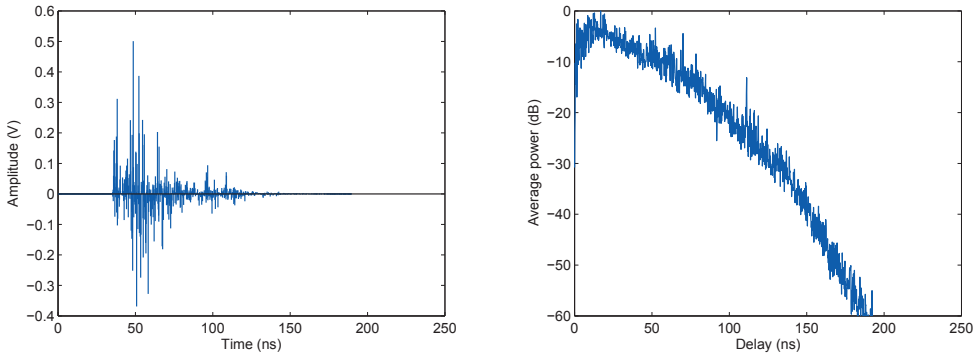

(a) Impulse Response (b) Power Decay Profile

Figure 1.13: IEEE 802.15.3a CM3 channel model

Typical realizations from the four channel models are shown in Figs. 1.11-1.14, where the time resolution is 167ps. A quick inspection of the figure indicates that the delay spread increases with the distance between the transmitter and the receiver because the propagation paths become more nonuniform as the distance increases [Zhu03]. Table 1.1 summarizes the parameters for different channel models.

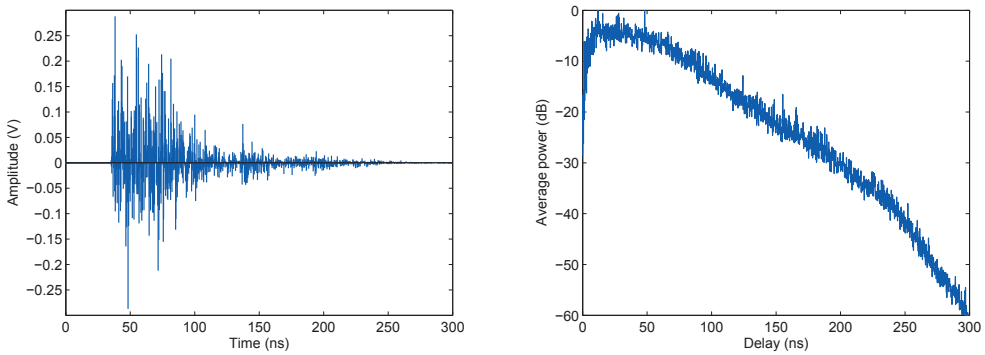

(a) Impulse Response (b) Power Decay Profile

Figure 1.14: IEEE 802.15.3a CM4 channel model

1.7.2 IEEE 802.15.4a Channel Model

To adapt to a larger number of potential applications, the IEEE 802.15.4a Working Group proposed an extended model in both frequency and types of environments [Mol04]. Target applications are of low data-rate (1 kbit/s to several Mbit/s), indoor environments (residential and office), external but also industrial (factories, etc..) and wireless body area network (WBAN) applications. Two frequency bands of UWB are considered: 3 to 10 GHz and 0,1 to 1 GHz.

We only discuss briefly the model corresponding to the high frequency band. The general form of the statistical model is similar to IEEE 802.15.3a model. However, some differences in the impulse response can be noted:

- The number of clusters is a Poisson-distributed random variable with PDF

$$pdf_L(L) = \frac{\left(\bar{L}^L\right)\exp\left(-\bar{L}\right)}{L!} \tag{1.27}$$

  where the mean $\bar{L}$ completely characterizes the distribution and is a parameter of the model.

- The ray arrival times are modeled with a mixture of two Poisson processes as follows

$$p(\tau_{k,l}|\tau_{k-1,l}) = \beta\lambda_1\exp[-\lambda_1(\tau_{k,l}-\tau_{k-1,l})] + (1-\beta)\exp[-\lambda_2(\tau_{k,l}-\tau_{k-1,l})], \quad k>0 \tag{1.28}$$

  where β is the mixture probability and λ_1 and λ_2 are the reay arrival rates.

- And finally, the cluster decay rates are found to depend linearly on the arrival time of the cluster:

$$\gamma_l = k_\gamma T_l + \gamma_0 \tag{1.29}$$

  where k_γ describes the increase of the decay constant with delay.

The main difference of the IEEE 802.15.4a model from IEEE 802.15.3a model resides in taking into account a realistic modeling of propagation losses, both in distance and frequency. The proposed model is intended as independent of the antennas used. This model has the advantage of being very complete, at the price of an increased complexity. Several sets of parameters are provided, based on experimental measurements for each environment: residential [Cho04], office [Bal04, Sch04], industrial [Kar04b] and outdoor [Bal04, Kei04].

1.8 IR-UWB Receiver Types

Different types of receivers have been used for IR-UWB communication systems. UWB receivers can be broadly classified into coherent and non-coherent receivers.

1.8.1 Coherent Rake Receiver

One of the key advantages of UWB signals is the immunity to fading. Depending on the bandwidth, a receiver can resolve MPCs whose path lengths differ by a few tens of centimeters, e.g., 15 cm for a signal bandwidth of 2 GHz. An increase in the transmission bandwidth improves the capability of resolving MPCs. Each of the resolved MPCs can be viewed as independently fading, thereby providing a high degree of diversity (delay diversity, frequency diversity) for the transmission. However, in order to utilize the available diversity, the receiver must be able to extract and process the different MPCs.

The most common approach to exploit the high degree of multipath diversity is to use RAKE receivers, as implemented successfully in the "traditional" wideband CDMA systems. Therefore, it is straightforward to apply this concept for detection in IR-UWB. Basically, a RAKE receiver consists of multiple correlators (also called RAKE fingers). Each finger matches (correlates) the received pulse sequence (spread by the multipath channel) with a delayed version of a template pulse $v(t - \tau_i)$

Combining all resolvable paths as in the All-Rake (A-Rake) receiver is quivalent to matched filter (MF) and therefore (with known channel coefficients) optimum with respect to the BER performance. However, the number of MPCs that can be utilized in a typical Rake combiner is limited by power consumption constraints, complexity considerations, and the availability of channel estimates. In typical UWB scenarios, the available number of MPCs at the receiver is often more than 100; hence the A-Rake UWB receiver serves only as a benchmark and provides a bound on the performance that is achievable by other suboptimal combining schemes. The complexity can be reduced, at the price of a performance penalty, by employing the Selective RAKE (S-RAKE) receiver structure, which combines a subset of the available resolved MPCs, namely the instantaneously strongest N MPCs. The S-RAKE provides a reduction in the number of correlators and thus reduces power consumption. However, the selection procedure still requires full channel estimation, which may not be easily available. Further simplicity can be achieved by using Partial RAKE (P-RAKE) receiver structure, which combines the first arriving N paths out of the available resolved MPCs. This technique requires only synchronization but not full channel estimation, at the expense of performance degradation.

Fig. 1.15 shows the block diagram of the Rake receiver with N fingers. The received signal is correlated with a given template $v(t - \tau_i)$ for the i^{th} finger and then combined based on the combining scheme used. According to ways of combining, RAKE receivers can be categorized into either equal gain combining (EGC) RAKE receivers or maximum ratio combining (MRC) RAKE receivers. Equal gain combiner simply sums up signal from all multi-paths, i.e., the RAKE receiver taps are all equal to unit. On the other hand, in maximal gain combiner, the RAKE receiver tap weights are chosen to be the complex conjugate of the channel gain, i.e., the channel phase shift is compensated and the signal is enhanced by a factor that is proportional to the signal strength. If the channel attenuation and phase shift can be perfectly estimated or known, maximal ratio combiner is the optimal combiner.

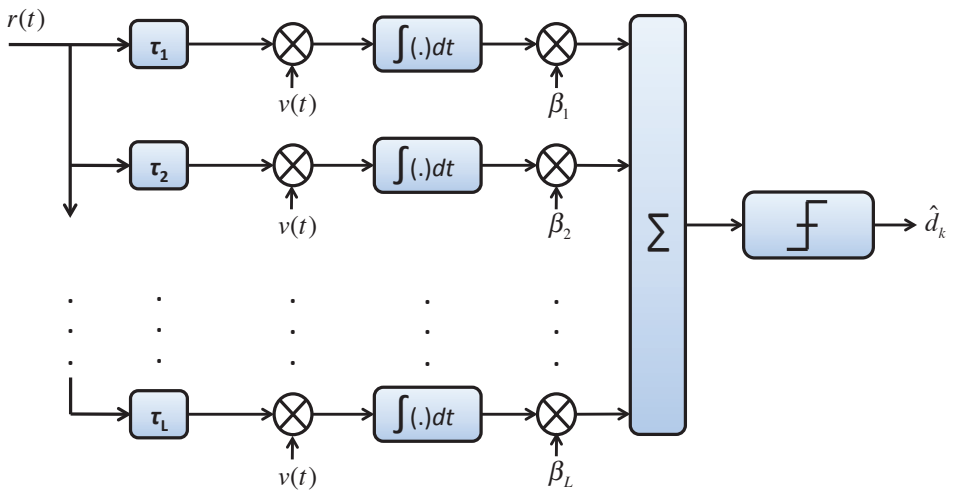

Figure 1.15: Block diagram of Rake receiver.

1.8.2 Non-coherent Receivers

Non coherent receivers do not require channel state information (CSI) at the receiver. From the implementation point of view, non coherent receivers give a simple option at the cost of some performance loss. Transmit reference receiver, differential detectors and energy detectors are common non-coherent receivers.

1.8.2.1 Transmit Reference Receiver

While the RAKE concept is used to estimate individual multipath components of the channel, the Transmitted Reference (TR) systems were devised as a method of communicating in unknown or random channels [Rus64], under the assumption that the channel is stationary during the transmission of the reference signal followed by the message signal. Luckily, UWB pulses are ultra-short in time duration and they are supposed to be transmitted at much higher rates (than the traditional narrowband systems), which allows the channel to be stationary over an even longer time span e.g. frame or symbol period.

It is known that, in general, the problem of single user optimal detection leads to the use of a matched filter, i.e., a convolution by the transmitted waveform including the effects of the channel. This waveform is not known and would need to be estimated. The idea of a TR system is that by transmitting a reference signal through the same channel as the message, it can be used in the convolution, so that channel state information is not needed to estimate the information.

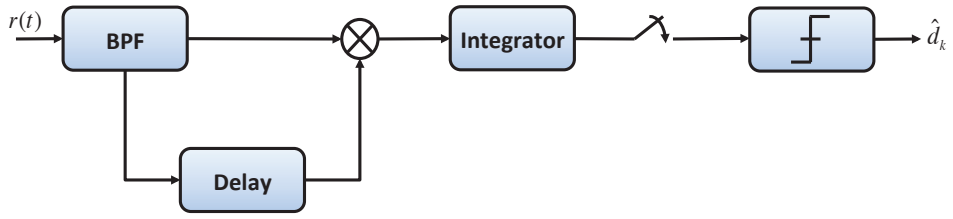

Figure 1.16: Block diagram of the transmit reference receiver.

For example, consider a simple transmission of a pulse pair (also called a doublet) consisting

of a reference pulse $s(t)$ and an information-bearing pulse $d.s(t-D)$. After being sent through a multipath channel, the received signal is

$$r(t) = g(t) + d.g(t-D) \tag{1.30}$$

where d is the data symbol and $g(t)$ is the composite channel. Fig. 1.16 illustrates the received signal and the basic receiver structure of a TR-UWB system.

Assuming $\tau_{max} + T_p < D$ so that there will be no interpulse interference, the data symbol can be detected by cross-correlating the signal with the delay-by-D version of itself, which can be viewed as matched filter with a noisy template

$$\hat{d} = \text{sign}\left\{\int r(t)r(t-D)\right\} \tag{1.31}$$

In this TR-UWB scheme, the data symbols can be detected without channel estimation. No synchronization is needed at the analog part of the receiver (the data and the reference pulse are always spaced at a fixed and known time interval D). Furthermore, no matter how the UWB pulses are distorted, their distortions as well as the channel spread are the same, and only one sample is needed per frame for the detection.

1.8.2.2 Differential Detector

The differential detector (DD) is similar to the TR scheme. Instead of sending reference pulses for correlating the received signal, the data pulses corresponding to the previous symbol is used as the template [Ho02, Cha03, Pau04]. This requires differentially encoding the transmitted bits before modulation, so that the information is in the difference of the two consecutive symbols. Avoiding the use of reference pulses in differential detectors increases spectral efficiency and hence doubles the data rates compared with the TR scheme.

Similar concerns as mentioned in TR scheme are also valid for differential detector receivers. The previous symbols that are used as a reference are noisy, degrading the performance of the receiver. The delay used for differential detector is a symbol length delay which is less robust to timing errors. The accuracy of the delays used at the transmitter and receiver affect the performance, as in the case of TR scheme. A slight difference in the delays will degrade the performance significantly. Note also that the channel needs to be time-invariant over the two-symbol period. For high mobility and larger symbol duration, this might be an issue that needs to be taken into account.

Even though it has been mentioned that the differential detector provides a 3 dB advantage compared with the TR scheme, this might not be true in a practical system design. First of all, the differential detector does not provide the flexibility of TR scheme in terms of adjusting the power, position, and number of the reference signal. Averaging the reference information in a differential detector is not possible. Also, as mentioned in the previous section, the TR scheme can also use the data pulses for improving the template waveform, which indirectly allows improvement of the spectral efficiency of TR schemes. As a result, even though in its basic form, the differential detector might have the advantage over the TR scheme, the TR scheme seems to have more potential for future enhancement and provides a better path towards more coherent receivers as the technology evolves.

1.8.2.3 Energy Detector

An energy detector (ED) (see Figure 1.17) is a simple suboptimal noncoherent IR-UWB receiver scheme, which can be implemented with modulations like OOK or PPM. When OOK is employed, a threshold must be set and used, where the bit decision is 0 if the received energy is less than the threshold, and 1 if it is larger than the threshold. The optimum threshold is the intersection of probability density functions corresponding to energies for 0 and 1. On the other hand, if the PPM is used, the threshold problem disappears, but that may sacrifice the data rate, as the pulses that represent different bits should be adequately separated (more than maximum excess delay of the channel).

Figure 1.17: Block diagram of an energy detector based on OOK.

The UWB energy detector receiver approach generally requires only coarse synchronization, which makes the system robust against clock jitter and triggering inaccuracy [Paq04, Rab04]. It is also not sensitive to distortion and phase nonlinearity of devices like antennas, amplifiers or filters [Paq04].

In spite of its simplicity, conventional energy detectors as implemented in fiberoptic channels perform poorly [Hum91]. This is one of the reasons why energy detectors have not been heavily considered for UWB applications. However, the performance can be improved with a careful receiver design. One of the improvements would be in averaging the received signal before the square device to reduce the noise effect (i.e., improve the signal-to-noise-ratio). The averaging algorithm can be implemented using a single delay line with variable pulse-to-pulse duration or using multiple delay lines using fixed pulse-to-pulse durations. Similarly, averaging can be done using digital samples if the sampling is employed before the square device. However, this will increase the sampling rate and ADC requirements.

Another improvement is in finding an accurate and simple threshold estimation technique for OOK modulation. The choice of the threshold plays an extremely important role in the performance of the receiver. The conventional receivers assume a fixed threshold for decision-making. However, the radio channel and noise statistics vary significantly, suggesting the use of an adaptive threshold that depends on the variation of the signal power and noise power.

Similar to TR, the integration interval can also be adapted depending on the maximum excess delay of the channel [Aka04]. Choosing an integration interval that sacrifices the insignificant multipath components in order to decrease the collected noise energy will improve the performance [Wei04a, Fra04]. Therefore, an optimal integration interval that minimizes the BER exists, and depends on the channel statistics and the noise variance.

1.9 Thesis Framework

In this thesis, we aim to focus on the TH based IR-UWB system (dubbed as TH-IR-UWB hereafter). A general architecture of the considered TH-IR-UWB system, whose performance has been evaluated in [Akb09], is shown in the Fig. 1.18.

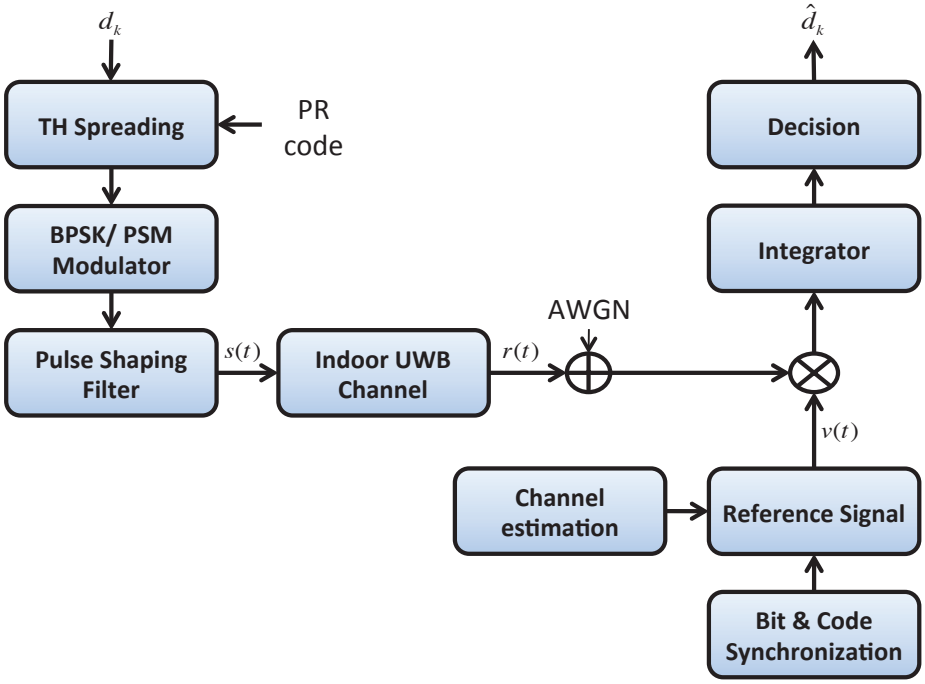

Figure 1.18: A general architecture of TH-PSM transceiver for IR-UWB signals [Akb09]

The reason to choose TH-IR-UWB as the preferred system is manifold. First, let us talk about the two data randomization and multi-access techniques, i.e. TH and DS. The non-continuous low duty-cycle operation of TH suggests a lower achievable data rate with TH as compared to DS schemes, where continuous transmission is employed. Thus, in terms of possible achievable data-rate, DS is certainly superior to TH. However, what really goes in favour of the TH scheme is its possible flexibility. The low duty-cycle transmission ensures much robust performance of such systems over the multipath channels due to low inter-pulse interference (IPI). Thus, a relatively low data-rate but robust transmission can be achieved with TH.

Another advantage of TH over DS is under the multi-acces scenarios. A relative performance comparison of BPSK for DS and TH techniques in an additive white gaussian noise (AWGN) channel has been presented in [Opp04]. The BER for up to 60 simultaneous users was examined. Both synchronous and asynchronous transmissions were considered and all users assumed to have the same power. There was a substantial difference between synchronous and asynchronous performance for the DS system. The synchronous DS system has the pulses for all users transmitted at the same time. The only feature which can be used to suppress multiple access interference is the de-spreading (pulse combining) process in the receiver. When the asynchronous system is used, the lower cross correlation values that occur at different pulse alignments means that there is substantially less interference per bit to be suppressed. The performance of the synchronous and asynchronous systems for the TH system is shown to be very similar. This is because each user has a different pulse transmit instant associated with his pseudorandom (PR) sequence, so the pulses are offset even if the time hopping frames are aligned. The performance of the TH and DS asynchronous systems are found to be very similar.

Another decisive factor to effectively mitigate the multi-access interference (MAI) is the design of optimal PR codes for both TH and DS. It has been shown in [KK09] that unlike DS, TH scheme guarantees to obtain sufficiently optimal pair of codes when increasing the number of chips per

frame for a fixed repetition factor. All this indicates the TH superiority over DS.

Next, consider the choice of impulse radio over multicarrier/ multiband (MC/MB) approaches. IR was exclusively used as the first solution to UWB in the early literature. However, with the time, new proposals emerged to counteract some of the limitation of IR. Among those limitations, the two most critical research challenges of IR are the narrowband interference mitigation and extremely high sampling at (or above) the Nyquist frequency. The multicarrier solutions relax those challenges to certain extent by dividing the 7.5 GHz band into multiple low sub-bands. However, this brings in other issues such as increased complexity and higher cost as the baseband operation of IR is lost. Both of these factors are equally undesirable for low-cost applications which is the main application area of UWB. Thus, the choice between IR and MC/MB really comes to the specific needs and eventual trade-offs. The IR along with TH makes it an appealing solution for communication as well as for plethora of radar and localization based applications, thus selected.

And finally, for modulation purposes, either PAM or PSM will be used. PAM is the most efficient modulation type for the binary case (equivalent to BPSK). However, for high order modulations (M-*ary*), which are required to increase the data-rate, PAM performance degrades significantly. So, PSM can be seen as an attractive solution under this scenario. The application of orthogonal signal sets also enables multiple access techniques to be considered. This can be attained by assigning a group of orthogonal pulses to each user, who uses the assigned set for PSM. The transmission will then be mutually orthogonal and different user signals will not interfere with each other, thus minimizing the MAI. The BER performance in a two user environment using the MHP-based PSM has been studied in [Wei04a], where the signal from one of the users acts as an interference. It is shown that MHP-based OPM has a significant performance improvement over traditional PPM.

Having talked about the considered system, we now discuss the four issues tackled in this research work.

Narrowband interference (NBI) in UWB As discussed before, the extremely low transmission power and large bandwidth enable UWB systems to co-exist with other narrowband systems without interfering with them. However, the effect of the narrowband signals on the UWB signal can be significant and may jam the UWB receiver completely. Even though the narrowband signals interfere with only a small fraction of the UWB signal spectrum, due to the large relative power of the narrowband signals with respect to the UWB signal, the performance and capacity of UWB systems can be affected considerably. Therefore, the UWB receivers might need to employ NBI suppression techniques to improve the performance, capacity, and range of communication.

The current trend in NBI is to avoid the transmission (using MC and MB approaches) of the UWB signal over the part of the frequency where NBI is strong. However, this restricts the transmission of UWB waveforms. The NBI can also be suppressed at the receiver, which relaxes the transmission format. However, this increases the receiver complexity.

The introduction of cognitive features along with opportunistic spectrum usage can enhance the IR-UWB co-existence. Efficient spectrum sensing is used to detect the presence of any active primary system/user in the UWB emission band.

Adaptive UWB waveform design To detect the presence of primary user is the first step to mitigate NBI. The next step is to benefit from this knowledge, therefore we must be able to design the UWB waveform which can skip the occupied band yet exploits efficiently the rest of the available band. Also, due to PSM modulation, we need to generate multiple

mutually orthogonal pulses. Thus, the design of UWB waveform is the most critical issue on the transmitter side. An efficient adaptive pulse design approach will not only mitigate the NBI using the spectrum sensing knowledge but will also reduce MAI using orthogonality.

Synchronization Synchronization can be roughly described as the process of providing the same time reference for the receiver as is used for the transmitter. In other words, the synchronization operation is a search operation, where the receiver searches for the correct timing of the transmitted signal and locks onto it. In UWB, synchronization is more difficult compared with other narrowband systems. Fast and accurate acquisition with low overhead is desired. Without a correct timing synchronization, demodulation and data detection are not possible.

Synchronization in general can be grouped as coarse and fine synchronization. Coarse synchronization involves detection of the existence of the signal and aligning the receiver with the correct transmitted pulse and symbol sequence. The fine synchronization is locking the receiver to the correct pulse timing. In Rake receivers, the receiver needs to lock into the appropriate path positions. Estimation of the proper finger positions is part of the synchronization process. Note that often timing estimation of the strongest path is not enough for dispersive NLOS channels as the energy from the other paths is not exploited. Therefore, estimation of multiple finger locations increases the synchronization complexity.

UWB Channel Parameters Estimation As we opt for coherent Rake receiver due to its near optimal performance in our considered system, the channel estimation is indispensable. In UWB, the transmission bandwidth is extremely large, which leads to multiple resolvable paths. For a given transmitted power, the power is distributed over extremely large bandwidths, and hence causes very low interference to narrowband users. In time domain, the high resolvability due to wide bandwidth can affect the receiver performance. Since the total power is distributed over many multipath components, the power in each of these individual paths will be very low [Cas03].

As long as the receiver is able to estimate the channel influence on the transmitted signal, it can accurately recover the information sent. The channel estimation includes estimation of the multipath delays, multipath coefficients, and the estimation of the received pulse due to the effect of the channel. Since the channel is random and time-varying, the estimation process needs to be continuous to be able to adapt the changes in the channel.

1.10 Conclusions

In this chapter we have examined the main concepts and challenges in ultra wideband wireless communications. UWB systems may be primarily divided into IR systems and MB systems. Multiband systems offer the advantage of potentially better utilization of spectrum.

However, IR systems have the significant advantage of simplicity, and so are potentially lower cost. In addition, IR is essentially a baseband technique. The IR-UWB concepts investigated support many modulation schemes including orthogonal and antipodal schemes. Basic modulation must also include some form of spectrum randomization techniques to limit the interference caused by the transmitted pulse train. Both TH and DS randomization techniques were examined. The standard channel models proposed by IEEE have also been studied. Several receiver options for TH-IR based UWB systems have been discussed.

A thesis framework is finally presented along with the focus of the research work.

Chapter 2

Cognitive UWB Radio: From Spectrum Sensing to Spectral Adaptation

- Abstract -

This chapter explores the concept of integrating UWB with cognitive radio (CR). First, the salient features of CR are reviewed and a close resemblance between the UWB features and CR requirements is observed. Due to this similarity, UWB technology itself can be considered as a potential candidate for realizing CR technology. On the other hand, by incorporating some CR features into UWB systems, some of the challenges faced by these systems can also be eliminated. Therefore, a mutual benefit exists by fusing these two interesting technologies together. Owing to this observation, we then focus on the spectrum sensing (SS) which is a key element of CR and propose a rapid method using finite random matrix theory. Next, an adaptive UWB waveform is designed which can help to efficiently utilize the available spectral resources and can also mitigate the interference from other systems.

Contents

2.1 Cognitive Radio

CR is a novel concept for future wireless communications, and it has been gaining significant interest among the academia, industry, and regulatory bodies. A CR is a radio that is aware of its surroundings and adapts intelligently [MI99b]. Regardless of the fundamental research and development challenges faced in bringing this technology to practice, the notion of efficiently utilizing the radio resources has attracted the spectrum regulatory bodies around the world. Hence, the research and technological investment in this field are currently experiencing a rapid continuous growth.

2.1.1 Motivation

The need for CRs is motivated by many factors. Principally, the need for cognition is driven by the complexity of the radio systems themselves. Wireless communications are routinely used today for a large variety of applications including voice, data transfer, Internet access, audio, and video streaming, etc. Pushed by the insatiable demand for bandwidth and pulled by the steady improvement of semiconductor technology (Moore's law), the performance offered by wireless standards is certain to improve with the years, seemingly without bounds, as illustrated in Fig. 2.1.

Future communications systems will have to seamlessly and opportunistically integrate these multiple radio technologies. From a user perspective, it is indeed very attractive to have a single hand-held device that can support a large number of these wireless standards enabling ubiquitous connectivity through seamless horizontal and vertical handovers. The concept of software-defined radio (SDR) in which a common hardware platform is used for different standards supports this

trend [Bur00, Dil03]. A closer inspection of standards specifications reveals that a large variety of bit rates, modulation formats, physical bandwidths, and carrier frequencies has to be supported.

Besides the adaptability constraint, spectrum is also becoming a major resource bottleneck, due to the accelerated deployment of broadband personal communication and the continuously increasing demand for higher data rates. For nearly a century, allocation of spectrum throughout the world has been based on a model of static allocation. Each application has been allocated a band definitively and exclusively, e.g. the band between 88-108 MHz for FM radio or 925-960 MHz for GSM 900.

More recently, it has been realized that this static model leads to gross inefficiencies. Recently, the FCC Spectrum Policy Task Force has reported [FCC02b] vast temporal and geographic variations in the usage of allocated spectrum with utilization ranging from 15% to 85% in the bands below 3 GHz. At frequencies above 3 GHz the actual utilization is also dramatically low. Fig. 2.2 shows the spectrum occupancy measurements taken in New York on 1st September 2004 by *Shared Spectrum Company* (SSC) [SSC]. It is clear from Fig. 2.2a that the band between 2.4 to 2.48 GHz is well-occupied while Fig. 2.2b reveals an under-utilization of the band between 700 to 800 MHz in the same timing. New paradigms for efficiently exploiting the spectrum are clearly needed. A current trend is the evolution toward dynamic and open access to spectrum, motivated by the under-utilization of many licensed frequency bands.

The demand for wireless connectivity and crowding of unlicensed spectra has pushed the regulatory agencies to be ever more aggressive in providing new ways to use spectra. In order to promote more flexibility in spectrum sharing, the FCC has provided new opportunities for unlicensed spec-

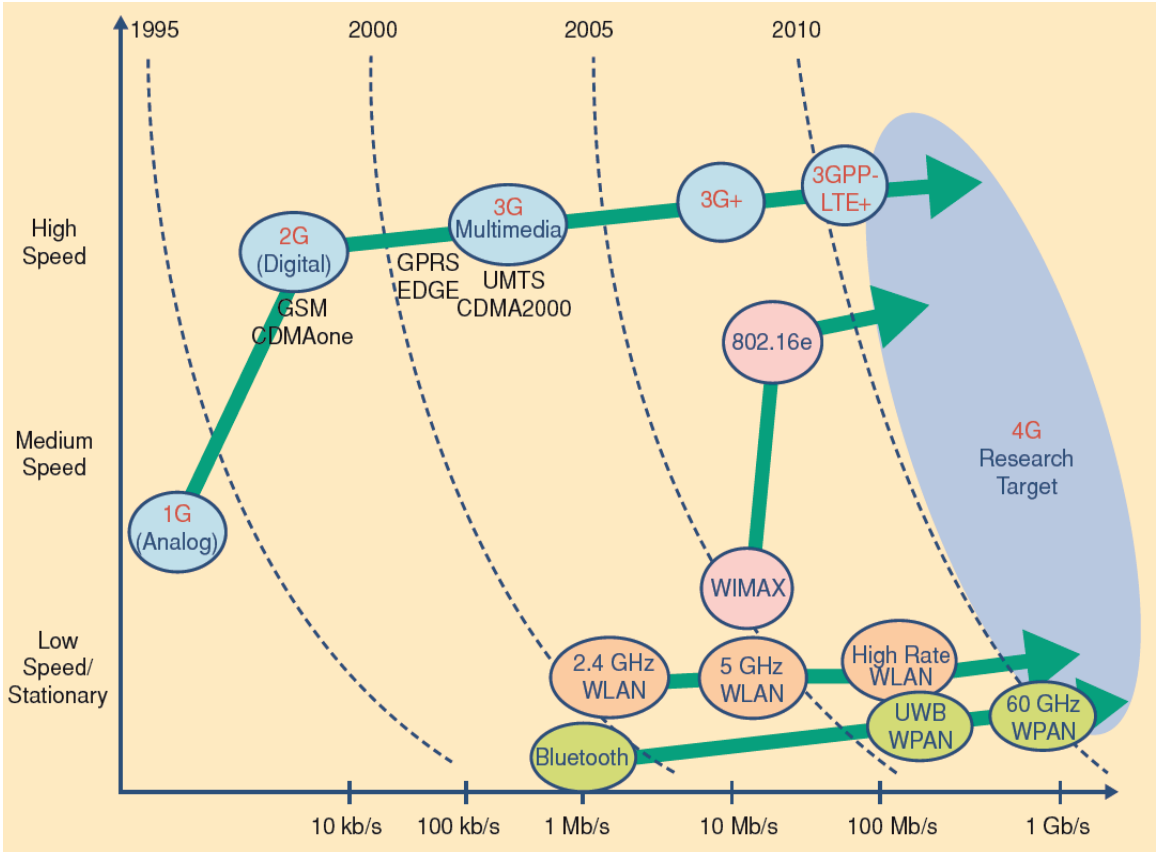

Figure 2.1: Evolution of wireless standards.

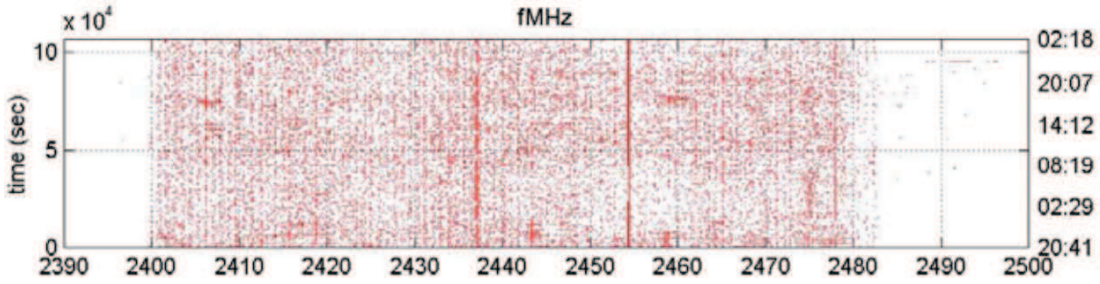

(a) 2390 MHz - 2500 MHz

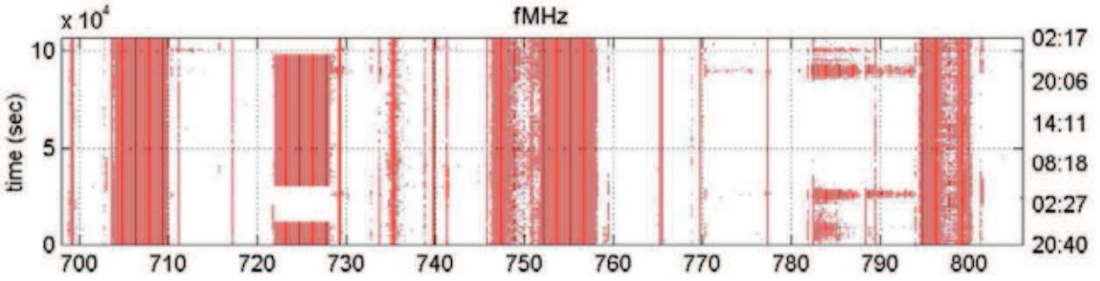

(b) 700 MHz - 800 MHz

Figure 2.2: Spectral occupancy measurements taken by SSC in New York [SSC]

trum usage with fewer restrictions on radio parameters. In order to utilize these spectrum 'white spaces', the FCC has issued a Notice of Proposed Rule Making [FCC03] advancing CR technology as a candidate to implement negotiated or opportunistic spectrum sharing.

2.1.2 Definitions

Joe Mitola is credited as defining the field of CR [MI99a, MI99c, MI00] with an interest in using the radio system as a personal assistant of sorts that intelligently reacts to the user's perceived needs.

In his thesis [MI00], J. Mitola defines CR as: "The term cognitive radio identifies the point at which personal digital assistant (PDAs) and the related networks are sufficiently computationally intelligent about radio resources and related computer to computer communications to:

1) Detect user communications needs as a function of use context, and

2) Provide radio resources and wireless services the most appropriate to these needs"

The definition of CR has been under debate since its introduction. In particular, much of the early work in CR deals with the concept of Dynamic spectrum access (DSA), that is, dynamically selecting frequency channels to enable spectrum sharing and reuse. While this is one of the applications of CR, the Mitola's original vision was much more than that as is clear by the definition. The other aspects of CR develop more of a service-oriented view of communications whereby the entire communications system is adapted to offer better quality of service (QoS). The service model extends beyond the DSA model by looking at the system performance and not just the slice of spectrum allocated.

Since then, the CR concept has evolved to include various meanings in several contexts and many organizations have adopted their own definitions, which we list below : According to FCC [FCC03] : "A cognitive radio is a radio that can change its transmitter parameters based on interaction with the environment in which it operates"

- European Telecommunications Standards Institute (ETSI) has proposed : "Cognitive radio system is a radio system, which has the following capabilities:
  - to obtain the knowledge of radio operational environment and established policies and to monitor usage patterns and user's needs
  - to dynamically and autonomously adjust its operational parameters and protocols according to this knowledge in order to achieve predefined objectives, e.g. more efficient utilization of spectrum
  - to learn from the results of its actions in order to further improve its performance"
- International Telecommunications Union (ITU) has defined : "Cognitive Radio System (CRS) is a radio system employing technology that allows the system to obtain knowledge of its operational and geographical environment, established policies and its internal state; to dynamically and autonomously adjust its operational parameters and protocols according to its obtained knowledge in order to achieve predefined objectives; and to learn from the results obtained"
- Haykin adopted the ideal CR definition of Mitola to emphasize more on spectrum-agile radio concept in [Hay05] : "Cognitive radio is an intelligent wireless communication system that is aware of its surrounding environment (i.e., outside world), and uses the methodology of understanding-by-building to learn from the environment and adapt its internal states to statistical variations in the incoming radio frequency stimuli by making corresponding changes in certain operating parameters (e.g., transmit power; carrier-frequency, and modulation strategy) in real-time, with two primary objectives in mind: (i.) highly reliable communication whenever and wherever needed and (ii.) efficient utilization of the radio spectrum."

We notice that these recent definitions are compatible with the much larger original definition of Mitola.

2.1.3 Cognitive Cycle

The cognitive cycle is the term describing the activities involving the intelligence of the radio device such as sensing, learning and adapting. In [MI99c], Mitola had presented a generic cognitive cycle that corresponds to his view of ideal CRs. Mitola's cognitive cycle appeared as a directed graph that includes various states such as Observe, Orient, Learn, Plan, Decide, and Act, as shown in Fig. 2.3.

According to this cycle, a CR may adapt to its environment thanks to :

- Ability to sense: The radio consists of sensors to capture the information regarding its operational environment.
- Ability to decide: The radio exploits the information gathered by sensors to decide the best-adopted configuration and learn from its experiences using inherent intelligence.

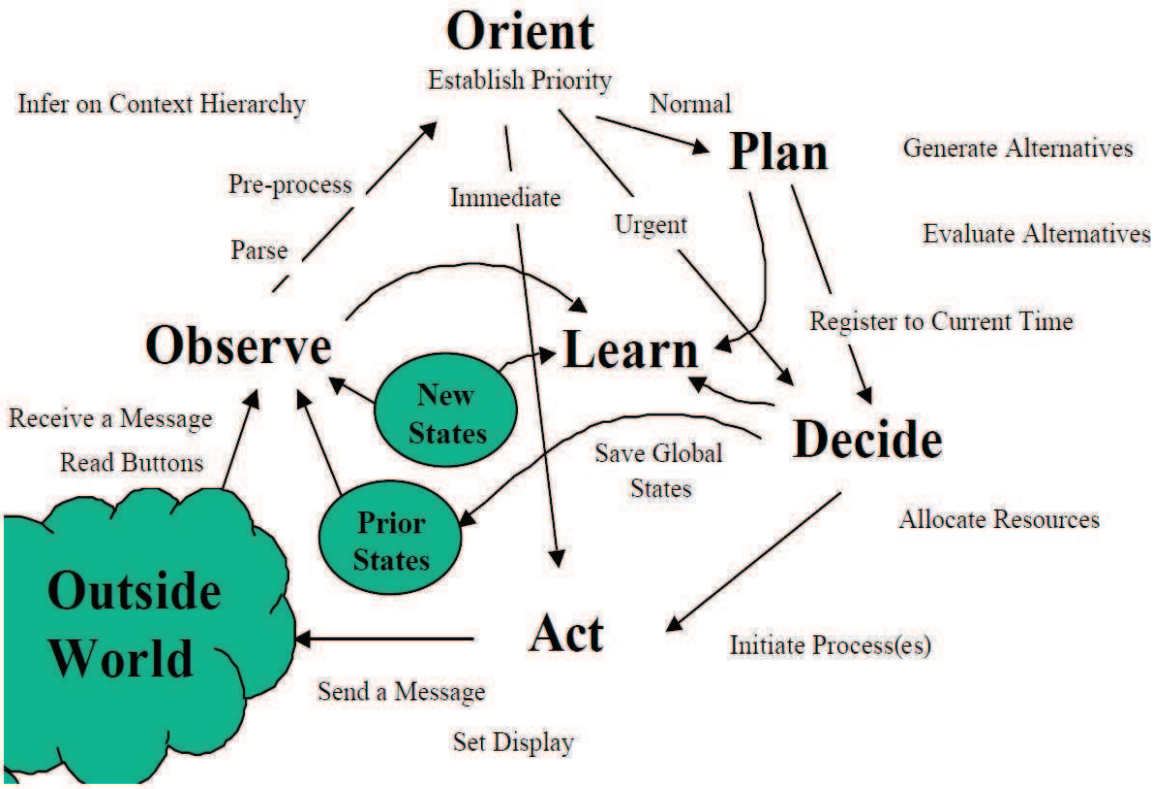

Figure 2.3: Cognition cycle proposed by Mitola [MI99c]

- Ability to reconfigure: The ability to act based on the decision dynamically and autonomously. This ability is generally achieved by SDR support.

A simplified cognition cycle based on these three essential elements is shown in Fig. 2.4. The

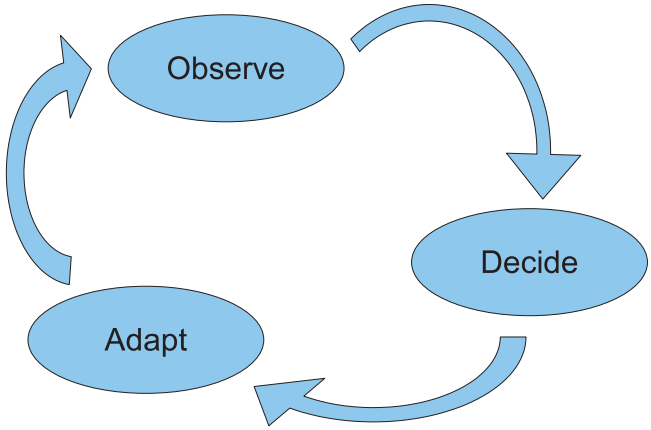

Figure 2.4: Simplified three-step Cognition cycle

notion of sensing as first block in the cognition cycle is vast. It may correspond to any means of information which can be helpful to the cognitive engine for making decisions, from many of radio's operational parameters to the protocols etc. This information may come from the real physical sensors, signal processing algorithms, information exchange within the network etc.

2.1.4 Spectral Sharing

At the moment, most attention given to the use of CR technology is on opportunistic spectrum access whereby CRs are able to identify "unused" portions of spectrum and share that spectrum without affecting the existing users as illustrated in Fig. 2.5. Therefore, for such CRs, to learn from environment generally corresponds to SS which is one of the crucial part in realizing them. CR enables the usage of unused spectrum, which is referred to as *spectrum hole* or *white space*. If this band is further used by a licensed user, the CR moves to another spectrum hole or stays in the same band, altering its transmission power level or modulation scheme to avoid interference

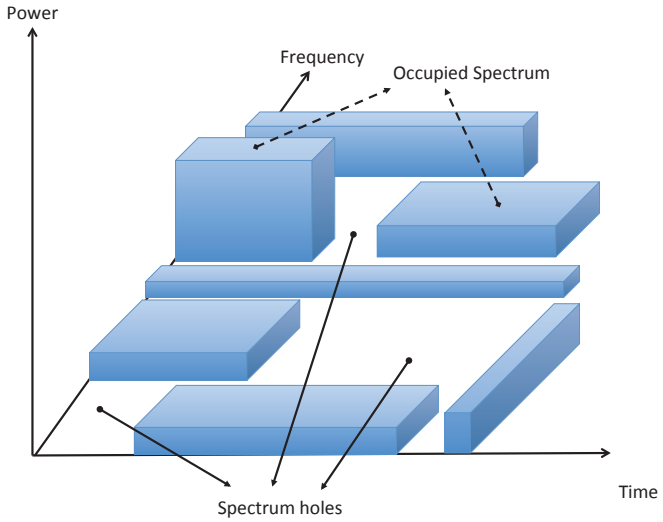

Figure 2.5: Spectrum hole concept

With CR technology the concept of 'primary users (or licensed users)' and 'secondary users (or secondary users)' of the spectrum is developed. The primary users are the incumbent users with the exclusive rights to use the spectrum at anytime and the secondary users, also known as the CR users, are the users that use the spectrum without interfering with the primary users. There are different spectrum sharing techniques considered for CR networks for maximizing the spectral efficiency between the primary and the secondary users.

2.1.4.1 Horizontal and vertical sharing

Spectrum sharing can be done either with the licensed radio systems or with the non-licensed systems.

- *Vertical Sharing*: One approach to sharing spectrum can be referred to as vertical sharing where the CR shares spectrum with the existing users. The CR is only allowed to utilize frequencies within the band as long as the existing user(s) is not affected, i.e. the CR must not cause harmful interference to the existing users. Depending on the spectrum rights of the primary user(s), the conditions under which the CR devices can operate are to be defined in advance by the regulator or could be left to the primary user.
- *Horizontal Sharing*: An alternative or complementary approach to vertical spectrum sharing is when CR technologies have the same rights to access the spectrum. Therefore this type of sharing is referred to as horizontal sharing. The established policies including the sharing

conditions should be transparent and non-discriminatory. In this model, regulatory intervention is required to define the conditions to ensure appropriate protection for other users or devices.

Fig. 2.6 graphically explains the concept.

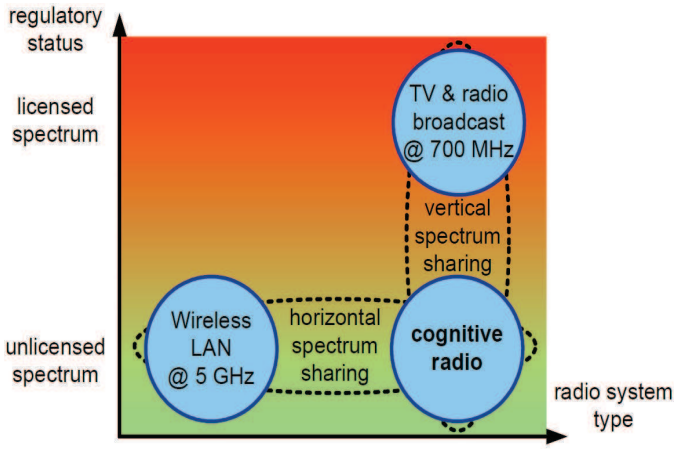

Figure 2.6: Horizontal or vertical spectrum sharing [Ber05]

2.1.4.2 Overlay and underlay techniques

- *Underlay technique*: In this method, the secondary users can utilize the spectrum simultaneously with the primary users without exceeding a predefined interference level to the primary users. Secondary users in this case can share the spectrum such that the total interference power from the secondary users to the primary users are controlled below the interference limit set by the relevant regulatory authorities. The characterization of such interference limit is given in the next subsection. UWB radio technology due to the low powered transmissions in the ultra wide band frequency range is therefore a potential candidate for deploying spectrum underlay technology for spectral sharing. Using the low powered transmissions and making sure that the interference limit is not exceeded, UWB radios can potentially share the spectrum with the primary users and coexist.
- *Overlay technique*: In this method, the CRs can identify the spectrum holes in the spatio-temporal domain and opportunistically utilize them by giving higher priority to the primary users. Whenever a primary user is not using the spectrum, secondary users (cognitive radios) are allowed to transmit. However, when a primary user is detected in that particular band, then secondary users need to immediately vacate the band by stopping transmitting in that particular band. In this sense SS and primary user detection become a crucial functionality for reliably detecting the primary users in the environment in the spatio-temporal domain.

A visual illustration of the idea is shown in Fig. 2.7.

2.1.4.3 Spectrum Pooling

The notion spectrum pool was first mentioned in [MI99a]. It basically represents the idea of merging spectral ranges from different spectrum owners (military, trunked radio, etc.) into a common pool.

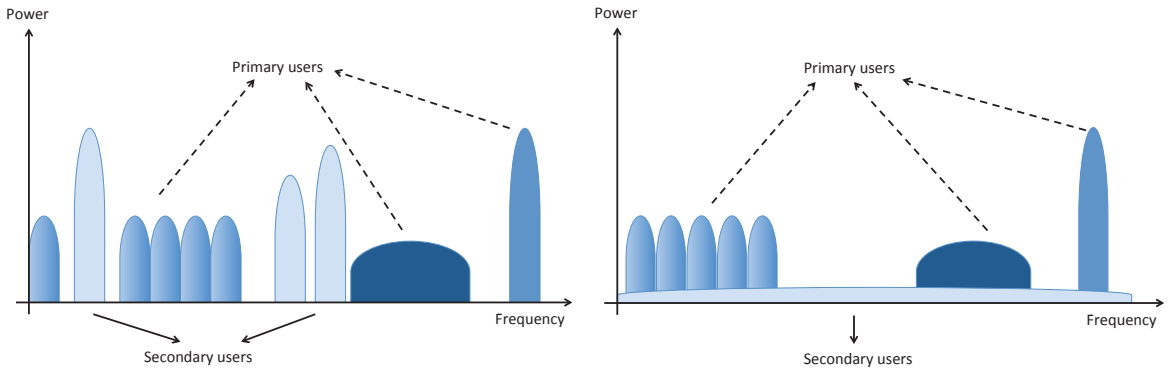

Figure 2.7: Spectrum sharing techniques, (a) Overlay (b) Underlay

From this common spectrum pool hosted by the so-called licensed system public rental, users may temporarily rent spectral resources during idle periods of licensed users. The basic proposition is that the licensed system does not need to be changed. The installed hardware can be operated like there was no other system present in the same frequency range. The standards based on multi-carrier modulation schemes such as OFDM are particularly well-suited to the concept of spectrum pool [Wei04b].

2.2 UWB based CR

The opportunistic, primary aware reuse of spectrum espoused by the CR community contrasts with the underlay, primary unaware philosophy behind the development of UWB technology. UWB devices seek to provide non-interference guarantees to primary users by spreading their transmit power over a very large bandwidth which ensures that the transmit power in any individual band is very low. Hence UWB devices appear as noise to most primary users.

It is evident that both CR and UWB represent contrasting philosophies to address the spectrum sharing problem. However, gains can be achieved by merging these two technologies; by adding cognitive technology to UWB radios. Some of the gains from this merger are as follows:

- **UWB as an alternative to CR**: First, if the main properties of impulse radio based UWB are considered, it is seen that there is a strong match between what the CR requires and what IR-UWB offers. IR-UWB inherently possesses many features such as negligible interference to existing systems, flexible pulse shape and bandwidth, adaptable data-rate and QoS, transmit power, limited cost etc. This makes UWB itself a potential candidate to reuse the spectrum efficiently.
- **Continuous transmission by CRs**: Implementing CR with UWB will ease the dependence on spectrum holes as it will enable the inherent low power underlay transmission mode as well. If there are unused portions in the spectrum, the cognitive UWB radio will benefit overlay mode by increasing the transmitted UWB power to a certain level that is comparable to the power of licensed systems. If the band is claimed by a licensed user, the cognitive UWB radio alters its transmission power level to function in underlay mode. Thus, a continuous transmission by CRs can be assured.
- **Interference mitigation in UWB**: Since UWB covers such a large bandwidth, it is there-

fore apparent that it will overlap with several communication systems and services with different technical and operational characteristics. These include WLAN, remote local area network (RLAN), WiMax, 3rd and 4th Generation Mobile systems, etc. UWB spectrum in Europe and parts of Asia Pacific overlaps with WiMax spectrum [Mis07]. Due to this overlap, an UWB transmitter in close proximity to a WiMax customer premise equipment (CPE) can impact the CPE's ability to receive transmissions from a WiMax base station [Mis07]. Hence regulators in Europe and the Asia Pacific are considering requiring UWB radios to detect the presence of WiMax receivers and to abandon the band if a potential victim is detected. Thus, the SS module of CR will help in mitigating the interference to and from UWB to other systems.

- **Improved functionality of UWB**: Furthermore, UWB radios that possess cognitive technology may also be allowed greater transmit power in bands where the primary users can be identified and avoided. Depending on the spectrum opportunities, the signaling and the spectrum of the transmitted signal can be shaped in such a way that part of the spectrum is occupied in an underlay mode, and some other parts are occupied in an overlay mode. This overlay mode will result in higher data-rates and increased range capability of UWB.

However, it has to be kept in mind that under the current FCC regulations, the overlay mode of UWB is not permitted, and similar spectral limitations are mandated upon UWB systems in other regions of the world, as well. Under these conditions, it should be stated that IR-UWB can be the technology for CR only when the regulatory agencies are convinced that IR-UWB devices are equipped with advanced sensing and spectrum shaping capabilities that leave zero possibility to interfering with licensed users. Thus, the key aspects for the development of cognitive UWB radio are:

1) **Spectrum sensing** to detect the primary user
2) **Spectral adaptation** to mitigate interference

In the remainder of this chapter, we will focus on the above two tasks. SS algorithms are discussed first and then a fast and efficient SS algorithm is proposed using finite random matrices. To avoid the interference and to enable simultaneous underlay/overlay operation, flexible spectrum sharing is inevitable. Since the IR-UWB communication is basically realized via the transmission of short pulses, varying the duration or the shape of the pulses directly alters the occupied spectrum. So, in the latter part of the chapter, we will concentrate on the design of adaptive UWB waveform.

2.3 State of the Art for Spectrum Sensing

As discussed before, SS is a fundamental element in a CR to enable its capability to measure, learn, and be aware of the radio's operating environment. Conventional sensing methods usually relate to sensing the spectrum in the three dimensions, defined as *a band of frequencies that are not being used by the primary user of that band at a particular time in a particular geographic area* [Kol01], i.e. in frequency, time, and spatial domains. However, there exists other possibilities such as the recent developments in beam technology can be used to transmit in particular directions while orthogonal codes can be employed in spread spectrum technique, to transmit in the same band without causing interference to primary users (PUs). These dimensions need to be explored further for spectrum opportunity.

Research Challenges

Before getting into the details of SS techniques, it is important to mention the potential challenges associated with the SS for CR [Yuc09, Zen10]. There are several factors which make SS really challenging such as

- **Low SNR of Primary Users** The secondary users (SUs) usually need to detect the PUs at very low SNR. For example, the future wireless regional area network (WRAN) which is based on CR technology, needs to detect the PU at a SNR of -22dB [Ste06].
- **Fading and Time Dispersion Channels** Fading will cause the received signal's power to fluctuate dramatically while the time dispersion will render coherent detection unreliable [Cab04, Sah05]. Also, severe multipath fading or shadowing observed by SUs while scanning for PU's transmissions may cause *hidden node* problem. A typical example is shown in Fig. 2.8 where SU can not detect the PU transmitter due to the operating range of devices.
- **Noise Uncertainty** Receiver device noise uncertainty due to non-linearity of components and thermal noise in components [Tan05a,Sah05] while environment noise uncertainty caused by transmissions of other users, makes it very difficult to obtain the accurate noise power, which is needed for some SS methods.
- **Hardware Requirements** A CR should be able to capture and analyze a relatively larger band for identifying spectrum opportunities. This impose additional requirements on the RFs components such as antennas and power amplifiers as well. Furthermore, high speed processing units (digital signal processors (DSPs) or FPGAs) are needed for performing computationally demanding signal processing tasks with relatively low delay.
- **Spread Spectrum Primary User Detection** Primary users that use spread spectrum signaling techniques such as frequency-hoping spread spectrum (FHSS) or direct sequence spread spectrum (DSSS), are difficult to detect as the power of the primary user is distributed over a wide frequency range.
- **Sensing Time and Frequency** CR should be able to identify the presence of primary users as quickly as possible and should vacate the band immediately. This requirement poses a limit on the performance of SS algorithm and creates a challenge for CR design. Sensing frequency, i.e. how often CR should perform SS, is a design parameter that needs to be chosen carefully. The optimum value depends on the capabilities of CR itself and the temporal characteristics of primary users in the environment.
- **Security** In CR, a selfish or malicious user can modify its air interface to mimic a primary user. Hence, it can mislead the SS performed by legitimate primary users.

The most efficient way to detect spectrum holes is to detect the primary users that are receiving data within the communication range of a CR user. In reality, however, it is difficult for a CR to have a direct measurement of a channel between a primary receiver and a transmitter. Thus, the most recent work focuses on primary transmitter detection based on local observations of cognitive users, called as local SS.

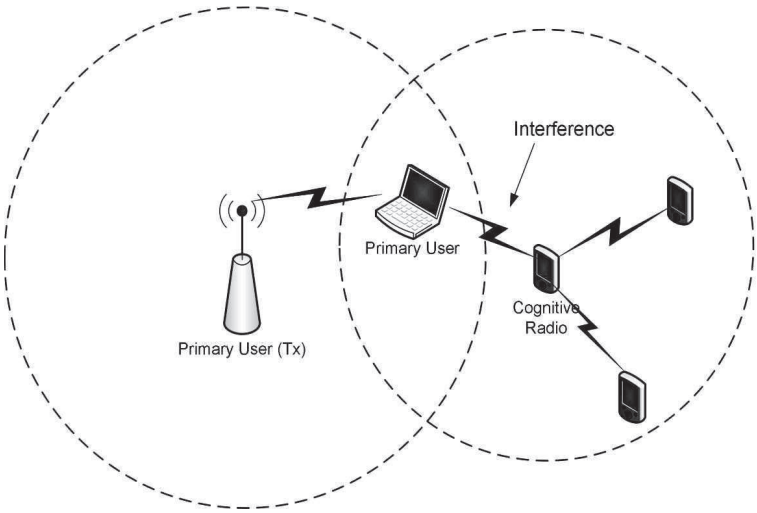

Figure 2.8: Hidden primary user problem in CRs [Yuc09]

Classification of Spectrum Sensing Techniques

From the perspective of signal detection, SS techniques can be classified into two broad categories: coherent and non-coherent detection. In coherent detection, the primary signal can be coherently detected by comparing the received signal or the extracted signal characteristics with *a-priori* knowledge of primary signals. In non-coherent detection, no *a-priori* knowledge is required for detection. Another way to classify SS techniques is based on the bandwidth of the spectrum of interest for sensing: narrowband and wideband. The classification of SS techniques is shown in Fig. 2.9.

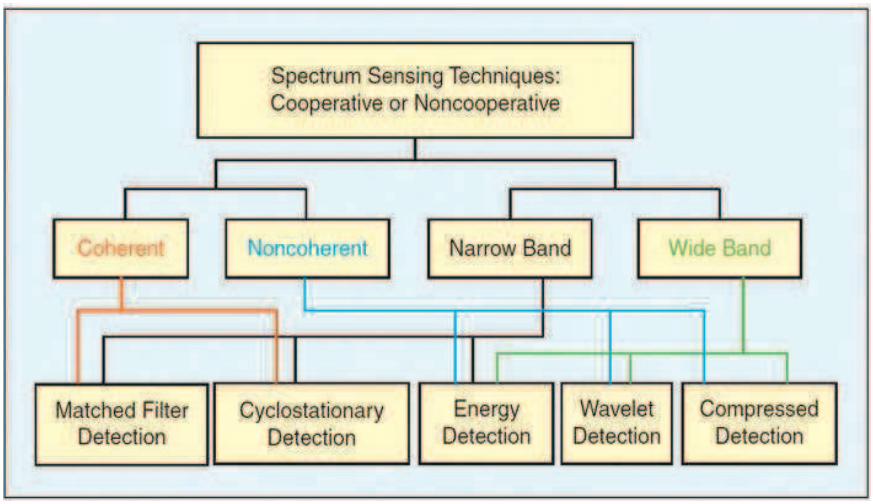

Figure 2.9: Classification of spectrum sensing techniques [Aky11]

Spectrum Sensing Concept

Typically, local sensing for primary signal detection can be formulated as a binary hypothesis problem as follows

$$\begin{aligned} \mathcal{H}_0 &: h(i) = n(i) \\ \mathcal{H}_1 &: h(i) = s(i) + n(i) \end{aligned} \tag{2.1}$$

where $h(i)$ denotes the received signal at the CR user, $s(i)$ is the transmitted PU signal including the effects of path loss, multipath fading and time dispersion, $n(i)$ is the zero-mean AWGN, $\mathcal{H}_0$ and $\mathcal{H}_1$ denote the hypothesis of the absence and the presence, respectively, of the PU signal in the frequency band of interest. The objective of SS is to make a decision on the binary hypothesis testing (choose $\mathcal{H}_0$ or $\mathcal{H}_1$) based on the received signal $h(i)$.

The performance of a SS algorithm is generally indicated by two metrics: probability of detection (P_d), which defines at the hypothesis $\mathcal{H}_1$, the probability of the algorithm correctly detecting the presence of the primary signal; and probability of false alarm (P_{fa}), which defines at the hypothesis $\mathcal{H}_0$, the probability of the algorithm mistakenly declaring the presence of the primary signal. Based on P_d, the probability of miss-detection (P_m), can be obtained by $P_m = 1 - P_d$. The plot that demonstrates P_d versus P_{fa} is called the receiver operating characteristic (ROC) curve, which is the metric for the performance evaluation of SS techniques. A SS algorithm is called "optimal" if it achieves the highest P_d for a given P_{fa} with a fixed number of samples, though there could be other criteria to evaluate the performance of a SS algorithm.

2.3.1 Traditional Spectrum Sensing Techniques

Quite a few algorithms have been proposed in literature for PUs detection. According to the *a priori* information they require and the resulting complexity and accuracy, SS techniques can be categorized in the following types:

2.3.1.1 Energy Detection

Energy detector (ED) is the most common type of SS because of its low computational and implementation complexities [Urk67, Leh05, Dig07, Vis08]. It is an example of a noncoherent detection method capable of performing optimally where there is no *a-priori* knowledge about the PUs' signal.

The detection statistics of the energy detector can be defined as the average (or total) energy of observed samples

$$T = \frac{1}{N} \sum_{i=1}^{N} |h(i)|^2 \tag{2.2}$$

The decision on whether the spectrum is being occupied by the PU is made by comparing the detection statistics with a predetermined threshold η.

Besides its low computational and implementation complexity, there also exist some challenges in designing a good energy detector. First, the detection threshold depends on the noise power, which may change over time and hence is difficult to measure precisely in real time. Below an SNR

threshold, a reliable detection cannot be achieved by increasing the sensing duration. This SNR threshold for the detector is called SNR wall [Son92]. With the help of the PU signal information, the SNR wall can be mitigated, but it cannot be eliminated [Tan08]. Moreover, an energy detector can only decide the PU's presence by comparing the received signal energy with a threshold; thus, it cannot differentiate the primary user from other unknown signal sources. As such, it can trigger false alarm frequently.

In spite of these limitations, the energy detection method remains the most common detection mechanism currently in use in cooperative sensing (a scheme to exploit the spatial diversity) [Aky06]. This is because some of its performance degradation due to noise uncertainty can be mitigated by the diversity gain resulting from cooperation.

2.3.1.2 Feature Detection

There are specific features associated with the information transmission of a primary user. For instance, the statistics of the transmitted signals in many communication paradigms are periodic because of the inherent periodicities such as the modulation rate, carrier frequency, etc. Such features are usually viewed as the cyclostationary features, based on which a detector can distinguish cyclostationary signals from stationary noise.

The cyclostationarity based detection algorithms can differentiate noise from PUs' signals. This is a result of the fact that noise is wide-sense stationary (WSS) with no correlation while modulated signals are cyclostationary with spectral correlation due to the redundancy of signal periodicities [Cab05]. Furthermore, cyclostationarity can be used for distinguishing among different types of transmissions and PUs [Lun07].

Different from an energy detector which uses time-domain signal energy as test statistics, a cyclostationary feature detector performs a transformation from the time-domain into the frequency feature domain and then conducts a hypothesis test in the new domain. Specifically, it can be realized by analyzing the cyclic autocorrelation function (CAF) of the received signal $h(i)$, expressed as

$$R_h^{\alpha}(\tau) = E[h(i+\tau/2)h^*(i-\tau/2)e^{j2\pi\alpha i}] \tag{2.3}$$

where $E[.]$ is the expectation operation, $*$ denotes complex conjugation, and α is the cyclic frequency.

CAF can also be represented by its Fourier series expansion, called cyclic spectrum density (CSD) function [Gar88], denoted as

$$S(f,\alpha) = \sum_{\tau=-\infty}^{\infty} R_h^{\alpha}(\tau)e^{-j2\pi f\tau} \tag{2.4}$$

The CSD function have peaks when the cyclic frequency α equals to the fundamental frequencies of the transmitted signal $h(i)$. Under hypothesis $\mathcal{H}_0$, the CSD function does not have any peaks since the noise is, in general, non-cyclostationary.

Compared to energy detectors that are prone to high false alarm probability due to noise uncertainty and cannot detect weak signals in noise, cyclostationary detectors become good alternatives because they can differentiate noise from PU's signal and have better detection robustness in low

SNR regime.

In a more general sense, features can refer to any intrinsic characteristics associated with a PU's transmission. Generalized feature detection refers to detection and classification that extracts more feature information other than the cyclostationarity due to the modulated primary signals, such as the transmission technologies used by a primary user, the amount of energy and its distribution across different frequencies [Var01, Meh01], channel bandwidth and its shape [Yuc06, Pal03], power spectrum density [Qua09], center frequency [Yuc06], idle guard interval of OFDM [Kha07], fast fourier transform (FFT)-type feature [Leu05], etc. By matching the features extracted from the received signal to the *a priori* information about PUs' transmission characteristics, PUs can be identified.

2.3.1.3 Matched Filter Detection

If SUs know information about a PU's signal *a priori*, then the optimal detection method is the matched filtering [Pro00], since a matched filter can correlate the already known primary signal with the received signal to detect the presence of the PU and thus maximize the SNR in the presence of additive stochastic noise.

The merit of matched filtering is the short time it requires to achieve a certain detection performance such as a low P_{md} and P_{fa} [Sah05], since a matched filter needs less received signal samples. However, the required number of signal samples also grows as the received SNR decreases, so there exists a SNR wall for a matched filter. In fact, the required number of samples grows as $O(1/SNR)$ for a target P_{fa} at low SNRs for matched filtering [Tan05a]. Also, matched filtering requires perfect knowledge of the PU's signal, such as the operating frequency, bandwidth, modulation type and order, pulse shape, packet format, etc. to demodulate the received signals. In addition, its implementation complexity and power consumption is too high [Cab04], because the matched filter needs receivers for all types of signals and corresponding receiver algorithms to be executed.

2.3.1.4 Waveform Based Detection

The detection performance of matched filter will be degraded a lot, if wrong information about the PU's signal is used. On the other hand, most wireless communication systems exhibit certain patterns, such as pilot tones, preambles, mid-ambles, spreading codes, and etc., which are used to assist control, equalization, synchronization, continuity, or reference purposes. Even though perfect information of a PU's signal may not be attainable, if a certain pattern is known from the received signals, waveform-based sensing (a.k.a coherent detection) can be used to decide whether a PU is transmitting or not [Sah06]. As an example, the procedure of coherent detection using pilot pattern is explained as follows [Sah06].

There are two hypothesis in the coherent detection:

$$\begin{aligned} \mathcal{H}_0 &: h(i) = n(i) \\ \mathcal{H}_1 &: h(i) = \sqrt{(\epsilon)}s_p(i) + \sqrt{(1-\epsilon)}s(i) + n(i) \end{aligned} \tag{2.5}$$

where $s_p(i)$ is a known pilot tone, ϵ is the fraction of energy allocated to the pilot tone, $s(i)$ is the desired signal assumed to be orthogonal to the pilot tone. The test statistics of the coherent

detection is defined as the projected received signal in the pilot direction, i.e.,

$$T = \frac{1}{N}\sum_{i=1}^{N} h(i)\hat{s_p}(i) \tag{2.6}$$

By comparing with a pre-determined detection threshold, one can decide the presence of a PU.

Coherent detection is shown to be robust to noise uncertainty, and not limited by the SNR wall [Sah06]] as N is large enough. Moreover, coherent detection outperforms energy detection in the sensing convergence time [Cab06, Tan05b], because the sensing time of energy detection increases quadratically with the SNR reduction, while that of coherent detection only increases linearly [Tan05b].

However, the measurement results presented in [Cab06] show that the detection performance is susceptible to synchronization errors. Also, information about the waveform patterns is a prerequisite for implementing coherent detection; the more precise information a coherent detector has, the better the sensing performance will be.

2.3.1.5 Other Spectrum Sensing Techniques

There are several other SS techniques proposed in recent literature, and some of them are variations inspired by the above-mentioned SS techniques.

Wavelet Based Spectrum Sensing: Wavelets are a good tool for modeling and detecting singularities in the spectrum such as band edges. A wavelet based approach for spectrum holes detection has been proposed in [Tia06]. Once the edges, which correspond to transitions from an occupied band to an empty band or vice versa, are detected, the powers within bands between two edges are estimated. Using this information and edge positions, the frequency spectrum can be characterized as occupied or empty in a binary fashion. The assumptions made in [Tia06], however, need to be relaxed for building a practical SS algorithm. The method proposed in [Tia06] is extended in [Tia07] by using sub-Nyquist sampling. Analog implementation of wavelet-transform based SS is proposed in [You06] for coarse sensing. The disadvantages of this sensing method consist in the difficulty of knowing information about the frequency of received signals which imply relatively complicated hardware compared to the FFT based method.

Statistical Covariance Based Spectrum Sensing: Since the statistical covariance matrices of the received signal and noise are generally different, the difference is used in [Zen09b] to differentiate the desired signal component from background noise. The eigenvalues of the covariance matrix of the received signal can also be used for primary detection [Zen09a]. These methods based on statistical covariances are shown to be more robust to noise uncertainty while requiring no prior information of the signal, the channel, and noise power. A detailed discussion about this category will be presented in section 2.3.2.

Filter-Based Spectrum Sensing: Application of a specific class of filter banks for SS in CR systems is proposed in [FB08]. When filter banks are used for multicarrier communications in CR networks, the SS can be performed by only measuring the signal power at the outputs of subcarrier channels with virtually no computational cost. The multitaper method [Hay05] can also be thought as a filter bank spectrum estimation with multiple filter banks.

Higher Order Statistics based PU detection: An algorithm to detect the DTV Signals

in Gaussian noise using Higher Order Statistics (HOS) is presented in [Mod07]. The algorithm performs non-Gaussianity check in the frequency domain in the vicinity of the Pilot. This technique relies on the non-Gaussianity of a signal to separate it from the Gaussian noise. In the Time Domain, DTV Signals show a Gaussian characteristic. However, in the Frequency Domain they are non-Gaussian and this characteristic is exploited to detect the signals in AWGN. Use of Higher Order Statistics is an efficient metric for detecting non-Gaussian signals at low SNRs.

Random Hough transform based PU detection: Random Hough transform of received signal is used in [Cha04] for identifying the presence of radar pulses in the operating channels of IEEE 802.11 systems. This method can be used to detect any type of signal with a periodic pattern as well.

Fast Spectrum Sensing: By utilizing the theory of quickest detection, which performs a statistical test to detect the change of distribution in spectrum usage observations as quickly as possible, an agile and robust SS is achieved in [Li08]. The unknown parameters after a primary user appears can be estimated using the proposed successive refinement, which combines both generalized likelihood ratio and parallel cumulative sum tests. An efficient sensing-sequence is developed in [Kim08] to reduce the delay due to spectrum opportunity discovery. The probability that a frequency band is available at sensing, the sensing duration and the channel capacity are three factors that determine the sensing sequence.

Measurements-Based Spectrum Sensing and Modeling: By collecting data over a long period of time at many base stations, [Wil08] provides a unique analysis of cellular primary usage. The collected data is dissected along different dimensions to characterize the primary usage. With the aid of spectrum observatory, [Bac08] extends short-term spectrum usage measurements to study the spectrum usage trend over long periods, observes spectrum usage patterns, and detects the positions of spectrum white space in time and spatial domains. Such information can be greatly helpful in developing good dynamic access protocols and governing secondary systems.

2.3.1.6 Comparison

A summary of three main SS techniques is presented in Table 2.1 and a relative comparison in terms of complexity versus accuracy is shown in Fig. 2.10.

The energy detector is the simplest method however its performance is limited if the noise is non-stationary and its variance is unknown. The coherent methods such as waveform based sensing and matched filter are more robust than energy detection and feature detection, however there should be prior information about the PU's signal or known patterns and pilot tones. Cyclostationarity based methods are more robust than energy detector when the noise becomes non-stationary, which is the case in the presence of co-channel interference. However, these methods are prone to channel fading and sampling clock offsets [Tka07].

The characteristics of primary users are the main factor in selecting a method. While selecting a sensing method, some trade-offs among accuracy, complexity and sensing time should be considered [Zha12, dA11].

Type	Detection statistic	Advantages	Drawbacks
Energy Detection	Comparing the detected energy with a threshold	• Low complexity • No prior knowledge needed	• High false alarm due to noise uncertainty • Very unreliable in low SNR regimes
Feature Detection	Exploiting the cyclostationarity (or other intrinsic) properties of the signal	• More robust against noise uncertainty than energy detection • Ability to distinguish primary systems	• Systems with known signal patterns • Vulnerable to sampling clock offsets
Matched Filtering	Project received signal onto already known primary signal	• More robust against noise uncertainty than feature detection • Less sensing time	• Precise prior knowledge about PU's signal • High complexity

Table 2.1: Summary of three main spectrum sensing techniques

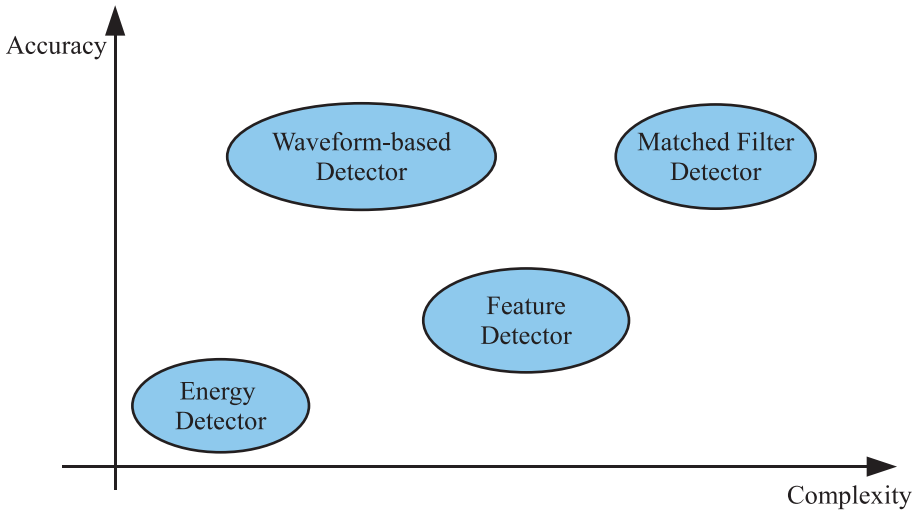

Figure 2.10: A comparison of main spectrum sensing techniques

2.3.2 Spectrum Sensing using Random Matrix Theory

A brief summary of classical SS techniques in the previous section shows that none can fully cope with all the requirements of CR networks. Based on some latest results from random matrix theory (RMT), it has been recently shown that blind detection algorithms of superior performance and robustness can be developed [Zen07,Car08,Zen09a,Pen09b] using eigenvalues of the received signal's covariance matrix. The statistical standard condition number (SCN) based approach in [Zen07, Zen09a] can be used for various signal detection algorithms. These algorithms has also been shown to outperform energy detection, when the signals to be detected are highly correlated.

The basic advantage of the RMT methods employing SCN criterion with respect to classical methods is that they do not require any prior information on the primary signal or on the noise power. This blindness feature is particularly attractive in crowded spectrum scenarios where background interference aggregate into AWGN with power dependent on the number of active users. Due to their attractive features, we focus on the eigenvalue based algorithms hereafter. In the following, we first discuss the previous work done in this category for SS. Based on their limitations, we will then present an efficient and fast SS algorithm using RMT in the subsequent section.

Denote with K the number of collaborating receivers (or antennas) and with N the number of samples during the sensing time; let $\mathbf{h}(i) = [h_1(i) \dots h_K(i)]^T$ be a $K \times 1$ vector containing K received samples at time i and $\mathbf{H} = [\mathbf{h}(1) \dots \mathbf{h}(N)]$ a $K \times N$ matrix containing all the received samples. The sample covariance matrix $\mathbf{W}(N) = \frac{1}{N}\mathbf{H}\mathbf{H}^\dagger$, converges to statistic covariance matrix $\mathbf{W} = \mathrm{E}\left[\mathbf{h}\mathbf{h}^\dagger\right]$ for a fixed K and $N \to \infty$. From the eigenvalues of $\mathbf{W}(N)$, it is possible to infer the presence or absence of the primary signal.

Let λ_{max} and λ_{min} be the largest and the smallest eigenvalues of $\mathbf{W}(N)$, and l_{max} and l_{min} those of normalized covariance matrix, defined as $\mathbf{W}'(N) = \frac{N}{\sigma^2}\mathbf{W}(N)$.

2.3.2.1 Asymptotic Model for Eigenspectrum Distribution

Under hypothesis $\mathcal{H}_0$, $\mathbf{W}'(N)$ turns out to be a white Wishart matrix and its eigenvalues follow the Marchenko-Pastur (MP) law [Mar67]. The MP law establishes that under $\mathcal{H}_0$, the eigenvalue support of $\mathbf{W}'(N)$ is finite, the smallest (l_{min}) and the largest (l_{max}) eigenvalues converge almost surely to

$$l_{min} \to a = \left(\sqrt{N} - \sqrt{K}\right)^2 \tag{2.7}$$

$$l_{max} \to b = \left(\sqrt{N} + \sqrt{K}\right)^2 \tag{2.8}$$

in the limit $(N, K) \to \infty$ with $0 < K/N < 1$ is a constant.

On the other hand, under hypothesis $\mathcal{H}_1$, the behavior of eigenvalues of $\mathbf{W}'(N)$ is related to the study of spiked population models [Bai06], which state that the largest eigenvalue converges almost surely to a value $b' > b$ under $\mathcal{H}_1$. Based on these results, two simple detection rules were proposed [Car08]:

1) Noise distribution unknown but variance known: Let l_i be any eigenvalue of $\mathbf{W}'(N)$, then if $\lambda_i \in [a, b]$, $\mathcal{H}_0$ is validated otherwise $\mathcal{H}_1$ holds true.

2) Noise distribution and variance both unknown: The ratio of the maximum and the minimum

eigenvalue of $\mathbf{W}'(N)$ does not depend upon noise variance. Therefore, a blind algorithm can be developed by using the following decision threshold

$$\gamma_{MP} = \frac{b}{a} \tag{2.9}$$

If the test statistic $T = l_{max}/l_{min} = \lambda_{max}/\lambda_{min} \leq \gamma_{MP}$, the detector decides $\mathcal{H}_0$, otherwise $\mathcal{H}_1$.

2.3.2.2 Semi-asymptotic Model for Eigenspectrum Distribution

A limiting distribution of l_{max} has been found in [Joh01] which states that the random variable

$$L_{max} = \frac{l_{max} - b}{\nu} \tag{2.10}$$

with

$$\nu = \left(\sqrt{N} + \sqrt{K}\right)\left(\frac{1}{\sqrt{N}} + \frac{1}{\sqrt{K}}\right)^{1/3} \tag{2.11}$$

converges (with probability one) to Tracy-Widom (TW) distribution of order 2 (order 1 for real noise) [Tra96, Tra00], under the same assumptions of $(N, K) \to \infty$ with $0 < K/N < 1$. This property has been exploited in [Zen07, Zen09a] to design a sensing algorithm, in which the Tracy-Widom cumulative distribution function (CDF) is used to model the random nominator, while the asymptotic MP law in (2.7) is maintained for the constant denominator, leading to an approximate SCN distribution used to relate the test threshold γ_{TW} to a prescribed probability of false alarm P_{fa}. The threshold can be written as

$$\gamma_{TW} = \gamma_{MP}.\left(1 + \frac{\left(\sqrt{N} + \sqrt{K}\right)^{-2/3}}{(NK)^{1/6}} F_{TW2}^{-1}(1 - P_{fa})\right) \tag{2.12}$$

where $F_{TW2}^{-1}(.)$ is the inverse TW CDF of order 2.

2.3.2.3 Semi-asymptotic Model for SCN Distribution

A recent result in [Fel10] showed that l_{min} also converges to TW distribution as $(N, K) \to \infty$, up to a proper rescaling factor. Thus, the random variable

$$L_{min} = \frac{l_{min} - a}{\mu} \tag{2.13}$$

converges in distribution to TW of order 2, with

$$\mu = \left(\sqrt{K} - \sqrt{N}\right)\left(\frac{1}{\sqrt{K}} - \frac{1}{\sqrt{N}}\right)^{1/3} \tag{2.14}$$

As $0 < K/N < 1$, μ is always negative. The test statistic may be written as

$$T = \frac{l_{max}}{l_{min}} = \frac{\nu L_{max} + b}{\mu L_{min} + a} \tag{2.15}$$

Applying the Curtiss formula on the ratio distribution of random variates [Cur41], combined with the previously explained limiting distributions of the smallest and the largest eigenvalues, leads to a more accurate model of SCN, which is exploited in [Pen09a, Pen09b] to develop a SS algorithm, which we dub as Tracy-Widom-Curtiss (TWC). The decision threshold can be given as

$$\gamma_{TWC} = F_{TWC}^{-1}(1 - P_{fa}) \tag{2.16}$$

where $F_{TWC}^{-1}(.)$ is CDF corresponding to limited eigenvalue ratio distribution of T.

2.3.2.4 Comments on Asymptotic Models Based Sensing

A comparative analysis of the methods relying on asymptotic random matrix models is presented in [Zha12]. It is shown that the TWC based sensing algorithms (Sec. 2.3.2.3) are generally superior to TW based algorithms (Sec. 2.3.2.2), which in turn outperform MP based method (Sec. 2.3.2.1).

The under-performance of the MP based algorithm results from the inaccuracy of the model with small sample sizes. In practical conditions, that may be characterized by small number of observations due to time-varying channel and/or detection in the shortest possible time, the asymptotic threshold turns out to be very unbalanced with respect to the actual eigenvalue ratio distribution [Pen09b]. Furthermore, this approach does not allow to tune the threshold as a function of a target P_{fa}.

The TW based approach admits a tolerated P_{fa} to be accommodated in the hypothesis test, but it is still based on the asymptotic limit for the smallest eigenvalue and it becomes inaccurate when N decreases. It exhibits better performance than MP alternatives but only for large SNR values.

The TWC based algorithm outperforms the others across a wide SNR range, however TW distribution and Curtiss formula are highly involved functions and hard to evaluate numerically. Thus, the improvement achieved by moving from MP based to TWC based methods comes at the expense of an increase in complexity and a loss of mathematical tractability.

Nevertheless, an interesting observation is that none of the aforementioned techniques require the knowledge of noise power. This blind feature is highly desirable in practical situations. Unfortunately, this potential advantage is undermined by the fact that all these methods are asymptotic and thus, only approximately applicable to finite and small numbers of samples. This in turn implies (contradictorily) that an accurate estimate of the average noise power can be obtained directly from the samples, with accuracy proportional to their number [Tan08]. Once we have the accurate knowledge about noise power, it will be more appealing to apply the simple energy detector.

In conclusion, it is reasonable to say that in order to truly exploit the potential of RMT based approaches to blind SS, novel techniques addressing the SS problem from a **finite random matrix theory (FRMT)** perspective are required. This is the subject of the subsequent section.

2.4 Fast Spectrum Sensing Using Finite Random Matrix Theory

In this section, we ought to develop efficient SS algorithms, that require only few number of samples, keeping the blindness feature in tact. Recently, Zhang *et al.* [Zha12] presented interesting

SS algorithms by invoking novel results on the exact distribution of SCNs of dual Wishart random matrices. Although the algorithms are robust and appealing, the authors left few questions unanswered which motivated us to develop them further. Thus, the work presented herein can be considered as an extension of their contribution.

2.4.1 Received Sample Model

Considering a single PU in the standard AWGN model, the i^{th} sample of the received signal is given as

$$h(i) = \sqrt{\beta}s(i) + n(i) \tag{2.17}$$

where β is the SNR, $s(i)$ is the PU signal with channel effect, $n(i)$ are independent, identically distributed (i.i.d) variates such that $n(i) \sim \mathcal{N}_{\mathbb{C}}(0,1)$ in which $\mathcal{N}_{\mathbb{C}}(0,1)$ denotes the circularly symmetric complex standard normal distribution and the notation $x \sim f(x)$ indicates that "$f(x)$" is the distribution of "x".

The primary user detection problem is formulated as a three hypotheses problem in [Zha12], defined by

$$\begin{aligned}
&\mathcal{H}_0 : h(i) = n(i) \\
&\mathcal{H}_1^c : h(i) = \sqrt{\beta}s(i) + n(i), \qquad |s| = 1 \\
&\mathcal{H}_1^r : h(i) = \sqrt{\beta}s(i) + n(i), \qquad s(i) \sim \mathcal{N}_{\mathbb{C}}(0,1)
\end{aligned} \tag{2.18}$$

where $\mathcal{H}_0$ corresponds to the hypothesis of the absence of PU signal while $\mathcal{H}_1^c$ and $\mathcal{H}_1^r$ denote the hypothesis of the presence of constant and random PU signal respectively.

The hypothesis $\mathcal{H}_1^c$ models the case when a single symbol of the PU over an AWGN channel is observed, in which case $s(i)$ may be an unknown arbitrary complex constant with $|s| = 1$. The hypothesis $\mathcal{H}_1^r$ models the case when the PU signal is sampled subject to uncorrelated (fast) Rayleigh fading, and/or is modulated within the received block of samples, in which case $s(i)$ are i.i.d. variates such that $s(i) \sim \mathcal{N}_{\mathbb{C}}(0,1)$.

Following the model described by (2.17), if a number $M = K \times N$ of samples is available, the receiver may build either of the following $K \times N$ random matrices

$$\mathbf{H} = \begin{cases} \mathbf{H}_n & \text{if } \mathcal{H}_0 \text{ is true} \qquad (2.19a) \\ \sqrt{\beta}.\mathbf{H}_s + \mathbf{H}_n & \text{if } \mathcal{H}_1 \text{ is true} \qquad (2.19b) \end{cases}$$

In [Zha12], two SS algorithms corresponding to $\mathcal{H}_0$ and $\mathcal{H}_1^c$ are proposed. However, the authors provide no solution for the extreme $\mathcal{H}_1^r$ case. Also, we found that the finite model used for SCN distribution in $\mathcal{H}_1^c$ case provide poor fit to the actual distribution.

In the sequel, we develop algorithms corresponding to the three hypotheses, using recent finite RMT results for the eigenspectrum and SCN's of Wishart matrices $\mathbf{W} \triangleq \mathbf{H}\mathbf{H}^{\dagger}$, where $\dagger$ denotes transpose conjugate (Hermitian), with $\mathbf{H}$ as given in (2.19). The PDFs and CDFs are denoted by f and F under $\mathcal{H}_0$, $\mathcal{H}_1^c$ and $\mathcal{H}_1^r$ respectively. Finally, without loss of generality [Zha12], all results to follow are for $K = 2$[1] and $K \leq N$ such that $\mathbf{W}$ is full-rank.

[1]Notice that for the binary hypothesis problem at hand, $K = 2$ is sufficient. In addition, choosing a lower value of K ensures that $\mathbf{W}$ is better-conditioned.

	SNR = -5 dB	SNR = 0 dB	SNR = 5 dB	SNR = 10 dB
RMT (eq. (2.20))	0.99	0.98	0.99	0.98
Lognormal	0.05	0.05	0.07	0.05
GEV	0.92	0.91	0.92	0.89

Table 2.2: Chi-square GOF test for hypothesis $\mathcal{H}_0$ – Mean acceptance rate vs SNR for three candidate distributions

2.4.2 Test based on SCN distribution under $\mathcal{H}_0$

A closed-form expression for the distribution of the SCN of finite dual uncorrelated Wishart matrices has been recently reported in [Mat10], which is of particular relevance to our purpose.

SCN distribution of uncorrelated central Wishart matrix under $\mathcal{H}_0$

Theorem 1 - PDF and CDF for $\mathcal{H}_0$:
Let λ_1, λ_2 be the sorted eigenvalues of $\mathbf{W}$ and $T|_{\mathcal{H}_0} \triangleq \lambda_2|_{\mathcal{H}_0}/\lambda_1|_{\mathcal{H}_0} \geq 1$ denote the SCN of dual uncorrelated central Wishart matrices $\mathbf{W}$, with $\mathbf{H}$ as in (2.19a). Then as given in [Zha12],

$$T|_{\mathcal{H}_0} \sim f^{(0)}_{SCN}(r;N) \triangleq \frac{S_1(r;N)}{2(N-1)!(N-2)!} \tag{2.20}$$

$$F^{(0)}_{SCN}(r;N) = \frac{S_2(r;N) - S_1(1;N)}{2(N-1)!(N-2)!} \tag{2.21}$$

where

$$S_i(r;N) \triangleq \Delta_i(r;N,N-1) - 2\Delta_i(r;N-1,N) + \Delta_i(r;N-2,N+1) \tag{2.22}$$

with $i = \{1,2\}$ and

$$\Delta_1(r;M,N) \triangleq \frac{(N-1)!}{(r+1)^2}\left[\sum_{n=0}^{N-1}\frac{\left(M+1-\frac{n}{r}\right)}{r^n}\prod_{m=1}^{M}\frac{n+m}{r+1}\right], \tag{2.23}$$

$$\Delta_2(r;M,N) \triangleq (N-1)!\left[M! - \frac{1}{r+1}\sum_{n=0}^{N-1}\frac{r^n}{(r+1)^n}\prod_{m=1}^{M}\frac{n+m}{r+1}\right] \tag{2.24}$$

Unlike the previous asymptotic models for the eigenvalue and condition number distributions of complex Wishart matrices given in section 2.3.2, the above expressions are valid irrespective of the number of samples. It may also be emphasized that despite the appearance of being somewhat involved, the above PDF and CDF are actually very simple and fast to evaluate, since they are indeed simple rational functions.

The accuracy of the model described by (2.20) is validated using chi-square test. The acceptance rate for the model in (2.20) and two reference distributions of lognormal and GEV, against the empirical data for four different SNR values, is given in Table 2.2. Clearly, the proposed model fits best the empirical data for all the SNRs. The same fact can also be observed in Fig. 2.11.

The exact and relatively simple PDF and CDF expressions of (2.20) and (2.21) can be readily employed in the design of spectrum-sensing algorithms [dA10]. In the vast majority of SS techniques

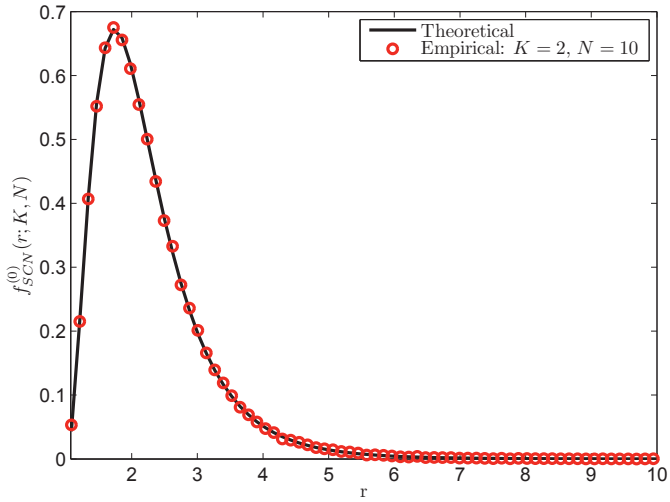

Figure 2.11: Probability density function and corresponding empirical distribution of the SCN of uncorrelated central Wishart matrices at SNR = 0dB

proposed [Yuc09], the threshold is determined from a given P_{fa}. Using the finite RMT tool described above, this "standard" detection scheme can be easily set up, with the threshold given by $\gamma^{(0)}_{SCN} = F^{(0)^{-1}}_{SCN}(1 - P_{fa})$ (see Eq. (15) [Pen09b]).

Specifically, given a prescribed P_{fa} and $2 \times N$ samples h_{kn}, the SS algorithm based on the above model is described by

Algorithm 1

1) Construct $\mathbf{H} \triangleq [h_{kn}]_{k=\{1,2\} \times n=\{1,\ldots N\}}$
2) Compute the eigenvalues (λ_1, λ_2) of $\mathbf{W} \triangleq \mathbf{H}\mathbf{H}^{\dagger}$
3) Evaluate the SCN $T \triangleq \lambda_2/\lambda_1$
4) Accept $\mathcal{H}_0$ if and only if $T \leq F^{(0)^{-1}}_{SCN}(1 - P_{fa})$

For conciseness, we shall hereafter loosely refer to the test described above as the **"SCN$_0$ Test"**.

2.4.3 Test based on SCN distribution under $\mathcal{H}_1^c$

Let the signal matrix in equation (2.19b) be $\mathbf{H}_s = s.\mathbf{1}_{K \times N}$ where $\mathbf{1}_{K \times N}$ is a matrix whose elements are all 1's, while s is an unknown complex constant with $|s| = 1$. Then, the received data matrix

$$\mathbf{H} = \sqrt{\beta} s.\mathbf{1}_{K \times N} + \mathbf{H}_n \tag{2.25}$$

is a complex non-central Wishart matrix.

The main difficulty in evaluating the SCN distribution of non-central Wishart matrices is the lack of simple closed-form expressions for the extreme eigenvalue distributions. On the other hand, both exact and asymptotic extreme eigenvalue distributions for correlated central Wishart matrices

are possible to obtain [Tan83, Zan08, Bai08]. Therefore, a natural idea is to move the effect of the non-centrality into the correlation part of the central matrix. Consider the $K \times N$ correlated complex normal distribution $\mathbf{Y}$ as

$$\mathbf{Y} = \mathbf{\Sigma}^{1/2}\mathbf{S} \tag{2.26}$$

where $\mathbf{S} \sim \mathcal{N}_{\mathbb{C}^{K\times N}}(0,1)$ and $\mathbf{\Sigma}^{1/2}$ stands for correlation matrix.

The first moment of the non-central Wishart matrix in (2.25) and the central Wishart matrix in (2.26) is given as

$$E\left[\mathbf{H}\mathbf{H}^{\dagger}\right] = \beta N \mathbf{1}_K + N\mathbf{I}_K \tag{2.27}$$

and

$$E\left[\mathbf{Y}\mathbf{Y}^{\dagger}\right] = N\mathbf{\Sigma}_K \tag{2.28}$$

respectively, where $E[.]$ denotes expectation and $\mathbf{I}_K$ is the $K \times K$ identity matrix.

Equaling these, we obtain an equivalent correlation matrix

$$\mathbf{\Sigma}_K = \beta \mathbf{1}_K + \mathbf{I}_K \tag{2.29}$$

The equivalent correlation matrix $\mathbf{\Sigma}_K$ incorporates the non-centrality of the original non-central Wishart matrix. The implication of this result is that the SCN distribution of the non-central complex Wishart matrices can be accurately approximated by that of a semi-correlated central complex Wishart matrix. In light of this result, a test can be designed based on the properties of semi-correlated central Wishart matrices.

SCN distribution of semi-correlated central Wishart matrix under $\mathcal{H}_1^c$

Theorem 2 - PDF and CDF for $\mathcal{H}_1^c$:
Let $T|_{\mathcal{H}_1^c} \triangleq \lambda_2|_{\mathcal{H}_1^c}/\lambda_1|_{\mathcal{H}_1^c} \geq 1$ still denote the SCN of dual semi-correlated central Wishart matrices $\mathbf{W} \triangleq (\mathbf{\Sigma}_2^{1/2}\mathbf{H}).(\mathbf{\Sigma}_2^{1/2}\mathbf{H})^{\dagger}$, with $\mathbf{H}$ as in (2.19a). $\mathbf{\Sigma}_2$, given in (2.29), denotes the associated correlation matrix and $\theta_1 > \theta_2$ are its corresponding ordered eigenvalues. Then as shown in [Zha12]

$$T|_{\mathcal{H}_1^c} \sim f_{SCN}^{(c)}(r; N, \theta_1, \theta_2) \triangleq \frac{S_3(r; N, \theta_1, \theta_2)}{\Phi(N, \theta_1, \theta_2)}, \tag{2.30}$$

$$F_{SCN}^{(c)}(r; N, \theta_1, \theta_2) = \frac{S_4(r; N, \theta_1, \theta_2) - S_4(1; N, \theta_1, \theta_2)}{\Phi(N, \theta_1, \theta_2)} \tag{2.31}$$

where

$$\Phi(N, \theta_1, \theta_2) \triangleq \frac{(\theta_2 - \theta_1).(N-1)!\,(N-2)!}{(\theta_1 - \theta_2)^{1-N}} \tag{2.32}$$

and

$$\begin{aligned} S_i(r; N, \theta_1, \theta_2) \triangleq\ & \Delta_i\left(r; N-1, N-1, \theta_1^{-1}, \theta_2^{-1}\right) - \Delta_i\left(r; N-2, N, \theta_1^{-1}, \theta_2^{-1}\right) \\ & - \Delta_i\left(r; N-1, N-1, \theta_2^{-1}, \theta_1^{-1}\right) + \Delta_i\left(r; N-2, N, \theta_2^{-1}, \theta_1^{-1}\right), \end{aligned} \tag{2.33}$$

with $i = \{3, 4\}$ and

$$\Delta_3(r; M, N, \theta_1, \theta_2) \triangleq \frac{(N-1)!}{(\theta_1 + \theta_2)^{m+2}} \left[\sum_{n=0}^{N-1} \frac{\left(M + 1 - \frac{n}{r}\right).(\theta_1.r)^n}{(\theta_1.r + \theta_2)^n} \prod_{m=1}^{M}(n+m)\right] \tag{2.34}$$

	SNR = -5 dB	SNR = 0 dB	SNR = 5 dB	SNR = 10 dB
RMT (eq. (2.30))	0.89	0.08	0	0
Lognormal	0.32	0.7	0.41	0.08
GEV	0.96	0.98	0.99	1

Table 2.3: Chi-square GOF test for hypothesis $\mathcal{H}_1^c$ – Mean acceptance rate vs SNR for three candidate distributions

$$\Delta_4\left(r;M,N,\theta_1,\theta_2\right) \triangleq \frac{(N-1)!}{(\theta_1)^N}\left[\frac{M!}{\theta_2^{M+1}}\frac{1}{(\theta_1.r+\theta_2)^{M+1}}\sum_{n=0}^{N-1}\frac{(\theta_1.r)^n}{(\theta_1.r+\theta_2)^n}\prod_{m=1}^{M}(n+m)\right] \tag{2.35}$$

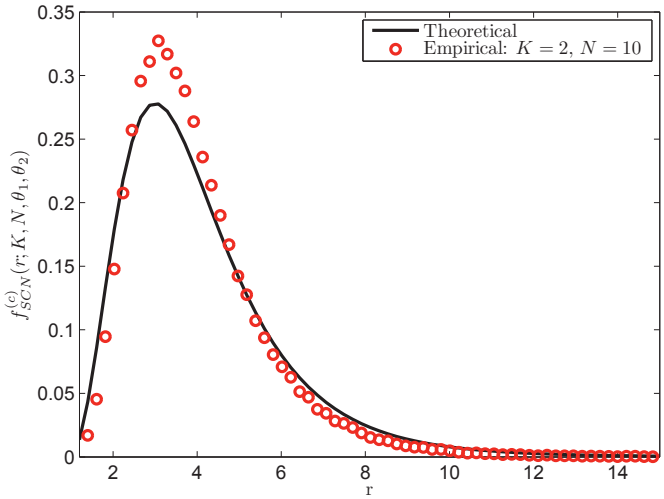

Figure 2.12: Probability density function of the SCN of semi-correlated dual Wishart matrices with correlation given in equation (2.29) and corresponding empirical distribution of non-central dual Wishart matrices at SNR = 0dB

A SS algorithm based on the above SCN distribution model is proposed in [Zha12]. However, as demonstrated by Fig. 2.12, the theoretical distribution as calculated by equation (2.30) provide poor fit to the empirical distribution. Therefore, the sensing algorithm based on this model is prone to exhibit unsatisfactory performance.

By applying the GOF tests on the empirical data, we observed that the GEV distribution provide a very good fit to the empirical SCN distribution under $\mathcal{H}_1^c$. The acceptance rate for GEV along with $f_{SCN}^{(c)}$ in (2.30) and lognormal distributions against the empirical data for four different SNR values is given in Table 2.3. Clearly, GEV distribution fits very well the empirical data for all the SNRs while the $f_{SCN}^{(c)}$ performs very poor. This GEV fitness fact is also graphically depicted in Fig. 2.13. Consequently, we propose a better-suited GEV model for SCN distribution.

Theorem 3 - PDF and CDF for $\mathcal{H}_1^c$:

Let $T|_{\mathcal{H}_1^c} \triangleq \lambda_2|_{\mathcal{H}_1^c}/\lambda_1|_{\mathcal{H}_1^c} \geq 1$ denote the SCN of dual non-central Wishart matrices $\mathbf{W}$, with $\mathbf{H}$

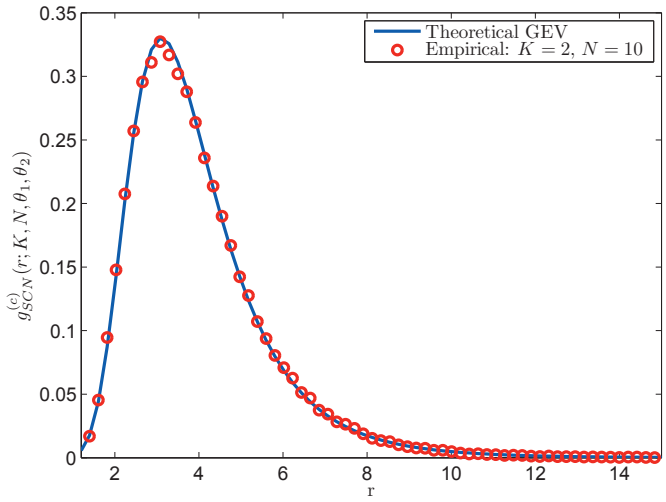

Figure 2.13: Probability density function of the GEV and the empirical distribution of the SCN of non-central dual Wishart matrices at SNR = 0dB

as in (2.19b). Then

$$T|_{\mathcal{H}_1^c} \sim g^{(c)}_{SCN}(r;\mu^{(c)},\sigma^{(c)},\xi^{(c)}) = \frac{1}{\sigma^{(c)}}\left[1+\xi^{(c)}\left(\frac{r-\mu^{(c)}}{\sigma^{(c)}}\right)\right]^{\left(-1/\xi^{(c)}\right)-1} \exp\left\{-\left[1+\xi^{(c)}\left(\frac{r-\mu^{(c)}}{\sigma^{(c)}}\right)\right]^{-1/\xi^{(c)}}\right\} \tag{2.36}$$

$$G^{(c)}_{SCN}(r;\mu^{(c)},\sigma^{(c)},\xi^{(c)}) = \exp\left\{-\left[1+\xi^{(c)}\left(\frac{r-\mu^{(c)}}{\sigma^{(c)}}\right)\right]^{-1/\xi^{(c)}}\right\} \tag{2.37}$$

for $1+\xi^{(c)}(r-\mu^{(c)})/\sigma^{(c)} > 0$, where

- $\mu^{(c)} \in \mathbb{R}$ is the location parameter
- $\sigma^{(c)} > 0$ is the scale parameter
- $\xi^{(c)} \in \mathbb{R}$ is the shape parameter.

A test analogous to $\mathbf{SCN}_0$ can be performed using the above GEV model, such that a prescribed probability of miss-detection P_{md} is not violated.

To this end, all that needs to be done is to replace the threshold $\gamma^{(c)}_{SCN} \triangleq G^{(c)^{-1}}_{SCN}(P_{md})$. Given a prescribed P_{md} and $2 \times N$ samples h_{kn}, the test can be summarized as

Algorithm 2

1) Construct $\mathbf{H} \triangleq [h_{kn}]_{k=\{1,2\}\times n=\{1,\dots N\}}$
2) Compute the eigenvalues (λ_1, λ_2) of $\mathbf{W} \triangleq \mathbf{H}\mathbf{H}^\dagger$
3) Evaluate the SCN $T \triangleq \lambda_2/\lambda_1$
4) Accept $\mathcal{H}_1^c$ if and only if $T \geq G^{(c)^{-1}}_{SCN}(P_{md})$

For conciseness, we shall hereafter loosely refer to the test described above as the **"SCN$_1$ Test"**.

2.4.4 Test based on Eigenvalues distribution under $\mathcal{H}_1^r$

SCN distribution of uncorrelated central Wishart matrix under $\mathcal{H}_1^r$

PDF and CDF for $\mathcal{H}_1^r$:
Let $T|_{\mathcal{H}_1^r} \triangleq \lambda_2|_{\mathcal{H}_1^r}/\lambda_1|_{\mathcal{H}_1^r} \geq 1$ denote the SCN of dual uncorrelated central Wishart matrices $\mathbf{W}$, with $\mathbf{H}$ as in (2.19b) and $\mathbf{H}_s \sim \mathcal{N}_{\mathbb{C}^{K\times N}}(0,1)$. Then as found by [Zha12],

$$T|_{\mathcal{H}_1^r} \sim f_{SCN}^{(0)}(r;N) \tag{2.38}$$

$$\Pr\left\{T|_{\mathcal{H}_1^r} \leq r\right\} = F_{SCN}^{(0)}(r;N) \tag{2.39}$$

Since $\mathbf{H}_n \sim \mathcal{N}_{\mathbb{C}^{K\times N}}(0,1)$, therefore $\mathbf{H} \sim \mathcal{N}_{\mathbb{C}^{K\times N}}(0,1+\beta)$. Consequently, $\lambda_k|_{\mathcal{H}_1^r}$ behaves as $(1+\beta).\lambda_k|_{\mathcal{H}_0}$. In other words, $\lambda_k|_{\mathcal{H}_1^r}$ follows same distribution as of $\lambda_k|_{\mathcal{H}_0}$, scaled by $(1+\beta)$, which in turn implies that $\lambda_2|_{\mathcal{H}_1^r}/\lambda_1|_{\mathcal{H}_1^r}$ follows the same distribution as $\lambda_2|_{\mathcal{H}_0}/\lambda_1|_{\mathcal{H}_0}$.

This fact is illustrated in Fig. 2.14. It is clear that the two SCNs distributions corresponding to hypotheses $\mathcal{H}_0$ and $\mathcal{H}_1^r$ superpose and therefore can not be separated. This means that SCN based test statistics can not be used to design the SS algorithms for detecting the presence of PUs with random i.i.d. signals.

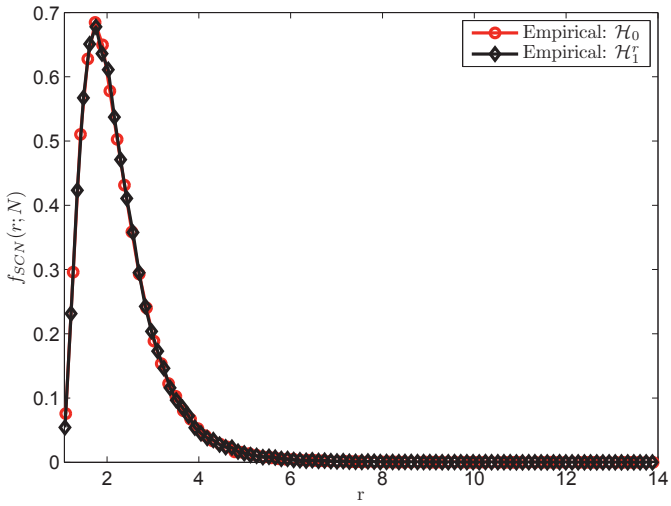

Figure 2.14: Probability density function of the SCN distribution of uncorrelated central Wishart matrices at SNR = 0dB for $K = 2$, $N = 10$.

The failure of SCN statistics calls for alternate solutions in this scenario. In the following, we develop two algorithms based on the eigenspectrum distribution.

A - BSL Finite Model for Eigenspectrum Distribution

1) PDF Under $\mathcal{H}_0$:

Let $\lambda|_{\mathcal{H}_0}$ denote any eigenvalue of $\mathbf{W}$, with $\mathbf{H}$ as in equation (2.19a). Then by [Bro65] and [Shi03],

$$\lambda|_{\mathcal{H}_0} \sim f_{EV}^{(0)}(r;K,N) \triangleq \frac{1}{K}\sum_{k=0}^{K-1}\frac{k!r^{N-K}e^{-r}}{(N-K+k)!}\left[L_k^{N-K}\right]^2, \tag{2.40}$$

where $L_a^b(x)$ is the Laguerre polynomial of order a,

$$L_a^b(x) = \sum_{l=0}^{a}(-1)^l.\binom{a+b}{a-l}.\frac{x^l}{l!} \tag{2.41}$$

2) PDF Under $\mathcal{H}_1^r$:
Let $\lambda|_{\mathcal{H}_1^r}$ denote any eigenvalue of $\mathbf{W}$, with $\mathbf{H}$ as in equation (2.19b) and $\mathbf{H}_s \sim \mathcal{N}_{\mathbb{C}^{K\times N}}(0,\beta)$. Then,

$$\lambda|_{\mathcal{H}_1^r} \sim f_{EV}^{(r)}(r;K,N,\beta) \triangleq \frac{1}{1+\beta}.f_{EV}^{(0)}\left(\frac{r}{1+\beta};K,N\right) \tag{2.42}$$

This result follows directly from the discussion after equation (2.39).

The CDFs corresponding to PDFs in (2.40) and (2.42) can be found by the numerical integration of respective PDFs. The resulting eigenspectrum is represented in Fig. 2.15. We observe that the Bronk-Shin-Lee model does not fit well the empirical data at low SNRs but as the SNR improves, it estimates the PDF quite accurately. In addition, the eigenspectrum distributions for $\mathcal{H}_0$ and $\mathcal{H}_1^r$ are quite distinct and thus can be used to design the SS algorithm.

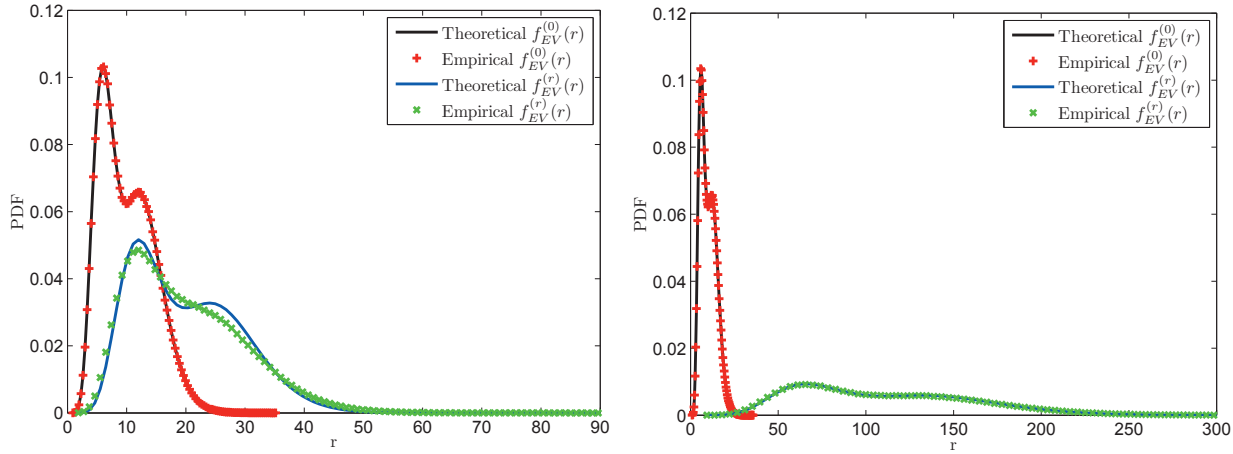

Figure 2.15: Probability density function of all eigenvalues by BSL model and corresponding empirical distributions of all eigenvalues with $K = 2$, $N = 10$; at (a) SNR $= 0$ dB (b) SNR $= 10$ dB

In the following, we summarize an approximate SS approach using eigenspectrum distribution. Given a prescribed P_{fa} and $2 \times N$ samples h_{kn}:

Algorithm 3

1) Construct $\mathbf{H} \triangleq [h_{kn}]_{k=\{1,2\}\times n=\{1,\ldots N\}}$
2) Compute the eigenvalues (λ_1, λ_2) of $\mathbf{W} \triangleq \mathbf{H}\mathbf{H}^\dagger$

3) Select the threshold $\gamma_{EV}^{(r)} = F_{EV}^{(r)^{-1}}(P_{md})$

4) Decide using the following reasoning

$$\begin{cases} \lambda_1 < \gamma_{EV}^{(r)} \text{ and } \lambda_2 < \gamma_{EV}^{(r)}, & \text{Decide } \mathcal{H}_0 \\ \lambda_1 > \gamma_{EV}^{(r)} \text{ and } \lambda_2 > \gamma_{EV}^{(r)}, & \text{Decide } \mathcal{H}_1^r \\ \lambda_1 < \gamma_{EV}^{(r)} \text{ and } \lambda_2 > \gamma_{EV}^{(r)}, & \Rightarrow \begin{cases} |\lambda_1 - \gamma_{EV}^{(r)}| > |\lambda_2 - \gamma_{EV}^{(r)}|, & \text{Decide } \mathcal{H}_0 \\ |\lambda_1 - \gamma_{EV}^{(r)}| < |\lambda_2 - \gamma_{EV}^{(r)}|, & \text{Decide } \mathcal{H}_1^r \end{cases} \end{cases} \tag{2.43}$$

For brevity, we shall hereafter loosely refer to the test described above as the **"EV Test"**.

B - Gamma Distribution for Sum of Eigenvalues It is well-known that the summation of eigenvalues of a matrix is the trace of a matrix. Also, this eigenvalues' sum (EVS) is shown to be almost same as the signal energy [Zen09a]. Therefore, EVS is equivalent to energy detection which is considered optimal for i.i.d. signals [Kay88a]. Based on EVS, therefore we can develop a SS algorithm for $\mathcal{H}_1^r$.

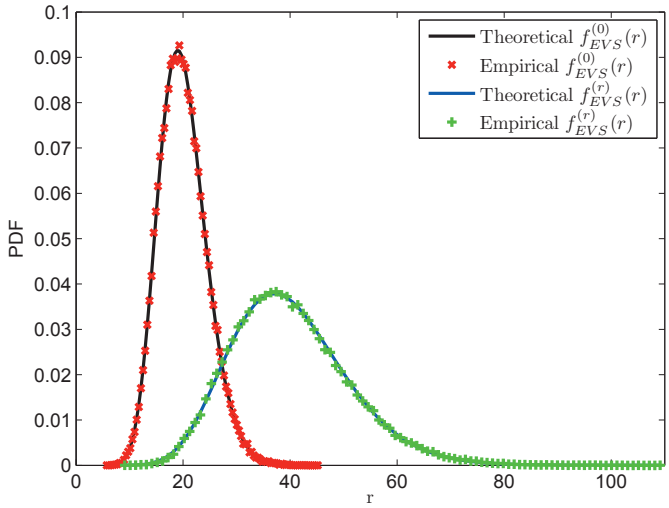

Figure 2.16: Probability density function of the sum of eigenvalues by Gamma distribution and corresponding empirical distribution at SNR = 0dB for $K = 2$, $N = 10$.

Using again the GOF test, we found that sum of eigenvalues follows a gamma distribution. This is reasonable as the test statistic in case of energy detector follows chi-square distribution [Dig03], which is a special case of Gamma distribution. This acceptance rate of Gamma distribution against empirical data against four different SNR values is provided in Table 2.4. The acceptance rate of BSL distribution is also given in the Table 2.4. It is clear from the test result that the Gamma distribution fits well the data for all the SNR values for both hypotheses. On the other hand, the BSL distribution matches well in case of hypothesis $\mathcal{H}_0$ and only for high SNR value for hypothesis $\mathcal{H}_1^r$. This is in accordance with the Fig. 2.15.

Let $T|_{\mathcal{H}_1^r} \triangleq (\lambda_1 + \lambda_2)\,|_{\mathcal{H}_1^r}$ denote the SCN of dual uncorrelated central Wishart matrices $\mathbf{W}$, with $\mathbf{H}$ as in (2.19b) and $\mathbf{H}_s \sim \mathcal{N}_{\mathbb{C}^{K\times N}}(0, \beta)$. Then

$$T|_{\mathcal{H}_1^r} \sim f_{EVS}^{(r)}(r; k^{(r)}, \zeta^{(r)}) \sim \frac{1}{\zeta_{k^{(r)}}^{(r)}} \frac{1}{\Gamma(k^{(r)})} r^{k^{(r)}-1} e^{-\frac{r}{\zeta^{(r)}}} \tag{2.44}$$

	SNR = -5 dB	SNR = 0 dB	SNR = 5 dB	SNR = 10 dB
Hypothesis $\mathcal{H}_0$				
BSL	0.99	0.99	1	1
Gamma	0.99	0.98	0.97	1
Hypothesis $\mathcal{H}_1^r$				
BSL	0.2	0.01	16	94
Gamma	0.99	0.98	0.97	1

Table 2.4: Chi-square GOF test – Mean acceptance rate vs SNR for the considered distributions

$$F_{EVS}^{(r)}(r;k^{(r)},\zeta^{(r)}) = \frac{\gamma\left(k^{(r)},\frac{r}{\zeta^{(r)}}\right)}{\Gamma(k^{(r)})} \tag{2.45}$$

where $\Gamma(k)$ is the gamma function, $\gamma\left(k, r/\zeta\right)$ is lower incomplete gamma function and $(r;k^{(r)},\zeta^{(r)}) > 0$ with

- k is the shape parameter
- ζ is the scale parameter

The accuracy of gamma distribution fitting the sum of eigenvalues is also illustrated in Fig. 2.16. Thus, it can be concluded that Gamma distribution can fit the EVS statistic under both hypotheses of no signal and random i.i.d. signal. We will denote the Gamma distribution under $\mathcal{H}_0$ by $f_{EVS}^{(0)}(r;k^{(0)},\zeta^{(0)})$. Given a prescribed P_{fa} and $2\times N$ samples h_{kn}, a novel test can be developed as

Algorithm 4

1) Construct $\mathbf{H} \triangleq [h_{kn}]_{k=\{1,2\}\times n=\{1,\ldots N\}}$
2) Compute the eigenvalues (λ_1,λ_2) of $\mathbf{W} \triangleq \mathbf{H}\mathbf{H}^\dagger$
3) Evaluate the EVS $T \triangleq (\lambda_1+\lambda_2)$
4) Accept $\mathcal{H}_1^r$ if and only if $T \geq F_{EVS}^{(0)^{-1}}(1-P_{fa})$

For conciseness, we shall hereafter loosely refer to the test described above as the **"EVS Test"**.

In practical applications the values of $F^{-1}(.)$, evaluated numerically off-line, can be stored in a look-up table and then used by the receiver to set the proper threshold as a function of N, K and target P_{fa} or P_{md}.

2.5 Performance Evaluation of Spectrum Sensing Algorithms

In the following, we will evaluate the SS algorithms using a) constant envelope PU signal ($\mathcal{H}_1^c$) b) random i.i.d. PU signal ($\mathcal{H}_1^r$) and c) random correlated PU signal (we term it $\mathcal{H}_1^{rc}$). The number

Method	Decision variable	Distribution Model	Test Statistic	Threshold
SCN_0	Standard Condition Number	Matthaiou *et al.* [Mat10]	$T\|_{\mathcal{H}_0}$	$F_{SCN}^{(0)^{-1}}(1-P_{fa})$
SCN_1	Standard Condition Number	Generalized Extreme Value (GEV)	$T\|_{\mathcal{H}_1^c}$	$G_{SCN}^{(c)^{-1}}(P_{md})$
EV	Eigenvalue spectra	Bronk-Shin-Lee [Bro65, Shi03]	$\lambda\|_{\mathcal{H}_0}$	$F_{EV}^{(r)^{-1}}(P_{md})$
EVS	Eigenvalues Sum	Gamma	$T\|_{\mathcal{H}_1^r}$	$F_{EVS}^{(0)^{-1}}(1-P_{fa})$

Table 2.5: Summary of spectrum sensing algorithms from radom matrix theory

of samples are assumed 20 ($K = 2$, $N = 10$) throughout and the results are averaged over 10^4 Monte-Carlo realizations.

First, the SCN based algorithms SCN_0 and SCN_1 are tested for $\mathcal{H}_1^c$ and the corresponding results are plotted in Figs. 2.17 and 2.18. It can be observed that P_{md} (P_{fa}) of less than 10% is achieved under a constrained $P_{fa} = 0.05$ ($P_{md} = 0.05$), with an SNR as less as 3 dB by the test SCN_0 (SCN_1). The exact estimated P_{fa} (P_{md}), corresponding to the prescribed probabilities P_{md} (P_{fa}) for the two tests, is a direct consequence of the accurate SCN models of (2.20) and (2.36).

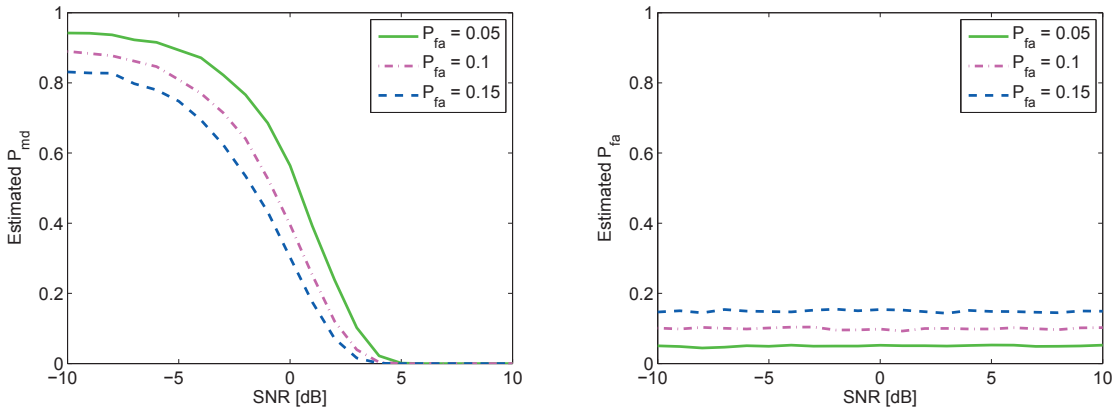

(a) (b)

Figure 2.17: Performance of spectrum sensing algorithm SCN_0 under $\mathcal{H}_1^c$, as a function of SNR and tolerated P_{fa}.

A direct comparison of the two schemes reveals that they exhibit almost similar performance. However, it must be noted that test SCN_0 does not need any prior knowledge about the signal or the noise power, therefore can be classified as a totally *blind* scheme. The test SCN_1, on the other hand, does need to estimate the SNR to determine the threshold, therefore making it a *semi-blind* approach. This makes us to believe that the test SCN_0 is more attractive from practical viewpoint. At the same point, it is important to emphasize that from the CR standpoint, maintaining a low P_{md} is relatively more desirable than a low P_{fa}, so that any eventual interference to the licensed users can be avoided. This, in turn implies that the test SCN_1 is more appealing as it uses P_{md} as a default tolerated probability. Thus, the two tests are tempting and fulfill different needs. However, an additional advantage of being able to find simple and exact models for the SCN distributions

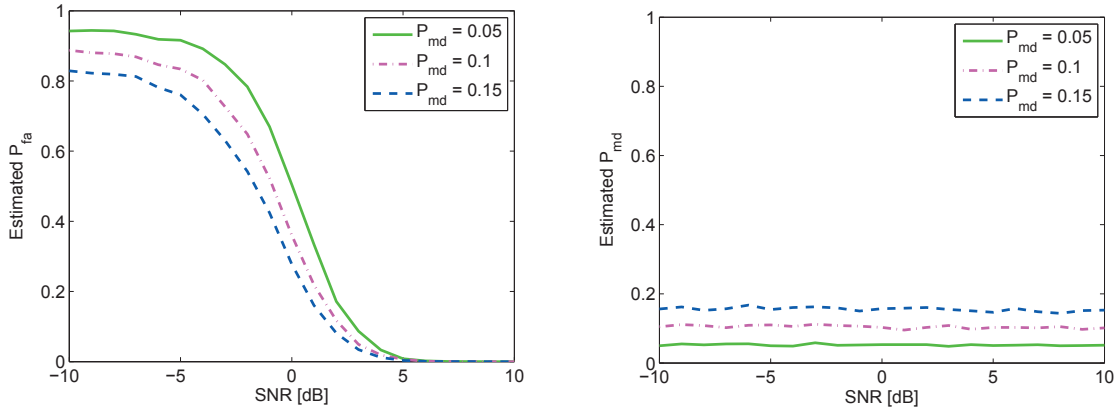

(a) (b)

Figure 2.18: Performance of spectrum sensing algorithm SCN_1 under $\mathcal{H}_1^c$, as a function of SNR and tolerated P_{md}.

under the two hypotheses is that a simple relationship between P_{fa} and P_{md} can be drawn, as

$$P_{fa} = 1 - F_{SCN}^{(0)}\left\{G_{SCN}^{(c)^{-1}}\left(P_{md}\right)\right\} \tag{2.46a}$$

$$P_{md} = G_{SCN}^{(c)}\left\{F_{SCN}^{(0)^{-1}}\left(1 - P_{fa}\right)\right\} \tag{2.46b}$$

This relationship allows to apply a specific test, starting from any prescribed probability, be it P_{fa} or P_{md}. For example, to apply test SCN_0 with a target P_{md}, desired generally in CR as explained above, we can set the threshold as

$$\gamma_{SCN}^{(0)} = F_{SCN}^{(0)^{-1}}\left[1 - \left\{1 - F_{SCN}^{(0)}\left(G_{SCN}^{(c)^{-1}}\left(P_{md}\right)\right)\right\}\right] \tag{2.47}$$

In Fig. 2.19, we plot the results obtained by using the test SCN_1 directly with target P_{md} and applying the test SCN_0 with target P_{md}, using the relationship in (2.46a) to find the threshold as explained in (2.47). Almost similar performance by the two tests allows us to develop the idea of skipping the test SCN_1 and always using test SCN_0 even when the tolerated probability is P_{md}, by converting it into an equivalent P_{fa} exploiting the expression in (2.46a). From hereon, we will refer to test SCN_0 as "**SCN Test**" (dropping the subscript).

As explained in section 2.4.4 that the SCN based tests can not function under $\mathcal{H}_1^r$, we next evaluate the SCN test with random correlated source signal $\mathcal{H}_1^{rc}$ and the Fig. 2.20 illustrates the corresponding performance. The algorithm is again proved to be robust and show almost similar performance as for the constant envelope PU case. This result is particularly interesting because the algorithm is based on the SCN distribution model under the hypothesis $\mathcal{H}_0$, but yet is able to effectively detect the correlated signals too. Thus, in conclusion, the SCN test can be used to detect the constant and correlated random signals with significant accuracy with as few as 20 samples, and is totally blind if P_{fa} is used as the target probability or semi-blind if P_{md} is employed.

The one scenario where SCN test can not function is the presence of random i.i.d. signals as in (2.19b). We proposed two algorithms based on eigenvalues distributions in previous section to deal with this case and we now move on to assess their performances under $\mathcal{H}_1^r$. The result for EV test is presented in Fig. 2.21 while for EVS test is shown in Fig. 2.22. As expected, the EVS test

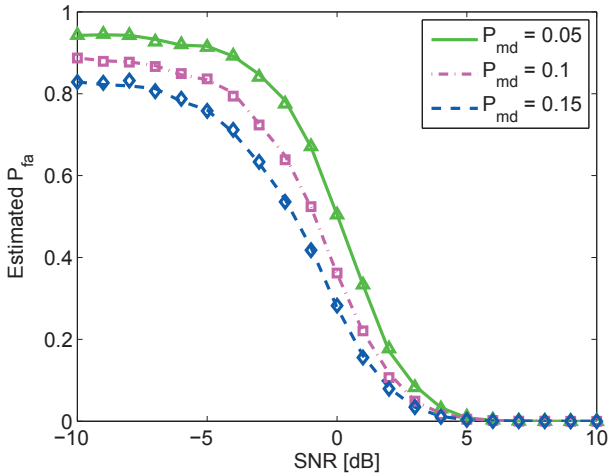

Figure 2.19: Performance comparison of spectrum sensing algorithm SCN_1 (lines) and SCN_0 (markers) under $\mathcal{H}_1^c$, as a function of SNR and tolerated P_{md}.

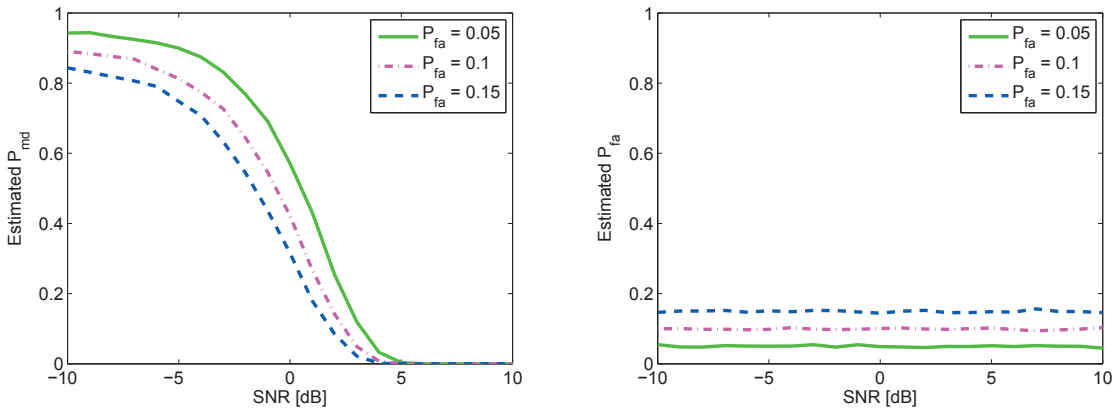

(a) (b)

Figure 2.20: Performance of the SCN test under $\mathcal{H}_1^{rc}$, as a function of SNR and tolerated P_{fa}.

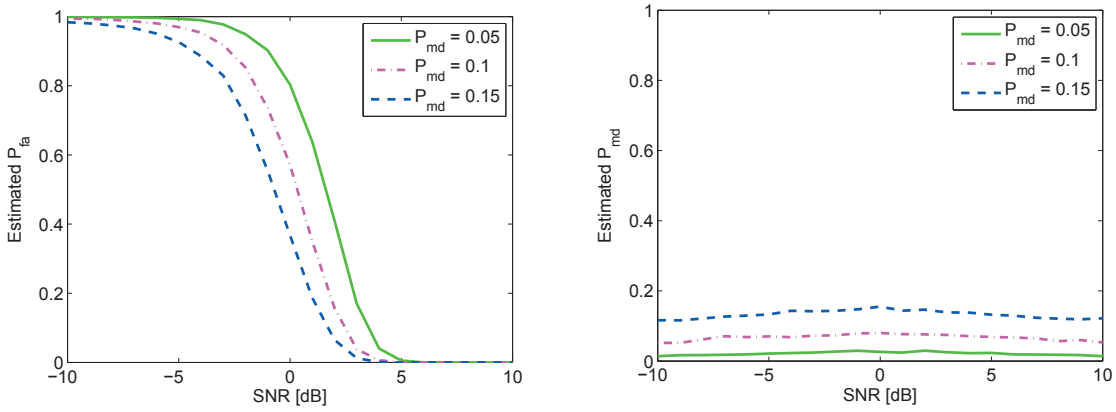

(a) (b)

Figure 2.21: Performance of spectrum sensing algorithm EV under $\mathcal{H}_1^r$, as a function of SNR and tolerated P_{md}.

exhibits much better performance compared to EV test and also estimated P_{fa} corresponds well to the tolerated P_{fa} for EVS test. The estimated P_{md} in case of EV test is a little higher than the tolerated P_{md}, which can be justified by the fact that we devised an approximate decision criteria (step 4 of EV test) and is not based on the exact model.

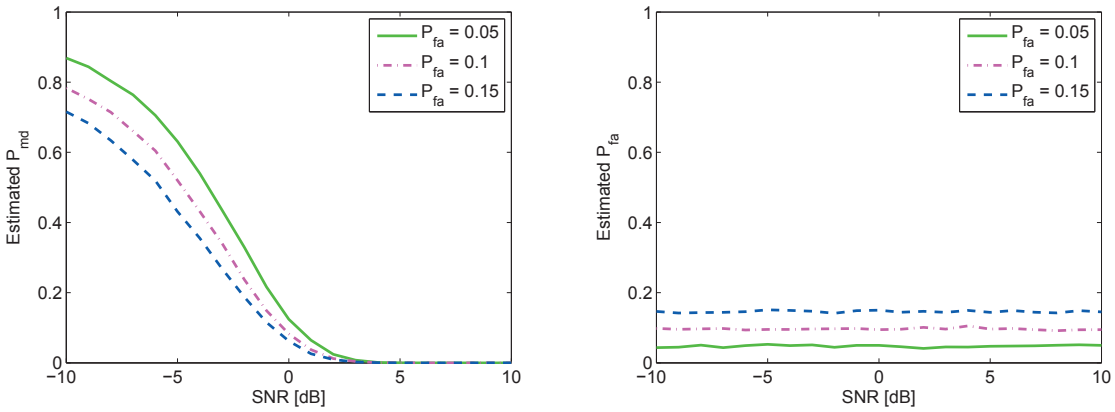

(a) (b)

Figure 2.22: Performance of spectrum sensing algorithm EVS under $\mathcal{H}_1^r$, as a function of SNR and tolerated P_{fa}.

Using the similar relationship between P_{fa} and P_{md} as for the SCN test in (2.46), we can set the threshold for EVS test with a prescribed P_{md} as

$$\gamma_{EVS}^{(0)} = F_{EVS}^{(0)^{-1}}\left[1 - \left\{1 - F_{EVS}^{(0)}\left(F_{EVS}^{(r)^{-1}}\left(P_{md}\right)\right)\right\}\right] \tag{2.48}$$

The performance with EVS test using prescribed P_{md} is represented in Fig. 2.23. Comparing

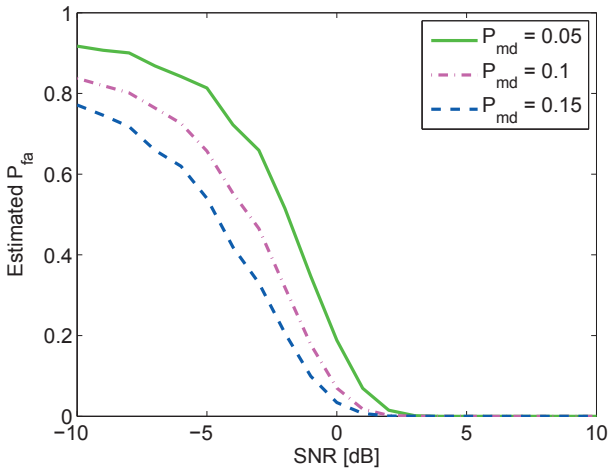

Figure 2.23: Performance of spectrum sensing algorithm EVS under $\mathcal{H}_1^r$, as a function of SNR and tolerated P_{md}.

Fig. 2.23 with Fig. 2.21, it is clear that converting target P_{md} into equivalent P_{fa} and then applying EVS test results in better performance than applying EV test directly. Both, these tests are semi-blind as they need knowledge about the noise power. From these results, we may conclude to skip the EV test and always use the test EVS for detecting the i.i.d. random signals. The theoretical relationship between P_{fa} and P_{md} for the two tests using (2.46), is plotted in Fig. 2.24, for various

values of SNR.

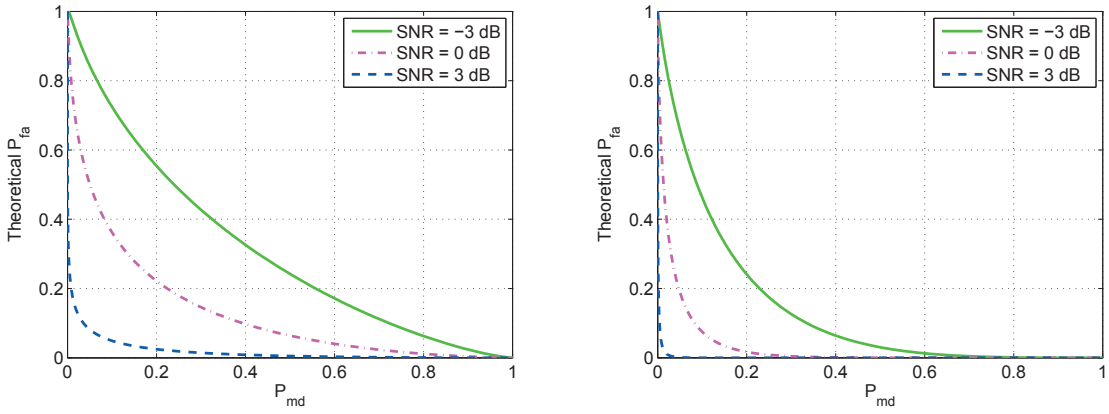

(a) SCN Test (b) EVS Test

Figure 2.24: Theoretical relationship between P_{fa} and P_{md}.

The performance under $\mathcal{H}_1^c$ and $\mathcal{H}_1^r$ using SCN and EVS tests respectively, in terms of number of sample N is shown in Fig. 2.25. The performance improves monotonically with N for both tests.

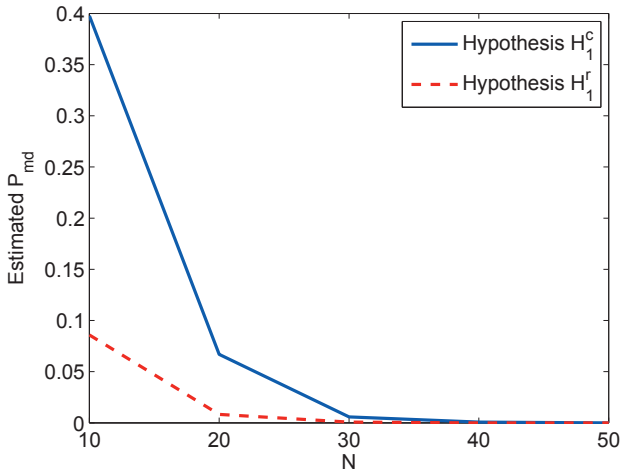

Figure 2.25: Performance of spectrum sensing algorithms SCN and EVS, as a function of N, with tolerated $P_{fa} = 0.1$ and SNR $= 0dB$.

The above discussion helps us to select the two tests which perform best under different hypotheses with minimum possible prior knowledge required, namely the SCN test and EVS test. However, SCN would fail to detect the i.i.d. random signals, while EVS would need an estimation of noise power to function. In the sequel, we present a compromised solution based on a double threshold detection scheme.

2.6 Two-stage Spectrum Sensing Approach

The preference of SCN test is obvious due to its tempting blindness feature with tolerated P_{fa}, however its limitation of not being able to detect the i.i.d. random signals must be apprehended.

This prompts us to develop the two-stage scheme where the advantages of both SCN and EVS tests are benefited while minimizing their drawbacks. The block diagram of the scheme is shown in Fig. 2.26. All the blocks are needed if P_{md} is used as the tolerated probability while only the dashed blocks will be required if P_{fa} is the tolerated probability.

The first stage consists of the SCN test as explained earlier. As the results demonstrated in previous section, SCN test will effectively detect the presence of constant or highly correlated signals. However, in case of i.i.d. random signals, there will be ambiguity between $\mathcal{H}_0$ and $\mathcal{H}_1^r$, and the SCN test will be inconclusive. At this point, we move to the second stage which comprises of the EVS test. The ambiguity between $\mathcal{H}_0$ and $\mathcal{H}_1^r$ will be solved by EVS test efficiently.

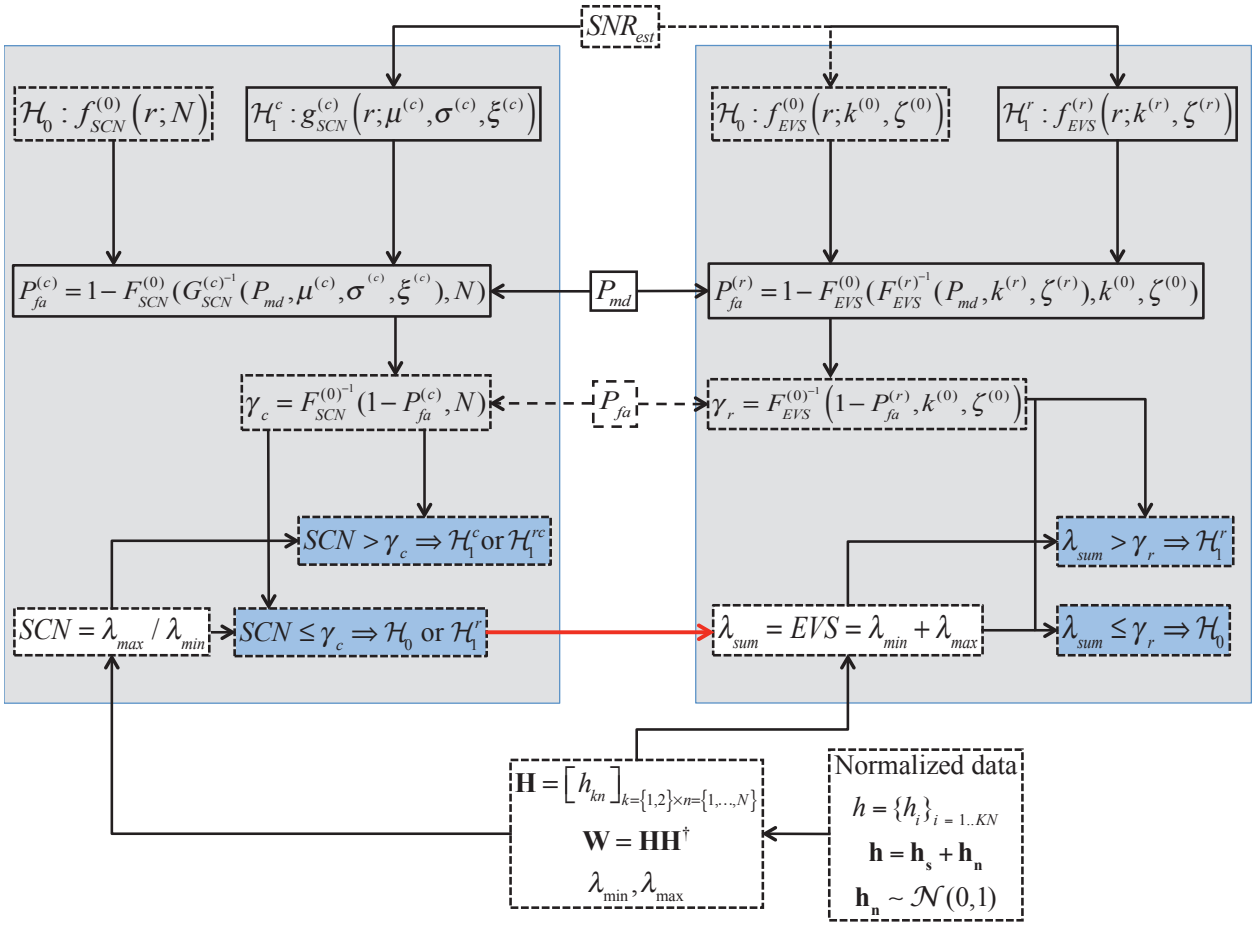

Figure 2.26: General PU detection schematic.

Using this double detection scheme, the i.i.d. random variates will be successfully detected, while the EVS test will only be employed occasionally when the SCN statistic is lower than the threshold of first stage. In practice, the received signal samples are usually correlated in time due to several reasons [Zen10]: the received signal is oversampled, the propagation channel is time-dispersive or the transmitted signal is correlated in time. Further, the received samples are also spatially correlated in case of single input multiple output (SIMO)/multiple input multiple output (MIMO), as the samples at different antennas/receivers are generated from the same source signal. Therefore, it is fair to assume that the most of the cases will be handled by the first stage and only under the rare extreme case of uncorrelated fading in single input single output (SISO), the second stage will be executed. Also, it is important to clarify that the EVS test under the particular configuration of $K = 2$ is equivalent to classic energy detection. However, we used EVS as the

minimum and the maximum eigenvalues have already been found in the first stage and thus can be reused to avoid any further computational load.

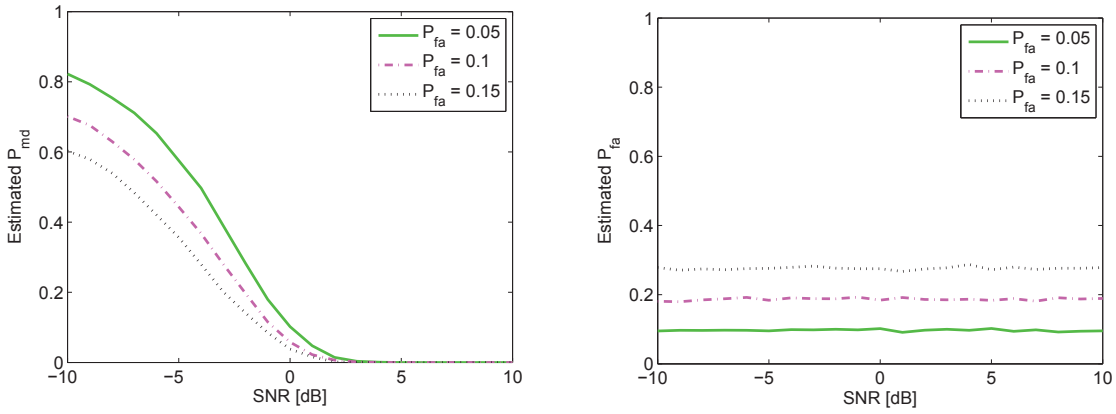

(a) (b)

Figure 2.27: Performance of two-stage spectrum sensing scheme using constant and random correlated/uncorrelated signals, as a function of SNR and tolerated P_{fa}.

Now, we evaluate the performance of this two-stage scheme by numerical simulations. The received signal samples are generated randomly at each iteration using one of the three hypotheses, namely $\mathcal{H}_1^c$, $\mathcal{H}_1^r$, $\mathcal{H}_1^{rc}$. The resulting curves using prescribed P_{fa} are plotted in Fig. 2.27. An interesting observation can be made from Fig. 2.27b that the estimated P_{fa} is twice of the target P_{fa}. This was expected as the first stage will produce the same P_{fa} as the target but then for the other $1 - P_{fa}$ cases, the decision is directed to the second stage which will also give same P_{fa} as intended, resulting in turn almost twice of the target P_{fa}. More precisely, $P_{fa-out} = P_{fa-1\text{st}} + (1 - P_{fa-1\text{st}}) . (P_{fa-2\text{nd}}) \approx 2P_{fa}$. This certainly appears as a bottleneck in establishing the two-stage detection approach. Using similar reasoning as for P_{fa}, the estimated P_{md} can be justified as; $P_{md-out} = (P_{md-1\text{st}}) . (P_{md-2\text{nd}})$. This will result in much lower P_{md}, compared to what have been achieved if only SCN test would have been applied, as can be verified by comparing Fig. 2.27 with Fig. 2.17. Thus, the double estimated P_{fa} problem can be resolved by using the prescribed P_{fa} half than the intended one, as it will increase P_{md} a little but still keeping it low than the one in Fig. 2.17 with alone SCN test.

We finally test the scheme against an OFDM signal and a QPSK signal with raised-cosine filter. At each iteration, one type of signal is generated and then 20 samples are randomly picked from within the symbol. The OFDM signal, in particular, is generated according to IEEE 802.11a WLAN standard specifications as it operates in 5GHz band, making it a potential interferer for UWB communications. As the OFDM signal has a gaussian-like nature [Ara12], it can be considered as complying to hypothesis $\mathcal{H}_1^r$, while the QPSK signal shows weak correlation conforming to hypothesis $\mathcal{H}_1^{rc}$. The resulting performance is illustrated in Fig. 2.28, which is almost identical to the previous general case.

2.7 Adaptive UWB Waveform Design

The design of UWB waveform is very critical because the pulses transmitted by IR-UWB are very influential on the spectrum occupied. A careful design of the set of pulses to be utilized is essential

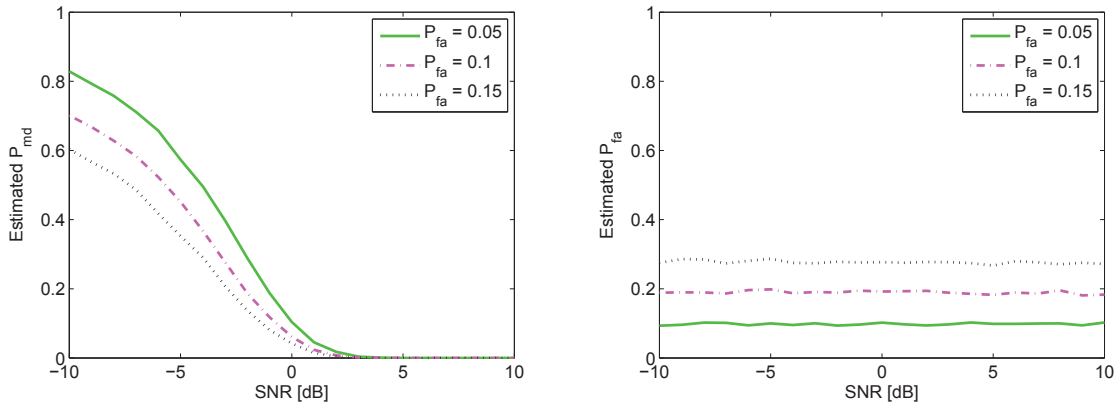

(a) (b)

Figure 2.28: Performance of two-stage spectrum sensing scheme using QPSK and OFDM signals, as a function of SNR and tolerated P_{fa}.

for an opportunistic spectrum usage.

UWB pulses have to comply with the FCC masks (or other masks defined by different regulatory bodies around the world) for the EIRP (Effective Isotropic Radiation Power). This compatibility is necessary in order to ensure sufficiently low levels of power (comparable with the noise) in some spectral bands already occupied by widely used applications (the GPS for example) and thus avoid introducing disturbances. At the same time, the allowed spectral resource is to be efficiently occupied, so that maximum energy can be transmitted while remaining compatible with the specifications of the considered spectral mask. The third objective is both to increase the transmission rate and to minimize the symbol interference using several mutually orthogonal UWB signals. Under the assumption that the regulation authorities allow the overlay mode of transmission, the UWB pulses also need to be enough adaptive so that their transmitted power is under the allowed mask for the occupied band while it is comparable to licensed system's power in the vacant band.

2.7.1 Literature review

UWB pulse design has been the focus of research for several years and many different pulses have been proposed till now like Gaussian pulses, modified Hermite pulses, prolate spheroidal wave functions, pulses based on digital filter design, pulses based on eigenvectors etc.

The most common UWB pulses have been Gaussian monocycle and its higher order derivatives. Although traditionally employed for UWB systems, these shapes poorly exploit the permissible power under the FCC mask. Even the Gaussian 5th derivative pulse, which presents high spectral levels at low frequencies (less than 3GHz) and low levels at very high frequencies and inherently considered superior to the Gaussian monocycle pulse in terms of meeting the spectral mask constraints, cannot reach the power efficiency of optimally designed pulses.

An attempt to solve the problem described in the discrete-time domain has been presented in [Par03], using pulses that are eigenvectors corresponding to the largest eigenvalues of a matrix calculated by sampling FCC's spectrum mask. Pulses generated from different eigenvectors are mutually orthogonal, and conform to the FCC spectral mask. However, they do not achieve the optimal spectral utilization as they try to match the mask only in the flat band, and require a high

sampling rate (64 GHz) that could lead to implementation difficulties. A set of orthogonal UWB pulse waveforms, based on the modified Hermite polynomials (MHP) is introduced in [Oue05]. However, in order for the modified HP pulses to comply with the FCC's spectrum mask, both filtering and up-conversion has to be done [Hu05].

By using the discrete-time prefiltering paradigm, different methods, originally developed for the design of the FIR digital filters in frequency domain, were applied for the design of the spectrally efficient UWB waveforms. In [Luo03], the FCC mask compliant UWB waveforms were designed by applying the Parks-McClellan (PM) algorithm. The PM design facilitates good approximations of the FCC spectral mask in a mini-max sense but does not directly optimize the spectral utilization of the pulse. Moreover, trial-and-error may be required to find suitable values for the parameters implicit in a PM design, such as the edges tolerances of the pass- and stop-bands, and the frequency weighting of the approximation error. In [Wu04] and [Wu06], families of orthogonal UWB waveforms that comply with the FCC's spectrum mask, were designed by using second-order cone programing (SOCP). However, since the method described in [Wu04] and [Wu06] is limited to the waveforms with linear phase, the number of waveforms designed was relatively small. Furthermore, the spectral efficiency decreased rapidly with the increase of the index of a designed orthogonal pulse waveform. A similar method which can design pulses with linear as well as non-linear phase was proposed in [Dot07].

It is clear that although several methods exist for UWB waveform design, each has drawbacks. For example, methods based on modified Hermite polynomials need frequency shifting and bandpass filters, the implementation complexity of the circuit for the eigenvector based solution is too high in practice whereas the FIR based methods can generate only a few number of pulses.

2.7.2 B-spline based pulse design

In this section, we propose a spectrally efficient and adaptive orthogonal UWB waveform design using B-spline functions [Akb10a].

The basis functions employed for designing pulses are B-splines [Sch46] having the following properties: (i) The B-splines are time-limited piecewise polynomials. (ii) They are rectangular pulses when their order is one and they converge to band-limited functions at the limit that their order tends to infinity [Kam88]. (iii) There are an analog circuit [Kam95] and a fast digital filter [Ich98] for the generation of B-splines.

The main idea behind this approach is that any signal can be represented as a linear combination of B-spline functions [Mat05]. These functions can be obtained as the output of a simple analog circuit (see Fig. 2.29) using following recursive equations [Kam95]:

$$\begin{cases} \varphi_1(t) = 1, & 0 \le t \le T \\ \varphi_m(t) = \displaystyle\int_0^{mT} [\varphi_{m-1}(t) - \varphi_{m-1}(t-T)]\, dt, & m = 2, 3, \ldots \end{cases} \tag{2.49}$$

where $\varphi_m(t)$ is a B-spline function of order m and knot interval T.

Also, the partial derivative of these functions is given by

$$\frac{d}{dt}\varphi_{m+1}(t) = \varphi_m(t) - \varphi_{m-1}(t-T) \tag{2.50}$$

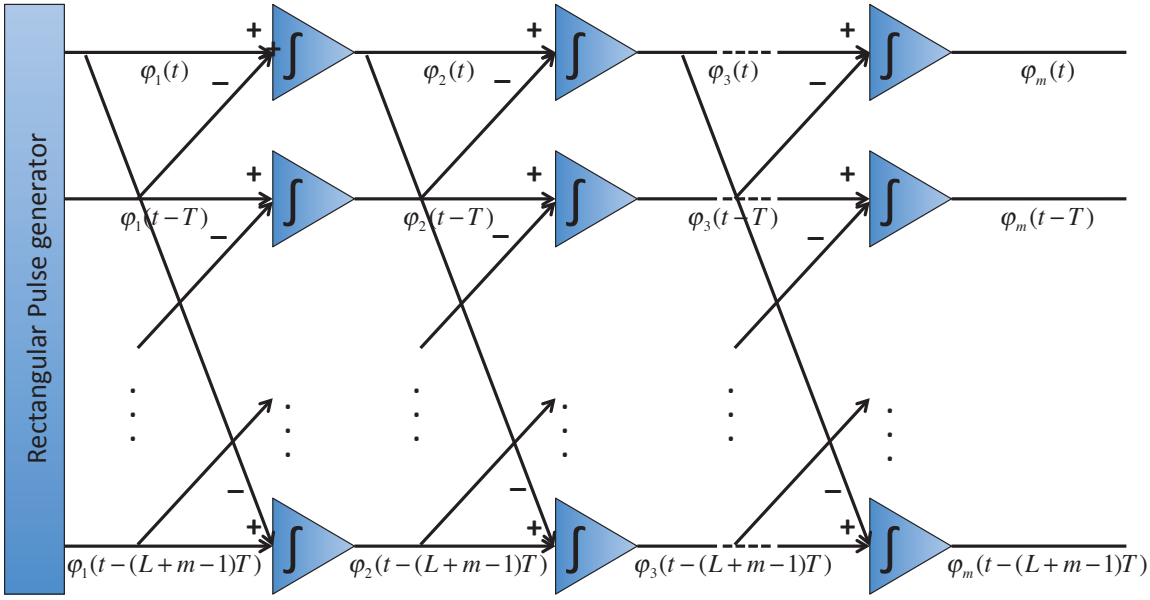

Figure 2.29: Analog circuit for the generation of B-splines [Mat05]

Then, the UWB pulses can be constructed by a linear combination of m-order B-splines as

$$\psi_l(t) = \sum_{k=0}^{N_s-1} c_{l,k}\varphi_m(t-kT), \quad l = 1, 2, \ldots, L \tag{2.51}$$

where $N_s = L + m - 1$ is the number of B-splines, L is the number of UWB pulses generated and $c_{l,k}$ are real number weight coefficients, obtained from an optimization procedure, which will be described next.

First, UWB pulses should not have any continuous component [Mat05], so they have to satisfy the following constraint:

$$\int_{-\infty}^{\infty} \psi_l(t)dt = 0, \quad l = 1, 2, \ldots, L \tag{2.52}$$

which in turn implies

$$\sum_{k=0}^{N_s-1} c_{l,k} \int_{-\infty}^{\infty} \varphi_m(t-kT)dt = 0 \tag{2.53}$$

In addition, the integration of B-spline functions is a constant [Sch73]:

$$\int_{-\infty}^{\infty} \varphi_m(t)dt = T \tag{2.54}$$

Combining (2.53) and (2.54) result in the first optimization constraint:

$$\sum_{k=0}^{N_s-1} c_{l,k} = 0, \quad l = 1, 2, \ldots, L \tag{2.55}$$

The generated UWB pulses are required to be mutually orthogonal in order to minimize the

symbol interference, which leads to the second constraint given as

$$\int_{-\infty}^{\infty} \psi_l(t)\psi_p(t)dt = E_\psi \delta_{lp} \tag{2.56}$$

where E_ψ is the energy of each one of the generated pulses and δ_{lp} is the Kronecker symbol.

The third constraint for UWB pulses is related to the given FCC mask specifications, given as

$$|\hat{\psi}_l(f)|^2 \leq S_{FCC}(f),\ \forall f \text{ and } l = 1, 2, \ldots, L \tag{2.57}$$

where $\hat{\psi}_l(f) = \int_{-\infty}^{\infty} \psi_l(t)e^{-j2\pi ft}dt$ and $S_{FCC}(f)$ stands for FCC's mask for PSD.

The generated pulses not only respect the FCC mask but also utilize the available resources efficiently. A normalized measure for the effectiveness of the spectral resources' use is defined for each UWB pulse as follows

$$\xi_l = \frac{\int_{-\infty}^{\infty} |\hat{\psi}_l(f)|^2 df}{\int_{-\infty}^{\infty} S_{FCC}(f)df} \times 100\% \tag{2.58}$$

The problem consists of determining the coefficients $c_{l,k}$ in such a way that the generated pulses satisfy the constraints of no direct current (DC) component (2.55), mutual orthogonality (2.56) and efficient spectral utilization (2.57).

The optimization problem can therefore be defined in the following form:

$$\begin{cases} \min\limits_{c_{l,k}} & \left[-\sum\limits_{l=1}^{L} \xi_l\right] \\ \text{subject to :} & \sum\limits_{k=0}^{N_s-1} c_{l,k} = 0,\ l = 1, 2, \ldots, L \\ \text{subject to :} & \int\limits_{-\infty}^{\infty} \psi_l(t)\psi_p(t)dt = E_\psi \delta_{lp},\ (l,p) \in \{1, 2, \ldots, L\} \\ \text{subject to :} & |\hat{\psi}_l(f)|^2 \leq S_{FCC}(f),\ l = 1, 2, \ldots, L \end{cases} \tag{2.59}$$

The problem in (2.59) is a non-linear optimization problem subject to both linear and non-linear constraints. In order to solve it we will use genetic algorithm (GA), which are well-known to be more effective than traditional numerical methods when the objective function is discontinuous, non-differential and consists of undefined gradients at many local points [Mic95].

2.7.3 GA based Optimization

The genetic algorithms are iterative methods handling a population of constant size. The population is formed by candidate points known as chromosomes, whose elements are called genes. At each iteration or generation, a new population is created with the same number of chromosomes. A generation consists of chromosomes "better adapted to their environment", such as it is represented by the objective function.

While the number of generations increases, the chromosomes will tighten towards the optimum of the objective function. The creation of a new population starting from the preceding one is

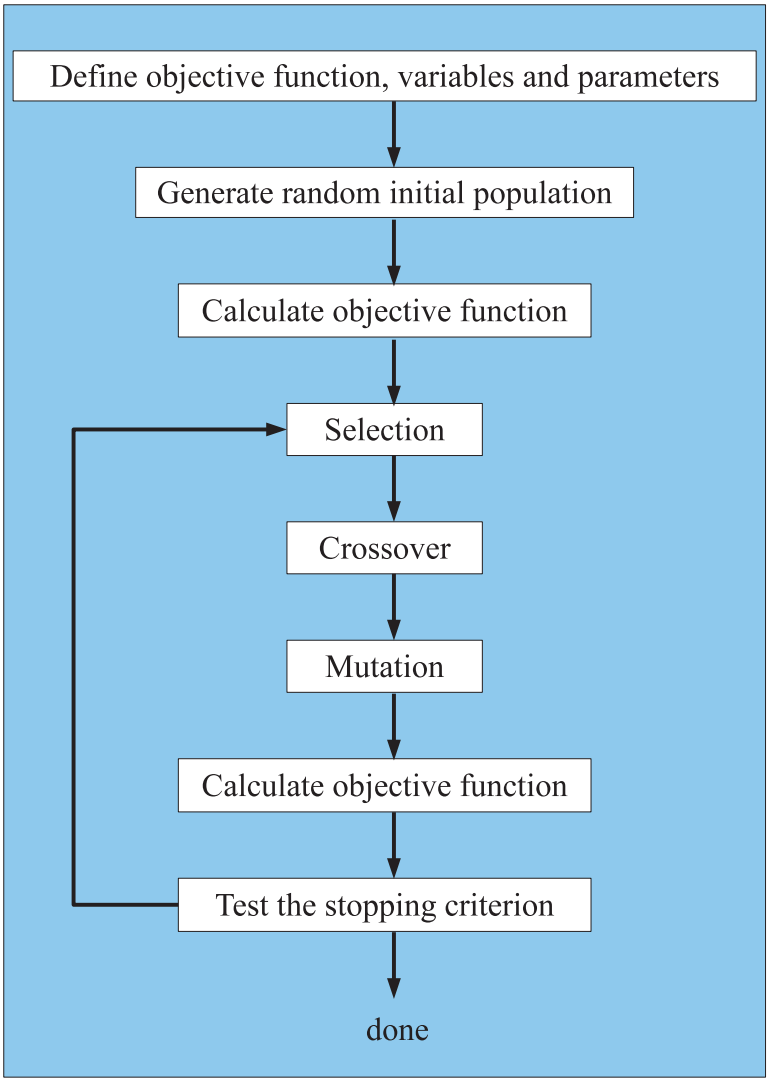

Figure 2.30: Flowchart of GA used for UWB waveform design

performed using the three genetic operators: selection, crossover and mutation. The selection of the best chromosomes is the first operation in a genetic algorithm. During this operation the algorithm selects the relevant elements which optimize the objective function. The crossover makes possible to generate two new ”children” chromosomes starting from two selected ”parents” chromosomes, while the mutation carries out the inversion of one or more genes of a chromosome to avoid the local minima. Fig.2.30 illustrates different steps of the algorithm.

2.7.4 Optimization Criteria for UWB pulse

GAs are typically able to solve a problem of nonlinear optimization with nonlinear constraints, linear constraints and bounds, having the following form

$$\begin{cases} \min\limits_{x} f(x) & f(x): \text{Objective function} \\ \text{subject to :} & \\ c_i(x) \leq 0,\ i = 1, 2, \ldots, m & \text{Non-linear inequality constraint} \\ \text{ceq}_i(x) = 0,\ i = m+1, 2, \ldots, L & \text{Non-linear equality constraint} \\ \text{A}.x \leq \text{b}, & \text{Linear inequality constraint} \\ \text{Aeq}.x = \text{beq}, & \text{Linear equality constraint} \\ \text{lb} \leq x \leq \text{ub}, & \text{Lower and upper bounds} \end{cases} \tag{2.60}$$

Fig. 2.31 demonstrates how to implement the system of equations (2.59) in the form of equations (2.60) to directly apply the optimization algorithm and obtain the appropriate values of the coefficients.

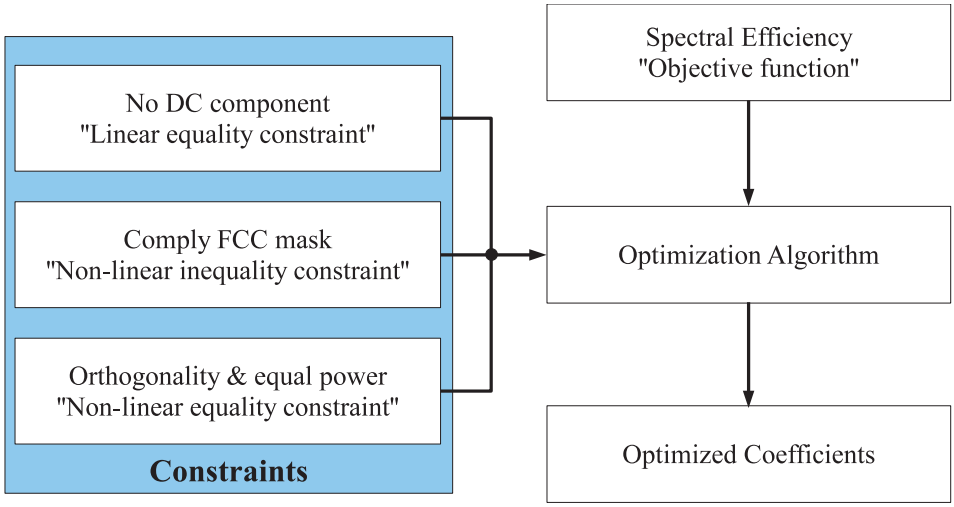

Figure 2.31: Optimization of UWB waveform coefficients using GA

Orthogonality and Equal Energy

These two properties are translated by the non-linear equality constraints for generating mutually orthogonal and same power signals.

$$\psi_l(t) = \sum_{k=0}^{N_s-1} c_{l,k}\varphi_m(t - kT), \quad l = 1, 2, \ldots, L$$

$$\begin{bmatrix} \psi_1 \\ \psi_2 \\ \vdots \\ \psi_L \end{bmatrix} = \begin{bmatrix} c_{1,0} & c_{1,1} & \cdots & c_{1,N_s-1} \\ c_{2,0} & c_{2,1} & \cdots & c_{2,N_s-1} \\ \vdots & \vdots & \vdots & \vdots \\ c_{L,0} & c_{L,1} & \cdots & c_{L,N_s-1} \end{bmatrix} \cdot \begin{bmatrix} \varphi_m(t-T) \\ \varphi_m(t-2T) \\ \vdots \\ \varphi_m(t-(N_s-1)T) \end{bmatrix}$$

$$\int_{-\infty}^{\infty} \psi_l(t)\psi_p(t)dt = E_\psi \delta_{lp}$$

$$\begin{bmatrix}\psi_1\\ \psi_2\\ \vdots\\ \psi_L\end{bmatrix}\begin{bmatrix}\psi_1^T & \psi_2^T & \cdots & \psi_L^T\end{bmatrix} = \begin{bmatrix}\langle\psi_1,\psi_1\rangle & \langle\psi_1,\psi_2\rangle & \cdots & \langle\psi_1,\psi_L\rangle\\ \langle\psi_2,\psi_1\rangle & \langle\psi_2,\psi_2\rangle & \cdots & \langle\psi_2,\psi_L\rangle\\ \vdots & \vdots & \vdots & \vdots\\ \langle\psi_L,\psi_1\rangle & \langle\psi_L,\psi_2\rangle & \cdots & \langle\psi_L,\psi_L\rangle\end{bmatrix} = \begin{bmatrix}E_\psi & 0 & \cdots & 0\\ 0 & E_\psi & \cdots & 0\\ \vdots & \vdots & \ddots & \vdots\\ 0 & 0 & \cdots & E_\psi\end{bmatrix}$$

$$\Rightarrow \begin{bmatrix}\|\psi_1\|^2 & \langle\psi_1,\psi_2\rangle & \cdots & \langle\psi_1,\psi_L\rangle\\ \langle\psi_2,\psi_1\rangle & \|\psi_2\|^2 & \cdots & \langle\psi_2,\psi_L\rangle\\ \vdots & \vdots & \vdots & \vdots\\ \langle\psi_L,\psi_1\rangle & \langle\psi_L,\psi_2\rangle & \cdots & \|\psi_L\|^2\end{bmatrix} - \begin{bmatrix}E_\psi & 0 & \cdots & 0\\ 0 & E_\psi & \cdots & 0\\ \vdots & \vdots & \ddots & \vdots\\ 0 & 0 & \cdots & E_\psi\end{bmatrix} = \begin{bmatrix}0\\0\\\vdots\\0\end{bmatrix}$$

$$\Rightarrow \begin{bmatrix}\|\psi_1\|^2 - E_\psi & \langle\psi_1,\psi_2\rangle & \cdots & \langle\psi_1,\psi_L\rangle\\ \langle\psi_2,\psi_1\rangle & \|\psi_2\|^2 - E_\psi & \cdots & \langle\psi_2,\psi_L\rangle\\ \vdots & \vdots & \vdots & \vdots\\ \langle\psi_L,\psi_1\rangle & \langle\psi_L,\psi_2\rangle & \cdots & \|\psi_L\|^2 - E_\psi\end{bmatrix} = \begin{bmatrix}0\\0\\\vdots\\0\end{bmatrix}$$

$$\Rightarrow \text{ceq}_i(\text{coeff}) = 0$$

No DC component

This property is reflected in the linear equality constraints for generating signals that have no DC component.

$$\int_{-\infty}^{\infty} \psi_l(t)dt = 0, \quad l = 1, 2, \ldots, L$$

$$\underbrace{\begin{bmatrix}1\ldots1 & 0\ldots0 & \cdots & 0\ldots0\\ 0\ldots0 & 1\ldots1 & \cdots & 0\ldots0\\ \vdots & \vdots & \vdots & \vdots\\ 0\ldots0 & 0\ldots0 & \cdots & 1\ldots1\end{bmatrix}}_{L\times L.N_s} \cdot \underbrace{\begin{bmatrix}c_{1,0}\\ c_{1,1}\\ \vdots\\ c_{1,N_s-1}\\ c_{2,0}\\ c_{2,1}\\ \vdots\\ c_{2,N_s-1}\\ \vdots\\ c_{L,0}\\ c_{L,1}\\ \vdots\\ c_{L,N_s-1}\end{bmatrix}}_{L.N_s\times 1} = \underbrace{\begin{bmatrix}0\\0\\\vdots\\0\end{bmatrix}}_{L\times 1}$$

$$\Rightarrow \text{Aeq.coeff} = \text{beq}$$

Fulfill FCC mask constraint

This property is translated by the non-linear inequality constraints to generate signals that meet the FCC mask requirements.

$$\begin{aligned} PSD_l(f) = |\hat{\psi}_l(f)|^2 \leq S_{FCC}(f), \quad \forall f \in \{f_1, f_2, \ldots, f_{Nfft}\} \\ \Rightarrow PSD_l(f) - S_{FCC}(f) \leq 0 \\ \Rightarrow - \begin{bmatrix} S_{FCC}(f) \\ S_{FCC}(f) \\ \vdots \\ S_{FCC}(f) \end{bmatrix} + \begin{bmatrix} PSD_l(f) \\ PSD_2(f) \\ \vdots \\ PSD_L(f) \end{bmatrix} \leq \begin{bmatrix} 0 \\ 0 \\ \vdots \\ 0 \end{bmatrix} \\ \Rightarrow \mathrm{c}_i(\mathrm{coeff}) \leq 0 \end{aligned}$$

Spectral Efficiency

This property is reflected by the objective function to generate signals which utilize the occupied band efficiently. Maximizing the spectral efficiency ξ_l, defined as in (2.58), is equivalent to minimizing the following expression

$$\acute{\xi}_l = \frac{\int S_{FCC}(f) - |\hat{\psi}_l(f)|^2 df}{\int S_{FCC}(f) df} \times 100\%, \quad l = 1, 2, \ldots, L$$

As the FCC mask and PSD of UWB signal are calculated for a finite number of frequencies $\{f_n\}_{n=2,\ldots,N_{fft}}$

$$\acute{\xi}_l = \frac{\sum_{n=2}^{N_{fft}} \left[S_{FCC}(f_n) - |\hat{\psi}_l(f_n)|^2 \right]}{\sum_{n=2}^{N_{fft}} S_{FCC}(f_n)} \times 100\%, \quad l = 1, 2, \ldots, L$$

where $\acute{\xi}_l$ is calculated from $n = 2$ because the pulses do not have DC component.

Consequently, the objective function to be minimized is given as

$$F_{obj} = \frac{\acute{\xi}_1 + \acute{\xi}_2 + \ldots + \acute{\xi}_L}{L}$$

2.7.5 Numerical Results

In this section, we validate the UWB waveform design by simulations. We use 3rd order B-spline functions throughout to generate the pulses, i.e. $m = 3$. The sampling frequency is $f_s = 100\,\mathrm{GHz}$ and $N_{fft} = 500$ points are used to calculate the generated signal's PSD. For optimization algorithm, the stopping criterion is specified by the minimum average change in the fitness function value Tolfun $= 10^{-32}$. In order to obtain the best trade-off between the optimization algorithm performance and convergence speed, the parameters have been set as follows

- Migration Function = 0.1

- Migration Interval = 10
- Crossover Function = 'Intermediate', with Ratio = 0.5
- Mutation Function = 'Gaussian', with Scale = 1 and Shrink = 1
- Population Type = 'Double Vector'
- Population Size = 100
- Selection Function = 'Stochastic Uniform'

The other GA related parameters take MATLAB predefined default values ("Genetic Algorithm and Direct Searc" Toolbox).

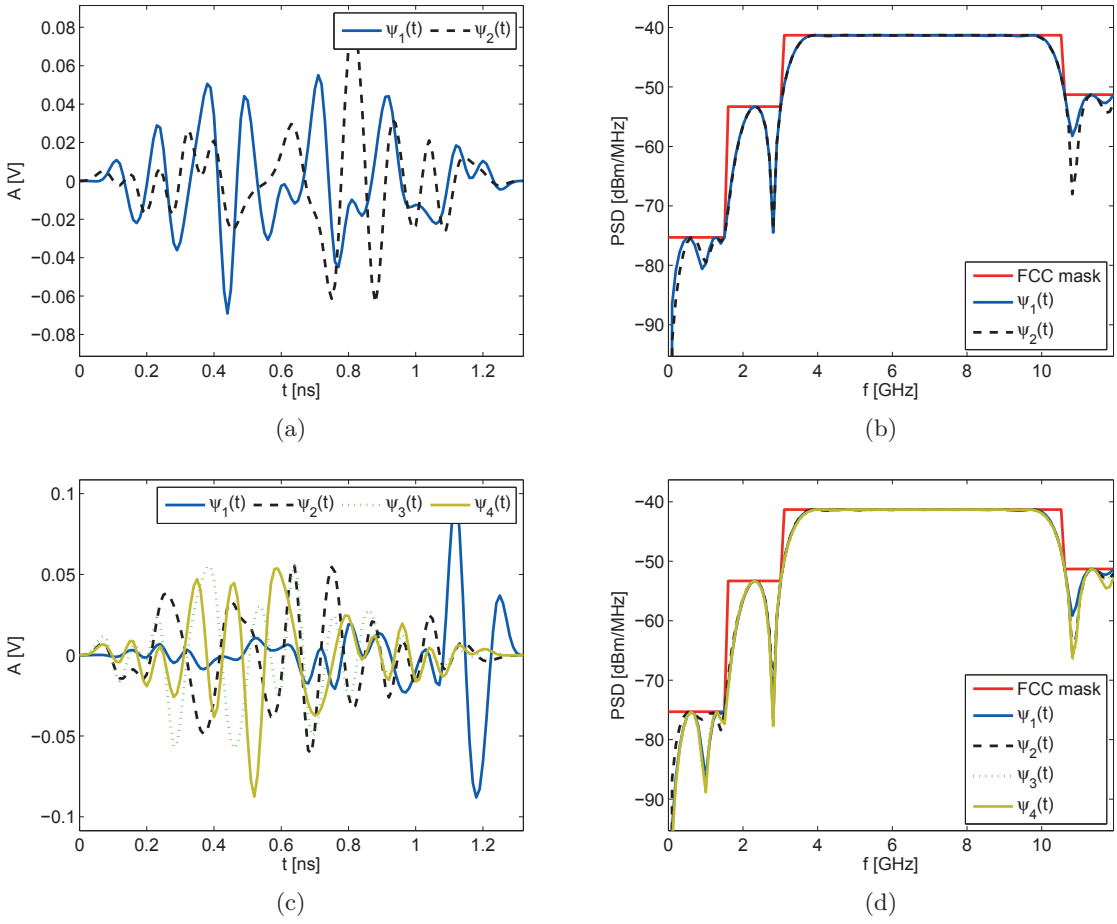

Figure 2.32: UWB pulses generated using $N_s = 30$ B-spline functions: [(*a*) and (*b*)] 2 pulses in time domain and corresponding PSDs, [(*c*) and (*d*)] 4 pulses in time domain and corresponding PSDs.

First, we generate multiple UWB pulses and the results are shown in Fig. 2.32. All the generated pulses have same duration equal to 1.28 ns. From Fig. 2.32, it is evident that all the pulses meet the FCC mask and also utilize the spectrum with high efficiency. In fact, the efficiency was approximately 91.5% in case of 2 and 4 pulses. Note that the mask used in the simulations is a modified version of the original FCC mask. The power in the band (0-0.96) GHz is restricted to -75.3 dBm/MHz instead of FCC's allowed -41.3 dBm/MHz. This is due to the presence of numerous narrowband systems in this band. Furthermore, it is found that the generated pulses are also mutually orthogonal.

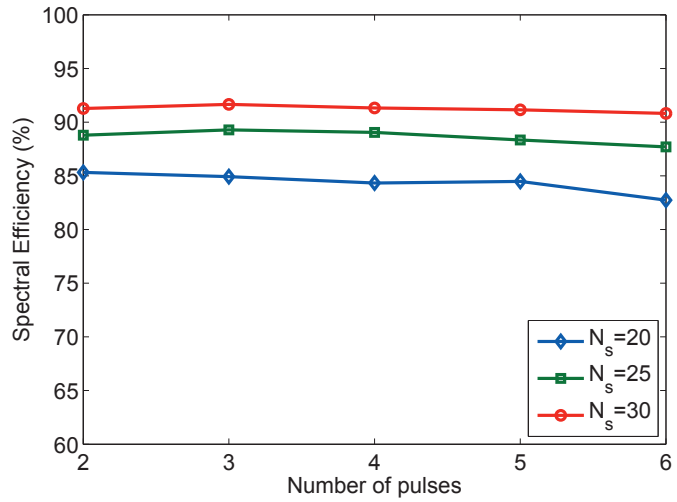

Figure 2.33: Impact of number of UWB pulses on the spectral efficiency

Next, we are interested to see the impact of number of generated pulses because as discussed in section 2.7.1 there are many algorithms which are efficient for the design of 2 pulses but their performance degrades markedly with high number of pulses. Also, we want to see the impact of the number of B-spline functions on the achieved efficiency. The result in Fig. 2.33 proves the robustness of our algorithm against the number of pulses generated. Also, the efficiency is improved with increasing number of B-splines as expected.

Finally, we show the spectrum adaptation ability of the proposed waveform design. It is assumed that there is a need to vacate the 5.2 GHz band due to the presence of WiFi (IEEE 802.11a) by users. Fig. 2.34 demonstrates that the B-splines based approach is very flexible in adapting to the

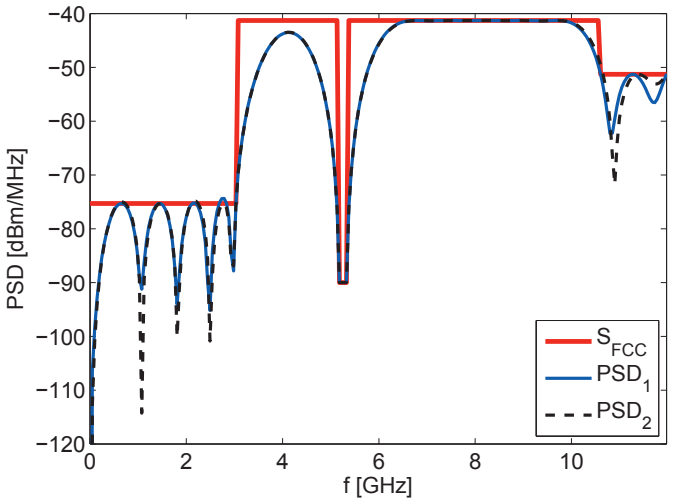

Figure 2.34: Spectrum adaptation ability in the presence of potential WiFi interference

specific needs.

2.8 Conclusions

In this chapter, we explored the concept of cognitive UWB radio. Although the UWB and CR appear as two contrasting ideas, UWB does have many features which qualify it directly as a potential candidate for CR. Furthermore, the UWB and CR can supplement each other to counter some of their limitations. Specifically, integrating the SS requirement of CR into UWB will help it to mitigate the strong primary systems' interference, thereby improving its performance. On the contrary, if CR is implemented with UWB, the underlay mode of UWB will help the cognitive users to transmit continuously, thus increasing its throughput. This provoked us to look into two major issues in realizing the cognitive UWB radios, first the SS and second the flexible design of UWB pulse for efficient spectrum utilization and interference mitigation.

The recent results of random matrix theory are invoked to develop efficient SS algorithms with limited number of samples. In fact, standard condition number (SCN) is used as a test statistic and the exact distribution of SCN of dual random Wishart matrices found recently under the hypothesis of no signal is used to determine the threshold. The SCN based approach is particularly attractive as it does not need any knowledge about the signal or noise power (blindness). Next, we found that under the presence of a complex signal, the SCN distribution can fit the GEV distribution, thus providing another alternate SS algorithm. Simulation results illustrated that the two test are almost equivalent, but the first one is more appealing due to blindness.

The SCN statistics, however, can not detect the PU under $\mathcal{H}_1^r$ hypothesis, thus inciting to look for alternatives. We then presented two methods, one based on any eigenvalues distribution and the other based on the eigenvalues sum distribution (EVS). Both of these algorithms, effectively distinguish between the $\mathcal{H}_0$ and $\mathcal{H}_1^r$, with second algorithm giving better performance. However, these algorithms need the estimation of noise power, making them only semi-blind.

Due to the inability of SCN to detect PU under $\mathcal{H}_1^r$ hypothesis and the dependence of EVS on noise power, we then proposed an intermediate two-stage solution to provide a trade-off between the two cited issues. The first stage of this two-stage scheme is based on SCN statistics while the second on the EVS. The first stage generally is sufficient as in practice majority of signals are correlated which it can detect efficiently. The second stage will only be required every now and then to tackle the $\mathcal{H}_1^r$ case.

In the second part of the chapter, we focused on the design of flexible UWB waveform. The UWB waveform should be capable to fulfill the FCC power mask constraints, efficiently utilize the spectral resources and adaptable to occupy/leave certain portion of the spectrum as needed by CR. To this part, a B-spline based approach is exploited to satisfy these demands. The basic idea is that the UWB signal can be generated by a linear combination of B-splines with appropriate weight coefficients. The objective is thus condensed to optimize these coefficients. As our problem is a non-linear optimization problem subject to both linear and non-linear constraints, we use GA, which are well-known iterative methods to solve such problems. Numerical results confirm the efficient spectrum usage and adaptability of generated pulses.

Chapter 3

Synchronization in IR-UWB Systems

- Abstract -

This chapter addresses the timing synchronization issue in IR-UWB systems. First, the eventual challenges linked with synchronization in IR-UWB are discussed and a literature review is presented. Motivated by certain limitations of these methods, we then propose several low-complexity synchronization methods, each signifying its merits under particular operating scenarios. Extensive simulation results are provided to validate the robustness of the proposed schemes along with discussion about the practical feasibility.

Contents

3.1 Introduction

Accurate timing estimation is a key factor to ensure the stable operation and reliable performance of any communication system. As discussed in chapter 1, the unique features of IR-UWB systems include extremely wide bandwidth, low duty cycle signaling and relatively low power UWB pulses constrained by the regulatory bodies [FCC02a]. Due to these properties, UWB has been envisioned as a potential candidate for short-range high-speed wireless communications and for object tracking and positioning applications. However, the same unique characteristics of IR-UWB result in equally demanding design challenges. The stringent timing requirements at the receiver for successful demodulation is one among them and poses a major problem in the deployment of IR-UWB systems.

Although synchronization is a tough task to accomplish in any communication system, it becomes much more challenging in IR-UWB due to plethora of factors.

First, the wide bandwidth results in a fine time resolution, thereby imposing a large search space. The receiver needs to search through a large number of candidate time shifts which will result in a large synchronization time if the time shifts are evaluated in a serial manner and will result in a prohibitive complexity if a parallel solution is opted.

Second, the extremely low power transmission means the receiver needs to process long sequence in order to develop a reliable synchronization criterion. For high data-rate UWB applications, the long synchronization preamble would cause significant reduction in the throughput.

Furthermore, the transmitted signal is distorted by antennas and unknown frequency selective dense multipath channels [Cas02, Cra02], which further intricate the already challenging task. This problem makes it difficult to use the conventional coherent solutions such as matched filtering the received signal with a locally generated replica of the transmitted signal.

And finally, due to short duration of UWB pulses, many resolvable multipaths may exist. This could also cause the receiver to lock with more than one possible arriving multipath component and still perform satisfactorily, thus resulting in multiple correct timing shifts. These issues arising from the unique transmission characteristics of IR-UWB signify the importance of synchronization problem in IR-UWB and the need to deal efficiently with it.

3.2 System Model and Synchronization Preliminaries

We will first introduce the IR-UWB synchronization problematic in the simple case of a BPSK modulation, which is suitable to illustrate the related concepts (propagation channel, transmission/reception model, synchronization parameter).

3.2.1 BPSK Transmission Model

For a typical IR-UWB system in a single-user scenario, equipped with TH codes and employing BPSK modulation, the transmitted signal can be expressed as

$$\begin{aligned} s(t) &= \sum_{i} d(i) p_T(t - iT_s) \\ p_T(t) &:= \sum_{j=0}^{N_f-1} \psi(t - jT_f - c_j T_c) \end{aligned} \tag{3.1}$$

where $p_T(t)$ is the symbol-long transmitted waveform. Each information-bearing symbol $d(i) = \pm 1$ is conveyed using one ultra-narrow UWB pulse $\psi(t)$ with duration $T_\psi \ll T_f$.

Due to severe limitations imposed by FCC on transmission power, effective SNR per symbol is increased by repeating UWB pulses over N_f frames with one pulse per frame to represent each data bit $d(i)$. The symbol duration is thus $T_s = N_f T_f$ where T_f is frame duration. Spectrum smoothing and multi-access are established by time shifting UWB pulses at multiples of chip duration T_c using user-specific pseudo-random TH codes $c_j \in [0, N_h)$, with $N_h \leq N_c$ where N_c is the number of chips per frame satisfying $T_f = N_c T_c$. A larger user capacity is typically achieved by using larger value for N_c.

3.2.2 Reception Model

The UWB indoor propagation channel is frequency selective and can be modeled by a stochastic tapped-delay line [Cas02]. The frequency selective nature of channel can lead to distortion of transmitted pulse which varies from path to path. A typical UWB channel impulse response can be expressed as

$$h(t) = \sum_{l=0}^{L-1} \lambda_l f_l(t - \tau_l) \tag{3.2}$$

where $\{\lambda_l, \tau_l\}_{l=0}^{L-1}$ are channel path gains and delays respectively, satisfying $\tau_l < \tau_{l+1}, \forall\, l$. The function $f_l(t)$ includes the combined effect of individual pulse distortion and transmit/receive antennas effect. The UWB channel is also assumed to be quasi-static i.e. channel taps remain invariant over a block of several symbols but may vary from block to block. In order to isolate propagation delay τ_0 from channel delays, channel response can be rewritten as $h(t) = \sum_{l=0}^{L-1} \lambda_l f_l(t - \tau_{l,0} - \tau_0)$ where $\tau_{l,0} = \tau_l - \tau_0$ is the relative path delay. The received signal is then obtained as the convolution product $s(t) * h(t)$, corrupted by an additive white Gaussian noise $n(t)$ with double-sided power spectral density (PSD) $N_0/2$

$$\begin{aligned} r(t) &= \sum_{i} d(i) p_R(t - iT_s - \tau_0) + n(t) \\ p_R(t) &:= \sum_{j=0}^{N_f-1} g(t - jT_f - c_j T_c) \end{aligned} \tag{3.3}$$

where $p_R(t)$ is the received aggregate symbol-long waveform with $g(t) = \sum_{l=0}^{L-1} \lambda_l \psi_l(t - \tau_{l,0})$ representing the channel response to a single UWB pulse $\psi(t + \tau_0)$ and $\psi_l(t) = \psi(t) * f_l(t)$ is the received UWB pulse from l^{th} path.

3.2.3 Synchronization Parameter

The synchronization problem in IR-UWB can be defined in two different ways. The first scenario assumes that the receiver is always active and therefore the objective of the synchronization scheme is to estimate the propagation delay τ_0 in (3.3). This is equivalent to estimating the time-of-arrival (ToA). In the other scenario, known as "cold start-up" scenario, the receiver is supposed to be unaware of transmission starting time and channel's propagation delay τ_0. Assuming that the receiver gets active at some time $t_0 \geq \tau_0$ and setting $\tau_0 = 0$ as it only serves as a reference in this scenario, the observation signal can be written as

$$\begin{aligned} x(t) &= r(t + t_0) \\ &= \sum_i d(i) p_R(t - iT_s + t_0) + n(t + t_0) \\ &= \sum_i d(i) p_R(t - (i - N)T_s - t_\phi) + n(t + NT_s - t_\phi) \end{aligned} \tag{3.4}$$

where $t_0 = NT_s - t_\phi$, with $N = \lceil t_0/T_s \rceil$.

As the receiver aims at aligning to the starting time of the first information symbol after t_0, i.e. to the time $t = t_0 + t_\phi$, thus the required synchronization parameter to be estimated is $t_\phi \in [0, T_s)$. Fig. 3.1 gives a graphical illustration of the two possible synchronization frameworks respectively.

Due to the multi-frame signal structure of IR-UWB systems, the timing recovery problem is typically performed in two stages. During the first stage, called acquisition stage, a coarse synchronization is carried out to quickly identify the symbol starting frame. The second stage, known as the tracking stage, aims at refining the acquisition stage estimator and reducing down the timing mismatch to less than a pulse duration.

The required synchronization precision is dependent on the type of receiver employed. The optimal coherent correlation receivers need to align a locally generated template with the incoming received signal with an accuracy at the order of reciprocal of the signal bandwidth, which for UWB is in the order of tens of picoseconds.

The low-complexity noncoherent receivers (TR [Hoc02], DD [Ho02], etc.) slightly relax the synchronization requirements and typically need an accuracy in the nanosecond range [Wit09]. Nevertheless, in both cases the synchronization requirements remain very strict. It was shown in [Tia05a, Tia05b, He06] that a slight misalignment at the order of nanoseconds can severely degrade the IR-UWB systems' performance.

3.3 Synchronization Algorithms - A Literature Review

Synchronization schemes in IR-UWB can be divided into many classes according to the approach (estimation-theoretic or detection-based), criterion (correlator, energy detector, cyclostationarity), search strategies (serial, parallel or hybrid), detector (coherent or noncoherent) and *a-priori* knowledge (data-aided or blind).

In the estimation based methods [Akb12a, Akb12b], an estimate of the timing is typically obtained by maximizing a statistic over a set of candidate phases. These schemes thus do not involve a threshold comparison. Most of the estimation based schemes attempt to exploit the cyclostation-

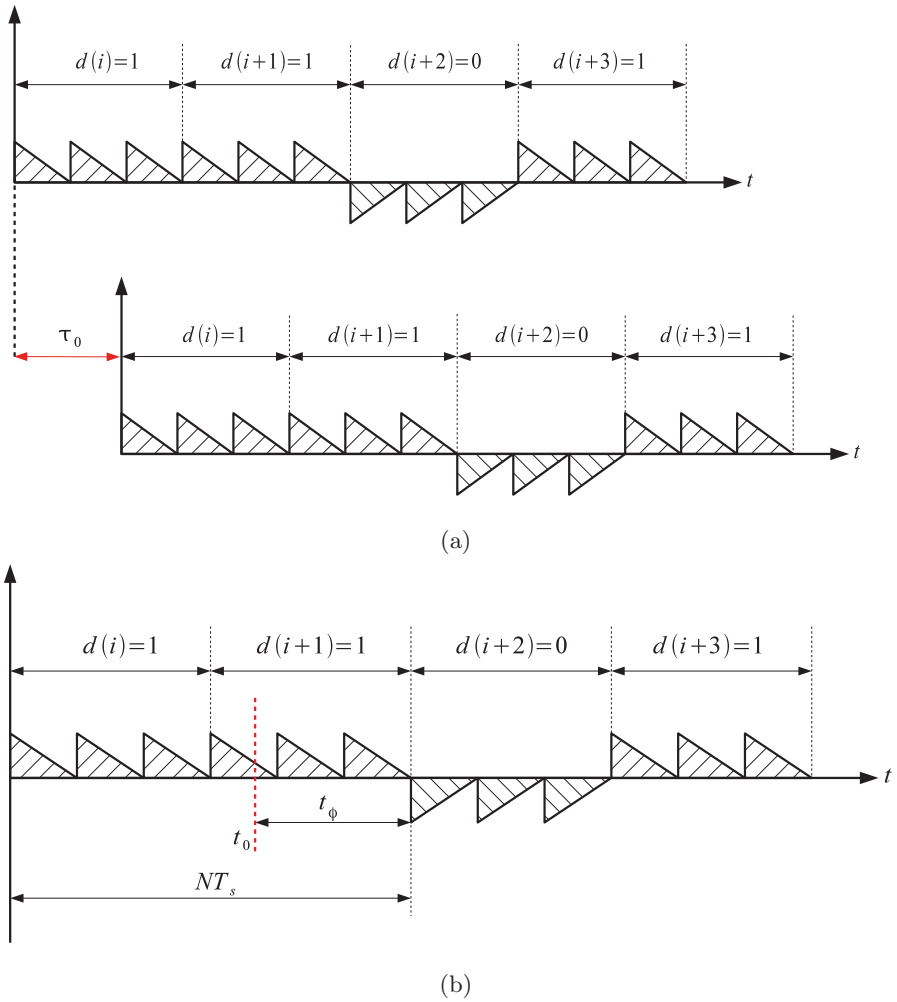

Figure 3.1: Received signal with $N_f = 3$ and synchronization parameter: (a) TOA estimation. (b) Cold start-up.

arity inherent in UWB signaling due to pulse repetition.

The synchronization methods which employ a detection based approach typically evaluate a candidate time shift by certain criterion and then compare it to a threshold in order to make a decision. These candidate shifts can be evaluated in a serial, parallel, or hybrid manner. The choice of search scheme is very important as it has direct connection with the rapid estimation of synchronization parameter and system's complexity. Thus, there has been much focus on the development of efficient search strategies to quickly evaluate the candidate shifts in the search space. Certain other schemes propose two-stage synchronization methods that achieve a reduction in the search space itself.

3.3.1 Estimation Based Approaches

A number of algorithms treat timing synchronization as part of channel estimation and aim at the joint estimation of timing offset and channel taps. In [Lot02], this is done using maximum-likelihood (ML) criterion, whereas a least square (LS) based method looking for the minimum of Euclidean distance between received signal samples and a local replica of their noiseless components is presented in [Car06]. However, a formidably high sampling rate up to several GHz raises concerns

over their implementations. Besides, very fast ADCs are needed in [Car06] as it is a fully digital approach.

Treating timing estimation as a harmonic retrieval problem, several subspace based methods have been proposed in [Mar03a, Mar03b, Kus03]. The implementation complexity involved in subspace analysis along with possible ill-conditioned Vandermonde systems in closely spaced multipaths limits its application in realistic UWB channels.

Timing is estimated in [Yan03, Tia02] by exploiting cyclostationarity, inherent in UWB due to pulse repetition. Under the assumption of known channel profile and absence of time-hopping (TH) codes, data-aided (DA) synchronization is performed in [Shi06].

The design of low-complexity synchronization schemes using either symbol-rate or frame-rate sampling is, therefore, highly motivated in UWB, in order to reduce the implementation complexity. One simple approach for synchronization in impulse radio is based on match-filtering the received signal with a locally generated "clean template" and peak-picking the correlation samples. Evidently, the reference template must encompass multipath channel effect which is unknown at synchronization, thus needing a cumbersome task of channel estimation.

A scheme, known as timing with dirty templates (TDTs), was proposed in [Yan05, Far05] to tackle this issue by utilizing pair of successive symbol long segments of the received signal, where one segment serves as template for the other. However, the main drawback of this approach is its poor performance due to the noise on noise effect from the dirty templates.

An algorithm using orthogonal pulses in an alternative manner and then applying TDT algorithm is presented in [Oue08]. Relying on periodic transmission of non-zero mean symbols, a group of joint timing and template recovery algorithms have been developed in [Luo04, Luo06a, Luo06b, Luo07], with universal applicability in the presence of ISI and multi-user interference (MUI). However, this asymmetric modulation aggravates the received SNR, thus deteriorating BER performance. Also, these algorithms need much longer sequence for reliable synchronization.

Another class of synchronization algorithms capitalizes on the fine correlation properties of binary codes. One such algorithm with improved performance using fewer number of symbols is proposed in [Yin08], which can be utilized under both non-data-aided (NDA) and DA scenarios. Exploiting the discriminative nature of similar binary codes, several other timing algorithms resilient to different types of interferences such as IFI & ISI [Liu10], MUI [Wu08], Near-Far [Li11] and a low-complexity demodulator [Lv11] have also been proposed.

3.3.2 Detection Based Approaches

Estimation based methods inevitably apply serial searching over all possible candidate time shifts. The large search space of IR-UWB systems, due to their extremely wide bandwidth, means that such linear search will lead to an increased mean synchronization time (MST).

A class of algorithms skipping the search technique have therefore been developed [Hom02, Gez03, Aed04, Wan07]. In [Hom02], it is shown that bin reversal search is the most efficient search technique with much reduced MST. Two-stage synchronization is adopted in [Gez03, Aed04], where the first stage performs a rapid coarse search and reduces the search space to a small subset while the second stage identifies exact timing using serial search in this subset. The algorithm in [Wan07] achieves synchronization exploiting the correlation property of binary code.

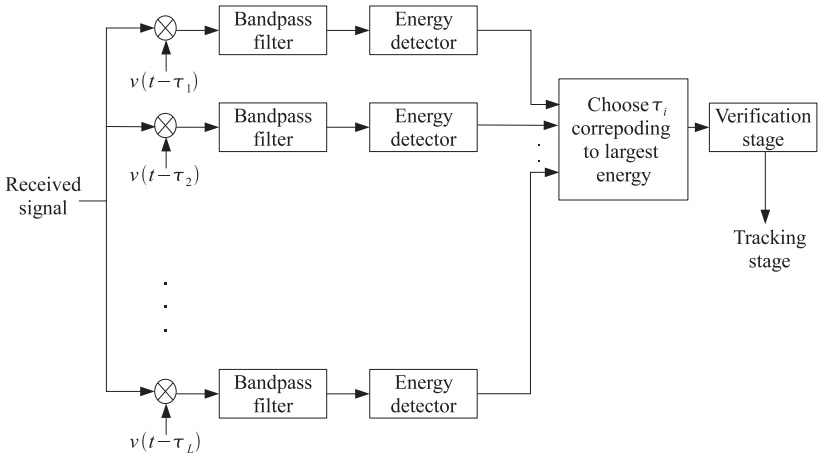

Figure 3.2: Block diagram of a parallel acquisition system where the received signal is correlated with template signal $v(t)$ delayed by all possible candidate shifts $\{\tau_i\}_{i=1}^{L}$ and then tested against the threshold simultaneously.

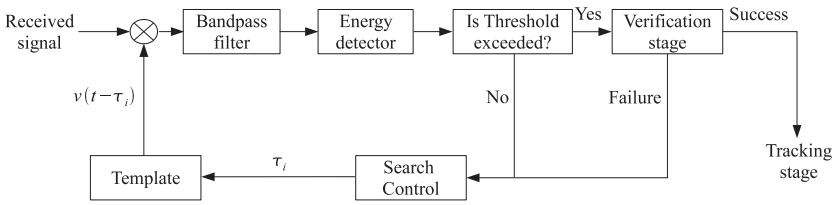

Figure 3.3: Block diagram of a serial acquisition system where the received signal is correlated with template signal $v(t)$ delayed by specific candidate shift τ_i and then tested against threshold. The process continues till the threshold is exceeded.

A class of optimal search strategies is presented in [Suw05, Suw07] where fundamental limits on achievable MST are also provided and it is shown that conventional serial search results in maximum MST. An attractive approach without search is presented in [Tia05c] for frame-level and pulse-level synchronization. Nevertheless, this approach employs a serial search first to achieve symbol-level synchronization, thus not completely independent of searching procedure. Exploiting orthogonality among UWB pulses, a promising algorithm is proposed in [Ren09]. However, it needs relatively high SNR to provide reasonable performance and also it is not functional in the presence of interfering users.

3.4 Motivation and objectives

Both detection and estimation based approaches have their benefits and problems. Estimation based schemes provide better accuracy as the maximization criterion is evaluated against each candidate time shift. However, an obvious problem will be the longer synchronization time as all the time shifts have to be evaluated and therefore the synchronization time is directly dependent on the employed search scheme. Two classic search strategies are parallel search and serial search (a typical example of both schemes is shown in Fig. 3.2 and Fig. 3.3 respectively).

The parallel search scheme is optimal in the sense that it needs the minimum possible time to

achieve a given probability. However, since it requires the number of correlators proportional to the number of candidate time shifts which may be extremely large in a UWB regime, the hardware complexity may be prohibitive. The serial search trades off the hardware complexity for an increased MST.

Detection based approaches, however, have the advantage that they can apply efficient search techniques such as bit reversal search and "look-and-jump-by-K-bins". However, the timing estimation is not optimal as it is not only dependent on the synchronization criterion but also on the search technique employed and the selected threshold.

Therefore, it all boils down to the trade-off between complexity and synchronization accuracy for the choice of algorithm. Also, most of the above-mentioned algorithms require one or more of the following assumptions: 1) known multipath channel; 2) absence of TH codes; 3) absence of IFI, ISI and MUI and 4) the timing error lies within first symbol. While the algorithms based on these assumptions are impractical for most realistic UWB settings, some methods such as the ones in [Yan05, Luo06b, Yin08] provide promising performance and generally take into account the practical UWB scenarios. Certain algorithms are also only capable of ToA estimation and not valid for estimating t_ϕ, such as subspace based methods [Mar03a, Mar03b, Kus03].

One common characteristic of the synchronization techniques in literature is that they are valid only for binary pulse amplitude modulation (BPAM) or/and binary pulse position modulation (BPPM), the two most popular modulation schemes in IR-UWB. These modulation schemes were widely adopted in the early years of UWB technology because of the difficulty to generate appropriate UWB pulses which can respect the severe FCC power constraints, thus limiting the choice.

However, in recent years, the possibility of generating multiple mutually orthogonal and spectrally efficient pulses with the same widths [Dot07, Wan08] has encouraged the use of alternative orthogonal modulation (OM) schemes [Maj07] for IR-UWB. PSM is an interesting OM scheme in which information is conveyed by the shape of pulse [Gha02, dA03]. These OM schemes are particularly attractive as high-rate multidimensional modulations, compared to high-order PAM and PPM [Pro00]. This feature along with possible robustness of PSM against MUI and ISI makes it the focus of research work presented in this thesis.

In the following, we develop several **low-complexity NDA** synchronization algorithms for IR-UWB systems. We preferred NDA algorithms as they do not interrupt the data transmission and can operate under "cold start-up" scenarios where the receiver is not aware of the transmission start time. The objective here is to develop algorithms which, under minimum *a-priori* knowledge available, can provide

1) Rapid coarse synchronization with resolution up to T_f for BPSK modulated IR-UWB systems.
2) Flexible synchronization up to any desired resolution for PSM modulated IR-UWB systems.

3.5 Rapid Synchronization with Search Eschewal

In this section, we focus on NDA timing synchronization of symbol boundaries in IR-UWB systems without sequential search. The proposed algorithm [Akb12c] uses a stream of alternating mutually orthogonal UWB pulses and asymmetric BPAM modulation with nonzero mean is applied. Ex-

ploiting this orthogonality available due to judicious signal design, head and tail energies of the received waveform are estimated which eventually assist in achieving frame-level synchronization. In the sequel, we explain the basic principle of the method for BPAM modulated system but the same approach can also be extended to PSM modulated systems with minor changes.

3.5.1 Modified BPSK System Model and Preliminaries

Our proposed scheme uses a pair of orthogonal pulses, transmitted in a judicious manner, in order to achieve synchronization. The resulting modified transmitted signal for point-to-point link in (3.1) is expressed as

$$\begin{aligned} s(t) &= \sum_i d(i) p_T(t - iT_s) \\ p_T(t) &:= \sum_{j=0}^{N_f-1} \psi_{\lfloor 3j/2N_f \rfloor}(t - jT_f - c_j T_c) \end{aligned} \tag{3.5}$$

where $p_T(t)$ is symbol-long waveform and N_f is supposed multiple of 3 ($\lfloor . \rfloor$ represents integer floor operation).

The information-bearing symbols $d(i)$ take values $\{\theta, -1\}$ equiprobably with nonzero mean, where $\theta > 1$. The ultra-short mutually orthogonal UWB pulses $\psi_0(t)$ and $\psi_1(t)$ of same duration $T_\psi \ll T_f$ and energy $E_\psi = \int_{-\infty}^{\infty} \psi_i^2(t)\, dt$ are used to represent one data symbol and satisfy $\int_0^{T_\psi} \psi_0(t)\psi_1(t)dt = \delta_{ij} E_\psi$, $(i, j) \in \{0, 1\}$. It is evident from the expression of $p_T(t)$ that it is further divided into three groups each with duration $T_{gr} = T_s/3$ and containing $N_{gr} = N_f/3$ frames, where the first two groups use $\psi_0(t)$ while third group employs $\psi_1(t)$ as the basic pulse. Alternatively, $p_T(t)$ can equivalently be expressed as $p_T(t) := \sum_{k=0}^{2} p_{T_{\lfloor k/2 \rfloor}}(t - kT_{gr})$ where $p_{T_i} = \sum_{j=0}^{N_{gr}-1} \psi_i(t - jT_f - c_j T_c)$, $i \in \{0, 1\}$. The TH codes are assumed group periodic i.e. $c_j = c_j + iN_{gr}$, $\forall i$ and $j \in [0, N_f)$.

The transmitted signal propagates through the linear tapped-delay line channel model $h(t) = \sum_{l=0}^{L-1} \lambda_l \delta(t - \tau_l)$ and the received signal is then given by

$$r(t) = \sum_i d(i) p_R(t - iT_s - \tau_0) + n(t) \tag{3.6}$$

where $p_R(t) := \sum_{j=0}^{N_f-1} g_{\lfloor 3j/2N_f \rfloor}(t - jT_f - c_j T_c)$ is the aggregate received symbol waveform of duration T_R and $g_n(t) = \sum_{l=0}^{L-1} \lambda_l \psi_n(t - \tau_{l,0})$, $n \in \{0, 1\}$ represents channel response to a single UWB pulse $\psi_n(t+\tau_0)$, with duration $T_g = T_\psi + \tau_{L,0}$. Like the transmitted symbol $p_T(t)$, the received waveform $p_R(t)$ can also be expressed in terms of groups as $p_R(t) := \sum_{n=0}^{2} p_{R_{\lfloor n/2 \rfloor}}(t - nT_{gr})$ where $p_{R_i}(t) = \sum_{j=0}^{N_{gr}-1} g_n(t - jT_f - c_j T_c)$, $i \in \{0, 1\}$.

Setting $\tau_0 = 0$ and assuming that receiver initiates at $t_0 \geq \tau_0$ like before, the observation signal can be written as

$$\begin{aligned} x(t) &= r(t + t_0) \\ &= \sum_i d(i) p_R(t - (i - N)T_s - t_\phi) + n(t + NT_s - t_\phi) \end{aligned} \tag{3.7}$$

Fig. 3.4 represents the received signal with the applied changes and synchronization parameter t_ϕ.

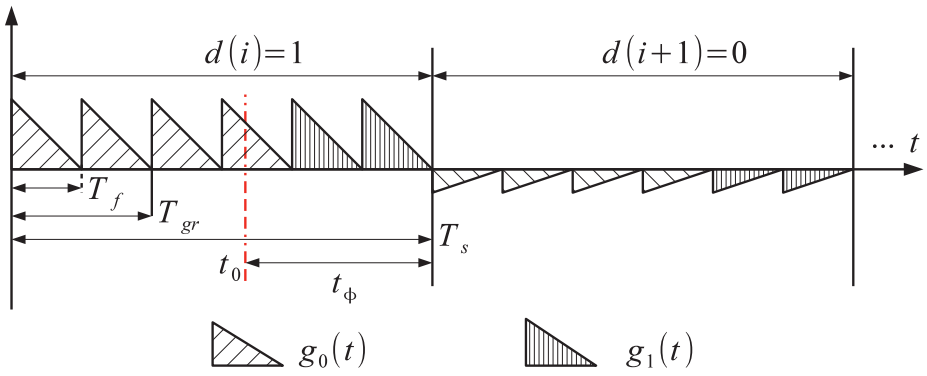

Figure 3.4: Received signal with synchronization parameter t_ϕ.

3.5.2 Orthogonal Signaling Based Synchronization Algorithm

Given $x(t)$, we will derive an algorithm exploiting the alternating orthogonal signaling and asymmetric modulation. The basic idea is to first estimate the tail and head energy of the groups within received symbol which will eventually provide the total energy scattered in each group.

First, we take T_s-long K segments from the observation signal $x(t)$, given by

$$\begin{aligned} x_k(t) &= x(t + kT_s), \qquad k \in [0, K-1],\ t \in [0, T_s) \\ &= \sum_i d(i) p_R(t - (i - N - k)T_s - t_\phi) + \eta(t) \end{aligned} \tag{3.8}$$

where $\eta(t) = n(t + (N + k)T_s - t_\phi)$. Assuming ISI free scenario, it is easy to observe that each segment $x_k(t)$ of size T_s will span at most two adjacent symbols of $p_R(t)$. Letting $i = N + k + q$ where $q \in \{0, -1\}$, (3.8) can be rewritten as

$$x_k(t) = \sum_{q=-1}^{0} d(N + k + q) p_R(t - qT_s - t_\phi) + \eta(t) \tag{3.9}$$

Next, the overlap-add operation is implemented on the observation signal as follows

$$\bar{x}(t) = \frac{1}{K} \sum_{k=0}^{K-1} \sum_{q=-1}^{0} d(N + k + q) p_R(t - qT_s - t_\phi) + \bar{\eta}(t) \tag{3.10}$$

where $\bar{\eta}(t)$ is the averaged noise term. We exploit the fact that $d(i)$ are independent, identically distributed (i.i.d.) symbols taking values $\{\theta, -1\}$, with mean $\mu = \mathrm{E}[d(i)] = 0.5\theta + 0.5(-1)$. Setting $\theta = 3$[1] and assuming that K is sufficiently large, the mean of observation signal $\bar{x}(t)$ in (3.10) can be simplified as

$$\bar{x}(t) = \sum_{q=-1}^{0} p_R(t - qT_s - t_\phi) + \bar{\eta}(t), \quad t \in [0, T_s) \tag{3.11}$$

Further, decomposing the synchronization parameter t_ϕ into group-level and subgroup-level

[1]This value of θ ensures a reasonable trade-off between transmission power, synchronization performance and averaging symbols K (see sections 3.5.3 and 3.8 for more details).

error i.e. $t_\phi = mT_{gr} + \epsilon$ where $m = \lfloor t_\phi / T_{gr} \rfloor$, $m \in \{0, 1, 2\}$ and $\epsilon \in [0, T_{gr})$, we get

$$\bar{x}(t) = p_R(t - mT_{gr} - \epsilon) + p_R(t - (m-3)T_{gr} - \epsilon) + \bar{\eta}(t) \tag{3.12}$$

Thus, estimating t_ϕ is equivalent to determine m and ϵ which we will pursue in the following.

Integrate and dump operations are performed on the products of groups within $\bar{x}(t)$ to estimate the tail and head energy of each group. Specifically,

$$\begin{aligned} X_1 &= \int_0^{T_{gr}} \bar{x}(t)\bar{x}(t + T_{gr})dt \\ X_2 &= \int_0^{T_{gr}} \bar{x}(t + T_{gr})\bar{x}(t + 2T_{gr})dt \\ X_3 &= \int_0^{T_{gr}} \bar{x}(t)\bar{x}(t + 2T_{gr})dt \end{aligned} \tag{3.13}$$

Let's analyze X_1. As different values of group-level misalignment m result in different energy capture by X_1, we first consider the case when $m = 2$. On this condition, substituting (3.12) into X_1 in (3.13) and simplifying using the fact that each group has a finite nonzero support of T_{gr}, we get

$$X_1 = \int_0^{T_{gr}} p_{R_0}^2(t + T_{gr} - \epsilon)dt + \int_0^{T_{gr}} p_{R_0}(t - \epsilon)p_{R_1}(t - \epsilon)dt + \zeta \tag{3.14}$$

where ζ stands for the Gaussian noise with variance σ^2.

Here, we make the assumption that $\int_{-\infty}^{-\infty} g_0(t)g_1(t)dt = 0$, which means that the received UWB waveforms remain orthogonal after propagating through channel. Invoking this assumption, we can write (3.14) as

$$X_1 = \int_{T_{gr}-\epsilon}^{T_{gr}} p_{R_0}^2(t)dt + \zeta = \mathcal{E}_{T0}(\epsilon) + \zeta \tag{3.15}$$

where $\mathcal{E}_{T0}(\epsilon)$ represents the tail energy of the first group. We also define the head energy of first group as $\mathcal{E}_{H0}(\epsilon) = \int_0^{\epsilon} p_{R_0}^2(t)dt$. As we use equal energy UWB pulses which are assumed to remain orthogonal after propagation, therefore $\mathcal{E}_{T0}(\epsilon) = \mathcal{E}_{T1}(\epsilon) = \mathcal{E}_T(\epsilon)$, $\mathcal{E}_{H0}(\epsilon) = \mathcal{E}_{H1}(\epsilon) = \mathcal{E}_H(\epsilon)$. We can find the value of X_1 corresponding to $m = 1$ and $m = 0$ following the same argumentation. Consequently, the mean squared value of X_1 can be summarized as

$$E\left[X_1^2\right] = \begin{cases} \mathcal{E}_H^2(\epsilon) + \sigma^2 & \text{if } m = 0 \\ \sigma^2 & \text{if } m = 1 \\ \mathcal{E}_T^2(\epsilon) + \sigma^2 & \text{if } m = 2 \end{cases} \tag{3.16}$$

Mimicking same steps as for X_1, the other two inter-group correlations can also be derived and are summarized in Table 3.1. A visual illustration of these correlations can be observed in Fig. 3.5. In order to identify the intended group i.e. value of m, we further calculate two correlations as

$$X_4 = \int_0^{T_{gr}/2} \bar{x}(t)\bar{x}(t + T_{gr})dt, \; X_5 = \int_{T_{gr}/2}^{T_{gr}} \bar{x}(t)\bar{x}(t + T_{gr})dt \tag{3.17}$$

Exploiting the particular orthogonal transmission format and correlation values in Table 3.1, we

	$E\left[X_1^2\right]$	$E\left[X_2^2\right]$	$E\left[X_3^2\right]$
$m=0$	$\mathcal{E}_H^2(\epsilon)+\sigma^2$	$\mathcal{E}_T^2(\epsilon)+\sigma^2$	σ^2
$m=1$	σ^2	$\mathcal{E}_H^2(\epsilon)+\sigma^2$	$\mathcal{E}_T^2(\epsilon)+\sigma^2$
$m=2$	$\mathcal{E}_T^2(\epsilon)+\sigma^2$	σ^2	$\mathcal{E}_H^2(\epsilon)+\sigma^2$

Table 3.1: Inter-group Correlation Functions

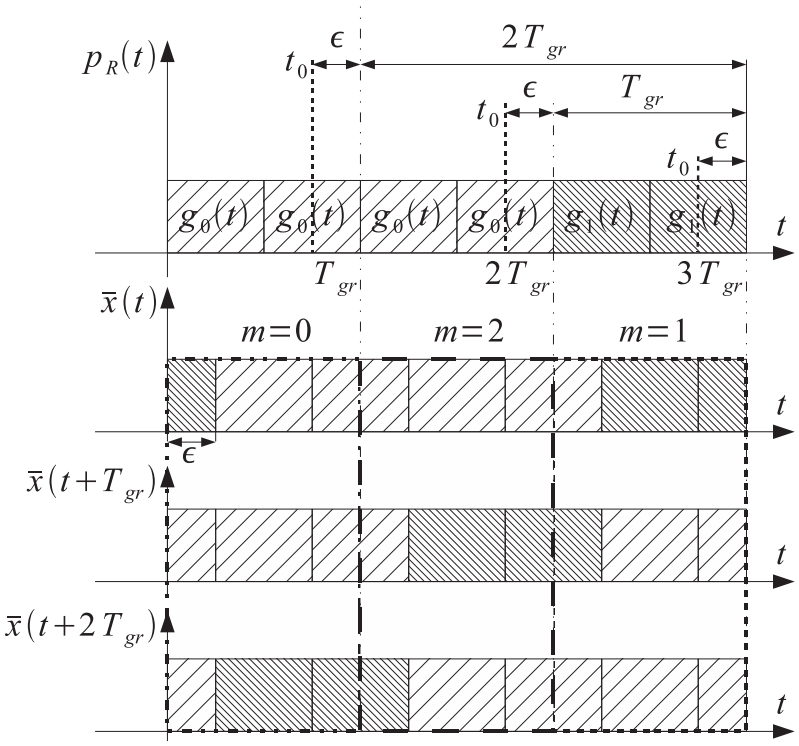

Figure 3.5: Observation signal and its delayed segments for different group-level m and subgroup-level ϵ misalignments.

can develop the following decision rule

$$\begin{cases} \hat{m}=2, & \text{if} \quad X_4^2 > X_5^2 \text{ and } X_4^2+X_5^2 > X_2^2 \\ \hat{m}=0, & \text{if} \quad X_4^2 < X_5^2 \text{ and } X_4^2+X_5^2 > X_3^2 \\ \hat{m}=1, & \text{otherwise} \end{cases} \tag{3.18}$$

Our next task is to determine subgroup-level timing error ϵ. Our algorithm focuses on frame-level synchronization, that is $|\epsilon-\hat{\epsilon}| \leq T_f$. The tail and head energies estimated through X_1, X_2 and X_3 include noise and can be better approximated to the true tail and head energies as indicated in Table 3.2. Using these estimated energies, $\hat{\epsilon}$ can be immediately calculated as

$$\hat{\epsilon} = \hat{\mathcal{E}}_T(\epsilon)/\hat{\mathcal{E}}_{Gr}(\epsilon) \tag{3.19}$$

where $\hat{\mathcal{E}}_{Gr}(\epsilon) = \hat{\mathcal{E}}_T(\epsilon) + \hat{\mathcal{E}}_H(\epsilon)$ is the total energy of group.

	$\hat{m}=0$	$\hat{m}=1$	$\hat{m}=2$
$\hat{\mathcal{E}}_T(\epsilon)$	$\sqrt{E\left[X_2^2\right]-E\left[X_3^2\right]}$	$\sqrt{E\left[X_3^2\right]-E\left[X_1^2\right]}$	$\sqrt{E\left[X_1^2\right]-E\left[X_2^2\right]}$
$\hat{\mathcal{E}}_H(\epsilon)$	$\sqrt{E\left[X_1^2\right]-E\left[X_3^2\right]}$	$\sqrt{E\left[X_2^2\right]-E\left[X_1^2\right]}$	$\sqrt{E\left[X_3^2\right]-E\left[X_2^2\right]}$

Table 3.2: Estimated Tail and Head Energies

Thus, the original synchronization parameter t_ϕ can be estimated using (3.18) and (3.19) as

$$\hat{t}_\phi = \hat{m}T_{gr} + \hat{\epsilon} \tag{3.20}$$

The proposed algorithm gives the exact estimation of t_ϕ when $\lceil \epsilon/T_f \rceil$ is an integer. However, when ϵ is not an integer i.e. there exists some tracking error, the algorithm will achieve synchronization with an error less than frame duration.

3.5.3 Discussion

Computational Complexity It is clear that the proposed algorithm does not employ any optimization criterion and avoids searching, therefore will result in significantly reduced MST. As for the computational complexity of proposition is concerned, it is mainly determined by the three integrals X_1, X_2 and X_3. As each of these integrals are computed over an interval $T_s/3$, the total complexity is proportional to the computation of one T_s-long integral or equivalently N_f T_f-long integral operations. Table 3.3 gives a comparison of computational complexity between proposed algorithm and some linear search based algorithms (see Appendix A). The table verifies the significantly reduced number of operations required with proposed algorithm, compared to the conventional serial search methods.

Method	Ref. [Yan05]	Ref. [Luo06b]	Ref. [Yin08]	Proposed
Complexity	$K(2N_f-1)$	$3N_f-1$	KN_f	N_f

Table 3.3: Complexity comparisons in terms of T_f-long integral

Impact of θ First, it is important to emphasize that the purpose of using asymmetric pulse amplitude modulation (A-PAM) with $(\theta, -1)$ as the constellation points is to enable NDA solution only and it has nothing to do with the functioning of the algorithm itself. In other words, a training based approach with $d(i) = 1$, $i \in [0, K)$ can also be developed using exactly the same argumentation as presented in previous section. However, as the NDA solutions are preferred due to their bandwidth efficiency and they do not need to interrupt the data transmission, we were motivated to discuss the NDA version of the algorithm. This in turn adds the flexibility to the algorithm, i.e. A-PAM can be used if the system can not afford rate loss and on the other hand if the low transmission power is indispensable, we can proceed with a training sequence.

Next, regarding the impact of theta, the choice of θ certainly has an impact on the synchronization performance. In fact, the value of θ should be such that a reasonable trade-off between transmission power, synchronization performance and averaging symbols K is achieved. Obviously,

selecting large θ will result in improved performance at fewer number of symbols K, but that will necessitate an exponential increase in the transmission power as well. Keeping this in mind, we selected $\theta = 3$ because this value under the assumption of large K will result in $\mu = \mathrm{E}[d(i)] = 1$, same as if a training sequence would have been employed. The drawback will be relatively large K needed, but it is not such a big issue as data transmission is continued during the synchronization phase.

The last thing which we want to mention is that this A-PAM modulation is adopted only during the synchronization phase. After the synchronization is done, the transmitter returns to the conventional power efficient zero-mean symmetric PAM (S-PAM). As this synchronization phase constitutes a very small fraction of the total transmission time, the effect on the overall demodulation performance will be negligible.

3.6 Flexible Synchronization with Linear Search

In this section, we propose two low-complexity algorithms for PSM modulated IR-UWB systems. The target metric here is to achieve any level of synchronization accuracy with much improved performance. The first algorithm exploits the first-order averaging while the second benefits from nice correlation property of bipolar codes.

3.6.1 Energy Detection Based Synchronization Algorithm

This algorithm [Akb11] uses simple overlap-add operation followed by energy detection to estimate the synchronization parameter. This algorithm has the advantage that it remains equally functional for higher-order PSM where orthogonal signaling is particularly more interesting than PAM [Pro00].

3.6.1.1 PSM System Model and Preliminaries

For a typical IR-UWB system in a single-user scenario, equipped with TH codes and employing orthogonal PSM, the transmitted signal can be expressed as

$$\begin{aligned} s(t) &= \sum_{i} p_{T,d(i)}(t - iT_s) \\ p_{T,d(i)}(t) &:= \sum_{j=0}^{N_f-1} \psi_{d(i)}(t - jT_f - c_jT_c) \end{aligned} \tag{3.21}$$

where $p_{T,d(i)}(t)$ is the symbol-long transmitted waveform. Each information-bearing symbol $d(i) \in \{0, 1, ..., M-1\}$ is conveyed using one of the ultra-narrow orthogonal UWB pulse in the set $S = \{\psi_0(t), \psi_1(t), \ldots, \psi_{M-1}(t)\}$, where M is the modulation order. Each pulse has a duration T_ψ and satisfies $\int_0^{T_\psi} \psi_i(t)\psi_j(t)dt = E_\psi \delta_{ij}$, $(i, j) \in \{0, 1, ..., M-1\}$, where $E_\psi = \int_{-\infty}^{\infty} \psi_i^2(t)\, dt$ is the pulse energy. TH codes are symbol periodic i.e. $c_j = c_{j+iN_f}$, $\forall i$ and $j \in [0, N_f)$.

To ease out synchronization, we first judiciously modify the conventional PSM symbol format

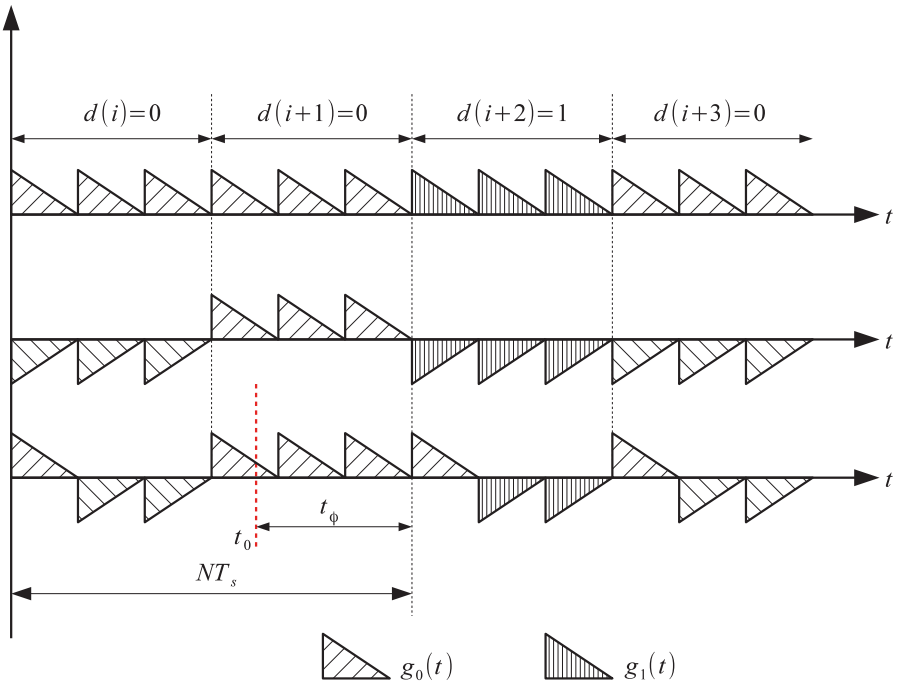

Figure 3.6: Received signal with the synchronization parameter t_ϕ and $N_f = 3$ a) original PSM signal format b) alternate signal inversion and c) information-free first frame, resulting in modified PSM signal format.

in (3.21) as follows

$$p_{T,d(i)}(t) = \psi_0(t - c_0 T_c) + \gamma_i \sum_{j=1}^{N_f - 1} \psi_{d(i)}(t - jT_f - c_j T_c) \tag{3.22}$$

where

$$\gamma_i = \sum_m \alpha_i^m \beta_i^m \,, \qquad m = 0, 1, ..., M-1 \tag{3.23}$$

with

$$\begin{aligned} \beta_i^m &= \beta_{i-1}^m \left[1 - 2\alpha_i^m\right] \\ \alpha_i^m &= \left[\left\lceil \frac{|d(i) - m| + M}{M} \right\rceil\right]_2 \end{aligned} \tag{3.24}$$

where $\alpha_i^m \in \{0, 1\}$ and $\{\beta_i^m, \gamma_i\} = \pm 1$.

From (3.22), it is clear that two changes have been made. First, the starting frame of each symbol is reserved and can be regarded as information-free pulse. Without loss of generality, we set $c_0 = 0$ hereafter. Secondly, pulses with alternate phase are used to represent a particular symbol i.e. the data symbol $d(i)$ is transmitted using $\psi_{d(i)}(t)$ and $-\psi_{d(i)}(t)$ alternately. The graphical explanation of these changes can be observed in Fig. 3.6.

Using same specifications for channel and receiver initialization as for previous proposition, the

observation signal can be given as

$$\begin{aligned} x(t) &= r(t+t_0) \\ &= \sum_i p_{R,d(i)}(t - iT_s + t_0) + n(t+t_0) \\ &= \sum_i p_{R,d(i)}(t - (i-N)T_s - t_\phi) + n(t + NT_s - t_\phi) \end{aligned} \tag{3.25}$$

where

$$p_{R,d(i)}(t) = g_0(t) + \gamma_i \sum_{j=1}^{N_f-1} g_{d(i)}(t - jT_f - c_jT_c) \tag{3.26}$$

3.6.1.2 Synchronization Algorithm

Now given $x(t)$ with $p_{R,d(i)}(t)$ defined as in (3.26), a simple ED based algorithm is proposed exploiting the judiciously designed signal format of (3.22). Let $T_g := \sup\{t|g_{d(i)}(t) \neq 0\}$ with $T_g = T_\psi + \tau_{L-1,0}$ and $T_R := \sup\{t|p_{R,d(i)}(t) \neq 0\}$ with $T_R = (N_f-1)T_f + c_{N_f-1}T_c + T_g$. For analytic tractability, we assume that both IFI and ISI are absent. This condition can be easily met by choosing $(N_h-1)T_c + T_g \leq T_f$. Note that this assumption is only imposed for analytic simplicity and we will show with numerical results the robustness of our algorithms against IFI and a moderate ISI.

First, just like for the method proposed in section 3.5.2, we take T_s-long K segments from received signal $x(t)$, given by

$$\begin{aligned} x_k(t) &= x(t + kT_s), \qquad k \in [0, K-1],\ t \in [0, T_s) \\ &= \sum_i p_{R,d(i)}(t - (i-N-k)T_s - t_\phi) + \eta(t) \end{aligned} \tag{3.27}$$

where $\eta(t) = n(t + (N+k)T_s - t_\phi)$.

As we have assumed that both IFI & ISI are absent, it is easy to observe that each segment $x_k(t)$ of size T_s will span at most two successive symbols of $p_{R,d(i)}(t)$. Letting $i = N + k + q$ where $q = 0$ or $q = -1$, (3.27) can be rewritten as

$$x_k(t) = \sum_{q=-1}^{0} p_{R,d(N+k+q)}(t - qT_s - t_\phi) + \eta(t) \tag{3.28}$$

Next, the mean of observation signal is found using sample mean estimator obtained from K segments as follows

$$\bar{x}(t) = \frac{1}{K}\sum_{k=0}^{K-1} x_k(t) = \frac{1}{K}\sum_{k=0}^{K-1}\sum_{q=-1}^{0} p_{R,d(N+k+q)}(t - qT_s - t_\phi) + \bar{\eta}(t) \tag{3.29}$$

where $\bar{\eta}(t)$ is averaged noise.

Ignoring noise brevity and substituting (3.26) in (3.29), we get

$$\bar{x}(t) = \sum_{q=-1}^{0} g_0(t - qT_s - t_\phi) + \frac{1}{K}\sum_{q=-1}^{0}\sum_{k=0}^{K-1}\sum_{j=1}^{N_f-1} \gamma_{N+k+q} g_{d(N+k+q)}(t - qT_s - jT_f - c_j T_c - t_\phi) \quad (3.30)$$

From (3.24), it can be seen that

$$\alpha_i^m = \begin{cases} 1 & \text{if } d(i) = m \\ 0 & \text{otherwise} \end{cases}, \; \beta_i^m = \begin{cases} -\beta_{i-1}^m & \text{if } d(i) = m \\ \beta_{i-1}^m & \text{otherwise} \end{cases} \quad (3.31)$$

therefore $\alpha_i^m \beta_i^m = -\beta_{i-1}^m$ for $d(i) = m$, resulting in mean of

$$\frac{1}{K}\sum_{k=0}^{K-1} \alpha_k^m \beta_k^m = \begin{cases} -1/K & \text{if } p^m \text{ is odd} \\ 0 & \text{otherwise} \end{cases} \quad (3.32)$$

where p^m is the total number of symbols in a sequence of length K having $d(k) = m$.

As K is sufficiently large, the sample mean can approximate to zero even when p^m is odd. Consequently,

$$\frac{1}{K}\sum_{k=0}^{K-1} \gamma_{N+k+q} = \frac{1}{K}\sum_{m}\sum_{k=0}^{K-1} \alpha_{N+k+q}^m \beta_{N+k+q}^m \approx 0 \quad (3.33)$$

Exploiting above fact, (3.29) can be simplified to

$$\bar{x}(t) = g_0(t - t_\phi) + g_0(t + T_s - t_\phi), \quad t \in [0, T_s) \quad (3.34)$$

From (3.34), it is clear that $\bar{x}(t)$ will have non-zero region only around t_ϕ. Exploiting the zeros guards, the objective function to estimate t_ϕ can be formulated as

$$\hat{t}_\phi = \arg \max_{\tau \in [0, T_s)} J(\tau)$$

where

$$J(\tau) = \int_0^{T_I} \bar{x}^2 \left([t + \tau]_{T_s} \right) dt \quad (3.35)$$

where $[.]_{T_s}$ is included as $\bar{x}(t)$ has size T_s while integration in (3.35) needs periodic extension of $\bar{x}(t)$ and T_I is the integration interval.

The integration region T_I has an impact on the synchronization accuracy of all flexible proposals as it is responsible for the signal energy capture. Ideally, it should be equal to the channel delay spread plus UWB pulse duration, i.e. $T_I = T_g$. However, if this value is not known, we can set it to $T_I = T_f - N_h T_c$ in the presence of TH codes and $T_I = T_f$ otherwise, provided that it captures sufficient energy.

In the sequel, we will show that $J(\tau)$ achieves its unique maximum only at t_ϕ i.e. $J(t_\phi) = \int_0^{T_I} g_0^2(t)dt$. Let $\Delta t = \tau - t_\phi$ be the relative misalignment between t_ϕ and candidate time shift τ with $\Delta t \in (-T_s, T_s)$. As value of Δt leads to different results, we consider the two following cases: $\Delta t \in (-T_s, 0]$ and $\Delta t \in (0, T_s]$, separately.

Specifically, if $\Delta t \in (-T_s, 0]$, the objective function $J(\tau)$ can be given as

$$J(\tau) = \int_0^{T_I} g_0^2(t + \Delta t)dt + \int_0^{T_I} g_0^2(t + T_s + \Delta t)dt \tag{3.36}$$

Recalling that $g(t)$ has a finite non-zero support within $[0, T_g)$, we get $J(\tau) = \int_0^{T_I+\Delta t} g_0^2(t)dt + \int_{T_s+\Delta t}^{T_I} g_0^2(t)dt$, which can be rearranged as

$$J(\tau) = J(t_\phi) - \int_{T_I+\Delta t}^{T_s+\Delta t} g_0^2(t)dt \tag{3.37}$$

Clearly, the objective function $J(\tau)$ is lower bounded by positive integral $\int_{T_I+\Delta t}^{T_s+\Delta t} g_0^2 dt > 0$, thus yielding a unique maximum if and only if (iff) $\Delta t = 0$ or equivalently $\tau = t_\phi$. Likewise, following the same steps when $\Delta t \in [0, T_s)$, we obtain

$$J(\tau) = J(t_\phi) - \int_{T_I+\Delta t-T_s}^{\Delta t} g_0^2 dt \tag{3.38}$$

Again, by a similar argument, we can conclude that $J(\tau)$ will achieve its maximum iff $\tau = t_\phi$, thus validating the algorithm.

3.6.1.3 Demodulation

The detection statistic for i^{th} symbol in conventional correlation based Rake receiver is given as

$$\hat{d}(i) = \arg \max_{m \in [0,M)} \left| \int_0^{T_s} x(t + iT_s + \hat{t}_\phi) v_m(t) dt \right| \tag{3.39}$$

where

$$v_m(t) = \sum_{l=0}^{L-1} \hat{\lambda}_l p_{T,m}(t - \hat{\tau}_{l,0})$$

is the reference signal with $\{\hat{\lambda}_l, \hat{\tau}_{l,0}\}_{l=0}^{L-1}$ representing estimated channel parameters and $p_{T,m}(t)$ is as given in (3.22) with $\gamma_i = 1$.

It is worth mentioning at this point that the reservation of one frame for synchronization purpose does not influence the BER performance to large extent. For example, consider the binary PSM and correlation based detection as in (3.39). To evaluate the probability of error, let us assume that $(d = 1)$ was transmitted, then the output of correlator in (3.39) inside modulus will be

$$\begin{aligned} r_0 &= \int_0^{T_s} x(t + iT_s + \hat{t}_\phi) v_0(t) dt = n_0 \\ r_1 &= \int_0^{T_s} x(t + iT_s + \hat{t}_\phi) v_1(t) dt = \sqrt{E_b} + n_1 \end{aligned} \tag{3.40}$$

where $\sqrt{E_b} = \sqrt{E_f} N_f$ is the bit energy with $\sqrt{E_f}$ being the frame energy. Then, the probability of error given $(d = 1)$ is transmitted is given by

$$P(e|d = 1) = P(r_1 < r_0 | d = 1) = P\left(|n_0 - n_1| > \sqrt{E_b}\right) \tag{3.41}$$

As n_1 and n_2 are i.i.d. random variables with $n_1, n_2 \sim \mathcal{N}(0, N_0/2)$, then the variable $n = n_0 - n_1$ will also be Gaussian with $n \sim \mathcal{N}(0, N_0)$. Thus,

$$\begin{aligned} P\left(|n| > \sqrt{E_b}\right) &= P\left(\sqrt{E_b} < n < -\sqrt{E_b}\right) \\ &= \frac{1}{\sqrt{2\pi N_0}} \int_{-\sqrt{E_b}}^{\sqrt{E_b}} e^{-x^2/2N_0} dx \\ &= \text{erfc}\left(\sqrt{\frac{E_b}{2N_0}}\right) \end{aligned} \tag{3.42}$$

where $\text{erfc}(x) = (2/\sqrt{\pi}) \int_x^\infty e^{-t^2} dt$ is the complementary error function. Now, when there is no reserved frame and conventional BPSM of (3.21) is used, then due to symmetry, the same error probability is obtained when we assume that $(d = 0)$ is transmitted. Sine the two signals are equiprobable, the average probability of error for coherent BPSM is

$$P_b = \text{erfc}\left(\sqrt{\frac{E_b}{2N_0}}\right) \tag{3.43}$$

However, when we intend to reserve a frame for achieving synchronization, as done in (3.22), then the symmetry no more exists when $(d = 0)$ is transmitted. Under this case, the two correlator outputs will be

$$\begin{aligned} r_0 &= \int_0^{T_s} x(t + iT_s + \hat{t}_\phi) v_0(t) dt = (N_f - 1)\sqrt{E_f} + n_0 \\ r_1 &= \int_0^{T_s} x(t + iT_s + \hat{t}_\phi) v_1(t) dt = \sqrt{E_f} + n_1 \end{aligned} \tag{3.44}$$

Then, the probability of error given $(d = 0)$ is transmitted is given by

$$P\left(e|d = 0\right) = P\left(r_0 < r_1 | d = 0\right) = P\left(|n_1 - n_0| > (N_f - 2)\sqrt{E_f}\right) \tag{3.45}$$

And thus,

$$\begin{aligned} P\left(e|d = 0\right) &= P\left((N_f - 2)\sqrt{E_f} < n < -(N_f - 2)\sqrt{E_f}\right) \\ &= \frac{1}{\sqrt{2\pi N_0}} \int_{-(N_f-2)\sqrt{E_f}}^{(N_f-2)\sqrt{E_f}} e^{-x^2/2N_0} dx \\ &= \text{erfc}\left((N_f - 2)\sqrt{\frac{E_f}{2N_0}}\right) \end{aligned} \tag{3.46}$$

Consequently, the average probability of error for coherent BPSM using signal with one information-free frame is

$$\begin{aligned} P_b &= \frac{1}{2}\text{erfc}\left(\sqrt{\frac{E_b}{2N_0}}\right) + \frac{1}{2}\text{erfc}\left(\frac{N_f - 2}{N_f}\sqrt{\frac{E_b}{2N_0}}\right) \\ &\approx \text{erfc}\left(\sqrt{\frac{E_b}{2N_0}}\right) \end{aligned} \tag{3.47}$$

where the approximation is achieved using the fact that N_f is chosen sufficiently large in IR-UWB in order to increase effective SNR per symbol, thus resulting in $(N_f - 2)/N_f \approx 1$. This BER expression is essentially same to one in (3.43) for conventional BPSM signaling.

Also, it important to clarify at this point that this information-free frame is adopted only during the synchronization phase. After the synchronization is done, the transmitter returns to the conventional PSM scheme. As this synchronization phase constitutes a very small fraction (say less than 5%) of the total transmission time [Luo06b], the effect on the overall demodulation performance will be negligible.

Although Rake receiver is considered to be optimal, unfortunately it needs L parallel correlators which makes its implementation unaffordable for practical UWB channels. Also, the performance of Rake receiver is very sensitive to mistiming [Tia05a, Tia05b] and channel estimation errors [Niu03]. These limitations of the Rake receiver motivate the use of non-coherent receivers for UWB [Hoc02, Wit09, Ho02], where the correlation between the received signal and a template derived from the received signal itself, is performed. Another interesting alternative to the Rake receiver is proposed in [Luo06b] where a template, called synchronized aggregate template (SAT), is achieved as a by-product of the synchronization algorithm. This SAT-based receiver has much lower complexity and exhibits very attractive performance in the SNR range of practical interest. In the following, we will show that by carefully designing the transmitted signal, we can develop a low-complexity SAT-based receiver for PSM-IR-UWB systems along with an improved synchronization algorithm.

3.6.2 SAT Extraction

Analyzing the mean of observation signal in (3.30), it is evident that the symbol-long segments of $\bar{x}(t)$ contain a version of $p_{R,d(i)}(t)$ circularly shifted by t_ϕ. Due to the careful change brought in the signal format by introducing γ_i in (3.22), the second part in the summation in (3.30) cancels out, leaving behind only the first frame. However, if we assume $\gamma_i = 1$ i.e. preserve the original PSM signal format of (3.21) and if t_ϕ were known, then (3.30) in case of binary PSM will result in

$$\hat{p}_R(t) = \frac{1}{K}\sum_{k=0}^{K-1} x_k(t + \hat{t}_\phi) = \hat{p}_{R,0}(t) + \hat{p}_{R,1}(t) \tag{3.48}$$

Applying the law of large numbers, one can see that $\lim_{K\to\infty} \hat{p}_R(t) = p_R(t)$ i.e. $\hat{p}_{R,0}(t) = p_{R,0}(t) = v_0(t)$ and $\hat{p}_{R,1}(t) = p_{R,1}(t) = v_1(t)$. Clearly, if we can separate the two parts of $\hat{p}_R(t)$ in (3.48), we will get the two desired reference signals as required for demodulation in (3.39) in case of binary PSM. This inspires us to think about an alternative solution which can provide not only the timing estimation but can also help in extracting the reference signals for demodulation.

Owing to the fact that the demodulator in (3.39) makes decision on the basis of the UWB waveform orthogonality, we may change the phase of the transmitted waveform in a way that it not only estimates the synchronization parameter but also separates the two template waveforms. Thus, instead of using $\psi_{d(i)}(t)$ for modulation, we will multiply $\psi_{d(i)}(t)$ with β_i, defined as

$$\begin{aligned} \beta_i &= \{[d(i) + \lfloor i/Q \rfloor]_2 + 1\} \, (\alpha_i)^{1+d(i)-\lfloor \frac{i}{Q} \rfloor}, \; \beta_i \in \{\pm 1, \pm 2\} \\ \alpha_i &:= \alpha_{i-1} \{2\lfloor i/Q \rfloor - 1\} \{1 - 2d(i)\}, \; \alpha_i \in \{1, -1\} \end{aligned} \tag{3.49}$$

where $Q \geq K$, with K being the number of symbols used for synchronization and Q being the number of symbols used for SAT recovery.

As $d(i)$ are independent and identically distributed (i.i.d) symbols taking the values $\{0, 1\}$ equiprobably, we can split them into two groups, denoted as $\mathcal{G}_0(i) := \{i : d(i) = 0\}$ and $\mathcal{G}_1(i) := \{i : d(i) = 1\}$. Choosing Q sufficiently large and using (3.49), the mean of the transmitted pulses can be shown to be

$$\begin{aligned}\frac{1}{Q}\sum_{i=0}^{Q-1}\beta_i\psi_{d(i)}(t) &= \frac{1}{Q}\left[\sum_{i=0}^{Q-1}\left[d(i)+1\right](\alpha_i)^{1+d(i)}\,\psi_{d(i)}(t)\right] \\ &\approx \frac{1}{Q}\left[\sum_{i\in\mathcal{G}_0(i)}\alpha_i\psi_0(t) + \sum_{i\in\mathcal{G}_1(i)}2\alpha_i^2\psi_1(t)\right] \\ &\approx \psi_1(t) \end{aligned} \tag{3.50}$$

Similarly, we can show that $(1/Q)\sum_{i=Q}^{2Q-1}\beta_i\psi_{d(i)}(t) \approx \psi_0(t)$. Thus, by judiciously changing the phase of the basic UWB pulse and performing two separate averaging operation once $\hat{t}_\phi$ is known, SAT can be recovered from (3.30) as

$$\begin{aligned}\hat{p}_{R,1}(t) &= Q^{-1}\sum_{k=0}^{Q-1}x_k(t+\hat{t}_\phi) = \hat{v}_1(t) \\ \hat{p}_{R,0}(t) &= Q^{-1}\sum_{k=Q}^{2Q-1}x_k(t+\hat{t}_\phi) = \hat{v}_0(t)\end{aligned} \tag{3.51}$$

Once SAT is recovered, we may proceed with our demodulation procedure in (3.39). It is worth mentioning that under the condition of large Q and equiprobable symbols, only Q out of $2Q$ symbols used for SAT recovery, are modulated by twice the amplitude of the others. As this value of Q is very small compared to the channel coherence time [Luo06b], received SNR will not be greatly aggravated and thus the impact on BER performance will be negligible.

3.6.3 Code Matching Based Synchronization Algorithm

The alternation of the symbols phase according to (3.49) effectively extracts the SATs for demodulation as long we know t_ϕ. As γ_i must be equal to 1 to extract SATs, it means that the energy detection based proposal can no more be used to achieve synchronization. So, our next aim is to estimate the synchronization parameter while preserving the phase alternation caused by β_i.

Code Matching Based Synchronization — Proposition 1

To achieve synchronization under the described signal format, we employ the well-known bipolar codes $\mathbf{b}$ having periodic autocorrelation function (PACF) defined as

$$R(n) = \sum_{j=0}^{N_f-1} b_j b_{[j+n]_{N_f}} = \begin{cases} N_f & n = kN_f \\ \pm 1 & \text{otherwise} \end{cases} \tag{3.52}$$

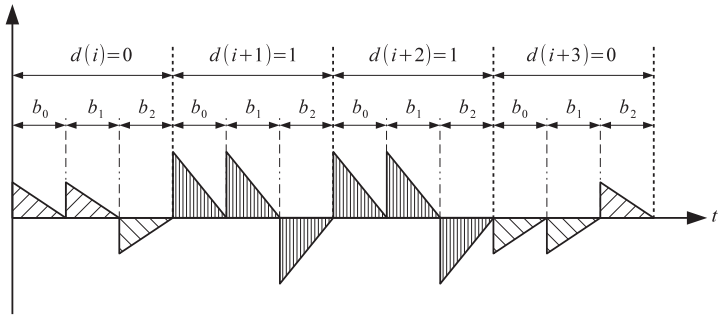

(a) $0 \leqslant i \leqslant (Q-1)$

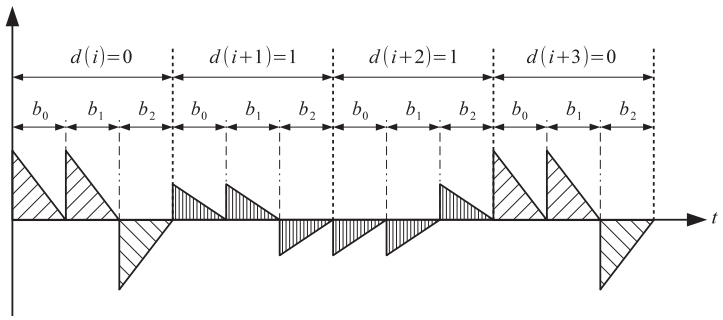

(b) $Q \leqslant i \leqslant (2Q-1)$

Figure 3.7: Observation signal with amplitude and phase alternation, $N_f = 3$ and $\mathbf{b} = [1, 1, -1]$.

with $k = 0, 1, 2, \cdots$.

Many sequences exhibit the above autocorrelation property (ACP), such as Maximum Length Shift Register sequences (m-sequence), Barker codes etc. The frames within each symbol are multiplied with these codes. Applying these modifications of multiplication by β_i and $\mathbf{b}$ to the original PSM transmitted symbol in (3.21), we get the resultant received symbol and observation signal as follows

$$\begin{aligned} p_{R,d(i)}(t) &= \sum_{j=0}^{N_f-1} b_j g_{d(i)}(t - jT_f - c_j T_c) \\ x(t) &= \sum_i \beta_i p_{R,d(i)}(t - (i-N)T_s - t_\phi) + n(t + NT_s - t_\phi) \end{aligned} \tag{3.53}$$

A graphical explanation of changes applied to transmitted signal can be seen in Fig. 3.7. The mean of observation signal is then given as

$$\begin{aligned} \bar{x}(t) &= \frac{1}{K} \sum_{k=0}^{K-1} x(t + kT_s), \quad K \leq Q,\ t \in [0, T_s) \\ &= \frac{1}{K} \sum_{k=0}^{K-1} \sum_i \beta_i p_{R,d(i)}(t - (i - N - k)T_s - t_\phi) \end{aligned} \tag{3.54}$$

Next, we take frame-long segments from $x_k(t)$ and compensate for random TH delays and binary

code $\{b_j\}_{j=0}^{N_f-1}$, followed by the signal aggregation operation.

$$\begin{aligned}\bar{x}_b(t,\tau) &= \sum_{m=0}^{N_f-1} b_m \bar{x}(t + mT_f + c_m T_c + \tau),\ t \in [0, T_f) \\ &= \frac{1}{K}\sum_{k=0}^{K-1}\sum_{i}\beta_i \sum_{m=0}^{N_f-1} b_m p_{R,d(i)}(t - (i-N-k)T_s - t_\phi + mT_f + c_m T_c + \tau)\end{aligned} \tag{3.55}$$

where $\tau \in [0, T_s)$ is the candidate time shift and the noise term is ignored for brevity hereafter.

Both synchronization parameter t_ϕ and candidate shift τ, can be expressed as an integer multiple of T_f plus a remnant, i.e. $t_\phi = n_\phi T_f + \epsilon_\phi, n_\phi = \lfloor t_\phi/T_f \rfloor \in [0, N_f)$, $\epsilon_\phi \in [0, T_f)$ and $\tau = n_\tau T_f + \epsilon_\tau, n_\tau = \lfloor \tau/T_f \rfloor \in [0, N_f)$, $\epsilon_\tau \in [0, T_f)$. Thus the relative misalignment at any specific time shift can be denoted as $t_e = \tau - t_\phi = [n_\tau - n_\phi]\, T_f + [\epsilon_\tau - \epsilon_\phi] = \tilde{n} T_f + \tilde{\epsilon}$, where $\tilde{n} \in [-n_\phi, N_f - 1 - n_\phi)$ and $\tilde{\epsilon} \in [-\epsilon_\phi, T_f - \epsilon_\phi)$. Consequently, (3.55) can be rewritten as

$$\bar{x}_b(t,\tau) = \frac{1}{K}\sum_{k=0}^{K-1}\sum_{i}\beta_i \sum_{m=0}^{N_f-1} b_m p_{R,d(i)}(t - (i-N-k)T_s + (m+\tilde{n})\, T_f + c_m T_c + \tilde{\epsilon}) \tag{3.56}$$

Substituting $p_{R,d(i)}(t)$ from (3.53), we get

$$\begin{aligned}\bar{x}_b(t,\tau) = \frac{1}{K}\sum_{k=0}^{K-1}\sum_{i}\beta_i \sum_{m=0}^{N_f-1}\sum_{j=0}^{N_f-1} b_m b_j g_{d(i)}(t - (i-N-k)T_s \\ + (m+\tilde{n}-j)\, T_f + (c_m - c_j)\, T_c + \tilde{\epsilon})\end{aligned} \tag{3.57}$$

To this end, it is worth noting that the dual purposes served by TH codes (i.e. spectrum smoothing and multi-access) can be equally achieved by the user-specific orthogonal polarity codes $\mathbf{b}$. Thus we assume $c_m = c_j = 0,\ \forall\,(m, j)$. As a result, (3.57) can be simplified as

$$\bar{x}_b(t,\tau) = \frac{1}{K}\sum_{k=0}^{K-1}\sum_{i}\beta_i \sum_{m=0}^{N_f-1}\sum_{j=0}^{N_f-1} b_m b_j g_{d(i)}(t - (i-N-k)T_s + (m+\tilde{n}-j)\, T_f + \tilde{\epsilon}) \tag{3.58}$$

As the value of $\tilde{\epsilon}$ leads to different results, we first consider the case when $\tilde{\epsilon} \in [-\epsilon_\phi, 0)$. Since the observed segments $\bar{x}_b(t,\tau)$ have a finite support $[0, T_f)$, only finite values of i, j will contribute to non-zero summands in (3.58) under the assumption of no IFI & ISI. So, it is easy to find that

$$i = N + k,\ j = m + \tilde{n} + q, \qquad q \in \{-1, 0\} \tag{3.59}$$

Also, by exploiting the explanation in (3.50), it is clear that $(1/K)\sum_{k=0}^{K-1}\beta_k g_{d(k)}(t) \approx g_1(t)$. Applying these simplifications, (3.58) can be expressed as

$$\begin{aligned}\bar{x}_b(t,\tau) &= \sum_{m=0}^{N_f-1}\sum_{q=-1}^{0} b_m b_{m+\tilde{n}+q} g_1(t - qT_f + \tilde{\epsilon}) \\ &= \sum_{m=0}^{N_f-1} b_m b_{m+\tilde{n}} g_1(t + \tilde{\epsilon}) + \sum_{m=0}^{N_f-1} b_m b_{m+\tilde{n}-1} g_1(t + T_f + \tilde{\epsilon})\end{aligned} \tag{3.60}$$

Capitalizing on the ACP of bipolar code $\mathbf{b}$ defined in (3.52), (3.60) simply reduces to

$$\bar{x}_b(t,\tau) = \begin{cases} N_f g_1(t+\tilde{\epsilon}), & n_\tau = n_\phi \\ N_f g_1(t+T_f+\tilde{\epsilon}), & n_\tau = n_\phi + 1 \\ \approx 0, & \text{otherwise} \end{cases} \tag{3.61}$$

It is easy to observe that when $\tilde{\epsilon} = 0$, the term corresponding to $n_\tau = n_\phi + 1$ in (3.61) disappears due to the fact that $T_g \leq T_f$ in the absence of IFI. Applying energy detection operation afterwards with integration interval equal to T_g, it is thus clear that $\bar{x}_b(t,\tau)$ achieves its maximum energy of $N_f^2 E_g$ only when $\tilde{n} = 0$, $\tilde{\epsilon} = 0$, i.e. $\tau = t_\phi$, where $E_g = \int_0^{T_g} g^2(t)\,dt$ is the energy of aggregate received segment.

Similarly, when $\tilde{\epsilon} \in [0, T_f - \epsilon_\phi)$, we can show following same procedure that

$$\bar{x}_b(t,\tau) = \begin{cases} N_f g_1(t-T_f+\tilde{\epsilon}), & n_\tau = n_\phi - 1 \\ N_f g_1(t+\tilde{\epsilon}), & n_\tau = n_\phi \\ \approx 0, & \text{otherwise} \end{cases} \tag{3.62}$$

Again, by similar argument we conclude that $\bar{x}_b(t,\tau)$ attains its maximum iff $\tau = t_\phi$. Building on above analytic analysis, timing offset t_ϕ can be estimated in NDA mode using the following optimization

$$\hat{t}_\phi = \arg \max_{\tau \in [0, T_s)} J(\tau)$$

where

$$J(\tau) = \int_0^{T_I} \bar{x}_b^2 \left((t,\tau)_{T_f} \right) dt \tag{3.63}$$

Note that $\bar{x}_b(t)$ has a size T_f whereas integration in (3.63) requires its periodic extension, thus a (mod T_f) operation is required, i.e. $\bar{x}_b(t,\tau) = \sum_{m=0}^{N_f-1} b_m \left[\bar{x}(t + mT_f + \tau)\right]_{T_f}$.

Due to the averaging in (3.54), PSD of the AWGN noise term $\bar{\eta}(t) := (1/K)\sum_{k=0}^{K-1} \eta(t + kT_s)$ is reduced to $N_0/2K$. This will result in improved synchronization accuracy. However, one drawback of proposition in (3.63) is that it will need a relatively long sequence to achieve the approximation in (3.50) and thus to establish a reliable estimation.

Under the assumption of a simplified linear channel model $h(t) = \sum_{l=0}^{L-1} \lambda_l \delta(t - \tau_l)$, we can develop a variant of above synchronization method to ensure much more efficient performance with fewer number of symbols. This proposition exploits the same ACP of bipolar codes $\mathbf{b}$ combined with orthogonality among UWB pulses, which we unfold next.

Code Matching Based Synchronization — Proposition 2

Let the UWB pulse correlation be $\Gamma_{a,b}(t) = \int_{-\infty}^{\infty} \psi_a(\tau)\psi_b(\tau - t)d\tau$, $[a,b] = \{0,1\}$. Relying on cross correlation between the observation signal in (3.53) with $\beta_i = 1$ and the two orthogonal pulses used for modulation i.e. $\psi_0(t)$ and $\psi_1(t)$, we get

$$y(t) = \int_{-\infty}^{\infty} x(\tau)\psi_0(\tau - t)d\tau + \int_{-\infty}^{\infty} x(\tau)\psi_1(\tau - t)d\tau \tag{3.64}$$

Defining $\Psi_a(t) = \Gamma_{0,a}(t) + \Gamma_{1,a}(t)$, $a = \{0, 1\}$, (3.64) can be rewritten as

$$\begin{aligned} y(t) &= \sum_i \breve{p}_{R,d(i)}(t - (i - N)\,T_s - t_\phi) \\ \breve{p}_{R,d(i)} &:= \sum_{j=0}^{N_f-1} b_j \breve{g}_{d(i)}(t - jT_f - c_j T_c) \end{aligned} \tag{3.65}$$

where $\breve{g}_{d(i)}(t) = \sum_{l=0}^{L-1} \lambda_l \Psi_{d(i)}(t - \tau_{l,0})$.

Clearly, if $\Psi_0(t) = \Psi_1(t)$ i.e. the autocorrelation and cross correlation functions of $\psi_0(t)$ and $\psi_1(t)$ are same, then we will have the same signal throughout and the signal dependence will be removed. We will show in next section how to ensure this property through the design procedure of the orthogonal UWB pulses $\psi_{d(i)}(t)$. Once we are able to find UWB pulses satisfying $\Gamma_{0,0}(t) = \Gamma_{1,1}(t)$ and $\Gamma_{0,1}(t) = \Gamma_{1,0}(t)$, then the symbol dependence will be removed and we can simply write

$$y(t) = \sum_i \breve{p}_{R,1}(t - (i - N)\,T_s - t_\phi) \tag{3.66}$$

The matched-filtering operation in (3.64) not only wipes out the signal dependence but also maximizes the received signal-to-noise ratio (SNR). As $y(t)$ is the same throughout, we can apply the same averaging and code matching operations of (3.54) and (3.55) on $y(t)$ as

$$\begin{aligned} \bar{y}(t) &= \frac{1}{K} \sum_{k=0}^{K-1} y(t + kT_s), \quad t \in [0, T_s) \\ \bar{y}_b(t, \tau) &= \sum_{m=0}^{N_f-1} b_m \bar{y}(t + mT_f + c_m T_c + \tau), \quad t \in [0, T_f) \end{aligned} \tag{3.67}$$

and can show using similar reasoning as for proposition 2 that $\bar{y}_b(t, \tau)$ will also achieve its maximum iff $\tau = t_\phi$, hence achieving synchronization.

Consequently, timing offset t_ϕ can be estimated in the absence of ISI without channel knowledge in NDA mode using the following optimization

$$\hat{t}_\phi = \arg \max_{\tau \in [0, T_s)} J(\tau) - T_\psi$$

where

$$J(\tau) = \int_0^{T_I} \bar{y}_b^2 \left([t, \tau]_{T_f} \right) dt \tag{3.68}$$

The term T_ψ is included due to the fact that $y(t)$ is a matched-filtered version of observation signal $x(t)$ with UWB pulses.

Next, we briefly explain the optimization procedure used to generate UWB pulses, with specific correlation properties as required by the synchronization algorithm to be functional.

Waveform Optimization

In previous chapter, we introduced a simple and flexible approach for generating UWB pulses using B-splines as basis functions. It was shown that spectrally efficient UWB pulses can be generated

by solving a non-linear optimization problem with linear and non-linear constraints. GA are then used to solve such discontinuous, non-differential objective function with undefined gradients at many local minimum points [Mic95].

To generate pulses with specific correlation properties as required by the last synchronization proposition, a new constraint has to be added to the previously defined ones and run again the optimization procedure. The required criteria can be mathematically written as

$$\begin{cases} \min\limits_{c_{l,k}} \left[-\sum\limits_{l=0}^{L-1} \xi_l \right] & \text{subject to :} \\ \sum\limits_{k=0}^{N_s-1} c_{l,k} = 0, & l = 0, 1, 2, \ldots, L-1 \\ |\hat{\psi}_l(f)|^2 \leq S_{FCC}(f), & l = 0, 1, 2, \ldots, L-1 \\ \int\limits_{-\infty}^{\infty} \psi_l(t)\psi_p(t)dt = E_\psi \delta_{lp}, & (l,p) \in \{0, 1, 2, \ldots, L-1\} \\ \Gamma_{0,0}(t) = \Gamma_{l+1,l+1}(t), & l = 0, 1, 2, \ldots, L-2 \\ \Gamma_{l,l+p}(t) = \Gamma_{l+p,l}(t), & p = l+1, \ldots, L-1 \end{cases} \tag{3.69}$$

where ξ_l is the objective function, $\hat{\psi}_l(f) = \int_{-\infty}^{\infty} \psi_l(t) e^{-2\pi f t} dt$, $S_{FCC}(f)$ is FCC spectral mask, and E_ψ is the pulse energy.

The first constraint in (3.69) is due to the requirement of zero DC component of transmitted signal while the remaining constraints correspond to respecting FCC mask, orthogonality and similar correlation functions respectively. Fig. 3.8 shows two orthogonal UWB pulses obtained using GA-based optimization along with their spectral properties and correlation functions.

As it can be seen these functions meet the criteria required by the last synchronization proposition. However, it should also be noted that the achieved efficiency is reduced compared to the one which would have been obtained without the new additional constraint (see the PSD notch around 7GHz in Fig. 3.8b).

3.7 Comparative Analysis of Proposed Algorithms

***A-priori* Information** In terms of *a-priori* knowledge, all the proposed algorithms need minimal information. Orthogonal signaling based synchronization (OSS) & energy detection based synchronization (EDS), however, have an edge over the others because they are totally blind in the sense that they do not need any knowledge whatsoever about the transmitted signal. Code matching based synchronization (CMS) propositions, on the other hand, do need *a-priori* knowledge about the user-specific TH codes and binary codes. All the methods except OSS also need information about the maximum channel delay spread in order to determine the integration region T_I.

Robustness to Transmission Characteristics From the applicability viewpoint, EDS is relatively more promising as it can be used in M-ary PSM. This is because γ_i in (3.23) changes the phase for all modulation indices $m = 0, 1, \cdots, M-1$ alternately. Thus, increasing the modulation-order will not affect the algorithm as long as the first frame is reserved and carries the same waveform

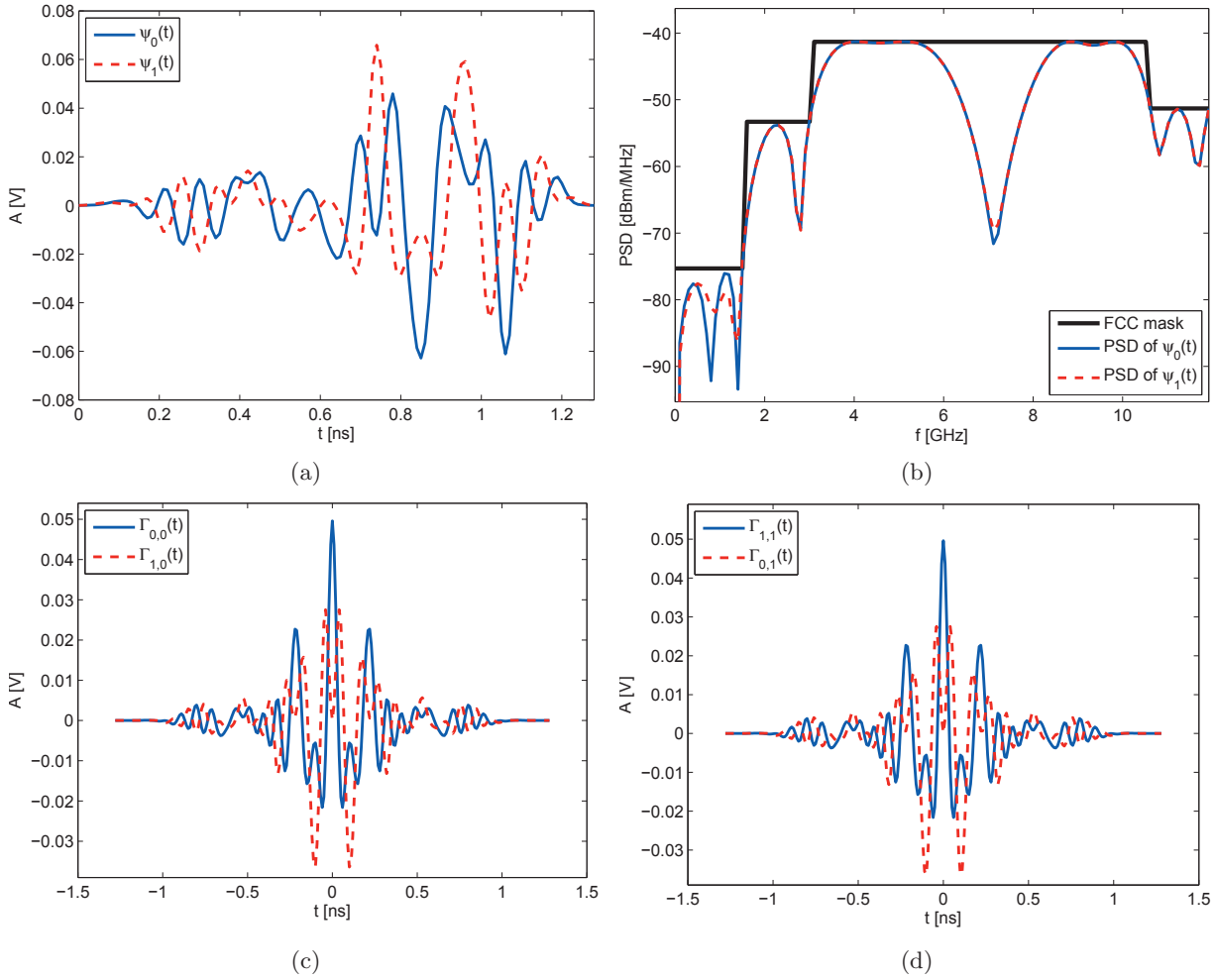

Figure 3.8: [(a) & (b)] Pair of orthogonal UWB pulses and their corresponding PSD. [(c) & (d)] Autocorrelation and cross-correlation of $\psi_0(t)$ and $\psi_1(t)$ respectively.

throughout.

Code matching based synchronization - proposition 2 (CMS2) can also be used in M-ary PSM but it will need cross-correlation between the observed signal and M basic pulses as in (3.64). Such cross-correlation with all M pulses will certainly increase the complexity of the system. Also, this will require the design of M orthogonal pulses with specific correlation properties among them using GA based waveform optimization, which is again difficult to accomplish for higher M.

Due to extremely wide bandwidth, the UWB channel usually exhibit non-linearity due to reflections, diffraction and scattering and should be modeled as (3.2). EDS & code matching based synchronization - proposition 1 (CMS1) are more appealing as they are robust to such frequency selective channels and to the distortions caused by antennas while OSS & CMS2 exploit the orthogonality of transmitted pulses, which can not be benefited in the presence of distorted received pulses.

Implementation Complexity With regards to implementation complexity, it mainly amounts to two factors, 1) shifting of observation signal by T_s to find the mean of observation signal and 2) the maximization of objective function $J(\tau)$ for the search based methods. The shifting can be done both in analog as well as in digital domain. Analog approaches have the advantage of avoiding the

sampling which can be very high in UWB regime. However, they need analog delay lines (on the order of symbol duration) for shifting which can be demanding especially for low-power circuits. Nonetheless, chips implementing analog delays from 20-2,000ns are available and can be used to implement the algorithms [ADL].

On the other hand, the digital implementation is relatively simple from the signal processing viewpoint and digital operations can be performed efficiently in modern on-chip technologies. However, it will need UWB receiver to digitize the signal at the Nyquist rate (usually several gigahertz). So the primary concern in digital implementation is the design of ultra-fast ADCs. Parallel ADCs can be used to achieve this feat where each ADC operates at a fraction of the effective sampling frequency [O'D05]. Nevertheless, if ultra-fast ADCs are available [DC], all propositions can be implemented in full-digital format.

As far the maximization itself is concerned, it is obvious that the continuous search over $[0, T_s)$ will result in prohibitive complexity. In practice, the objective function $J(\tau)$ is evaluated over a grid of finite equispaced values $\tau = nT_\delta$ where $n \in [0, \lfloor T_s/T_\delta \rfloor)$ and T_δ is the step interval.

$$\hat{n} = \arg \max_{n \in [0, \lfloor T_s/T_\delta \rfloor)} J(nT_\delta) \tag{3.70}$$

The estimated synchronization parameter will be then $\hat{t}_\phi = \hat{n}T_\delta$ with an ambiguity of T_δ. It is worth mentioning that the synchronization at any precision can be achieved by the maximization based proposals and is only constrained by the affordable complexity, thereby signifying their flexibility.

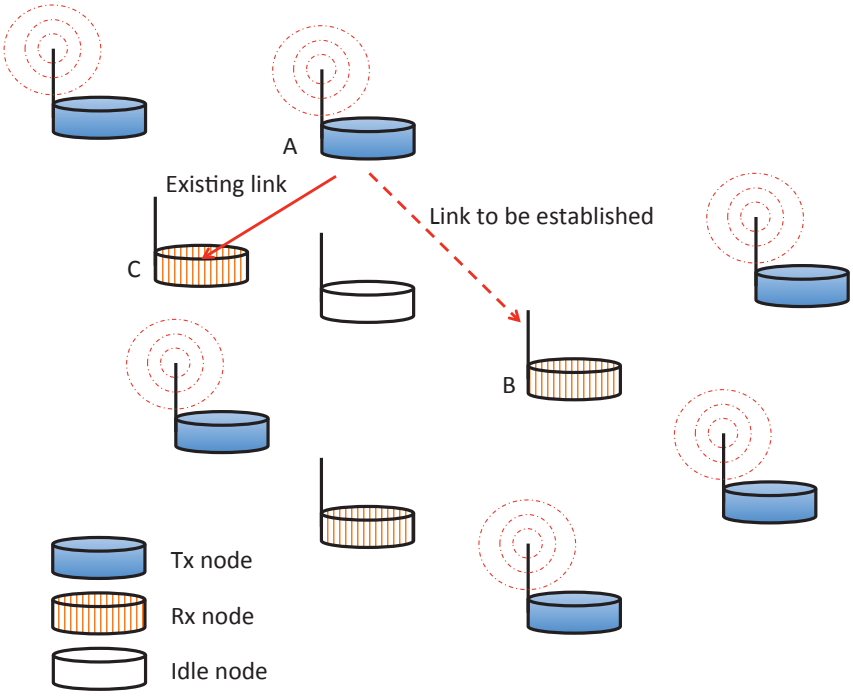

Figure 3.9: A multi-access ad hoc configuration (cluster topology) [Luo06b].

Application Framework From the perspective of possible application area, we envision a similar context and application framework for our methods as described in [Luo06b, Luo07] for UWB ad hoc networks such as wireless sensor networks (WSNs).

Consider a single piconet consisting of multiple nodes. A likely configuration of the overall pro-

tocol is outlined in [Luo06b]. Under multi-user interference, the essence of the proposed algorithms is that at any time, there is only one node (but not the same one all the time) which transmits peculiar signal format. This node is designated as a "master" node and takes the responsibility of synchronizing the other nodes designated as "slave" nodes. This is effectively the case with star or clustered topologies of ad hoc networks.

Let us outline the overall protocol we envision for a WSN setting using OSS proposition. With reference to Fig. 3.9, the master node A broadcasts regularly to its cluster the conventional zero-mean S-PAM symbols and occasionally transmits the A-PAM. An idle neighbor node B "wakes up" and starts averaging the symbols according to (3.10). As soon the A-PAM symbols are transmitted by node A, the averaging will effectively result in non-zero mean and at that time node B can proceed to synchronize using proposed OSS algorithm. Meanwhile, nodes with established links in the same cluster with A (e.g., node C) receive information without interruption which they demodulate using the conventional zero threshold detector.

3.8 Numerical Results

In this section, simulations are carried out to evaluate the performance of proposed synchronization algorithms in terms of probability of detection (P_D), normalized mean squre error (NMSE) and BER. In all ensuing simulations, specially designed B-spline based orthogonal UWB pulses meeting the optimization criteria of (3.69) are used with duration $T_\psi = 1.28\,\text{ns}$. Each symbol consists of $N_f = 13$ ($N_f = 12$ for OSS as it needs number of frames which are multiple of 3) frames while each frame contains $N_c = 15$ chips. The chip duration T_c is same as pulse duration T_ψ, resulting in frame duration of $T_f = 19.2\,\text{ns}$. We have used TH codes randomly taking integer values from $[0, N_h)$, where $N_h = 5$.

The multipath channel employed in simulations is CM1 indoor channel proposed by IEEE 802.15.3a working group [Mol03], having RMS delay spread $\tau_{rms} = 5\,\text{ns}$. The synchronization parameter t_ϕ is randomly generated from a uniform distribution over $[0, T_s)$ at each Monte Carlo trial. The binary code for code matching based propositions is selected as $\mathbf{b} = 202$ in decimal. The integration interval T_I is set equal to $T_f - N_h T_c$, so no knowledge about the maximum delay spread is needed. SNR is defined as P_g/σ^2 where P_g is the received power per pulse (after the convolution of transmitted pulse with channel impulse response).

The synchronization performance is assessed under three different conditions namely;

Test A. Absence of IFI & ISI: To avoid any interference among frames and symbols, the channel is truncated beyond $(T_f - N_h T_c) = 12.8\,\text{ns}$ and the energy is normalized to unity.

Test B. Moderate IFI & ISI: Addition of moderate interference is ensured by extending the channel delay spread to T_f and hence spreading $N_h T_c$ long tail of dispersed pulse into the subsequent frame. The tail of last frame in each symbol will also spread into the first frame of subsequent symbol, thereby also inducing a small ISI.

Test C. Introduction of MUI: We return to the original setting of Test A, but this time we assume that there are two interfering users also present in the system. The two users are assumed to transmit according to (3.53) with $\beta_i = 1$ and employ user-specific TH codes but same polarity codes $\mathbf{b}$ as the desired user for CMS propositions, according to conventional PSM as in (3.21) for EDS and according to conventional power efficient zero-mean A-PAM for OSS. As $N_h = 5$, the

user-specific TH codes can not widely separate the three users, thus a severe interference exists among them.

These settings effectively satisfy the envisioned protocol outlined in the previous section as all the interfering users utilize the conventional signaling format and only a single node which takes the responsibility of synchronizing neighbors applies judicious changes in the transmission format.

3.8.1 Synchronization Performance

We first evaluate the synchronization accuracy of proposed algorithms in terms of detection probability which is defined as $P_D = \Pr\left[|\hat{t}_\phi - t_\phi| \leq T_\delta\right]$. As OSS method can synchronize up to frame-level accuracy, we set step interval $T_\delta = T_f$ for a fair comparison among all proposed algorithms.

The detection probability performance curves under different tests are shown in Fig. 3.10. Each proposed algorithm is also compared with one algorithm in literature based on similar criterion. For instance, we compare OSS with "Dispensing with search (DS)" [Ren09], EDS with "Low-complexity blind synchronization (LCBS)" [Luo06b] and CMS propositions with "Code-assisted blind synchronization (CABS)" [Yin08]. The reason for this choice is that DS also exploits orthogonal pulses like OSS, LCBS is also based on energy detection like EDS and CABS utilizes bipolar codes much like our CMS schemes; thus providing a good basis for relative comparison.

It is worth mentioning, however, that all these compared algorithms deal with IR-UWB systems employing BPAM and are used only to give a benchmark performance. A pronounced improvement in performance is evident with proposed algorithms compared to referenced algorithms under all operating conditions. Note that the LCBS method uses $2K$ symbols in case of Test A and $3K$ in case of Test B. The DS approach does not function in the presence of MUI at all while OSS proposition still provides quite satisfactory performance.

In case of IFI/ISI, the performance curves are almost identical to the ideal case of no interference for all propositions. This is justified due to the fact that channel is truncated beyond 12.8ns which is more than twice the τ_{rms} and as the PDP of CM1 decays exponentially, the interference is not severe enough to affect the performance.

On the other hand, the performance degradation is more visible in case of MUI. However, the performance is not degraded dramatically compared to the ideal case of no interference and the synchronization parameter can still be estimated with reasonable precision. Also, it is important to notice that the performance of OSS will be less affected in the presence of MUI. This is because OSS employs A-PAM modulation while the interfering users keep on transmitting the S-PAM symbols. Thus the averaging operation in (3.10) will result in the suppression of MUI automatically.

The maximization based propositions EDS and CMS, however, focus on PSM and although each of them also apply averaging as the first step in algorithm, such averaging will not cancel out MUI. Further, we have considered the worst scenario where the two interfering users also employ the same binary codes as the desired user in case of CMS. Therefore, it is reasonable to assume that by choosing orthogonal binary codes for different users in CMS1 & CMS2 and larger separation by TH codes in all propositions, the performance under MUI may improve but the effect of MUI will certainly be more adverse than OSS.

As discussed before that the choice of θ is an important factor for OSS method, we are interested to see the impact of θ on the detection probability of OSS. Fig. 3.11 provides the P_D of OSS against

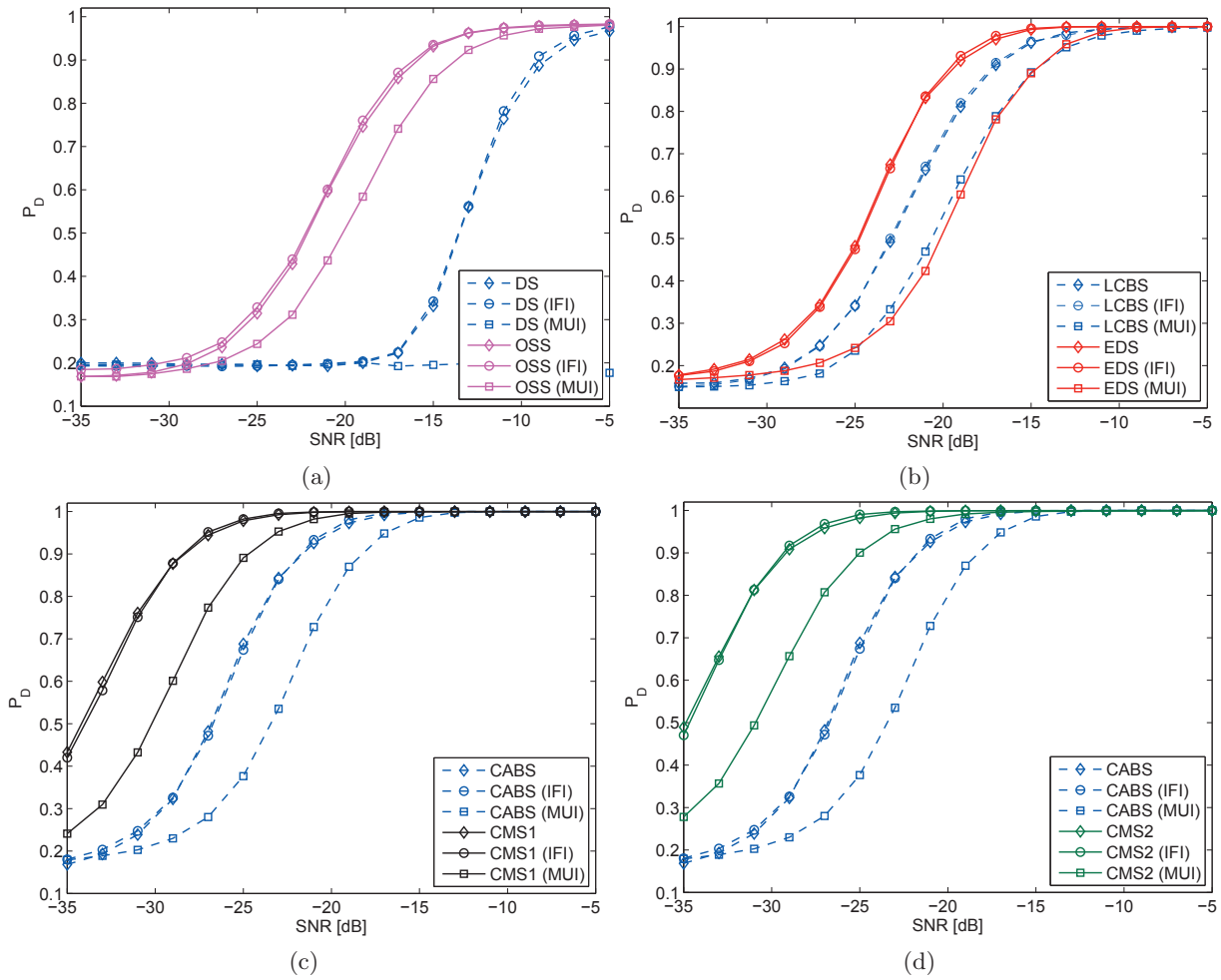

Figure 3.10: Detection probability comparison with $K = 64$ symbols under different operating conditions: (a) OSS and reference [Ren09], (b) EDS and reference [Luo06b], (c) CMS1 and reference [Yin08], (d) CMS2 and reference [Yin08].

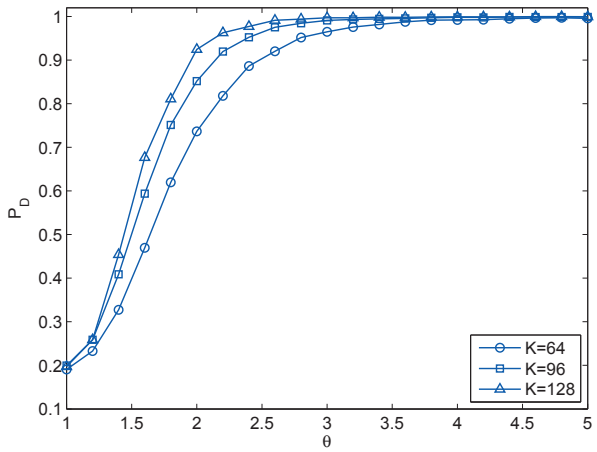

Figure 3.11: Detection Probability against θ at SNR $= -15$dB.

various values of θ under Test A. The resulting curves justify our choice of $\theta = 3$ as performance with more than 90% is achieved even with $K = 64$ symbols.

Fig. 3.12a provides a comparison between the proposed algorithms themselves in terms of P_D

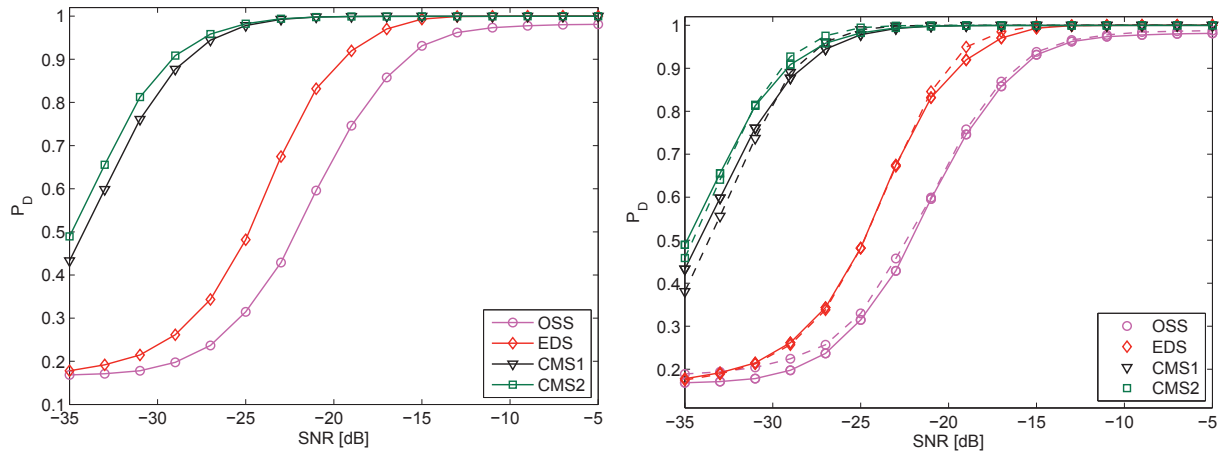

Figure 3.12: Detection probability performance comparison between proposed algorithms with $K = 64$ symbols: (a) CM1. (b) CM1 (solid) and CM2 (dotted).

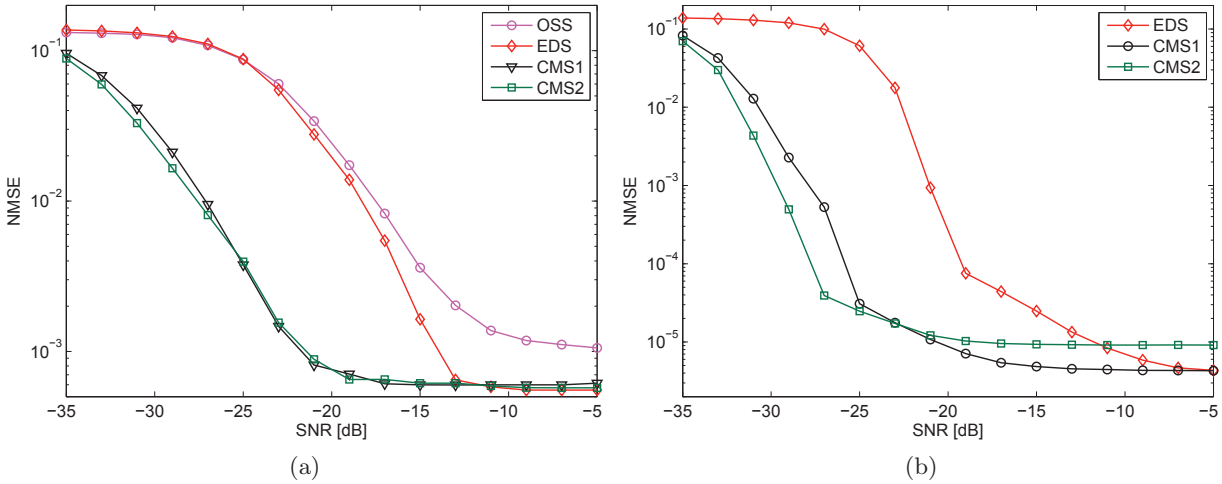

Figure 3.13: NMSE performance comparison between proposed algorithms with $K = 64$ symbols: (a) Frame-level. (b) Chip-level.

under Test A. It is clear that maximization based methods provide much better performance, which was expected as they evaluate all candidate time shifts. Among maximization based approaches, code matching solutions provide significantly improved performance compared to EDS, thanks to the fine correlation properties of binary codes.

In Fig. 3.12b, the performance is compared in both line-of-sight (LOS, CM1) and non line-of-sight (NLOS, CM2) propagation channels of the IEEE 802.15.3a standard with $T_\delta = T_f$. The simulation results in Fig. 3.12b show that the performance is almost identical in LOS and NLOS channels. Even slight improvement is observed for some SNR values, this is because CM2 is more dense channel and there are less empty bins compared to CM1, thus the algorithms can exploit better the orthogonality and energy capture.

Next, the NMSE performance is evaluated and the results are shown in Fig. 3.13. The performance curves decrease monotonically for all synchronizers before reaching an error floor. This error floor is obvious since synchronization is performed with a finite resolution of T_f in Fig. 3.13a and with T_c in Fig. 3.13b. The error floor is almost 6×10^{-4} in Fig. 3.13a corresponding to a timing error standard deviation around 6.11 ns which is less than the intended accuracy of $T_f = 19.2$ ns.

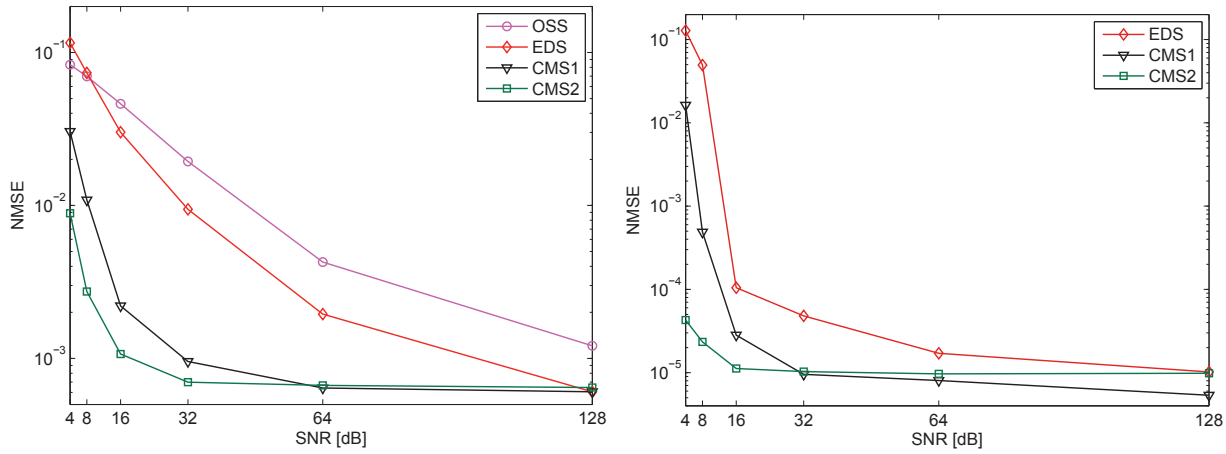

Figure 3.14: Performance comparison in terms of NMSE between proposed algorithms with various values of K symbols at SNR $= -15$dB: (a) Frame-level. (b) Chip-level.

Similarly, in Fig. 3.13b, the error floor is around 5×10^{-5} resulting in timing error standard deviation of about 0.79 ns which is again less than the intended accuracy of $T_c = 1.28$ ns. Note that, Fig. 3.13b does not show OSS because it can only provide frame-level synchronization.

The effect of various lengths of the observation window K on detection probability of the proposed algorithms can be seen in Fig. 3.14. It is clear that the performance is improved with increasing K due to the fact that the signal averaging operation employed by all propositions can better mitigate the noise effect with large K. Clearly, CMS approaches need much fewer symbols compared to other methods for a reasonable accuracy. Among CMS1 & CMS2, we observe from Fig. 3.14b that as few as 4 symbols are sufficient for synchronization with CMS2. This is due to the fact that no undesired part is needed to be eliminated by first-order averaging, in contrast to other methods.

3.8.2 BER Performance

We now translate the synchronization performance into BER performance. Fig. 3.15 exhibit BER using demodulator of (3.39), after estimating synchronization parameter by the proposed synchronization algorithms with $T_\delta = T_f$ for OSS while $T_\delta = T_c$ for the rest. We suppose that channel estimation is done after synchronization and that it was error-free. We average over 10^3 channel realizations where in each realization after estimating t_ϕ, we demodulate 10^3 symbols using A-Rake. We also plot BER using A-Rake under perfect timing as a reference.

As CMS can precisely synchronize with much fewer symbols, we can achieve BER similar to the case of perfect timing even with $K = 8$ symbols for CMS2 and and $K = 32$ symbols for CMS1. However, EDS needs higher and OSS needs even more symbols to achieve reasonable BER performance.

Finally, we extract SATs as in (3.51) and use them as reference signals in (3.39). These SATs can be obtained from CMS1 after synchronization stage. The resulting performance is compared against A-Rake and selective Rake (S-Rake) with 5 correlators corresponding to 5 strongest paths, under perfect timing. S-Rake is practically a more viable solution compared to A-Rake due to its prohibitive complexity.

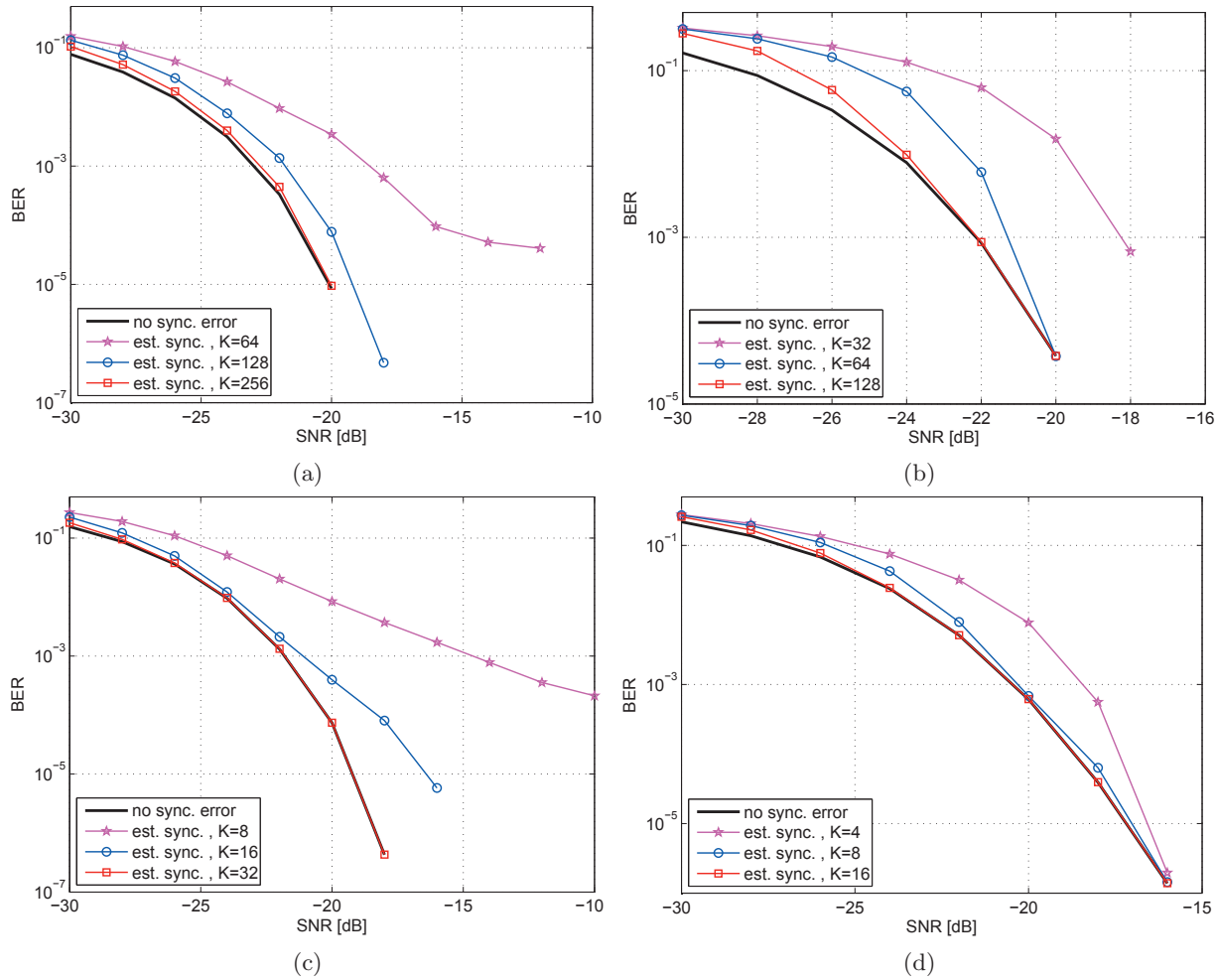

Figure 3.15: BER Performance comparison for various values of K symbols: (a) OSS. (b) EDS. (c) CMS1. (d) CMS2.

The results shown in Fig. 3.16 demonstrate that the BER performance of SAT-based receiver is very close to S-Rake, especially at high SNR. It can also be observed that SAT-based receiver can even outperform S-Rake by increasing the number of averaging symbols Q in (3.51), while S-Rake on the other hand is dependent on number of fingers to capture sufficient energy.

3.9 Conclusions

In this chapter, the issue of synchronization in time-hopping IR-UWB systems is addressed and several new synchronization algorithms are proposed.

The central idea of all these new methods is to take advantage of some useful properties of UWB pulses achieved via waveform optimization (orthogonality, correlation properties), in order to design **non-data-aided**, **low-complexity** and **effective** synchronization algorithms.

The key contributions of the work presented in this chapter can be summarized as follows.

1) First, a rapid synchronization scheme (OSS) is proposed without the need to search hundreds of bins. This approach follows a detection based approach and benefits from the orthogonal pulses and asymmetric PAM to achieve coarse frame-level synchronization.

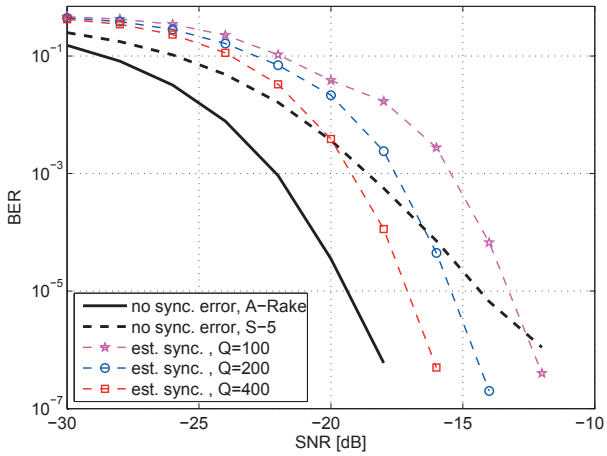

Figure 3.16: BER performance comparison of Rake and SAT-based receiver of CMS1 proposition.

2) Next, an energy detection based synchronization algorithm (EDS) is proposed which exploits the first order averaging. Unlike the first method it follows an estimation based approach and makes use of PSM instead of PAM. The transmitted signal is judiciously designed in a way that by simple overlap-add operations followed by energy detection, one can estimate the synchronization time. This algorithm has the advantage of achieving synchronization with no *a-priori* knowledge and remain equally valid for higher-order PSM.

3) The energy detection based proposition, however, has a limitation that the judicious change in the signal format results in the loss of one frame per symbol, thereby making it a semi NDA algorithm. So, next we propose another approach (CMS1) which exploits the discriminative nature of well-designed binary codes and does not incur any data loss. This approach estimates the timing offset by code matching followed by aggregating received signal segments and energy detection. This estimation based approach provides much improved performance than the first one, especially in case of relatively high number of symbols.

4) Although, the code matching based proposition (CMS1) is full NDA, it needs relatively large number of symbols to achieve synchronization. This limitation is overcome by using a second code matching based proposition (CMS2) which makes use of specially designed UWB pulses and matched filtering the received signal with them before applying code matching. This effectively reduces the number of symbols for acceptable synchronization accuracy.

5) In the course of establishing synchronization using CMS1 proposition, we also get as a by-product an aggregate template which we use to develop a new non-coherent demodulation scheme for binary PSM, similar to the one proposed for BPAM in [Luo06b]. This receiver bypasses the cumbersome task of channel estimation and can collect the full multipath energy. Also, it inherently captures the pulse distortion caused by antennas and other receiver effects. Results show that it can achieve performance comparable to the widely adopted S-Rake in medium to high SNR range.

A comparative study is also provided about merits and eventual challenges in the realization of proposed methods. Extensive simulations are carried out under different operating conditions to validate the robustness of proposed algorithms.

Chapter 4

Channel Estimation in IR-UWB

- Abstract -

In this chapter, we address the channel estimation problem which is another critical issue for the realization of coherent Rake receivers. First, a literature review is presented regarding channel estimation in IR-UWB. It was found that most of the methods available in literature are based on either maximum-likelihood (ML) or orthogonal subspace (OS) approaches. Motivated by certain limitations of these methods, we then propose a joint ML/OS channel estimation method. The simulation results prove the increased efficiency of the proposed algorithm in terms of resolution and accuracy.

Contents

4.1 Introduction

In a Rake receiver, each signal echo is correlated with a locally generated time-hopping pulse train and then combined into a single test variable for final decision. Time alignment is required between the code sequence in each echo and the corresponding locally generated reference. Also, the attenuations incurred by the various echoes must be known to maximize SNR in the decision variable (maximum ratio combining). Performing Rake reception with appropriate weights on individual fingers entails estimation of the channel impulse response. This poses a major challenge in UWB communications because even if one opts to utilize only a few (say the ten strongest out of hundreds of) returns, accurate estimation of the ten strongest channel gains and their corresponding delays is required.

Although channel estimation is also critical in the context of narrowband and spread-spectrum systems, and the channel estimators developed for Direct Sequence Code Division Multiple Access

(DS-CDMA) can be adapted to UWB systems, one main distinction is that the number of parameters to be estimated, i.e. the number of delays and amplitudes, can be as large as 100 for a typical UWB indoor channel. This calls for alternatives specifically designed for UWB characteristics.

4.2 UWB Channel Model

A typical model for the impulse response of a multipath fading channel is given by

$$h_{\boldsymbol{\alpha},\boldsymbol{\tau}}(t) = \sum_{l=1}^{L} \alpha_l \delta(t - \tau_l) \tag{4.1}$$

where $\{\alpha_l, \tau_l\}_{l=0}^{L-1}$ are channel path gains and delays respectively. Although this model does not adequately reflect specific frequency dependent effects, it is commonly used for diversity reception schemes in conventional wideband receivers (e.g., RAKE receivers). Equation (4.1) can be interpreted as saying that a received signal $y(t)$ is made up of a weighted sum of attenuated and delayed replicas of the transmitted signal $s(t)$, that is

$$y(t) = \sum_{l=1}^{L} \alpha_l s(t - \tau_l) + \eta(t) \tag{4.2}$$

where $\eta(t)$ denotes AWGN noise.

The objective is to estimate the unknown channel parameters $\{\boldsymbol{\alpha}, \boldsymbol{\tau}\}$ using the received signal $y(t)$.

4.3 Literature Review

In order to estimate the unknown delays and propagation coefficients, several classes of algorithms have been developed so far. In [Car03], the authors propose a least-square (LS) procedure, taking into account the clustered structure of the channel. However, such an approach requires the Nyquist sampling rate (that is, a sub-pulse rate) and has prohibitively high computational requirements. Another class of algorithms is based on the ML criterion for estimating the channel parameters [Lot02, Win02]. For example, in [Lot02], the authors use the ML parameter estimation of UWB multipath channels in the presence of MUI. In particular, the impulse response estimates are formed using either training symbols or information-bearing symbols, while treating MUI as white Gaussian noise. Similarly to the LS approach, the computational complexity of the ML estimator increases rapidly as the number of multipath components increases, and becomes almost unaffordable in real-time applications. Besides, the sampling rate suggested in [Lot02] is in the range $12.5/T_p$ - $25/T_p$ (where T_p denotes the pulse duration). With a typical value of $T_p = 1\,\text{ns}$, the required sampling rate is prohibitively high and ranges between 12.5 GHz and 25 GHz.

The ML criterion for channel estimation also requires a multidimensional optimization of a highly oscillatory error function, implying a huge, complex computational solution. For these reasons, several suboptimal ToA algorithms jointly estimating the channel parameters, based on a simple peak detection process have been proposed in [Fal06]. In particular, a novel estimation strategy able to cope with the presence of unresolved multipath, is developed by the authors.

It is shown in [Che10] that the performance of the approximate NDA ML estimate derived in [Lot02] can be further improved and so a new NDA near-ML estimator for the delays and attenuations in an UWB channel by using a new approximation to the ML equation is proposed. However, the performance gain is achieved at the cost of a more complicated estimator structure. Therefore, the new estimators are only desirable in applications where performance is more important than complexity.

The channel estimation issues in aperiodic TH systems are studied in [Xu06] and both LS and correlation matching (CM) techniques are developed. First, a pulse-rate discrete-time system model is introduced to transform original PPM-based TH-UWB signals. Through this modeling, a unique time-dependant code matrix for each user in each symbol interval can be defined. Then it is observed that channel parameters are embedded either linearly in the first-order or quadratically in the second-order statistics of received signals. Applying a mean-matching technique via a LS criterion, multiuser channels can be estimated without ambiguity. Meanwhile, after defining a rank-one channel-dependent matrix for each user, a CM technique can be applied to estimate each channel up to a scalar ambiguity. Although reliable estimation of the mean or correlation by sample averaging is not feasible due to the time-varying nature of hopping codes, it is shown that instantaneous estimates of those statistics can still be exploited to achieve reliable channel estimates with appropriate cost functions. If interfering users' hopping codes are not known, corresponding single-user versions of LS and CM estimators are developed after approximating the sum of all interfering signals and noise as a stationary process with unknown statistics. Thanks to the time-varying property of TH codes, those statistics can be jointly estimated with unknown channel parameters of the desired user using similar matching criteria, unique for aperiodic TH-UWB systems.

A UWB (space alternating generalized expectation maximization (SAGE)) based channel estimation method is proposed in [Han03]. This algorithm is an extension of conventional SAGE algorithm which is often adopted for wideband channel estimation. The algorithm divides the measured data into individual ray paths and estimates the directions of arrival, propagation time, and the variation of the amplitude and phase during the propagation for each signal. UWB-SAGE algorithm is based on the ML estimation and has a high resolution in separating the incident waves.

The expectation-maximization (EM) algorithm [Dem77] provides a numerical method for obtaining maximum likelihood of estimates that might not be available otherwise. The EM algorithm has been studied in [Mek08] to estimate the channel parameters of an M-PPM UWB communication. A training sequence is first exploited to get an initial estimate of the channel, then the equalizer is performed and feeds the channel decoder which in turn gives updated probabilities to the EM estimator.

A successive interference cancellation (SIC) type implementation of the ML-based estimator is done in [Han06] to estimate channel parameters. Although the main drawback of the SIC-type path detection is error propagation, the fine time resolution offered by UWB signals can mitigate it, since the detection and removal of the paths are conducted in an accurate manner. The SIC-type procedure is equivalent to the EM algorithm with the number of paths equals to one. In SIC, first the strongest path is estimated and then the data corresponding to this path is reconstructed and then subtracted from the received signal. This process is continued until the number of paths reaches a predefined number. In finding a value of the strongest model parameters at the start, a combination of a coarse global mesh search based on the EM algorithm and a fine local search based on the SAGE algorithm was employed. In the coarse global mesh search, we find the region which

may include the values of parameters that give the maximum value of the log-likelihood function. After the region is specified, a fine local search is conducted inside the region to find the value of parameters accurately.

To avoid the high sampling rate and reduce complexity, there has been a renewed interest in using the so-called TR signaling; that is, rather than estimating the channel impulse response h(t), one should estimate the aggregate analog channel $s(t) * h(t)$. Namely, the idea is to couple each information-bearing pulse $s(t)$ with an unmodulated (or pilot) pulse. For example, the transmitted pulse can be of the form $p(t) = s(t) + b.s(t - T_f)$, $b = \{\pm 1\}$, where the frame duration T_f is chosen such that, after multipath propagation, the information and pilot pulses do not overlap. The receiver then correlates the received signal $y(t)$ with its delayed version $y(t-T_f)$ to yield the symbol estimate, assuming that the timing of each pulse is known. While such an approach requires only frame-rate samples, it results in 50% energy or rate loss, as half of the transmitted waveforms are used as pilot symbols. Recently, several modifications of the TR scheme have been also proposed in the literature. In [Cha03], some generalized likelihood ratio test (GLRT) schemes were investigated, whereas in [Zha03] the authors propose a maximum-likelihood approach, which computes the autocorrelation of the channel impulse response at various delays. Yet, such techniques trade off computational requirements for performance, and have nearly the same complexity as the methods developed in [Win02].

The UWB propagation study and associated channel modeling suggest clustering occurs in both space and time for indoor environments. Relying on a channel model based on clusters, UWB channel estimation is carried out in two steps in [Car04]: a coarse localization of the local scatterers and then a more refined identification of the principal multipath components within each cluster. Different schemes are investigated. The ML estimation followed by the EM algorithm assures good performance, but care must be taken when initializing both schemes. Also, convergence can be very slow at low SNR. Alternatively, when the initial conditions are not close to the truth and low complexity is required, the LS estimation followed by the space-time correlation turns out to be a more appropriate choice and results in a slight performance loss.

The idea of multiple pulse transmissions is exploited in [Gei10] to obtain highly accurate channel and range estimates using the low-complexity ED. A single ED is employed for channel estimation and ranging whose sampling rate is shifted with respect to the pulse repetition frequency. It is demonstrated that the signal model of the IEEE 802.15.4a standard allows the application of the proposed receiver architecture.

Note from (4.2) that the received signal $y(t)$ has only $2L$ degrees of freedom, the time delays τ_l and the propagation coefficients α_l. Although these parameters can be estimated using the time domain model (4.2), an efficient, closed-form solution is possible if we consider the problem in the frequency domain.

Let $Y(\nu)$ denote the Fourier transform of the received signal

$$Y(\nu) = \sum_{l=1}^{L} \alpha_l S(\nu) \exp(-j2\pi\nu\tau_l) + N(\nu) \;\Rightarrow\; \frac{Y(\nu)}{S(\nu)} = \sum_{l=1}^{L} \alpha_l \exp(-j2\pi\nu\tau_l) + N(\nu) \tag{4.3}$$

where $S(\nu)$ and $N(\nu)$ are the Fourier transforms of $s(t)$ and $\eta(t)$, respectively.

Clearly, the received and transmitted signals spectra ratio is given by a sum of complex exponentials, where the unknown time delays appear as complex frequencies while propagation coefficients

appear as unknown weights. Thus the problem of estimating the channel parameters can be considered as a special case of harmonic retrieval problem that are well studied in spectral estimation literature.

High-resolution harmonic retrieval is well-studied: there exists a rich body of literature on both theoretical limits and efficient algorithms for reliable estimation [Hua90,Hua91,Roy89,Rao92] There is a particularly attractive class of model-based algorithms, called super-resolution methods, which can resolve closely spaced sinusoids from a short record of noise-corrupted data. In [Rao92, Sto97], a polynomial realization is discussed, where the parameters are estimated from zeros of the so-called prediction or annihilating filter. In [Rao92], a state space method is proposed to estimate parameters of superimposed complex exponentials in noise, which provides an elegant and numerically robust tool for parameter estimation using a subspace-based approach. The ESPRIT algorithm is developed in [Roy89], which can be viewed as a generalization of the state space method applicable to general antenna arrays. In [Hua91], several subspace techniques for estimating generalized eigenvalues of matrix pencils are addressed, such as the Direct matrix pencil algorithm, Pro-ESPRIT, and its improved version TLS-ESPRIT. Subspace methods can achieve performance close to that of the ML estimator [Hua90], and are thus considered to be a viable alternative, provided that a low-rank system model is available.

4.4 A Joint ML/OS Channel Estimation Approach

The algorithm we propose [Akb10b] is based on a joint ML and superresolution approach. Basically, our algorithm consists of three steps. In the first step, we get a coarse estimation of the time delays and corresponding amplitudes using ML estimation. In particular, we will employ a SIC based implementation of ML. In the next step, these estimated MPCs are validated using the noise projection vector, formed by the eigenanalysis of the received signal correlation matrix. And finally, the remaining paths which the ML estimator was not able to find will be estimated by MUltiple Signal Classification (MUSIC). In the following, we will first represent the two algorithms which form the building blocks of our proposed algorithm and then we will elaborate the detailed description of merging these algorithms to propose a joint estimation method.

4.4.1 Search, Subtract and Readjust Algorithm

In the case of Gaussian noise, ML criterion is equivalent to the mean squared error minimization. So the ML estimate of the channel parameters $\boldsymbol{\alpha}$ and $\boldsymbol{\tau}$ are the values which will minimize the following mean squared error:

$$S(\boldsymbol{\alpha}, \boldsymbol{\tau}) = \frac{1}{M} \|\mathbf{y} - \hat{\mathbf{y}}_{\boldsymbol{\alpha},\boldsymbol{\tau}}\|^2 \tag{4.4}$$

where $\mathbf{y}$ and $\hat{\mathbf{y}}_{\boldsymbol{\alpha},\boldsymbol{\tau}}$ contain the samples of $y(t)$ and $s(t) \star \hat{h}_{\boldsymbol{\alpha},\boldsymbol{\tau}}(t)$ respectively, with $\hat{h}_{\boldsymbol{\alpha},\boldsymbol{\tau}}(t)$ is the estimated CIR.

The ML estimation used as a basis here is one proposed in [Fal06], namely search, subtract and readjust (SSR) algorithm, which is similar to SIC. The idea is simply to calculate the correlation between received signal and reference signal via a MF and finding the largest peak in each iteration, which will correspond to value of τ. The algorithm consists of the following steps:

- Match-filter the received signal with transmitted pulse.
- Find the sample corresponding to the largest peak of the absolute value of the MF output and convert the index into the corresponding time location to estimate $\hat{\tau}_1$.
- Calculate the amplitude estimate of $\hat{\tau}_1$ as:

$$\hat{\alpha}_1 = \left(\mathbf{s}_1^T \mathbf{s}_1\right)^{-1} \mathbf{s}_1^T \mathbf{y} \tag{4.5}$$

  where $\mathbf{s}_1$ represents the sampled replica of UWB pulse $s(t)$ shifted by delay τ_1.
- Reconstruct data of the strongest path and remove it from received signal to form a new observation signal, i.e. $\acute{\mathbf{y}} = \mathbf{y} - \hat{\alpha}_1 \mathbf{s}_1$.
- Use the new observation signal and return to step 1 to estimate the next multipath
- The amplitudes $\boldsymbol{\alpha}$ in k-th iteration are calculated by

$$\begin{bmatrix} \hat{\alpha}_1 \\ \hat{\alpha}_2 \\ \vdots \\ \hat{\alpha}_k \end{bmatrix} = \left([\mathbf{s}_1, \mathbf{s}_2, \cdots, \mathbf{s}_k]^T [\mathbf{s}_1, \mathbf{s}_2, \cdots, \mathbf{s}_k] \right)^{-1} [\mathbf{s}_1, \mathbf{s}_2, \cdots, \mathbf{s}_k]^T \mathbf{y} \tag{4.6}$$

- Continue the same process until the N strongest paths are found.

The detailed description of this method can be seen in [Fal06, Win02]. A block diagram depicting different steps of SSR is shown in Fig. 4.1.

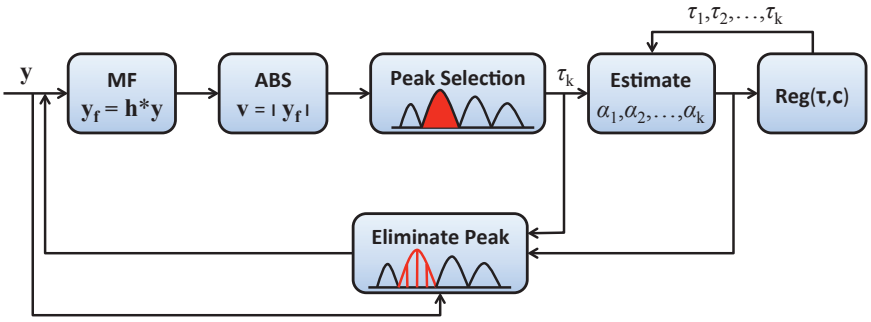

Figure 4.1: Block diagram of the SSR algorithm.

4.4.2 MUSIC Algorithm

For superresolution based method, we will use the classic MUSIC approach which can be summarized by the following steps:

- Construct the data matrix using spectral smoothing procedure.
- Apply eigenanalysis of the data matrix and decompose the observation space into two orthogonal subspaces, i.e. signal subspace and noise subspace.
- Estimate the signal subspace dimension using information theoretic criteria.
- Constitute the projection operator on noise subspace as $\Pi_n^{\perp} = \mathbf{V}_n \mathbf{V}_n^H$, where $\mathbf{V}_n$ is the column matrix of the noise subspace eigenvectors.

- Calculate the channel profile using maxima of $CP_{MUSIC}(\tau_i) = \dfrac{1}{\mathbf{a}_i^H \prod_n^{\perp} \mathbf{a}_i}$ where $\mathbf{a}_i$ is the search vector which will explore the whole parameter space.

The detailed description of MUSIC is given in Appendix B. A generic block diagram explaining different steps of OS based MUSIC method is given in Fig. 4.2.

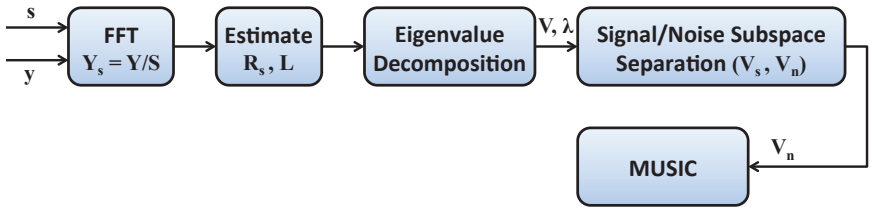

Figure 4.2: Block diagram of the OS based MUSIC algorithm.

Limitations ML based estimations are relatively simple but may pose some limitations in UWB channels. Mainly, they have limited resolution ability, making them less attractive for UWB channels. Also the estimation degrades significantly for MPCs of small amplitude in the noisy case. One key advantage is that as the algorithm focuses on similarity between received signal and estimated signal, it can provide a low mean-squared error even at low SNR.

OS based methods theoretically can provide infinite resolution, but in practice show some limitations. Firstly, the autocorrelation matrix is generally not known, so its estimation is subject to errors. Secondly, as it is a parametric approach, precise information about the number of MPCs to be estimated is needed. For this purpose some estimation procedure is used such as Akaike Information Criterion (AIC) or Maximum Description Length (MDL) [Wax85]. Again this estimation is not reliable for low SNR and under-estimation of MPCs present in the received signal may cause errors. These effects become very prominent at low SNR, causing estimation to degrade drastically and making them unsuitable for low SNR scenarios.

4.4.3 Proposed Algorithm (OS-SSR)

The main idea of the algorithm proposed is to combine SSR and MUSIC approaches in order to take advantage of their attractive features and to overcome some of their limitations. The block diagram of the proposed algorithm is shown in Fig. 4.3, while the detailed description of different steps is given below:

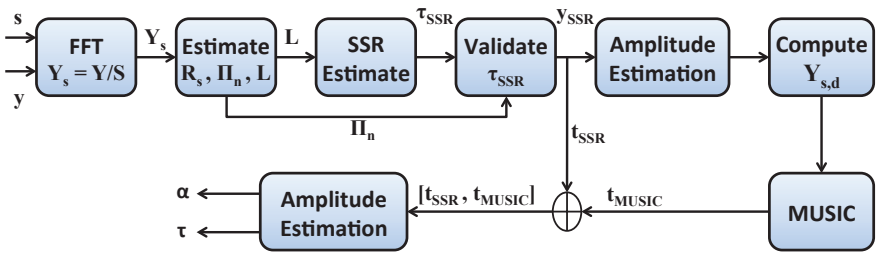

Figure 4.3: Block diagram of the proposed algorithm.

1) Compute the FFT coefficients for the received signal $y(t)$ and the UWB pulse $s(t)$ and form the corresponding vectors $\mathbf{Y}$ and $\mathbf{S}$ respectively. Actually, only the coefficients corresponding to the frequency band of interest (3.1 to 10.6 GHz) are used to further calculate the ratio $\mathbf{Y}_s = \mathbf{Y}/\mathbf{S}$, in order to avoid the risk of dividing by zero.

   The Nyquist condition is satisfied here in terms of delays as $1/\Delta f \geq 2\tau_{max}$, where Δf is the frequency sampling interval and τ_{max} is the maximum delay of channel.

2) Form the $p \times q$ data matrix using the $\mathbf{Y}_s$ vector elements:

$$\mathbf{D}_s = \begin{bmatrix} \mathbf{Y}_s(1) & \cdots & \mathbf{Y}_s(q) \\ \mathbf{Y}_s(2) & \cdots & \mathbf{Y}_s(q+1) \\ \vdots & \ddots & \vdots \\ \mathbf{Y}_s(p) & \cdots & \mathbf{Y}_s(N) \end{bmatrix} \tag{4.7}$$

   with $N = p + q - 1$ and $p, q \geq L$.

   Next, estimate the data autocorrelation matrix as follows

$$\hat{\mathbf{R}}_s = q^{-1} \left[\mathbf{D}_s \mathbf{D}_s^H + \mathbf{J}_p \mathbf{D}_s \mathbf{D}_s^H \mathbf{J}_p \right] \tag{4.8}$$

   where $\mathbf{J}_p$ is $p \times p$ anti-diagonal identity matrix.

   The estimate provided by (4.8) has been preferred to the standard one [Wax85] since it allows improving the Toeplitz structure of the data autocorrelation matrix.

3) Perform the $\hat{\mathbf{R}}_s$ matrix eigenanalysis and obtain the eigenvector matrix $\mathbf{V}$ and the eigenvalue diagonal matrix $\mathbf{\Lambda}$. The eigenvalues are sorted and then used by AIC or MDL criterion to estimate the signal subspace dimension, i.e. the number of MPCs L. The eigenvectors corresponding to the largest L eigenvalues span the signal subspace and form the $\mathbf{V}_s$ matrix. The others span the noise subspace and form the $\mathbf{V}_n$ matrix. The noise subspace projection operator is then calculated as:

$$\Pi_n^{\perp} = \mathbf{V}_n \mathbf{V}_n^H \tag{4.9}$$

4) Estimate the MPC delays $\boldsymbol{\tau}_{\text{SSR}} = [\tau_1, \tau_2, \cdots, \tau_L]$ using SSR algorithm and form the signal vectors:

$$\mathbf{a}_k = \left[1 \; e^{-j2\pi\nu_0\tau_k} \; \cdots e^{-j2\pi(p-1)\nu_0\tau_k} \right]^T \tag{4.10}$$

   Validate only the delays resulting in signal vectors orthogonal to the noise subspace, that is:

$$\mathbf{a}_k^H \Pi_n^{\perp} \mathbf{a}_k \cong 0 \tag{4.11}$$

   In the noiseless case false and true peaks are clearly separated. In the noisy case, it is more difficult, but still possible to classify most of them, using some suitable threshold for the projection values. The paths corresponding to projection values above that threshold are considered as false paths and thus eliminated.

5) Use the vector of validated delays, denoted by $\mathbf{t}_{\text{SSR}}$ in Fig. 4.3, to estimate the amplitudes of remaining true paths $\mathbf{c}_{\text{SSR}}$ according to (4.6).

6) Compute the signal $y_{\text{SSR}}(t)$ as:

$$y_{\text{SSR}}(t) = s(t) \star h_{c,t}^{\text{SSR}}(t) \tag{4.12}$$

Now derive a new observation vector, called difference vector, $\mathbf{Y}_{s,d} = (\mathbf{Y} - \mathbf{Y}_{\text{SSR}})/\mathbf{S}$, using only the FFT coefficients in the frequency band of interest, as done in step 1. This newly formed vector will now be used to estimate the remaining paths which were either not estimated at all by SSR or badly estimated and eventually dropped in the validation step.

7) Estimate the remaining MPCs from $\mathbf{Y}_{s,d}$ using MUSIC algorithm: follow steps 2 and 3 to estimate $\hat{R}_s$ and to split observation space into orthogonal signal and noise subspaces, then estimate multipath delays by projecting the vector $\mathbf{a}(\tau) = \left[1\, e^{-j2\pi\nu_0\tau_k} \cdots e^{-j2\pi(p-1)\nu_0\tau_k}\right]^T$ onto the noise subspace.

8) The final delays can be given as $\boldsymbol{\tau} = [\mathbf{t}_{\text{SSR}}, \mathbf{t}_{\text{MUSIC}}]$ while the corresponding amplitudes $\mathbf{c}_{\text{SSR}}$ and $\mathbf{c}_{\text{MUSIC}}$ are adjusted using (4.6) to give final coefficients $\boldsymbol{\alpha}$.

4.5 Simulation Results

In this section, performance of different algorithms is analyzed. We have used a specially designed, B-spline based UWB pulse with time duration $T_p = 1.28\,\text{ns}$, which fulfills the FCC mask constraints and also optimizes the spectral effectiveness [Akb09].

The example below shows how the proposed approach OS-SSR works on a typical IEEE 802.15.3a CM2 channel profile. In fact, it is truncated as shown on Fig. 4.4 in order to still be able to visually distinguish the channel estimation results and to compare the different methods. As it can be noticed from this figure, the channel profile contains 19 peaks, some of them being extremely close. For instance, the 17$^{\text{th}}$ and the 18$^{\text{th}}$ peaks are spaced by only 0.01 ns.

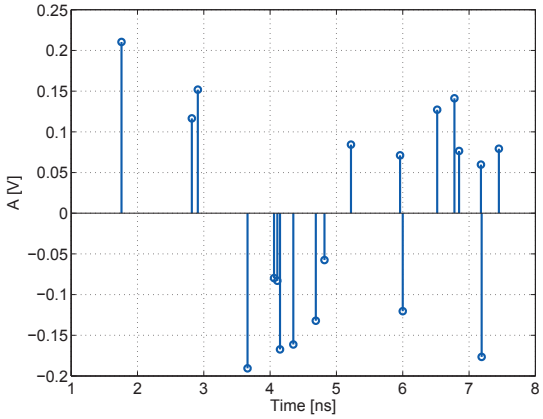

Figure 4.4: Truncated version of a typical IEEE 802.15.3a CM2 channel profile

When the UWB pulse depicted on the Fig. 4.5a is transmitted into this channel, the signal shown on the Fig. 4.5b is obtained at the receiver input, in the noiseless case.

Running the algorithms introduced in Section 4.4 on this example leads to the results shown on Fig. 4.6. As expected for the noiseless case, the superresolution method MUSIC provides an exact estimation of the channel profile irrespective of how closely spaced are its multipath, unlike the SSR method, whose resolution is finite and is the same as for the matched filtering.

In the framework of this thesis, the performance of channel estimation methods is assessed in terms of two complementary parameters. The first one is the normalized mean square error,

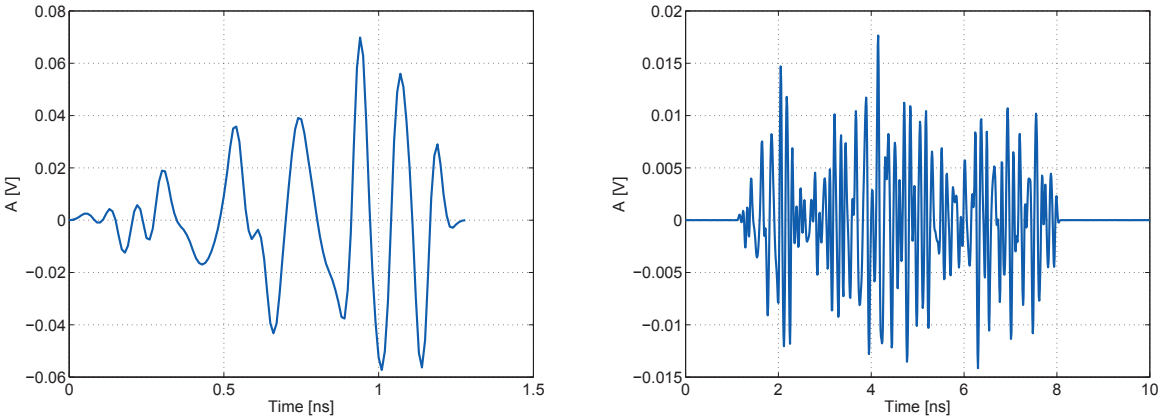

(a) (b)

Figure 4.5: (a) Transmitted UWB pulse and (b) received noiseless signal.

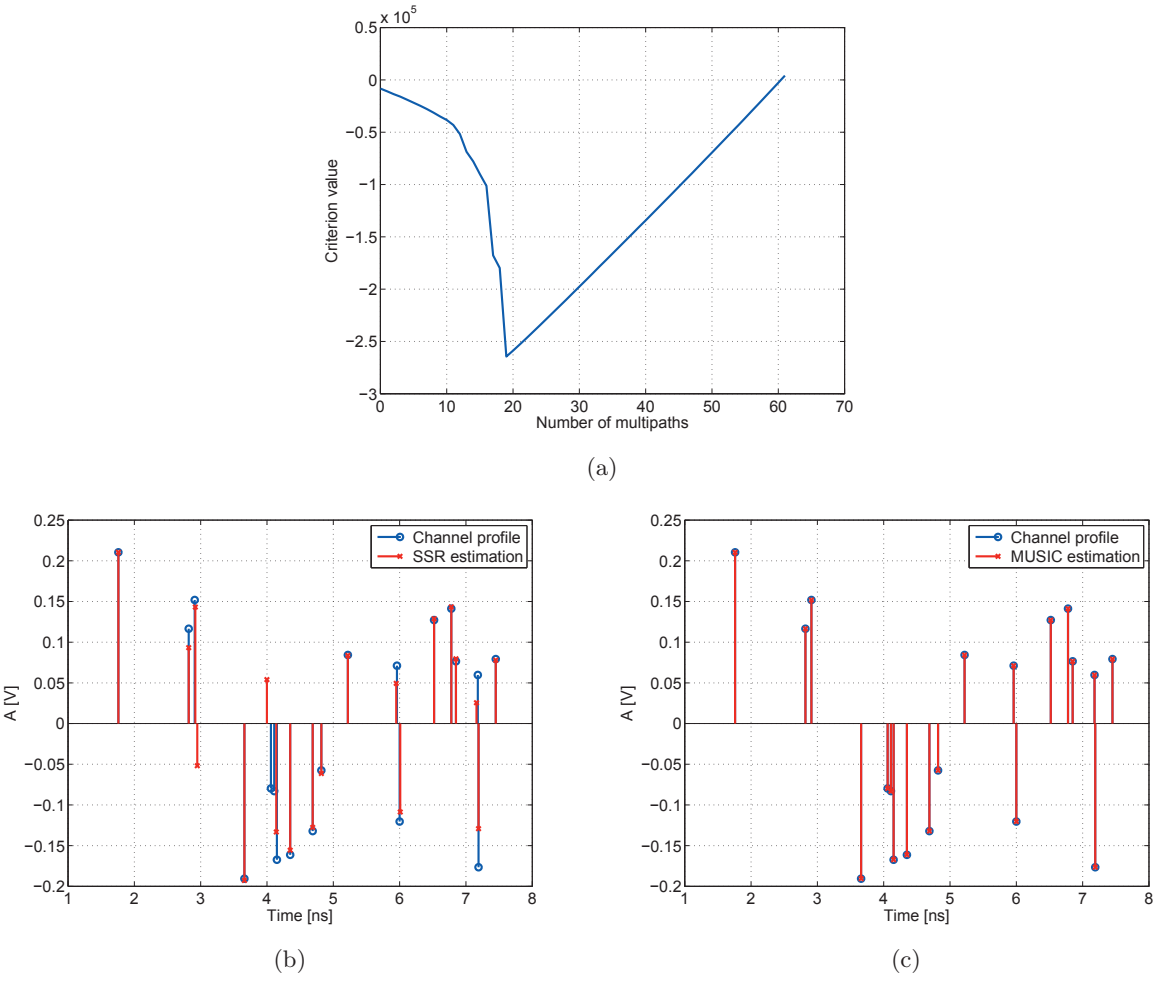

(a)

(b) (c)

Figure 4.6: Illustration of channel estimation methods: (a) estimation of the number of peaks with AIC, and channel profile estimations given by (b) SSR (c) MUSIC

denoted as S_n and given by:

$$S_n(\boldsymbol{\tau}, \boldsymbol{\alpha}) = \frac{\|\mathbf{y} - \hat{\mathbf{y}}_{\boldsymbol{\tau},\boldsymbol{\alpha}}\|^2}{\|\mathbf{y}\|^2} \tag{4.13}$$

Parameters	S_n		S_{ac}	
	SNR = 5 dB	SNR = 15 dB	SNR = 5 dB	SNR = 15 dB
MUSIC	0.278	0.22	0.816	0.825
SSR	0.153	0.153	0.738	0.738
OS-SSR	0.145	0.134	0.82	0.872

Table 4.1: Performance comparison of different channel estimation algorithms

The parameter S_n provides good information about matching between received signal and signal reconstructed using estimated channel parameters. However, a low S_n value does not necessarily mean good channel estimation. For instance, the S_n value for the SSR based channel estimation corresponding to the example above is 0.1239, while the time-delays of 7 paths over 19 are not correctly estimated. Due to this reason, performance is also assessed in terms of the correlation coefficient between the ideal channel profile and the estimated one, denoted by S_{ac} and defined as:

$$S_{ac}(\boldsymbol{\tau}, \boldsymbol{\alpha}) = \frac{\langle \mathbf{h}, \hat{\mathbf{h}}_{\boldsymbol{\tau},\boldsymbol{\alpha}} \rangle}{\|\mathbf{h}\|.\|\hat{\mathbf{h}}_{\boldsymbol{\tau},\boldsymbol{\alpha}}\|} \tag{4.14}$$

where $\hat{\mathbf{h}}_{\boldsymbol{\tau},\boldsymbol{\alpha}}$ is the estimated discrete time CIR and $\langle . \rangle$ stands for the scalar product.

S_{ac} value for the example considered here is 0.7462, which reflects better in this case the quality of the channel estimation. Thus, for a general case, it is more reasonable to think that a good estimation is one which is good both in terms of S_n and S_{ac}.

Despite of their high performance in the noiseless case, as it has been already stated in Section 4.4.2 the superresolution methods are subject to severe performance degradation in the case of noisy signals. The main interest of the proposed approach is then to take advantage of the robustness to noise of the SSR method and to increase its performance, especially in terms of time resolution, by using it in combination with MUSIC algorithm.

In order to illustrate the gain achieved with OS-SSR method in the case of the example above, channel estimation results are shown on the Fig. 4.7, for two SNR values, 15 dB and 5 dB respectively. The corresponding S_n and S_{ac} parameters are also provided in the Table. 4.1.

From Table. 4.1, note that the performance of SSR method remains roughly the same in the two cases, despite of the relatively large range of variation for the considered SNR. It is satisfying in terms of S_n, but poor in terms of S_{ac} because of the limited time resolution. The behaviour of the MUSIC algorithm is quite different, since it exhibits poor performance in terms of both of S_n and S_{ac} in the first case, but performs significantly better in the second case. The proposed method can be considered a good trade-off between these two techniques, because it is nearly as robust as the SSR algorithm, but compared to it, its performance is increased, especially in terms of S_{ac}.

Figure 4.8 represents the performance variation of different algorithms against SNR in terms of S_n and S_{ac} in the CM1 and CM2 channel models of IEEE 802.15.3a standard. At each iteration, the channel is randomly generated and then truncated beyond the 20^{th} path. The results are obtained by averaging over 1000 randomly generated realizations of CM1 or CM2. The results again prove our previous conclusion that the proposed algorithm provides the best trade-off in terms of S_n and S_{ac}.

Finally, Cramer-Rao lower bound (CRLB) is introduced to assess the performance for an academic context with 4 MPCs. The delays of MPCs are defined as $\boldsymbol{\tau} = [1\text{ns}, 1.45\text{ns}, 1.5\text{ns}, 2\text{ns}]$ while

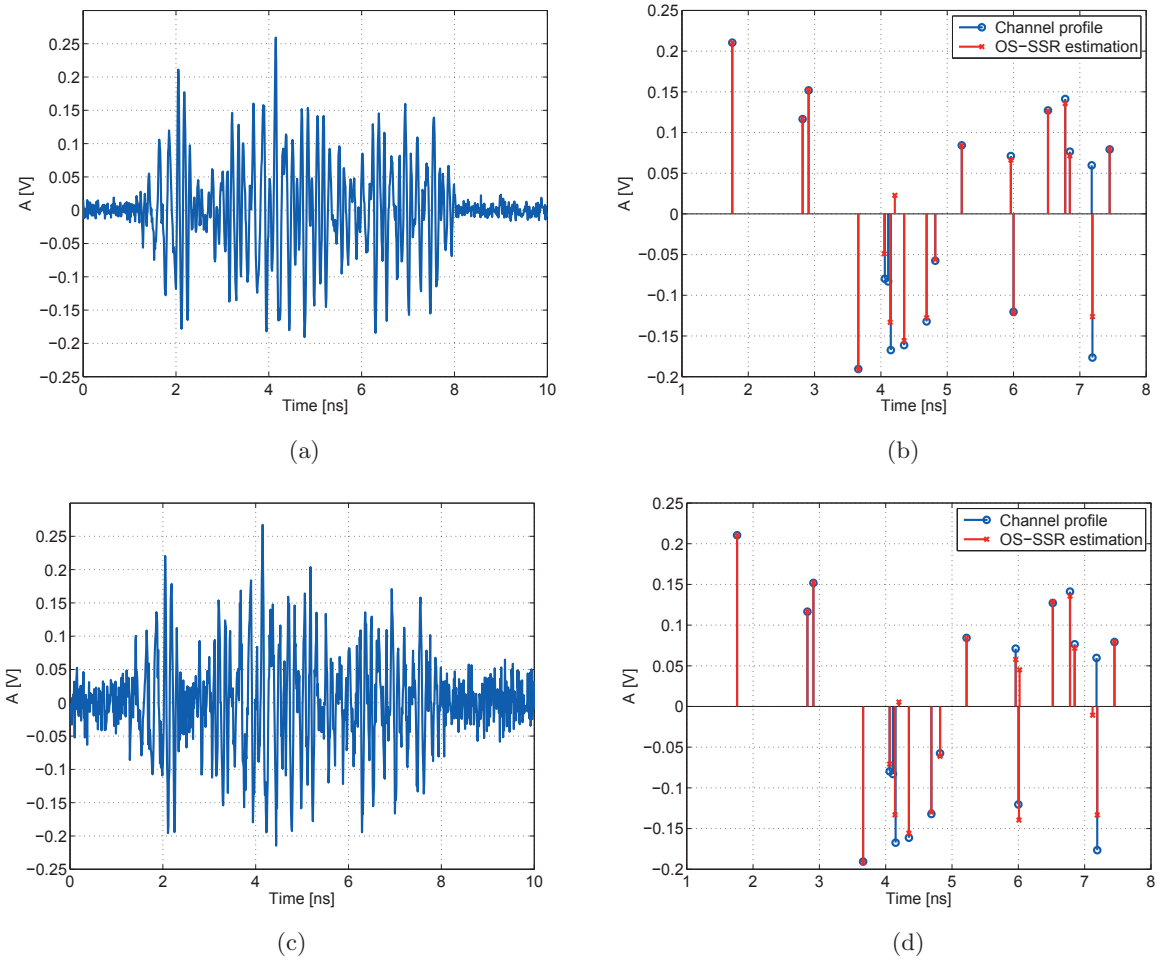

Figure 4.7: Channel estimation using the proposed approach: received signal for a SNR = 15 dB (a) and SNR = 5 dB (c), and the corresponding estimated channel profile provided by OS-SSR [(b) and (d)]

all MPCs have equal amplitudes. As explained before that the delay estimation is a special case of harmonic retrieval problem, CRLB for noisy exponentials is taken as a reference given by [Kay88b]:

$$\mathrm{var}(\tau_i) \geq \frac{\sigma_n^2 \left[\mathbf{M}^{-1}\right]_{ii}}{8\pi^2 \alpha_i^2} \tag{4.15}$$

where $\left[\mathbf{M}^{-1}\right]_{ii}$ is the [i,i] element of the inverse of the $2L \times 2L$ Fisher information matrix $\mathbf{M}$, with $i = 1, 3, \cdots, 2L-1$. Figure 4.9 represents comparison of studied methods with CRLB for 3rd MPC i.e. MPC with delay 1.5ns, as it is most severely affected by other MPCs. Clearly, SSR is suboptimal as it can not differentiate two peaks as close as 0.05ns. Our proposition exhibit similar performance to MUSIC at higher SNR while outclassing the latter for low SNR regime.

However, it has been observed that OS based methods are also sensitive to the number of multipaths to be estimated. This fact is already visible from Fig. 4.8 where 20 MPCs are estimated at each trial and in that case the performance of OS does not remain as optimal as suggested in 4.9 for 4 MPCs, where our algorithm still remains acceptable in both cases.

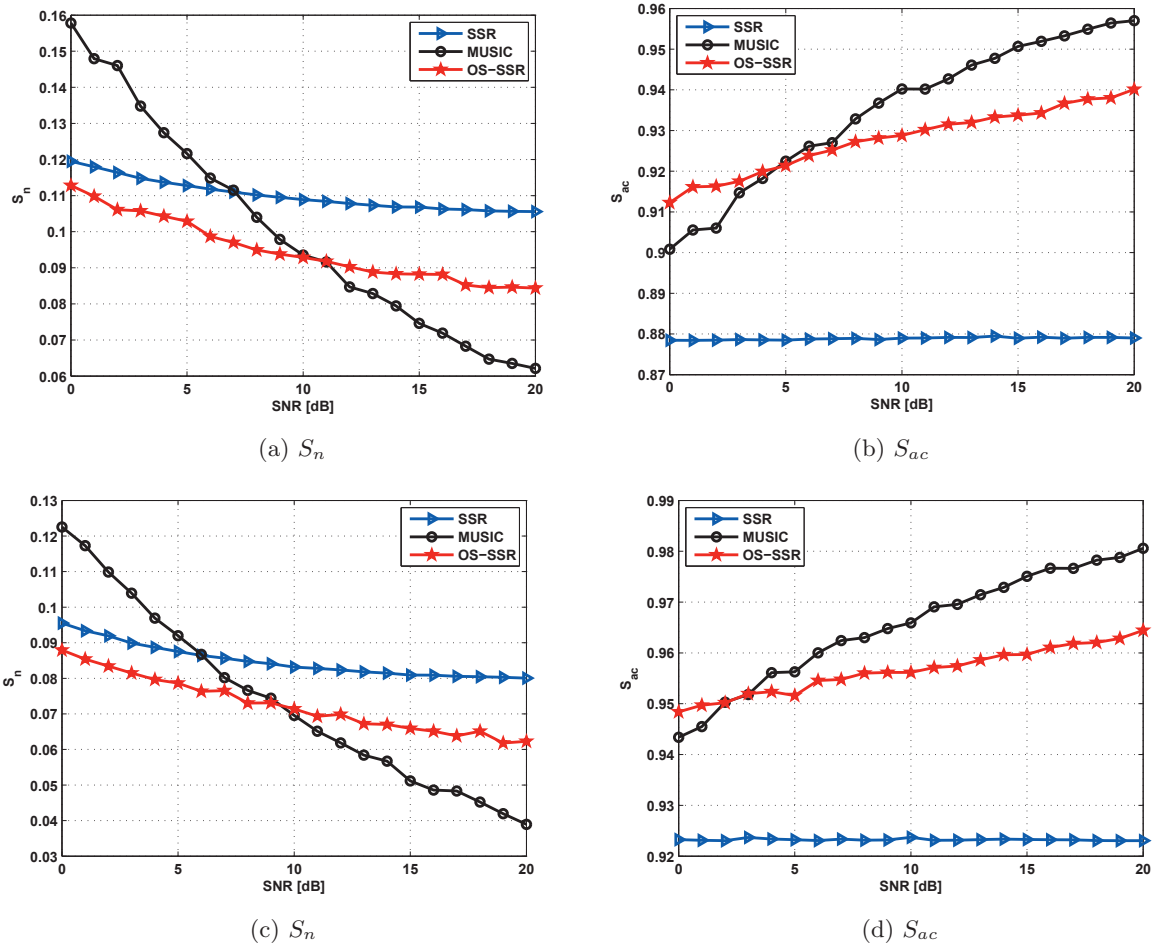

(a) S_n (b) S_{ac}

(c) S_n (d) S_{ac}

Figure 4.8: Performance of channel estimation algorithms against SNR in terms of S_n and S_{ac} in channel models [(a) & (b)] CM1 [(c) & (d)] CM2

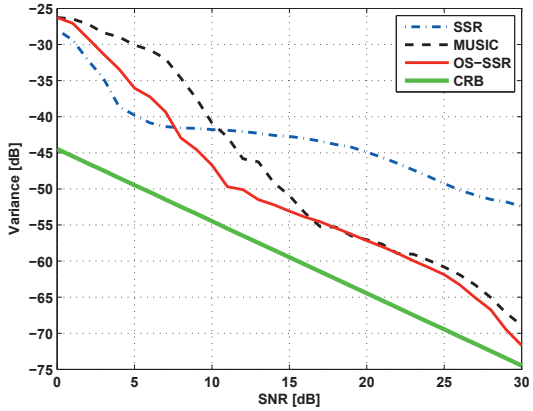

Figure 4.9: CRLB and variance of different methods against SNR

4.6 Conclusions

Channel estimation is a key point for any communication system and even more for a IR-UWB because of the dense multipath associated environment. ML estimators, which are implemented through MF, have been generally used so far, since they show robustness to noise. However, they

have limited resolution and are not able to resolve very close multipaths. This may become a critical point if the amplitudes of the unresolved multipath is higher enough to be taken into account by the S-Rake receiver for example. Time domain superresolution methods could be an interesting solution from this point of view, but they are too sensitive to noise. The method proposed n this chapter combines the advantages of the two approaches and removes their drawbacks to some extent. An ML estimator is used in the first stage, thus taking advantage of its robustness to noise. The provided solution is then validated using noise subspace projection operator and only the peaks satisfying the orthogonality constraint are conserved. A superresolution method is finally used to resolve the remaining peaks given the partial solution obtained previously. The proposed algorithm is compared to several reference methods and its performance is assessed in the framework of a realistic UWB channel model. It is shown that the new method can cope with noisy UWB channels and provides best performance in both low and high SNR scenarios.

Conclusions and Future Work

In this research work, we focused on time-hopping based IR-UWB systems coupled with cognitive radio. UWB has seen a renewed interest in recent years while cognitive radio has emerged as the most promising solution to the spectrum scarcity problem. Although the UWB and cognitive radio appear as two contrasting ideas, UWB does have many features which qualify it directly as a potential candidate for cognitive radio. Furthermore, the UWB and CR can supplement each other to counter some of their limitations. Specifically, integrating the spectrum sensing requirement of CR into UWB will help it to mitigate the strong primary systems' interference, thereby improving its performance. On the contrary, if CR is implemented with UWB, the underlay mode of UWB will help the cognitive users to transmit continuously, thus increasing its throughput. This provoked us to look into the major issues in realizing the cognitive UWB radios.

Thesis Contributions

As a result of huge spectral occupancy, UWB technology can provide unique and attractive features. For instance, this accounts for ultra-high-speed data rates, ultra-fine time resolution for precise positioning and ranging, multipath immunity and low probability of interception due to the low power spectral density. Nevertheless, formidable challenges must be faced in order to fulfill the expectations of UWB technology. In this thesis, we addressed the issues of efficient spectrum sensing to avoid NBI, adaptive UWB waveform design, synchronization and channel estimation. Directed at these challenging aspects, our research work has resulted in several original contributions, which can be summarized as follows:

- First, a cognitive radio based two-way approach is proposed to avoid NBI. The presence of primary system/user in a specific band is tested and then if the band is already occupied, a UWB waveform design approach is used to vacate that specific band while still using the rest of the available band to its full. Thus, it is evident that we need an efficient spectrum sensing algorithm for the first stage and an adaptive UWB waveform design algorithm in the second stage to avoid the NBI. Random matrix theory (RMT) based methods are particularly interesting due to their blindness features as they do not need any knowledge about the primary user signal or the noise power. However, most of the methods in literature are based on asymptotic models of eigenvalue distribution and thus are not applicable for finite number of samples. As sensing time is really critical, methods using finite number of samples must be employed for practical spectrum sensing purposes. This motivated us to develop spectrum sensing algorithms using fewer number of samples. In particular, we invoked some latest results on the distribution of standard condition number (SCN) from the finite random matrix theory (FRMT). Two types of hypotheses are considered; either the primary user signal is an unknown arbitrary complex constant or i.i.d Gaussian variate. Multiple spectrum sensing algorithms are then presented for these hypotheses. An algorithm based on the SCN distribution is presented for constant PU case. However, SCN based method does not work for the random i.i.d. user case for which spectrum sensing algorithm based on eigenvalues' sum distribution is then provided. Further, a two-stage method is then developed where first stage comprises of the SCN based test while the second stage consists of the eigenvalues based

test. The results prove interesting performance in terms of probability of false alarm P_{fa} and probability of miss-detection P_{md} for as few as 20 samples.

- Once detected the presence/absence of primary user, the next step is to consequently adapt the UWB pulse spectrum. The UWB waveform should be capable to fulfill the power mask constraints by the regulatory authorities, efficiently utilize the spectral resources and adaptable to occupy/leave certain portion of the spectrum to avoid NBI. To this part, a B-spline based approach is exploited to satisfy these demands. The basic idea is that the UWB signal can be generated by a linear combination of B-splines with appropriate weight coefficients. The objective is thus condensed to optimize these coefficients. In order to solve this non-linear optimization problem subject to both linear and non-linear constraints, we use genetic algorithm (GA), which are well-known iterative methods to solve such problems. Numerical results confirm the efficient spectrum usage and adaptability of generated pulses.
- Afterwards, we turn our attention to the issues that impact the performance of a coherent Rake receiver in IR-UWB. The extremely wide bandwidth and low duty cycle signaling of IR-UWB demand stringent synchronization requirements at the receiver for successful demodulation and poses a major problem in the deployment of IR-UWB systems. We have considered the BPSK and PSM modulated IR-UWB systems and propose several synchronization algorithms in chapter 3. The central idea of all these new methods is to take advantage of some useful properties of UWB pulses achieved via waveform optimization (orthogonality, correlation properties), in order to design non-data-aided, low-complexity and effective synchronization algorithms. A rapid method using UWB pulses' orthogonality for BPSK, a code matching based solution for PSM and an energy detection based approach for M-ary PSM are proposed. The results confirm efficient performance in terms of mean square error.
- Finally, we focus on channel estimation which is another performance-limiting factor for the design of Rake receivers. A joint maximum-likelihood (ML) and orthogonal subspace (OS) based approach is proposed in chapter 4. The ML estimation used is a variant to well-known SIC algorithm which calculates the correlation between received signal and reference signal via a matched filter (MF) and finds the largest peak in each iteration and subtract it for the subsequent iteration. OS based methods such as MUSIC and ESPRIT, also known as super-resolution techniques, are based on the eigenanalysis of the received signal autocorrelation matrix. The method proposed combines the advantages of the two approaches and removes their drawbacks. An ML estimator is used in the first stage, thus taking advantage of its robustness to noise. The provided solution is then validated using noise subspace projection operator and only the peaks satisfying the orthogonality constraint are conserved. A super-resolution method is finally used to resolve the remaining peaks given the partial solution obtained previously.

Perspectives

Some of the topics that have not been addressed in this dissertation but may be subject to further investigation are the following:

- The first contribution in the context of this work is related to spectrum sensing. The recent results of random matrix theory are invoked to develop efficient spectrum sensing algorithms with limited number of samples. Standard condition number (SCN) is used as a test statistic

to detect the constant envelope PU signal. The SCN based approach is particularly attractive as it does not need any knowledge about the signal or noise power (blindness). The SCN statistics, however, can not detect the PU under i.i.d signal hypothesis, thus inciting to look for alternatives. Two methods, one based on any eigenvalues distribution and the other based on the eigenvalues sum distribution (EVS) are then provided to circumvent this problem. However, these algorithms need the estimation of noise power, making them only semi-blind. This needs further study in this domain to look for the blind alternatives while keeping the finite number of symbols constraint intact.

- One of the most important challenges is to cope with the overwhelming distortion introduced by the intricate propagation physics of UWB signals. An optimal UWB receiver must take into account certain frequency-dependent effects on the received waveform. That is, due to the broadband nature of UWB signals, the components propagating along different paths typically undergo different frequency-selective distortions. This fact has been intentionally ignored in the development of some algorithms in this thesis. For example, the rapid synchronization methods OS in chapter 3 exploits the orthogonality between the transmitted and received signal, which may no more exist under such channel distortions. Also, the similar assumption is essential for the proposed joint ML/OS channel estimation algorithm. In this regard, a study on the UWB pulse impairments using UWB platform recently acquired by the laboratory will be beneficial for further improvements in the proposed methods.
- The UWB channel estimation method is based on transmitting an isolated pulse and applying the algorithm on the received waveform. It will be interesting to extend it using TH-IR-UWB signals for information-bearing symbols in the DA or NDA context.
- In the context of this thesis, we have throughout limited ourselves to the single-user scenario. While simulation results for few users have been provided in case of synchronization algorithms, a more detailed study on the impact of MUI will be interesting.
- An experimental validation of the theoretical results presented in this thesis is also planned for the near future using the UWB experimental platform. Although some measured data acquired with this platform is already available, it could not be used in the framework of this thesis because the conditions required for accurately matching the IEEE 802.15.3a environment have not yet been met. An already scheduled upgrade of our experimental UWB platform will lead to increased performance, especially in terms of bandwidth, and will enable an appropriate and meaningful comparison of the theoretical results presented in this thesis to those that will be obtained from measured data.

Appendix A

Complexity analysis of some synchronization algorithms

We compare the complexity of proposed rapid method (OSS) with some sequential search based methods in the literature. We assume IFI/ISI free scenarios and compute the complexity in terms of T_f long integrals while focusing on frame-level synchronization.

Timing with dirty templates [Yan05]:

Rewriting the equation (see (13) in [Yan05]) summarizing the algorithm, as follows

$$n_\tau = \arg \max_{n\in[0,N_f-1]} \left[\frac{1}{K}\sum_{k=1}^{K}\int_{2kT_s}^{(2k+1)T_s} r(t+nT_f)r(t+nT_f-T_s)dt\right]^2$$

$$= \arg \max_{n\in[0,N_f-1]} \left[\frac{1}{K}\sum_{k=1}^{K}\underbrace{\int_{2kT_s+nT_f}^{(2k+1)T_s+nT_f} r(t)r(t-T_s)dt}_{I_n}\right]^2$$

For $n=0$;

$$I_0 = \int_{2kT_s}^{(2k+1)T_s} r(t)r(t-T_s)dt = \sum_{m=0}^{m=N_f-1} \underbrace{\int_{(2k+m)T_f}^{(2k+m+1)T_f} r(t)r(t-T_s)dt}_{J_m}$$

$$I_0 = J_0 + J_1 + \ldots + J_{N_f-1}$$

As the same integral I_0 has to be calculated over K consecutive symbols, the overall complexity for $n=0$ is KN_f integrals of duration T_f.
For $n=1$;

$$I_1 = \int_{2kT_s+T_f}^{(2k+1)T_s+T_f} r(t)r(t-T_s)dt = \sum_{m=1}^{m=N_f} \underbrace{\int_{(2k+m)T_f}^{(2k+m+1)T_f} r(t)r(t-T_s)dt}_{J_m}$$

$$I_1 = J_1 + J_2 + \ldots + J_{N_f}$$

However, in this step only one new integral J_{N_f} is calculated because the integrals $J_1 \ldots J_{N_f-1}$ have already been calculated in the previous step. So, K new integrals are calculated for $n=1$.

Similarly for $n = 2$;

$$I_2 = \int_{2kT_s+2T_f}^{(2k+1)T_s+2T_f} r(t)r(t-T_s)dt = \sum_{m=2}^{m=N_f+1} \underbrace{\int_{(2k+m)T_f}^{(2k+m+1)T_f} r(t)r(t-T_s)dt}_{J_m}$$

$$I_2 = J_2 + J_3 + \ldots + J_{N_f+1}$$

Again, only one new integral N_f+1 is computed this time. Therefore, KN_f integrals are computed for $n = 0$ and then for all the other values of $n = 1, ..., N_f - 1$, K additional integral operation are calculated. Thereby in total, the maximization of n_τ needs $\mathbf{K(2N_f - 1)}$ integrals of T_f duration.

Low complexity blind synchronization [Luo06b]:

Rewriting the equation (see (9) in [Luo06b]) summarizing the algorithm, as follows

$$\begin{aligned} n_\tau &= \arg \max_{n\in[0,2N_f-1]} \int_0^{T_s} \left|\bar{r}((t+nT_f) \bmod 2T_s)\right|^2 dt \\ &= \arg \max_{n\in[0,2N_f-1]} \underbrace{\int_{nT_f}^{T_s+nT_f} \left|\bar{r}((t) \bmod 2T_s)\right|^2 dt}_{I_n} \end{aligned}$$

For $n = 0$;

$$I_0 = \int_0^{T_s} |\bar{r}(t)|^2 dt = \sum_{m=0}^{m=N_f-1} \underbrace{\int_{mT_f}^{(m+1)T_f} |\bar{r}(t)|^2 dt}_{J_m}$$

$$I_0 = J_0 + J_1 + \ldots + J_{N_f-1}$$

Thus we calculate N_f integrals for $n = 0$.
For $n = 1$;

$$I_1 = \int_{T_f}^{T_s+T_f} |\bar{r}(t)|^2 dt = \sum_{m=1}^{m=N_f} \int_{mT_f}^{(m+1)T_f} |\bar{r}(t)|^2 dt$$

$$I_1 = J_1 + J_2 + \ldots + J_{N_f}$$

However, in this step only one new integral J_{N_f} is calculated because the integrals $J_1 \ldots J_{N_f-1}$ have already been calculated in the previous step.
Similarly for $n = 2$;

$$I_2 = \int_{2T_f}^{T_s+2T_f} |\bar{r}(t)|^2 dt = \sum_{m=2}^{m=N_f+1} \int_{mT_f}^{(m+1)T_f} |\bar{r}(t)|^2 dt$$

$$I_2 = J_2 + J_3 + \ldots + J_{N_f+1}$$

Again, only one new integral $N_f + 1$ is computed this time. Therefore, N_f integrals are computed for $n = 0$ and then for all the other values of $n = 1, ..., 2N_f - 1$, one additional integral operation is calculated. Thereby in total, the maximization of n_τ needs $\mathbf{3N_f - 1}$ integrals of T_f duration.

Code assisted blind synchronization [Yin08]:

Rewriting the equation (see (3) in [Yin08]) summarizing the algorithm, as follows

$$n_\tau = \arg \max_{n\in[0,N_f-1]} \frac{1}{K}\sum_{k=1}^{K}\int_0^{T_f}\left|\sum_{j=0}^{N_f-1} d_j g_r(t) r(t+kT_s+jT_f+c_jT_c+nT_f)\right|^2 dt$$

It is evident by taking a closer look at the above equation that the complexity of this algorithm is at the order of $\mathbf{KN_f}$ integrals of duration T_f.

Proposed:

As the proposed algorithm does not need to search over multiple time shifts, the complexity is proportional to the calculation of 4 cross-correlations X_2, X_3, X_4 and X_5 whereas $X_1 = X_4 + X_5$ will be readily found afterwards. The energies X_2 and X_3 each need $N_f/3$ while X_4 and X_5 each require $N_f/6$ integrals of T_f duration. Thus, the total complexity is equivalent to computing $\mathbf{N_f}$ integrals of T_f duration.

This proves significant improvement in the detection speed by the proposed algorithm.

Appendix B

Short overview on 1D superresolution MUSIC method

In this appendix, we shall present a brief overview of well-known superresolution method MUSIC (MUltiple Signal Classification), which is an extrema-searching algorithm.

Matrix signal model

MUSIC performs very well when the analyzed signal can be expressed as a sum of weighted complex exponentials:

$$s(n) = \sum_{k=1}^{N} \gamma_k \exp(j\Phi_k) + u(n) \tag{B.1}$$

where $u(n)$ are noise samples.

In our problem, the IR-UWB channel is multipath, each of these multiple paths being characterized by its amplitude and time delay. The phase Φ_k will then carry the information concerning the time delays τ_k corresponding to the different paths.

Now assume a channel with N multiple paths and an equivalent signal model to that provided by equation (7), where discrete frequency samples $\nu_n = \nu_0 + n.\Delta\nu$, $n = 0, 1, \cdots, N_s - 1$ are considered instead of ν:

$$s(n) = \sum_{k=1}^{N} \gamma_k \exp(j2\pi f_n \tau_k) + u(n) \tag{B.2}$$

Thus, we can form the vector of complex samples given below:

$$\mathbf{s} = [s(0)\ s(1)\ \cdots\ s(N_s - 1)]^T \tag{B.3}$$

with:

$$\begin{aligned} s(n) &= \sum_{k=1}^{N} \gamma_k \exp\left[j2\pi(\nu_0 + n\Delta\nu)\tau_k\right] + u(n) \\ &= \sum_{k=1}^{N} \left[\gamma_k \exp(j2\pi\nu_0\tau_k)\right] \exp(j2\pi\Delta\nu n\tau_k) + u(n) \\ &= \sum_{k=1}^{N} \tilde{\gamma}_k \exp(j2\pi\Delta\nu n\tau_k) + u(n) \end{aligned} \tag{B.4}$$

and $\tilde{\gamma}_k = \gamma_k \exp(j2\pi\nu_0\tau_k)$.

In the following we will still use γ_k instead of $\tilde{\gamma}_k$ for simplicity. Eq. (B.4) written for all samples $s(n)$ results in:

$$\mathbf{s} = \sum_{k=1}^{N} \gamma_k \mathbf{a}_k + \mathbf{u} = \mathbf{A}\boldsymbol{\gamma} + \mathbf{u} \tag{B.5}$$

where

$$\mathbf{a}_k = [1 \exp(j2\pi\Delta\nu\tau_k) \cdots \exp(j2\pi\Delta\nu p\tau_k) \cdots \exp(j2\pi\Delta\nu(N_s-1)\tau_k)]^T$$

$$\mathbf{u} = [u(0)\ u(1) \cdots u(p) \cdots u(N_s-1)]^T$$

are the signal and noise vector respectively, and:

$$\mathbf{A} = [\mathbf{a}_1\ \mathbf{a}_2 \cdots \mathbf{a}_N], \qquad \boldsymbol{\gamma} = [\gamma_1\ \gamma_2 \cdots \gamma_N]^T$$

Autocorrelation matrix eigenanalysis

A preliminary step for the application of the superresolution methods is the autocorrelation matrix eigenanalysis. This matrix is defined as :

$$\mathbf{R}_s = \mathrm{E}\left[\mathbf{s}\mathbf{s}^H\right] \tag{B.6}$$

where $\mathrm{E}[.]$ stands for the operator of statistical average.

Since it is generally unknown, it can be estimated by averaging a set of N_{obs} observations:

$$\hat{\mathbf{R}}_s = \frac{1}{N_{obs}} . \sum_{i=1}^{N_{obs}} \mathbf{s}_i \mathbf{s}_i^H \tag{B.7}$$

The R_s matrix must be of full rank in order to resolve the multipaths. This averaging process would lead to an autocorrelation matrix of full rank only if the contributions of different paths were decorrelated. However, the multipath signals are coherent, so that increasing the number of observations does not have any effect on the autocorrelation matrix rank.

In order to decorrelate the multipath signals the p order autocorelation matrix can be estimated by the spatial smoothing technique [Mar87]:

$$\hat{\mathbf{R}}_s = (N-p+1)^{-1} \mathbf{D}_s \mathbf{D}_s^H \tag{B.8}$$

or:

$$\hat{\mathbf{R}}_s = (N-p+1)^{-1} \left[\mathbf{D}_s \mathbf{D}_s^H + \mathbf{J}_p \mathbf{D}_s \mathbf{D}_s^H \mathbf{J}_p\right] \tag{B.9}$$

where:

$$\mathbf{D}_s = \begin{bmatrix} \mathbf{s}(0) & \mathbf{s}(1) & \cdots & \mathbf{s}(N_s-p) \\ \mathbf{s}(1) & \mathbf{s}(2) & \cdots & \mathbf{s}(N_s-p+1) \\ \vdots & \vdots & \ddots & \vdots \\ \mathbf{s}(p-1) & \mathbf{s}(p) & \cdots & \mathbf{s}(N_s-1) \end{bmatrix}$$

is known as the p order data matrix.

This matrix is obtained by shifting an $N_s - p + 1$ length window along the data snapshot. The

columns of the $\mathbf{D}_s$ matrix belong to the observation space, which is p dimensional. Since no precise rule exists for the choice of p, an empirically recommended interval is between $N_s/2$ and $2N_s/3$.

The main idea behind all the subspace eigenanalysis based methods consists in splitting the observation space, spanned by the eigenvectors of the autocorrelation matrix, into two orthogonal subspaces, usually named the signal subspace and the noise subspace.

Using (B.5) the p order autocorrelation matrix can be also expressed as:

$$\hat{\mathbf{R}}_s = \sum_{k=1}^{K} |\gamma_k|^2 . \mathbf{a}_k . \mathbf{a}_k^H + \sigma^2 . \mathbf{I}_p = \mathbf{S}_p + \mathbf{W}_p \tag{B.10}$$

where $\mathbf{I}_p$ is the p order unit matrix and a white, zero mean and σ^2 variance noise is assumed in the equation above.

Let μ_i and $\boldsymbol{\nu}_i$ be the $\mathbf{S}_p$ matrix eigenvalues and eigenvectors respectively. There will be only N non-zero eigenvalues because of the rank of the $\mathbf{S}_p$ matrix. Hence, the following relationship holds:

$$\mathbf{S}_p = \sum_{i=1}^{p+1} \mu_i \boldsymbol{\nu}_i \boldsymbol{\nu}_i^H = \sum_{i=1}^{N} \mu_i \boldsymbol{\nu}_i \boldsymbol{\nu}_i^H \tag{B.11}$$

The unit matrix can be put in the same form, because all its eigenvalues are equal to 1 and any vector may be considered as its eigenvector:

$$\mathbf{I}_p = \sum_{i=1}^{p+1} \boldsymbol{\nu}_i \boldsymbol{\nu}_i^H \tag{B.12}$$

The following equation is then obtained:

$$\begin{aligned} \hat{\mathbf{R}}_s &= \sum_{i=1}^{N} \mu_i \boldsymbol{\nu}_i \boldsymbol{\nu}_i^H + \sigma^2 \sum_{i=1}^{p+1} \boldsymbol{\nu}_i \boldsymbol{\nu}_i^H \\ &= \sum_{i=1}^{N} \left(\mu_i + \sigma^2\right) \boldsymbol{\nu}_i \boldsymbol{\nu}_i^H + \sum_{i=N+1}^{p+1} \sigma^2 \boldsymbol{\nu}_i \boldsymbol{\nu}_i^H \end{aligned} \tag{B.13}$$

Consequently, the autocorrelation matrix eigenvectors corresponding to the largest N eigenvalues, known as the principal eigenvectors, span the same subspace as the signal vectors, while the other eigenvectors span the noise subspace. The superresolution method MUSIC takes advantage of the orthogonality of the two subspaces to find out very accurately the time delays corresponding to the channel multipaths.

MUSIC 1D algorithm

Let us define the data vector:

$$\mathbf{a}_i = \left[1 \ \exp(j2\pi\Delta\nu\tau_i) \ \cdots \ \exp(j2\pi\Delta\nu(p-1)\tau_i)\right]^T \tag{B.14}$$

When τ_i is varied this vector sweeps the whole observation space. It penetrates the signal subspace for $\tau_i = \tau_k$. It becomes then orthogonal to any linear combination of the eigenvectors which span the noise subspace. This means that the channel profile estimation:

$$CP_{MUSIC}(\tau_i) = \frac{1}{\mathbf{a}_i^H \left[\sum_{i=N+1}^{p} \boldsymbol{\nu}_i \boldsymbol{\nu}_i^H\right] \mathbf{a}_i} = \frac{1}{\mathbf{a}_i^H \Pi_n^{\perp} \mathbf{a}_i} \tag{B.15}$$

will theoretically have infinite value whenever it is evaluated at a time delay corresponding to a multipath. In the equation above $\Pi_n^{\perp} = \mathbf{V}_n \mathbf{V}_n^H$ stands for the projection operator on the noise subspace, where $\mathbf{V}_n$ is the column matrix of the noise subspace eigenvectors.

In practice, the function will be finite because of the estimation errors, but it will exhibit very sharp peaks.

Signal subspace dimension estimation

The most known technique to estimate the signal subspace dimension is the Akaike Information Criterion (AIC). The number of signal vectors is determined to realize the best concordance between the model and the observation data. Analytically, this condition is expressed in the form:

$$\hat{N} = \min_n \left[C(n)\right] \tag{B.16}$$

where $C(n)$ is a cost function related to the log likelihood ratio of the model parameters for $N = n$. However, the Akaike criterion yields an inconsistent estimate that tends, asymptotically, to overestimate the number of multipaths. To overcome this problem Rissanen has proposed the Minimum Description Length criterion (MDL). Although the estimate is consistent now, the signal subspace dimension will be underestimated, especially when the number of samples is small.

In our experiments we have used both the AIC and the MDL criteria adapted by Wax and Kailath [Wax85]. The cost functions in the two cases have the following expressions:

$$AIC(n) = 2\log \left[\frac{\frac{1}{p-n} \sum_{i=n+1}^{p} \lambda_i}{\prod_{i=n+1}^{p} \lambda_i^{1/(p-k)}} \right]^{(p-k)/N} + 2n(2p-n) \tag{B.17}$$

$$MDL(n) = \log \left[\frac{\frac{1}{p-n} \sum_{i=n+1}^{p} \lambda_i}{\prod_{i=n+1}^{p} \lambda_i^{1/(p-k)}} \right]^{(p-k)/N} + \frac{1}{2} n(2p-n)\log N \tag{B.18}$$

Publications

- R. Akbar, E. Radoi, S. Azou, "Performance Evaluation of Impulse Based UWB System in AWGN and Indoor Multipath Channel", MTA Review, ISSN 1843-3391, Vol. XIX, No. 4, pp. 419-438, Bucharest, Romania, 2009.

- R. Akbar, E. Radoi, S. Azou, "Conception d'une forme d'onde IR-UWB optimisée et analyse de ses performances dans le canal IEEE 802.15.3a", Proc. of MajecSTIC 2010 Conference, pp. 1-8, Bordeaux, France, October 13-15, 2010.

- R. Akbar, E. Radoi, S. Azou, "Maximum Likelihood and Orthogonal Subspace based Approach for Improved IR-UWB Channel Estimation", Proc. of 18th European Signal Processing Conference (EUSIPCO 2010), pp. 1145-1149, Aalborg, Denmark, August 23-27, 2010, ISSN 2076-1465.

- R. Akbar, E. Radoi, S. Azou, "Energy Detection based Blind Synchronization for Pulse Shape Modulated IR-UWB Systems", Proc. of IEEE 22nd International Symposium on Personal Indoor and Mobile Radio Communications (PIMRC 2011), pp. 864-868, Toronto, Canada, September 11-14, 2011, doi: 10.1109/PIMRC.2011.6140090.

- R. Akbar, E. Radoi, "An overview of synchronization algorithms for IR-UWB systems", invited paper in Proc. of International Conference on Computing, Networking and Communications (ICNC 2012), pp. 573-577, Jan. 30 – Feb. 2, 2012, Maui, Hawaï, doi: 10.1109/ICCNC.2012.6167487.

- R. Akbar, E. Radoi, S. Azou, "Comparative Analysis of some Low-Complexity Blind Synchronization Algorithms for IR-UWB Systems", Journal of Communications (JCM, ISSN 1796-2021), Vol. 7, No. 5, pp. 374-381, May 2012, doi: 10.4304/jcm.7.5.374-381.

- R. Akbar, E. Radoi, S. Azou, "A Non-Data-Aided Rapid Synchronization Method for UWB Impulse Radio", IEEE Communications Letters, Vol. 16 , No. 8, pp. 1308 – 1311, 2012, doi: 10.1109/LCOMM.2012.060112.120763.

- R. Akbar, E. Radoi, S. Azou, "Low-complexity synchronization algorithms for orthogonally modulated IR-UWB systems", submitted to Eurasip journal on Wireless Communications and Networking, 2012.

- R. Akbar, E. Radoi, S. Azou, "A spectrum sensing approach using low number of samples for IR-UWB cognitive radio", to be submitted to IEEE Transactions on Communications in 2013.

Bibliography

[ADL] "Analog & Digital Delay Lines". http://www.allenavionics.com/ADDL/ADDL.htm.

[Aed04] S. Aedudodla, S. Vijayakumaran, T. F. Wong. "Rapid ultra-wideband signal acquisition". Proc. IEEE Wireless Commun. and Networking Conf., pp. vol.2, 1148–1153, Mar. 2004.

[Aka04] H. Akahori, Y. Shimazaki, A. Kasamatsu. "Examination of the automatic integration time length selection system using PPM in UWB". Proc. Intl. Workshop on Ultra Wideband Systems, joint with Conf. on Ultrawideband Systems and Technologies. (Joint UWBST & IWUWBS), pp. 268–272, 2004.

[Akb09] R. Akbar, E. Radoi, S. Azou. "Performance evaluation of impulse based UWB system in AWGN and indoor multipath channel". MTA Review, vol. XIX, no. 4, Dec. 2009. ISSN 1843-3391.

[Akb10a] R. Akbar, E. Radoi, S. Azou. "Conception d'une forme d'onde IR-UWB optimisée et analyse de ses performances dans le canal IEEE 802.15.3a". Proc. MAnifestation des JEunes Chercheurs en Sciences et Technologies de l'Information et de la Communication (MajecSTIC'10), pp. 1–8. Bordeaux, France, Oct. 2010.

[Akb10b] R. Akbar, E. Radoi, S. Azou. "Maximum likelihood and orthogonal subspace based approach for improved IR-UWB channel estimation". Proc. European Sig. Process. Conf. (EUSIPCO'10), pp. 1145–1149. Aalborg, Denmark, Aug. 2010.

[Akb11] R. Akbar, E. Radoi, S. Azou. "Energy detection based blind synchronization for pulse shape modulated IR-UWB systems". Proc. IEEE Intl. Symp. Pers. Indoor and Mobile Radio Commun. (PIMRC'11), pp. 864–868. Toronto, Canada, Sep. 2011.

[Akb12a] R. Akbar, E. Radoi. "An overview of synchronization algorithms for IR-UWB systems". Proc. Int. Conf. Comput., Netw. and Commun. (ICNC), pp. 573–577. Maui, Hawaï, Jan. 2012. [Invited Paper].

[Akb12b] R. Akbar, E. Radoi, S. Azou. "Comparative analysis of some low-complexity blind synchronization algorithms for IR-UWB systems". Journal of Communications, vol. 7, no. 5: pp. 374–381, 2012.

[Akb12c] R. Akbar, E. Radoi, S. Azou. "A non-data-aided rapid synchronization method for UWB impulse radio". IEEE Commun. Lett., vol. 16, no. 8: pp. 1308–1311, Aug. 2012.

[Aky06] I. F. Akyildiz, W.-Y. Lee, M. C. Vuran, S. Mohanty. "NeXt generation/dynamic spectrum access/cognitive radio wireless networks: A survey". Computer Networks, vol. 50, no. 13: pp. 2127–2159, 2006.

[Aky11] I. F. Akyildiz, B. F. Lo, R. Balakrishnan. "Cooperative spectrum sensing in cognitive radio networks: A survey". Physical Communication, vol. 4, no. 1: pp. 40–62, Mar. 2011.

[Alf04] G. Alfano, A. Lozano, A. M. Tulino, S. Verdú. "Mutual information and eigenvalue distribution of MIMO ricean channels". Proc. Int. Symp. Information Theory and Its Applications (ISITA'04), vol. 4, pp. 1040–1045, 2004.

[Ara12] T. Araujo, R. Dinis. "On the accuracy of the gaussian approximation for the evaluation of nonlinear effects in ofdm signals". IEEE Trans. Commun., vol. 60, no. 2: pp. 346 –351, Feb. 2012.

[Bac08] R. B. Bacchus, A. J. Fertner, C. S. Hood, D. A. Roberson. "Long-term, wide-band spectral monitoring in support of dynamic spectrum access networks at the iit spectrum observatory". Proc. 3rd IEEE Int. Symp. New Frontiers in Dynamic Spectrum Access Networks (DySPAN), pp. 1–10, 2008.

[Bai06] J. Baik, J. W. Silverstein. "Eigenvalues of large sample covariance matrices of spiked population models". J. of Multivariate Analysis, vol. 97, no. 6: pp. 1382–1408, 2006.

[Bai08] Z. Bai, J. Yao. "Central limit theorems for eigenvalues in a spiked population model". Annales de l'Institut Henri Poincaré, Probabilités et Statistiques, vol. 44, pp. 447–474, 2008.

[Bal04] K. Balakrishnan, K. C. Wee, S. Xu, C. L. Chuan, F. Chin, C. Y. Huat, C. C. Choy, T. T. Thiang, P. Xiaoming, M. Ong, et al.. "Characterization of ultra wideband channels: Small-scale parameters for indoor & outdoor office environments". Document technique IEEE, pp. 802–15, 2004.

[Bar00] T. W. Barrett. "History of ultrawideband (UWB) radar & communications: pioneers and innovators". Proc. Progress in Electromagnetics Symposium, pp. 1–42, 2000.

[Bat04] A. Batra, et al.. "Multi-band ofdm physical layer proposal for ieee 802.15 task group 3a". Tech. Rep., 2004.

[Ben78] C. L. Bennett, G. F. Ross. "Time-domain electromagnetics and its applications". Proceedings of the IEEE, vol. 66, no. 3: pp. 299–318, 1978.

[Ber05] L. Berlemann, G. Dimitrakopoulos, K. Moessner. "Cognitive radio and management of spectrum and radio resources in reconfigurable networks". Wireless World Research Forum, Working Group 6 White Paper, 2005.

[Bro65] B. V. Bronk. "Exponential ensemble for random matrices". J. of Mathematical Physics, vol. 6: pp. 228–237, 1965.

[Bur00] E. Buracchini. "The software radio concept". IEEE Commun. Mag., vol. 38, no. 9: pp. 138–143, 2000.

[Cab04] D. Cabric, S. M. Mishra, R. W. Brodersen. "Implementation issues in spectrum sensing for cognitive radios". Proc. Asilomar Conf. on Signals, Systems and Computers, vol. 1, p. 772–776, 2004.

[Cab05] D. Cabric, R. W. Brodersen. "Physical layer design issues unique to cognitive radio systems". Proc. IEEE Intl. Symp. Pers. Indoor and Mobile Radio Commun. (PIMRC'05), vol. 2, pp. 759–763, 2005.

[Cab06] D. Cabric, A. Tkachenko, R. W. Brodersen. "Spectrum sensing measurements of pilot, energy, and collaborative detection". Proc. IEEE MILCOM'06, pp. 1–7, 2006.

[Car03] C. Carbonelli, U. Mengali, U. Mitra. "Synchronization and channel estimation for uwb signal". Proc. IEEE Global Telecommun. Conf., (GLOBECOM'03), pp. 764–768, 2003.

[Car04] C. Carbonelli, U. Mitra. "Clustered channel estimation for uwb signals". Proc. IEEE Conf. Commun., (ICC'04), vol. 4, pp. 2432–2436, 2004.

[Car06] C. Carbonelli, U. Mengali. "Synchronization algorithms for UWB signals". IEEE Trans. Commun., vol. 54, no. 2: pp. 329–338, Feb. 2006.

[Car08] L. S. Cardoso, M. Debbah, P. Bianchi, J. Najim. "Cooperative spectrum sensing using random matrix theory". Proc. 3rd Intl. Symp. Wireless Pervasive Computing (ISWPC), pp. 334–338, 2008.

[Cas02] D. Cassioli, M. Z. Win, A. F. Molisch. "The ultra-wide bandwidth indoor channel: from statistical model to simulations". IEEE J. Sel. Areas Commun., vol. 20, no. 6: pp. 1247–1257, Aug. 2002.

[Cas03] D. Cassioli, M. Z. Win, F. Vatalaro, A. F. Molisch. "Effects of spreading bandwidth on the performance of UWB rake receivers". Proc. IEEE Intl. Conf. Commun., (ICC'03), vol. 5, pp. 3545–3549, 2003.

[Cha03] Y. L. Chao, R. A. Scholtz. "Optimal and suboptimal receivers for ultra-wideband transmitted reference systems". Proc. IEEE Global Telecommun. Conf., (GLOBECOM'03), vol. 2, pp. 759–763, 2003.

[Cha04] K. Challapali, S. Mangold, Z. Zhong. "Spectrum agile radio: Detecting spectrum opportunities". Proc. Intl. Symp. Adv. Radio Technol., 2004.

[Che10] Y. Chen, N. C. Beaulieu. "A novel approximation of nda ml estimation for uwb channels". IEEE Trans. Commun., vol. 58, no. 10: pp. 2795–2798, 2010.

[Cho04] C. C. Chong, Y. Kim, S. S. Lee. "UWB indoor propagation channel measurements and data analysis in various types of high-rise apartments". Proc. IEEE Veh. Technol. Conf., VTC 2004-Fall, vol. 1, pp. 150–154, 2004.

[Cho05] C. C. Chong, Y. Kim, S. S. Lee. "A modified SV clustering channel model for the UWB indoor residential environment". Proc. IEEE Veh. Technol. Conf., VTC 2005-Spring, vol. 1, pp. 58–62, 2005.

[Con99] J. T. Conroy, J. L. LoCicero, D. R. Ucci. "Communication techniques using monopulse waveforms". Proc. IEEE Military Commun. Conf. (MILCOM'99), vol. 2, pp. 1181–1185, 1999.

[Cra02] R. J. M. Cramer, R. A. Scholtz, M. Z. Win. "Evaluation of an ultra-wide-band propagation channel". IEEE Trans. Antennas Propag., vol. 50, no. 5: pp. 561–570, 2002.

[Cur41] J. H. Curtiss. "On the distribution of the quotient of two chance variables". The Annals of Mathematical Statistics, vol. 12, no. 4: pp. 409–421, 1941.

[dA03] G. T. F. de Abreu, C. J. Mitchell, R. Kohno. "On the design of orthogonal pulse-shape modulation for UWB systems using Hermite pulses". J. of Commun. and Networks., vol. 5, no. 4: p. 328–343, Dec. 2003. Special issue on UWB Communications.

[dA10] G. T. F. de Abreu, W. Zhang, Y. Sanada. "Finite random matrices for blind spectrum sensing". Proc. IEEE 44th Asilomar Conf. Signals, Systems and Computers, pp. 116–120. IEEE, 2010.

[dA11] G. T. F. de Abreu, W. Zhang, Y. Sanada. "Spectrum sensing algorithms via finite random matrix theory". Proc. IEEE Intl. Conf. Commun. (ICC'11), pp. 1–5, 2011.

[DB06] M. G. Di Benedetto. UWB communication systems: a comprehensive overview, vol. 5. Hindawi Publishing Corporation, 2006.

[DC] "Data Converters | TI.com". http://www.ti.com/lsds/ti/analog/dataconverters/data_converter.page.

[Dem77] A. P. Dempster, N. M. Laird, D. B. Rubin. "Maximum likelihood from incomplete data via the em algorithm". Journal of the Royal Statistical Society. Series B (Methodological), pp. 1–38, 1977.

[Dig03] F. F. Digham, M. S. Alouini, M. K. Simon. "On the energy detection of unknown signals over fading channels". Proc. IEEE Int. Conf. Commun. (ICC'03), vol. 5, p. 3575–3579, 2003.

[Dig07] F. F. Digham, M.-S. Alouini, M. K. Simon. "On the energy detection of unknown signals over fading channels". IEEE Trans. Commun., vol. 55, no. 1: pp. 21 –24, Jan. 2007.

[Dil03] M. Dillinger, K. Madani, N. Alonistioti. Software Defined radio: Architectures, systems, and functions, vol. 1. John Wiley & Sons Inc, 2003.

[Dot07] I. Dotlic, R. Kohno. "Design of the family of orthogonal and spectrally efficient UWB waveforms". IEEE J. Sel. Topics Signal Process., vol. 1, no. 1: pp. 21–30, June 2007.

[ECC] ECC. "2009/343/ec: Commission decision of 21 april 2009 amending decision 2007/131/ec on allowing the use of the radio spectrum for equipment using ultra-wideband technology in a harmonised manner in the community". Official Jour. of European Union, pp. 9–13.

[Fal06] C. Falsi, D. Dardari, L. Mucchi, M. Z. Win. "Time of arrival estimation for uwb localizers in realistic environments". EURASIP J. Adv. Sig. Process., vol. 2006, 2006.

[Far05] S. Farahmand, X. Luo, G. B. Giannakis. "Demodulation and tracking with dirty templates for UWB impulse radio: algorithms and performance". IEEE Trans. Veh. Technol., vol. 54, no. 5: pp. 1595–1608, Sept. 2005.

[FB08] B. Farhang-Boroujeny. "Filter bank spectrum sensing for cognitive radios". IEEE Trans. Sig. Process., vol. 56, no. 5: pp. 1801–1811, 2008.

[FCC02a] "First report and order: Revision of part 15 of the commission's rules regarding ultra-wideband transmission systems". Tech. Rep., Federal Communications Commission, Apr. 2002. http://www.fcc.gov/Bureaus/Engineering_Technology/Orders/2002.

[FCC02b] "Report of the spectrum efficiency working group". Tech. Rep., FCC Spectrum Policy Task Force, Nov. 2002. http://www.fcc.gov/sptf/reports.html.

[FCC03] "FCC, ET Docket No 03-322, Notice of proposed rule making and order". Tech. Rep., Federal Communications Commission, Dec. 2003.

[Fel10] O. N. Feldheim, S. Sodin. "A universality result for the smallest eigenvalues of certain sample covariance matrices". Geometric And Functional Analysis, vol. 20, no. 1: pp. 88–123, 2010.

[Foe01] J. Foerster, E. Green, S. Somayazulu, D. Leeper, et al.. "Ultra-wideband technology for short-or medium-range wireless communications". Intel Technology Journal. Citeseer, 2001.

[Foe02] J. Foerster. "Channel modeling sub-committee report final". IEEE P802. 15-02/368r5-SG3a, 2002.

[Fow90] C. Fowler, J. Entzminger, J. Corum. "Assessment of ultra-wideband (UWB) technology". IEEE Aerospace and Electronic Systems Mag., vol. 5, no. 11: pp. 45–49, 1990.

[Fra04] S. Franz, U. Mitra. "Integration interval optimization and performance analysis for UWB transmitted reference systems". Proc. Intl. Workshop on Ultra Wideband Systems, joint with Conf. on Ultrawideband Systems and Technologies. (Joint UWBST & IWUWBS), pp. 26–30, 2004.

[Gar88] W. A. Gardner. "Signal interception: a unifying theoretical framework for feature detection". IEEE Trans. Commun., vol. 36, no. 8: pp. 897–906, 1988.

[Gei10] B. C. Geiger, T. Gigl, K. Witrisal. "Enhanced-accuracy channel estimation and ranging for ir-uwb energy detectors". Proc. IEEE Intl. Conf. on Ultra-Wideband, (ICUWB'10), pp. 513–518, 2010.

[Gez03] S. Gezici, E. Fishler, H. Kobayashi, H. Poor, A. Molisch. "A rapid acquisition technique for impulse radio". Proc. IEEE Commun., Comp. and signal Process. Conf., vol. 2, pp. 627–630 vol.2, Aug. 2003.

[Gha02] M. Ghavami, L. B. Michael, S. Haruyama, R. Kohno. "A novel UWB pulse shape modulation system". Kluwer Intl. J. on Wireless Pers. Commun., vol. 23, no. 1: pp. 105–120, Aug. 2002.

[Gha04a] S. S. Ghassemzadeh, R. Jana, C. W. Rice, W. Turin, V. Tarokh. "Measurement and modeling of an ultra-wide bandwidth indoor channel". IEEE Trans. Commun., vol. 52, no. 10: pp. 1786–1796, 2004.

[Gha04b] M. Ghavami, L. B. Michael, R. Kohno, I. Ebrary. Ultra wideband signals and systems in communication engineering, vol. 5. Wiley Online Library, 2004.

[Han03] K. Haneda, J. I. Takada. "An application of sage algorithm for uwb propagation channel estimation". Proc. IEEE Conf. on Ultra Wideband Systems and Technologies, pp. 483–487, 2003.

[Han06] K. Haneda, J. Takada, T. Kobayashi. "A parametric uwb propagation channel estimation and its performance validation in an anechoic chamber". IEEE Trans. Microwave Theory and Techniques, vol. 54, no. 4: pp. 1802–1811, 2006.

[Hay05] S. Haykin. "Cognitive radio: brain-empowered wireless communications". IEEE J. Sel. Areas Commun., vol. 23, no. 2: pp. 201–220, 2005.

[He06] N. He, C. Tepedelenlioglu. "Performance analysis of non-coherent UWB receivers at different synchronization levels". IEEE Trans. Wireless Commun., vol. 5, no. 6: pp. 1266–1273, June 2006.

[Ho02] M. Ho, V. S. Somayazulu, J. Foerster, S. Roy. "A differential detector for an ultra-wideband communications system". Proc. IEEE Vehicular Technol. Conf., vol. 4, pp. 1896–1900, May 2002.

[Hoc02] R. T. Hoctor, H. W. Tomlinson. "An overview of delay-hopped, transmitted-reference RF communications". Technique Information Series: General Electric Company Research and Development Center, pp. 1–29, Jan. 2002.

[Hom02] E. A. Homier, R. A. Scholtz. "Rapid acquisition of ultra-wideband signals in the dense multipath channel". Proc. IEEE Ultra Wideband Syst. and Technol. Conf., Digest of Papers, pp. 105–109, 2002.

[Hu05] B. Hu, N. C. Beaulieu. "Pulse shapes for ultrawideband communication systems". IEEE Tran. Wireless Commun., vol. 4, no. 4: pp. 1789–1797, 2005.

[Hua90] Y. Hua, T. K. Sarkar. "Matrix pencil method for estimating parameters of exponentially damped/undamped sinusoids in noise". IEEE Trans. Acoustics, Speech and Sig. Process., vol. 38, no. 5: pp. 814–824, 1990.

[Hua91] Y. Hua, T. K. Sarkar. "On svd for estimating generalized eigenvalues of singular matrix pencil in noise". IEEE Trans. Sig. Process., vol. 39, no. 4: pp. 892–900, 1991.

[Hum91] P. A. Humblet, M. Azizoglu. "On the bit error rate of lightwave systems with optical amplifiers". Journal of Lightwave Technology, vol. 9, no. 11: pp. 1576–1582, 1991.

[Ich98] K. Ichige, M. Kamada, R. Ishii. "A simple scheme of decomposing and reconstructing continuous-time signals by B-splines". IEICE TRANSACTIONS on Fundamentals of Electronics, Communications and Computer Sciences, vol. 81, no. 11: pp. 2391–2399, 1998.

[Joh01] I. M. Johnstone. "On the distribution of the largest eigenvalue in principal components analysis". The Annals of statistics, vol. 29, no. 2: pp. 295–327, 2001.

[Kam88] M. Kamada, K. Toraichi, R. Mori. "Spline function approach to digital signal processing", 1988.

[Kam95] M. Kamada, K. Toraichi, R. E. Kalman. "A smooth signal generator based on quadratic B-spline functions". IEEE Trans. Signal Process., vol. 43, no. 5: pp. 1252–1255, 1995.

[Kar04a] J. Karedal, S. Wyne, P. Almers, F. Tufvesson, A. F. Molisch. "Statistical analysis of the UWB channel in an industrial environment". Proc. IEEE Veh. Technol. Conf., VTC 2004-Fall, vol. 1, pp. 81–85, 2004.

[Kar04b] J. Karedal, S. Wyne, P. Almers, F. Tufvesson, A. F. Molisch. "UWB channel measurements in an industrial environment". Proc. IEEE Global Telecommun. Conf., (GLOBECOM'04), vol. 6, pp. 3511–3516, 2004.

[Kay88a] S. Kay. Fundamentals of Statistical Signal Processing: Detection Theory, vol. 2. Prentice-Hall, 1988.

[Kay88b] S. Kay. Modern Spectral Estimation: Theory and Applications. Prentice-Hall, 1988.

[Kei04] J. Keignart, N. Daniele. "Uwb channel measurements in snow-covered environment". Document technique IEEE, pp. 802–15, 2004.

[Kha07] N. Khambekar, L. Dong, V. Chaudhary. "Utilizing ofdm guard interval for spectrum sensing". Proc. IEEE Wireless Commun. Netw. Conf. (WCNC), pp. 38–42, 2007.

[Kim08] H. Kim, K. G. Shin. "Fast discovery of spectrum opportunities in cognitive radio networks". Proc. 3rd IEEE Int. Symp. New Frontiers in Dynamic Spectrum Access Networks (DySPAN), pp. 1–12, 2008.

[KK09] F. Kharrat-Kammoun, C. J. Le Martret, P. Ciblat. "Performance analysis of IR-UWB in a multi-user environment". IEEE Trans. Wireless Commun., vol. 8, no. 11: pp. 5552–5563, 2009.

[Kol01] P. Kolodzy, et al.. "Next generation communications: Kickoff meeting". Proc. DARPA, vol. 10, 2001.

[Kus03] J. Kusuma, I. Maravic, M. Vetterli. "Sampling with finite rate of innovation: channel and timing estimation for UWB and GPS". Proc. Intl. Conf. Commun., pp. 3540–3544, vol.5, May 2003.

[Leh05] J. Lehtomäki. Analysis of energy based signal detection, vol. 68, 2005.

[Leu05] A. E. Leu, K. Steadman, M. McHenry, J. Bates. "Ultra sensitive TV detector measurements". Proc. IEEE Int. Symp. New Frontiers in Dynamic Spectrum Access Networks (DySPAN), pp. 30–36, 2005.

[Li08] H. Li, C. Li, H. Dai. "Quickest spectrum sensing in cognitive radio". Proc. 42nd Annual Conf. Information Sciences and Systems (CISS'08), pp. 203–208, 2008.

[Li11] L. Li, J. K. Townsend. "Near-far resistant synchronization for UWB communications". IEEE Trans. Wireless Commun., vol. 10, no. 2: pp. 519–529, 2011.

[Liu10] B. Liu, T. Lv, H. Gao. "Blind synchronization and demodulation for noncoherent ultra-wideband system with robustness against ISI and IFI". Proc. IEEE Intl. Conf. Commun. (ICC'10), pp. 1–5, May 2010.

[Lot02] V. Lottici, A. D'Andrea, U. Mengali. "Channel estimation for ultra-wideband communications". IEEE J. Sel. Areas Commun., vol. 20, no. 9: pp. 1638–1645, Dec. 2002.

[Lun07] J. Lunden, V. Koivunen, A. Huttunen, H. V. Poor. "Spectrum sensing in cognitive radios based on multiple cyclic frequencies". Proc. CrownCom'07, pp. 37–43, 2007.

[Luo03] X. Luo, L. Yang, G. B. Giannakis. "Designing optimal pulse-shapers for ultra-wideband radios". Proc. IEEE Ultra Wideband Syst. and Technol. Conf., pp. 349–353, 2003.

[Luo04] X. Luo, G. B. Giannakis. "Blind timing and channel estimation for UWB multiuser ad hoc access". Asilomar Conf. Signals, Systems and Computers, pp. vol.1, 642–646, Nov. 2004.

[Luo06a] X. Luo, G. Giannakis. "Cyclic-mean based synchronization and efficient demodulation for UWB ad hoc access: Generalizations and comparisons". EURASIP J. Signal Process., vol. 86, no. 9: pp. 2139–2152, 2006.

[Luo06b] X. Luo, G. B. Giannakis. "Low-complexity blind synchronization and demodulation for (ultra-)wideband multi-user ad hoc access". IEEE Trans. Wireless Commun., vol. 5, no. 7: pp. 1930–1941, July 2006.

[Luo07] X. Luo, G. B. Giannakis. "Raise your voice at a proper pace to synchronize in multiple ad hoc piconets". IEEE Trans. Signal Process., vol. 55, no. 1: pp. 267–278, Jan. 2007.

[Lv11] T. Lv, Y. Qiao, Z. Wang. "Training-based synchronization and demodulation with low complexity for UWB signals". IEEE Trans. Veh. Technol., vol. 60, no. 8: pp. 3736–3747, Oct. 2011.

[Maj07] S. Majhi, A. S. Madhukumar, A. B. Premkumar, F. Chin. "Modulation schemes based on orthogonal pulses for time hopping ultra wideband radio systems". Proc. Intl. Conf. Commun., pp. 4185–4190. Scotland, June 2007.

[Mar67] V. A. Marčenko, L. A. Pastur. "Distribution of eigenvalues for some sets of random matrices". Mathematics of the USSR-Sbornik, vol. 1: p. 457, 1967.

[Mar87] S. L. Marple. Digital Spectral Analysis with Applications. Prentice-Hall, 1987.

[Mar03a] I. Maravic, J. Kusuma, M. Vetterli. "Low-sampling rate UWB channel characterization and synchronization". Journal of Communications and Networks, vol. 5, no. 4: pp. 319–327, 2003.

[Mar03b] I. Maravic, M. Vetterli. "Low-complexity subspace methods for channel estimation and synchronization in ultra-wideband systems". Proc. of Intl. Workshop on Ultra-Wideband (IWUWB). Oulu, Finland, 2003.

[Mat05] M. Matsuo, M. Kamada, H. Habuchi. "Design of UWB pulses based on B-splines". proc. IEEE Intl. Symp. on Circuits and Systems, pp. vol. 6, pp. 5425–5428. Japan, May 2005.

[Mat10] M. Matthaiou, M. R. McKay, P. J. Smith, J. A. Nossek. "On the condition number distribution of complex wishart matrices". IEEE Trans. Commun., vol. 58, no. 6: pp. 1705–1717, 2010.

[Meh01] M. Mehta, N. Drew, G. Vardoulias, N. Greco, C. Niedermeier. "Reconfigurable terminals: An overview of architectural solutions". IEEE Commun. Mag., vol. 39, no. 8: pp. 82–89, 2001.

[Mek08] S. Mekki, J. L. Danger, B. Miscopein, J. J. Boutros. "Em channel estimation in a low-cost uwb receiver based on energy detection". Proc. IEEE Intl. Symp. Wireless Commun. Syst., (ISWCS'08), pp. 214–218, 2008.

[MI99a] J. Mitola III. "Cognitive radio for flexible mobile multimedia communications". Proc. IEEE Intl. Workshop on Mobile Multimedia Commun., pp. 3–10, 1999.

[MI99b] J. Mitola III. Cognitive radio: Model-based competence for software radios. Ph.D. thesis, Royal Inst. Technol. (KTH), Stockholm, Sweden, 1999.

[MI99c] J. Mitola III, G. Q. Maguire Jr. "Cognitive radio: Making software radios more personal". IEEE Pers. Commun., vol. 6, no. 4: pp. 13–18, 1999.

[MI00] J. Mitola III. Cognitive radio: An integrated agent architecture for software defined radio. Ph.D. thesis, Royal Inst. Technol. (KTH), Stockholm, Sweden, 2000.

[Mic95] Z. Michalewicz. "A perspective on evolutionary computation". Progress in Evolutionary Computation, pp. 73–89, 1995.

[Mis07] S. M. Mishra, R. W. Brodersen, S. T. Brink, R. Mahadevappa. "Detect and avoid: an ultra-wideband/wimax coexistence mechanism [topics in radio communications]". IEEE Commun. Mag., vol. 45, no. 6: pp. 68–75, 2007.

[Mod07] A. Mody. "Spectrum sensing of the DTV in the vicinity of the pilot using higher order statistics", 2007. IEEE 802.22-07/0359r1.

[Mol03] A. F. Molisch, J. R. Foerster, M. Pendergrass. "Channel models for ultrawideband personal area networks". IEEE Wireless Commun., vol. 10, no. 6: pp. 14–21, Dec. 2003.

[Mol04] A. F. Molisch, K. Balakrishnan, D. Cassioli, C. C. Chong, S. Emami, A. Fort, J. Karedal, J. Kunisch, H. Schantz, U. Schuster, et al.. "IEEE 802.15. 4a channel model-final report". IEEE P802, vol. 15, no. 04, 2004.

[Mol05] A. F. Molisch. "Ultrawideband propagation channels-theory, measurement, and modeling". IEEE Trans. Veh. Technol., vol. 54, no. 5: pp. 1528–1545, 2005.

[Niu03] H. Niu, J. A. Ritcey, H. Liu. "Performance of UWB RAKE receivers with imperfect tap weights". Proc. Intl. Conf. Acoustics, Speech, and Signal Process., vol. 4, pp. 125–128, 2003.

[O'D05] I. O'Donnell, R. W. Brodersen. "An ultra-wideband transceiver architecture for low power, low rate, wireless systems". IEEE Trans. Veh. Technol., vol. 54, no. 5: pp. 1623–1631, Sept. 2005.

[Opp04] I. Oppermann, M. Hämäläinen, J. Iinatti. UWB theory and applications. Wiley, 2004.

[Oue05] M. Ouertani, H. Besbes, A. Bouallegue. "Modified hermite functions for designing new optimal UWB pulse-shapers", 2005.

[Oue08] M. Ouertani, H. Xu, H. Besbes, L. Yang, A. Bouallègue. "Orthogonal bi-pulse UWB: Timing and (de)modulation". Physical Communication, vol. 1, no. 4: pp. 237–247, 2008.

[Pal03] J. Palicot, C. Roland. "A new concept for wireless reconfigurable receivers". IEEE Commun. Mag., vol. 41, no. 7: pp. 124–132, 2003.

[Paq04] S. Paquelet, L. M. Aubert, B. Uguen. "An impulse radio asynchronous transceiver for high data rates". Proc. Intl. Workshop on Ultra Wideband Systems, joint with Conf. on Ultrawideband Systems and Technologies. (Joint UWBST & IWUWBS), pp. 1–5, 2004.

[Par00] J. D. Parsons. The mobile radio propagation channel, vol. 2, 2000.

[Par03] B. Parr, B. L. Cho, K. Wallace, Z. Ding. "A novel ultra-wideband pulse design algorithm". IEEE Commun. Lett., vol. 7, no. 5: pp. 219–221, 2003.

[Pau04] M. Pausini, G. J. M. Janssen. "Analysis and comparison of autocorrelation receivers for IR-UWB signals based on differential detection". Proc. IEEE Intl. Conf. Acoustics, Speech, and Sig. Process., (ICASSP'04), vol. 4, pp. iv–513, 2004.

[Pen09a] F. Penna, R. Garello. "Theoretical performance analysis of eigenvalue-based detection". Arxiv preprint arXiv:0907.1523, 2009.

[Pen09b] F. Penna, R. Garello, M. Spirito. "Cooperative spectrum sensing based on the limiting eigenvalue ratio distribution in wishart matrices". IEEE Commun. Lett., vol. 13, no. 7: pp. 507–509, 2009.

[Pro00] J. G. Proakis. Digital communications. McGraw-Hill, 4 edn., 2000.

[Qua09] Z. Quan, S. J. Shellhammer, W. Zhang, A. H. Sayed. "Spectrum sensing by cognitive radios at very low SNR". Proc. IEEE Global Telecom. Conf. (Globecom'09), pp. 1–6, 2009.

[Rab04] A. Rabbachin, I. Oppermann. "Synchronization analysis for UWB systems with a low-complexity energy collection receiver". Proc. Intl. Workshop on Ultra Wideband Systems, joint with Conf. on Ultrawideband Systems and Technologies. (Joint UWBST & IWUWBS), pp. 288–292, 2004.

[Raj03] A. Rajeswaran, V. S. Somayazulu, J. R. Foerster. "Rake performance for a pulse based UWB system in a realistic UWB indoor channel". Proc. IEEE Intl. Conf. Commun. (ICC'03), vol. 4, pp. 2879–2883, 2003.

[Rao92] B. D. Rao, K. S. Arun. "Model based processing of signals: A state space approach". Proceedings of the IEEE, vol. 80, no. 2: pp. 283–309, 1992.

[Rap02] T. S. Rappaport. Wireless communications: principles and practice. Prentice Hall, 2002.

[Ren09] Z. Ren, T. Lv. "A novel synchronization algorithm dispensing with searching for UWB signals". Proc. IEEE Global Telecom. Conf. (Globecom'09), pp. 1–5, Dec. 2009.

[Roy89] R. Roy, T. Kailath. "Esprit estimation of signal parameters via rotational invariance techniques". IEEE Trans. Acoustics, Speech and Sig. Process., vol. 37, no. 7: pp. 984–995, 1989.

[Rus64] C. Rushforth. "Transmitted-reference techniques for random or unknown channels". IEEE Trans. Inf. Theory, vol. 10, no. 1: pp. 39–42, 1964.

[Sah05] A. Sahai, D. Cabric. "Spectrum sensing: fundamental limits and practical challenges". Proc. IEEE Intl. Symp.on New Frontiers in Dynamic Spectrum Access Networks (DySPAN'05), 2005.

[Sah06] A. Sahai, R. Tandra, S. M. Mishra, N. Hoven. "Fundamental design tradeoffs in cognitive radio systems". Proc. First intl. workshop on Technology and policy for accessing spectrum, p. 2, 2006.

[Sal87] A. A. M. Saleh, R. Valenzuela. "A statistical model for indoor multipath propagation". IEEE J. Sel. Areas Commun., vol. 5, no. 2: pp. 128–137, Feb. 1987.

[Sch46] I. J. Schoenberg. "Contributions to the problem of approximation of equidistant data by analytic functions". Quart. Appl. Math, vol. 4, no. 2: pp. 45–99, 1946.

[Sch73] I. J. Schoenberg. Cardinal spline interpolation, vol. 12. SIAM, 1973.

[Sch93] R. Scholtz. "Multiple access with time-hopping impulse modulation". Proc. IEEE Military Commun. Conf., MILCOM'93, vol. 2, pp. 447–450, 1993.

[Sch04] U. Schuster, H. Bolsckei. "Indoor uwb channel measurements from 2 ghz to 8 ghz". Document technique IEEE, pp. 802–15, 2004.

[Shi03] H. Shin, J. H. Lee. "Capacity of multiple-antenna fading channels: Spatial fading correlation, double scattering, and keyhole". IEEE Trans. Inf. Theory, vol. 49, no. 10: pp. 2636–2647, 2003.

[Shi06] D. H. Shin, Y. H. Cho, D. J. Park. "A new synchronization scheme exploiting mean energy profile in UWB non-coherent receiver". Proc. Intl. Conf. Commun., vol. 12, pp. 5721–5725, June 2006.

[Son92] A. Sonnenschein, P. M. Fishman. "Radiometric detection of spread-spectrum signals in noise of uncertain power". IEEE Trans. Aerosp. Electron. Syst, vol. 28, no. 3: pp. 654–660, 1992.

[SSC] "Shared Spectrum Company". http://www.sharedspectrum.com/measurements/.

[Sta11] M. I. Stanciu. Sur l'estimation aveugle de paramètres de signaux UWB impulsionnels dans un contexte de radio intelligente. Ph.D. thesis, Univésité de Bretagne Occidentale (UBO), Apr. 2011.

[Ste06] C. R. Stevenson, C. Cordeiro, E. Sofer, G. Chouinard. "Functional requirements for the 802.22 WRAN standard". doc.: IEEE, pp. 802–22, 2006.

[Sto97] P. Stoica, R. L. Moses. Introduction to spectral analysis, vol. 51. Prentice Hall Upper Saddle River, NJ, 1997.

[Suw05] W. Suwansantisuk, M. Z. Win, L. A. Shepp. "On the performance of wide-bandwidth signal acquisition in dense multipath channels". IEEE Trans. Veh. Technol., vol. 54, no. 5: pp. 1584–1594, sept. 2005.

[Suw07] W. Suwansantisuk, M. Z. Win. "Multipath aided rapid acquisition: Optimal search strategies". IEEE Trans. Inf. Theory, vol. 53, no. 1: pp. 174 –193, Jan. 2007.

[Tan83] W. Y. Tan, R. P. Gupta. "On approximating the non-central wishart distribution with wishart distribution". Commun. Stat. Theory Method, vol. 12, no. 22: pp. 2589–2600, 1983.

[Tan05a] R. Tandra, A. Sahai. "Fundamental limits on detection in low SNR under noise uncertainty". Proc. Int. Conf. Wireless Netw., Commun. and Mobile Comput., vol. 1, p. 464–469, 2005.

[Tan05b] H. Tang. "Some physical layer issues of wide-band cognitive radio systems". Proc. IEEE Int. Symp. New Frontiers in Dynamic Spectrum Access Networks (DySPAN), pp. 151–159, 2005.

[Tan08] R. Tandra, A. Sahai. "SNR walls for signal detection". IEEE J. Sel. Topics Signal Process., vol. 2, no. 1: pp. 4–17, 2008.

[Tay94] J. D. Taylor. Introduction to ultra-wideband radar systems. CRC, 1994.

[Tia02] Z. Tian, L. Yang, G. B. Giannakis. "Symbol timing estimation in ultra wideband communications". Proc. Asilomar Conf. Signals, Systems and Computers, pp. vol.2, 1924–1928, Nov. 2002.

[Tia05a] Z. Tian, G. B. Giannakis. "BER sensitivity to mistiming in ultra-wideband impulse radios - part I: Nonrandom channels". IEEE Trans. Signal Process., vol. 53, no. 4: pp. 1550–1560, April 2005.

[Tia05b] Z. Tian, G. B. Giannakis. "BER sensitivity to mistiming in ultra-wideband impulse radios - part II: fading channels". IEEE Trans. Signal Process., vol. 53, no. 5: pp. 1897–1907, May 2005.

[Tia05c] Z. Tian, G. B. Giannakis. "A GLRT approach to data-aided timing acquisition in UWB radios-part I: algorithms". IEEE Trans. Wireless Commun., vol. 4, no. 6: pp. 2956–2967, Nov. 2005.

[Tia06] Z. Tian, G. B. Giannakis. "A wavelet approach to wideband spectrum sensing for cognitive radios". Proc. 1st Intl. Conf. Cognitive Radio Oriented Wireless Netw. Commun. (CrownCom), pp. 1–5, 2006.

[Tia07] Z. Tian, G. B. Giannakis. "Compressed sensing for wideband cognitive radios". Proc. IEEE Intl. Conf. Acoustics, Speech, and Sig. Process. (ICASSP'07), vol. 4, p. 1357–1360, 2007.

[Tka07] A. Tkachenko, A. D. Cabric, R. W. Brodersen. "Cyclostationary feature detector experiments using reconfigurable BEE2". Proc. 2nd IEEE Int. Symp. New Frontiers in Dynamic Spectrum Access Networks (DySPAN), pp. 216–219, 2007.

[Tra96] C. A. Tracy, H. Widom. "On orthogonal and symplectic matrix ensembles". Communications in Mathematical Physics, vol. 177, no. 3: pp. 727–754, 1996.

[Tra00] C. A. Tracy, H. Widom. "The distribution of the largest eigenvalue in the gaussian ensembles". Calogero-Moser-Sutherland Models, CRM Series in Mathematical Physics, vol. 4: pp. 461–472, 2000.

[Urk67] H. Urkowitz. "Energy detection of unknown deterministic signals". Proceedings of the IEEE, vol. 55, no. 4: p. 523–531, 1967.

[Var01] G. Vardoulias, J. Faroughi-Esfahani, G. Clemo, R. Haines. "Blind radio access technology discovery and monitoring for software defined radio communication systems: problems and techniques". Proc. 2nd Intl. Conf. 3G Mobile Commun. Technol., pp. 306–310, 2001.

[Vis08] F. E. Visser, G. J. M. Janssen, P. Pawelczak. "Multinode spectrum sensing based on energy detection for dynamic spectrum access". Proc. IEEE Vehi. Technol. Conf., (VTC'08) Spring, p. 1394–1398, 2008.

[Voj03] B. R. Vojcic, R. L. Pickholtz. "Direct-sequence code division multiple access for ultra-wide bandwidth impulse radio". Proc. IEEE Military Commun. Conf. (MILCOM'03), vol. 2, pp. 898–902, 2003.

[Wan07] J. Wang, L. Mai, Y. Peng, J. Han, X. Zeng. "An energy-proportion synchronization method for IR-UWB communications". Proc. IEEE Symp. on Circuits and Syst., pp. 2578–2581, May 2007.

[Wan08] M. Wang, S. Yang, S. Wu. "A GA-based UWB pulse waveform design method". Digital Signal Processing, vol. 18, no. 1: pp. 65–74, 2008.

[Wax85] M. Wax, T. Kailath. "Detection of signals by information theoretic criteria". IEEE Trans. Acoust., Speech, Signal Process., vol. 33, no. 2: p. 387–392, 1985.

[Wei04a] M. Weisenhorn, W. Hirt. "Robust noncoherent receiver exploiting UWB channel properties". Proc. Intl. Workshop on Ultra Wideband Systems, joint with Conf. on Ultrawideband Systems and Technologies. (Joint UWBST & IWUWBS), pp. 156–160, 2004.

[Wei04b] T. A. Weiss, F. K. Jondral. "Spectrum pooling: an innovative strategy for the enhancement of spectrum efficiency". IEEE Commun. Mag., vol. 42, no. 3: pp. S8–S14, 2004.

[Wil08] D. Willkomm, S. Machiraju, J. Bolot, A. Wolisz. "Primary users in cellular networks: A large-scale measurement study". Proc. 3rd IEEE Int. Symp. New Frontiers in Dynamic Spectrum Access Networks (DySPAN), pp. 1–11, 2008.

[Win02] M. Z. Win, R. A. Scholtz. "Characterization of ultra-wide bandwidth wireless indoor channels: a communication-theoretic view". IEEE J Sel. Areas Commun., vol. 20, no. 9: pp. 1613–1627, 2002.

[Wit09] K. Witrisal, G. Leus, G. Janssen, M. Pausini, F. Troesch, T. Zasowski, J. Romme. "Noncoherent ultra-wideband systems". IEEE Signal. Process. Mag., vol. 26, no. 4: pp. 48–66, Jul. 2009.

[Wu04] X. Wu, Z. Tian, T. N. Davidson, G. B. Giannakis. "Orthogonal waveform design for UWB radios". Proc. IEEE 5th Workshop on Signal Processing Advances in Wireless Communications, pp. 150–154, 2004.

[Wu06] X. Wu, Z. Tian, T. Davidson, G. B. Giannakis. "Optimal waveform design for UWB radios". IEEE Trans. Signal Process., vol. 54, no. 6: pp. 2009–2021, June 2006.

[Wu08] L. Wu, V. Lottici, Z. Tian. "Maximum likelihood multiple access timing synchronization for UWB communications". IEEE Trans. Wireless Commun., vol. 7, no. 11: pp. 4497–4501, Nov. 2008.

[Xu06] Z. Xu, J. Tang. "Blind channel estimation in aperiodic time-hopping ultra-wideband communications". IEEE Trans. Sig. Process., vol. 54, no. 6: pp. 2333–2346, 2006.

[Yan03] L. Yang, Z. Tian, G. B. Giannakis. "Non-data aided timing acquisition of ultra-wideband transmissions using cyclostationarity". Proc. IEEE Intl. Conf. Acoustics, Speech, and Sig. Process. (ICASSP'03), pp. 121–124. Hong Kong, China, Apr. 2003.

[Yan05] L. Yang, G. B. Giannakis. "Timing ultra-wideband signals with dirty templates". IEEE Trans. Commun., vol. 53, no. 11: pp. 1952–1963, Nov. 2005.

[Yin08] Y. Ying, M. Ghogho, A. Swami. "Code-assisted synchronization for UWB-IR systems: Algorithms and analysis". IEEE Trans. Signal Process., vol. 56, no. 10: pp. 5169–5180, Oct. 2008.

[You06] Y. Youn, H. Jeon, J. H. Choi, H. Lee. "Fast spectrum sensing algorithm for 802.22 WRAN systems". Proc. Intl. Symp. Communications and Information Technologies, (ISCIT'06), pp. 960–964, 2006.

[Yuc06] T. Yucek, H. Arslan. "Spectrum characterization for opportunistic cognitive radio systems". Proc. IEEE MILCOM'06, pp. 1–6, 2006.

[Yuc09] T. Yucek, H. Arslan. "A survey of spectrum sensing algorithms for cognitive radio applications". IEEE Commun. Surveys Tuts., vol. 11, no. 1: pp. 116–130, 2009.

[Zan08] A. Zanella, M. Chiani. "The pdf of the lth largest eigenvalue of central wishart matrices and its application to the performance analysis of mimo systems". Proc. IEEE Global Telecom. Conf. (Globecom'08), pp. 1–6, 2008.

[Zen07] Y. Zeng, Y. C. Liang. "Maximum-minimum eigenvalue detection for cognitive radio". Proc. IEEE Intl. Symp. Pers. Indoor and Mobile Radio Commun. (PIMRC'07), pp. 1–5, 2007.

[Zen09a] Y. Zeng, Y. C. Liang. "Eigenvalue-based spectrum sensing algorithms for cognitive radio". IEEE Trans. Commun., vol. 57, no. 6: pp. 1784–1793, 2009.

[Zen09b] Y. Zeng, Y. C. Liang. "Spectrum-sensing algorithms for cognitive radio based on statistical covariances". IEEE Trans. Veh. Technol., vol. 58, no. 4: pp. 1804–1815, 2009.

[Zen10] Y. Zeng, Y. C. Liang, A. T. Hoang, R. Zhang. "A review on spectrum sensing for cognitive radio: challenges and solutions". EURASIP J. Adv. Signal Process., vol. 2010, 2010.

[Zha03] H. Zhang, D. L. Goeckel. "Generalized transmitted-reference uwb systems". Proc. IEEE Conf. on Ultra Wideband Systems and Technologies, pp. 147–151, 2003.

[Zha12] W. Zhang, G. Abreu, M. Inamori, Y. Sanada. "Spectrum sensing algorithms via finite random matrices". IEEE Trans. Commun., vol. 60, no. 1, Jan. 2012.

[Zhu03] W. Zhuang, X. S. Shen, Q. Bi. "Ultra-wideband wireless communications". Wireless commun. and mobile computing, vol. 3, no. 6: pp. 663–685, 2003.

Abstract

Faced with an ever increasing demand of high data-rates and improved adaptability among existing systems, which in turn is resulting in spectrum scarcity, the development of new radio solutions becomes mandatory in order to answer the requirements of these emergent applications. Among the recent innovations in the field of wireless communications, ultra wideband (UWB) has generated significant interest. Impulse based UWB (IR-UWB) is one attractive way of realizing UWB systems, which is characterized by the transmission of sub nanoseconds UWB pulses, occupying a bandwidth up to 7.5 GHz with extremely low power density. This large bandwidth results in several captivating features such as low-complexity low-cost transceiver, ability to overlay existing narrowband systems, ample multipath diversity, and precise ranging at centimeter level due to extremely fine temporal resolution.

In this PhD dissertation, we investigate some of the key elements in the realization of an intelligent time-hopping based IR-UWB system. Due to striking resemblance of IR-UWB inherent features with cognitive radio (CR) requirements, a **cognitive UWB** based system is first studied. A CR in its simplest form can be described as a radio, which is aware of its surroundings and adapts intelligently. As sensing the environment for the availability of resources and then consequently adapting radio's internal parameters to exploit them opportunistically constitute the major blocks of any CR, we first focus on robust **spectrum sensing** algorithms and the **design of adaptive UWB waveforms** for realizing a cognitive UWB radio. The spectrum sensing module needs to function with minimum *a-priori* knowledge available about the operating characteristics and detect the primary users as quickly as possible. Keeping this in mind, we develop several spectrum sensing algorithms invoking recent results on the random matrix theory, which can provide efficient performance with a few number of samples. Next, we design the UWB waveform using a linear combination of B-splines with weight coefficients being optimized by genetic algorithms. This results in a UWB waveform that is spectrally efficient and at the same time adaptable to incorporate the cognitive radio requirements. In the 2nd part of this thesis, some research challenges related to signal processing in UWB systems, namely **synchronization** and dense multipath **channel estimation** are addressed. Several low-complexity non-data-aided (NDA) synchronization algorithms are proposed for BPSK and PSM modulations, exploiting either the orthogonality of UWB waveforms or the inherent cyclostationarity of IR-UWB signaling. Finally, we look into the channel estimation problem in UWB, which is very demanding due to particular nature of UWB channels and at the same time very critical for the coherent Rake receivers. A method based on a joint maximum-likelihood (ML) and orthogonal subspace (OS) approaches is proposed which exhibits improved performance than both of these methods individually.

Index terms – IR-UWB, cognitive UWB, time-hopping, orthogonal signaling, spectrum sensing, UWB waveform design, NDA synchronization, UWB channel estimation.

Résumé

Face à une demande sans cesse croissante de haut débit et d'adaptabilité des systèmes existants, qui à son tour se traduit par l'encombrement du spectre, le développement de nouvelles solutions dans le domaine des communications sans fil devient nécessaire afin de répondre aux exigences des applications émergentes. Parmi les innovations récentes dans ce domaine, l'ultra large bande (UWB) a suscité un vif intérêt. La radio impulsionnelle UWB (IR-UWB), qui est une solution intéressante pour réaliser des systèmes UWB, est caractérisée par la transmission des impulsions de très courte durée, occupant une largeur de bande allant jusqu'à 7,5 GHz, avec une densité spectrale de puissance extrêmement faible. Cette largeur de bande importante permet de réaliser plusieurs fonctionnalités intéressantes, telles que l'implémentation à faible complexité et à coût réduit, la possibilité de se superposer aux systèmes à bande étroite, la diversité spatiale et la localisation très précise de l'ordre centimétrique, en raison de la résolution temporelle très fine.

Dans cette thèse, nous examinons certains éléments clés dans la réalisation d'un système IR-UWB intelligent. Nous avons tout d'abord proposé le concept de **radio UWB cognitive** à partir des similarités existantes entre l'IR-UWB et la radio cognitive. Dans sa définition la plus simple, un tel système est conscient de son environnement et s'y adapte intelligemment. Ainsi, nous avons tout d'abord focalisé notre recherché sur l'analyse de la disponibilité des ressources spectrales (**spectrum sensing**) et la **conception d'une forme d'onde UWB adaptative**, considérées comme deux étapes importantes dans la réalisation d'une radio cognitive UWB. Les algorithmes de spectrum sensing devraient fonctionner avec un minimum de connaissances a priori et détecter rapidement les utilisateurs primaires. Nous avons donc développé de tels algorithmes utilisant des résultats récents sur la théorie des matrices aléatoires, qui sont capables de fournir de bonnes performances, avec un petit nombre d'échantillons. Ensuite, nous avons proposé une méthode de conception de la forme d'onde UWB, vue comme une superposition de fonctions B-splines, dont les coefficients de pondération sont optimisés par des algorithmes génétiques. Il en résulte une forme d'onde UWB qui est spectralement efficace et peut s'adapter pour intégrer les contraintes liées à la radio cognitive. Dans la 2ème partie de cette thèse, nous nous sommes attaqués à deux autres problématiques importantes pour le fonctionnement des systèmes UWB, à savoir la **synchronisation** et l'**estimation du canal UWB**, qui est très dense en trajets multiples. Ainsi, nous avons proposé plusieurs algorithmes de synchronisation, de faible complexité et sans séquence d'apprentissage, pour les modulations BPSK et PSM, en exploitant l'orthogonalité des formes d'onde UWB ou la cyclostationnarité inhérente à la signalisation IR-UWB. Enfin, nous avons travaillé sur l'estimation du canal UWB, qui est un élément critique pour les récepteurs Rake cohérents. Ainsi, nous avons proposé une méthode d'estimation du canal basée sur une combinaison de deux approches complémentaires, le maximum de vraisemblance et la décomposition en sous-espaces orthogonaux, d'améliorer globalement les performances.

Mots clefs – IR-UWB, radio UWB cognitive, time-hopping, spectrum sensing, conception de la forme d'onde UWB, synchronization non-assistée, estimation du canal UWB.